UNIVERSITÀ DEGLI STUDI DI TRIESTE

XXVII CICLO DEL DOTTORATO DI RICERCA IN

NANOTECNOLOGIE

DIGITAL CONTROL OF PROTEIN-NUCLEIC ACID INTERACTIONS WITH SELF-ASSEMBLED DNA NANOSYSTEMS

Settore scientifico-disciplinare: FIS/03

DOTTORANDO

ALEX STOPAR

COORDINATORE

PROF. LUCIA PASQUATO

SUPERVISORE DI TESI

DR. MATTEO CASTRONOVO

ANNO ACCADEMICO 2014 / 2015

Abstract (EN)

Understanding how enzymes access, transform or degrade a nucleic acid nanostructure is an essential step for the progress of functional DNA nanotechnology.

Most approaches for the analysis of nucleic acids require enzymatic reactions. For instance sequencing-by-synthesis of confined DNA molecules is a most established approach for the analysis of the entire genomic information in living organisms. Little is known however about the physical factors that regulate enzymes functions in highly confined systems.

In this doctoral thesis, I have investigated the activity of type II restriction enzymes (REs) on basic, two-dimensional DNA nanostructures (DNA origami, i.e. triangles and rectangles) that are formed upon the spontaneous hybridization of many single stranded (ss)DNA molecules over the 7,249-nt-long M13mp18 ssDNA phage genome that serves as scaffold for the inherent DNA self-assembly process.

The primary action of REs is DNA fragmentation, and they are a primary defensive mechanism to viral infection in bacteria. Type II REs have an exquisite ability to specifically recognize dsDNA binding sites (termed restriction sites) and irreversibly cleave the inherent DNA molecules within the sites. They are in addition essential tools for DNA cloning in current bioengineering and biotechnology applications. On the other hand, the M13mp18 scaffold naturally possesses a number of restriction sites for each of several, known restriction enzymes. In addition, DNA origami are comprised of different structural motifs that are responsible for molecular confinement of the involved DNA molecules and the peculiar mechanical properties of the shape.

My work primarily consists of an unprecedented investigation of the action of >10 type II restriction enzymes on two-dimensional (2D) DNA origami. For two enzymes in particular (*HhaI* and *Hin1II*) we fully mapped the site-specific action by activating one site at a time (by generating DNA origami mutants), and measuring the fragmentation pattern of the DNA scaffold by gel electrophoresis, after melting the DNA

nanostructure. With such mutational analysis of 2D DNA origami we found that (a) restriction reactions can be efficiently inhibited in 2D DNA origami, while similar inhibition cannot be achieved with the corresponding unfolded dsDNA scaffold (as expected). We argue that the observed behaviour of dense nucleic acid architectures naturally emerges as a result of reduction in spatial degrees of freedom near restriction sites, which can be controlled through small changes to the degree of mechanical stress (e.g. torsion) near the sites. (b) In 2D DNA origami, the action of REs on a site can be predicted from the structure of the three 16 bp-long adjacent dsDNA segments, with the site located in the central one (16 bp is the distance between two consecutive crossovers that join the dsDNA segments). Specifically, a site can be cleaved only if (c) it is located ≥4 bp from a crossover junction, and (d) near the site, each of the adjacent dsDNA segments presents a nick in one of the two strands that form the duplex.

This quantitative study reveals therefore that restriction enzyme action can be digitally controlled with the closest neighbouring 2D DNA structural pattern surrounding a restriction site. These unprecedented results also suggest how to design functional nucleic acid nanostructures, with important implications for the implementation of innovative nano-biosensor, that is briefly anticipated in the concluding section of this thesis.

Abstract (IT)

La comprensione di come gli enzimi accedano, trasformino o degradino le nanostrutture formate da un acidi nucleici è un passo essenziale per il progresso delle possibili funzionalità implementabili con le nanotecnologie di DNA .

La maggior parte dei metodi per l'analisi di acidi nucleici richiedono reazioni enzimatiche. Per esempio il sequenziamento per sintesi di molecole di DNA confinate è un approccio affermato per l'analisi dell'informazione genetica presente negli organismi viventi. Poco si sa invece sui fattori fisici che regolano le funzioni degli enzimi in sistemi in cui le molecole sono altamente confinate.

In questa tesi di dottorato, ho studiato l'attività di enzimi di restrizione (ER) di tipo II su nanostrutture di DNA bidimensionali (cioè DNA origami di forma triangolare e rettangolare) che si formano mediante l'ibridazione spontanea di molte molecole di DNA a singolo filamento (ss) e il ssDNA genomico del fago M13, lungo 7249 nt (M13mp18) che funge da impalcatura per il processo di auto-assemblaggio dello stesso DNA.

Gli ER di tipo II hanno la capacità di riconoscere specificamente un sito di legame a doppio filamento (ds)DNA (chiamati siti di restrizione) e irreversibilmente tagliare le molecole di DNA all'interno dello stesso. Attualmente, gli ER sono strumenti essenziali per la clonazione del DNA in applicazioni di bioingegneria e biotecnologia. D'altra parte, il DNA impalcatura di M13mp18 possiede naturalmente un certo numero di siti per ciascuno dei diversi ER noti. I DNA origami sono costituiti da diversi motivi strutturali che sono responsabili per il confinamento delle molecole di DNA coinvolte nella struttura, oltre a ciò, possiedono peculiari proprietà meccaniche che dipendono dalla forma del DNA origami.

Il mio lavoro di tesi consiste principalmente nell'indagine senza precedenti dell'azione di più di 10 ER di tipo II su DNA origami bidimensionali (2D). Per due enzimi in particolare (HhaI e Hin1II) abbiamo completamente mappato l'azione sito-specifica,

generando mutanti di DNA origami, che dopo il trattamento con l'enzima sono stati denaturati e la frammentazione del DNA impalcatura è stata analizzata mediante elettroforesi su gel. Con tale analisi mutazionale di DNA origami 2D abbiamo trovato che (a) le reazioni di frammentazione possono essere inibite in modo efficiente con i DNA origami 2D, mentre tale inibizione non può essere raggiunta con il corrispondente scaffold dsDNA non nanostrutturato (come previsto). Sosteniamo che il comportamento osservato nelle architetture di acido nucleico ad alto confinamento molecolare emerge naturalmente come risultato della riduzione dei gradi di libertà spaziale vicino ai siti di restrizione, che anche possono essere controllati attraverso piccole modifiche al grado di stress meccanico (ad esempio torsione) vicino ai siti. (b) Nei DNA origami 2D, l'azione dei ER su un sito può essere prevista dalla struttura dei tre segmenti di dsDNA, lunghi 16 nt, con il sito nel segmento centrale (16 nt è la distanza tra due giunzioni *crossover* consecutive che uniscono i segmenti di dsDNA). In particolare, un sito può essere scisso solo se (c) si trova ≥4 nt da un *crossover*, e (d) vicino al sito, ciascuno dei segmenti adiacenti dsDNA presenta un nick in uno dei due filamenti che lo formano.

Questo studio quantitativo rivela quindi che l'azione degli ER può essere controllata in modo digitale tramite il pattern strutturale 2D del DNA presente nell'area vicina e circostante al sito di restrizione. Questi risultati senza precedenti suggeriscono anche come progettare nanostrutture funzionali di acidi nucleici, con importanti implicazioni

Major key words:

- DNA
- Self-assembly
- Nanostructures
- Endonucleases
- Mechano-chemistry

Other key words:

- Atomic force microscopy
- Crowding
- Detection
- DNA origami design
- Enzymes
- Gel electrophoresis
- Hybridization
- Molecular modeling
- Molecular devices
- Nanomanipulation
- Nanomedicine
- Nanotechnology
- Nanoscale confinement
- Nucleases
- Nucleic acids
- Steric hindrance
- Surfaces
- Synthesis and purification

Table of content

Chapter 1 – Introduction, motivations and scope of the work

The facile self-assembly and nanomanipulation of nucleic acids hold great promise in the design of innovative, programmable materials, with applications ranging from biosensing to cellular targeting and drug delivery. Little is known, however, of the effects of confinement on biochemical reactions within such systems, in which the level of packing and crowding is similar to that of intracellular environments. In this chapter we outline novel, unexpected properties of nucleic acids that arise from nanoscale confinement, as mainly revealed by atomic force and electron microscopy, electrochemistry, fluorescence spectroscopy, and gel electrophoresis. We review selected scientific studies over the last decade that describe the novel behavior of nanoconfined nucleic acids with respect to hybridization, denaturation, conformation, stability, and enzyme accessibility. The nanoscale systems discussed include self-assembled, water-soluble, DNA or RNA nanostructures, ranging in width from a few to several tens of nm; gold nanoparticles coated with DNA monolayers; and self-assembled monolayers of DNA, from a few to several hundreds of bp in length. These studies reveal that the functionality of nucleic acid-based nanosystems is highly dependent upon the local density, molecular flexibility and network of weak interactions between adjacent molecules. These factors significantly affect steric hindrance, molecular crowding and hydration, which in turn control nucleic acid hybridization, denaturation, conformation, and enzyme accessibility. The findings discussed in this chapter demonstrate that nucleic acids function in a qualitatively different manner within nanostructured systems, and suggest that these novel properties, if better understood, can enable the development of powerful molecular tools for application in the life sciences and in particular in nanomedicine.

1.1 Effects of nanocale confinement on the functionality of nucleic acids: implications for nanomedicine – an overview

In addition to their essential biological functions, nucleic acids are promising building blocks for artificial nanostructured systems that have a potentially broad range of applications, from biology and medicine [1–4] to information technology [5–8] (see Figure 1.1). Nucleic acid-based molecular nanoengineering has experienced a rapid development, as it takes advantage of the inherent capacity of nucleic acids to self-assemble by Watson-Crick base pairing. Moreover, progress has been ably supported by the commercial availability of custom DNA and RNA molecules with a broad range of modifications, as well as diverse enzymes that can recognize, process or otherwise modify nucleic acids with high efficiency and selectivity.

The hybridization of short DNA sequences in solution allows formation of diverse structural motifs of several nanometers in width, such as double-helical and single-helical regions, sticky ends, hairpin loops, bulge loops, junctions, and crossovers [9]. With the aid of computer design, the assembly can be scaled up to form structures from a few to several hundreds of nanometers in width [9–12] (see Figure 1.2). Furthermore, relatively short single stranded (ss)DNAs can be efficiently conjugated to enzymes, proteins, antibodies and other biomolecules *via* click chemistry [3], and utilized to extend the functionality of nucleic acid arrays by linking the conjugates *via* hybridization of the complementary ssDNA strands (also termed DNA-directed immobilization) [3,13]. The DNA-probe conjugates in most cases are formed using commercially available ssDNA that is chemically modified with biotin, thiol or amine groups with standard procedures, and retain full functionality [14–17].

A novel approach to the design of water-soluble, dense DNA nanostructures (also termed “DNA origami”) was described by Rothemund in 2006, who created planar structures that are formed *via* Watson-Crick hybridization of several, short ssDNA sequences (also termed “staples”) with a long circular ssDNA molecule (the “scaffold”) [10]. The ssDNA scaffold, thermally treated in the presence of a large excess of staples, provides reproducible formation of different shapes (“DNA origami”). Since then, several studies demonstrated the functionalization of DNA origami with different probes, including aptamers, DNA, proteins, gold nanoparticles [18–21], as well as antibodies for immunodetection capability [17].

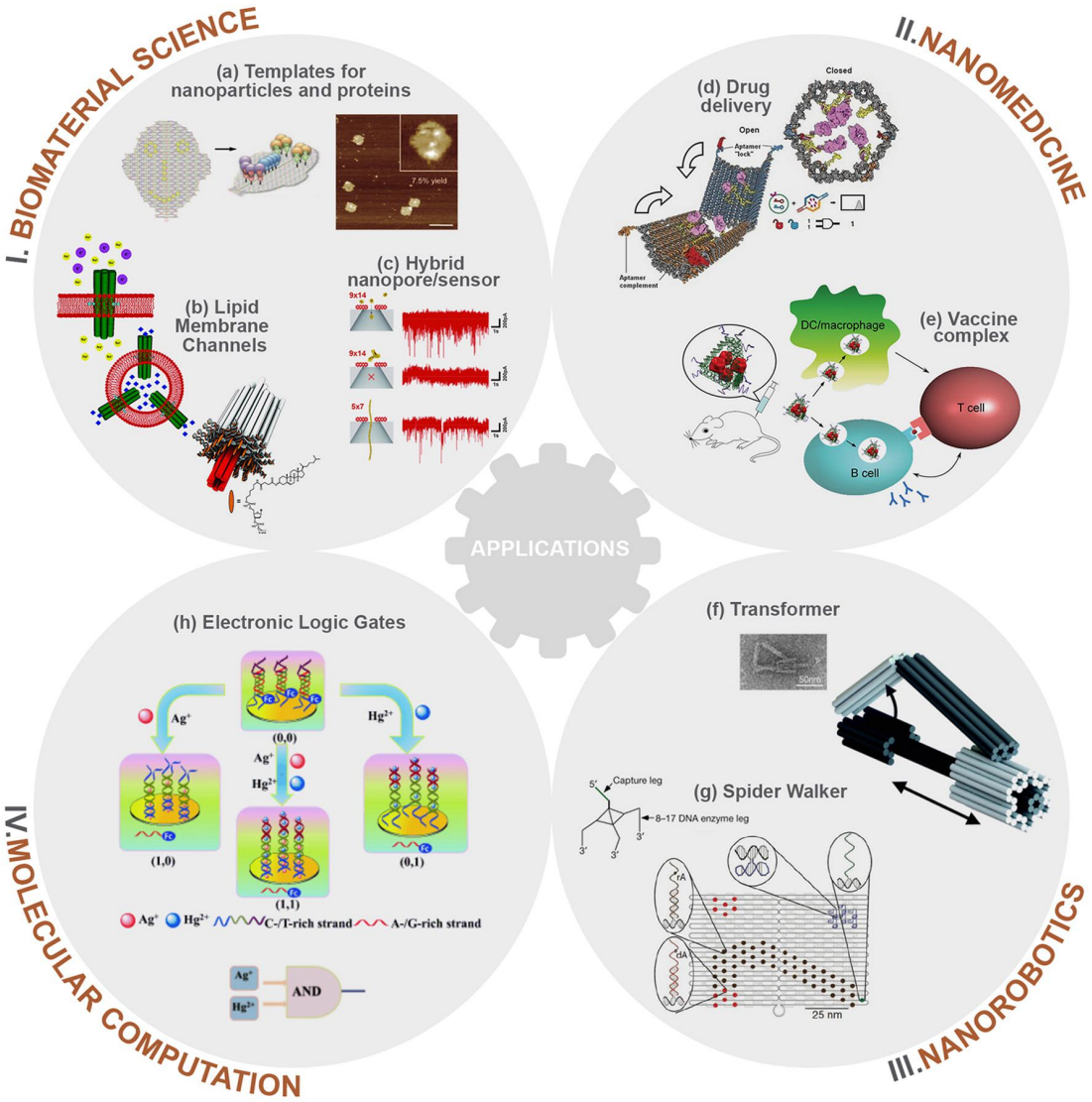

Figure 1.1. DNA nanotechnology has demonstrated that artificial nanostructured systems based on the inherent capacity of nucleic acids to self-associate have a potentially broad range of applications in several emerging research areas such as biomaterial science, nanomedicine, nanorobotics and molecular computation (adapted from [22]).

In most of these cases, the probes are linked to selected staples after their incorporation within the scaffold-staples-based nanostructure, formed during a single-step self-assembly process [14]. DNA-based nanochips can be created and used in biosensing, in particular in combination with atomic force microscopy (AFM) [2,21]. Using this approach Lindsay and co-workers produced an RNA detector, potentially applicable to analysis at the single-cell level [2] (see Figure 1.3).

DNA self-assembly allows the precise spatial positioning of fluorescent labels, generating materials with exquisite optical properties [23,24]. For example, Niemeyer and co-workers reported on the DNA-directed assembly of supramolecular Forster

Resonance Energy Transfer (FRET) systems, based on a few ssDNA staples (i.e. without a scaffold), and comprised of fluorescent proteins connected to a synthetic chromophore by a position-specific DNA linkage [25]. Tinnefeld and co-workers used a two-dimensional DNA origami as a molecular “breadboard” to allow the precise and programmable arrangement of fluorophores in a grid-like fashion by self-assembly [26,27]. They demonstrated that the 2D arrangement of fluorophores allows alternative energy-transfer pathways that is dependent upon incorporation of a “jumper” dye at specific positions [27].

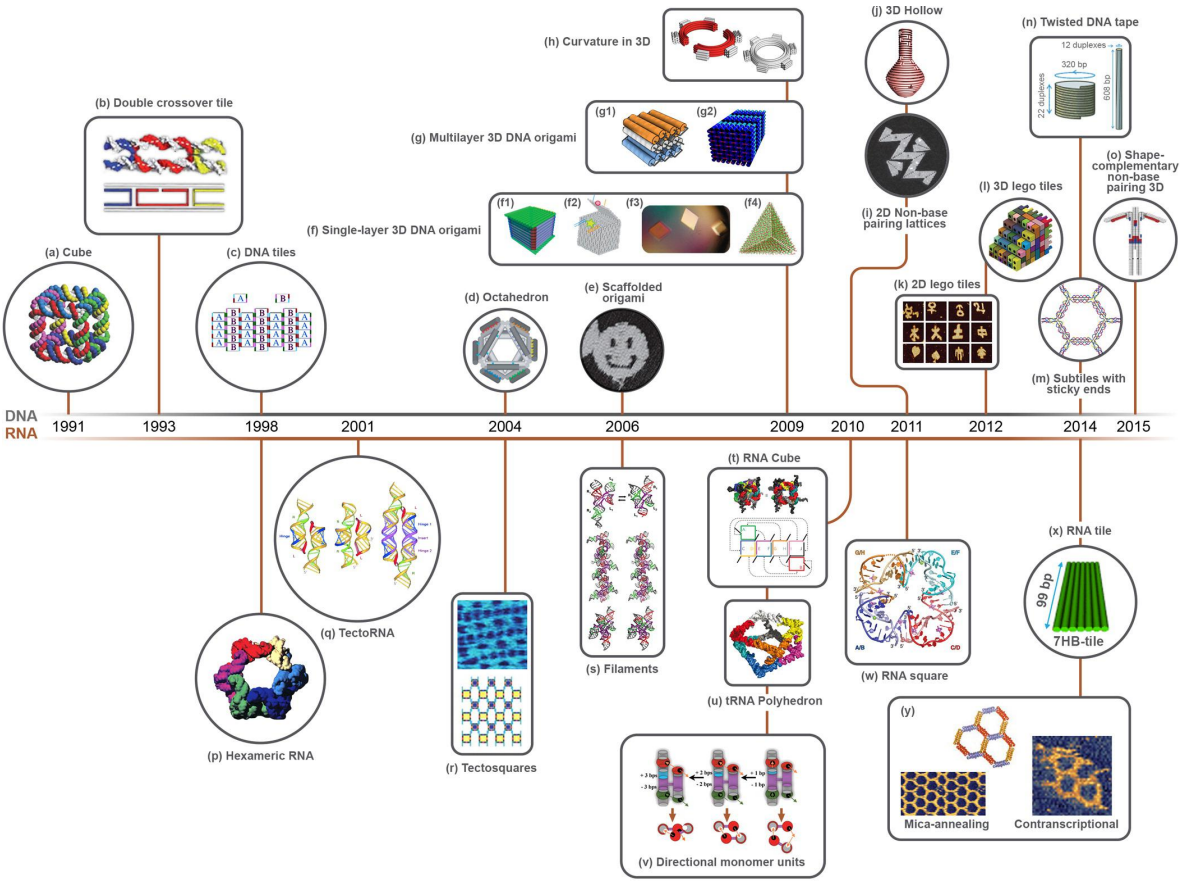

Figure 1.2. Timeline of the major achievements in DNA nanotechnology. With the aid of computer design, the assembly can be scaled up to form structures from a few to several hundreds of nanometers in width (adapted from reference [22]).

Nucleic acid self-assembly opens up the prospect of nanomachines that are able to control their shapes and perform operations in a programmable manner [28,29]. This has provided the basis for development of novel carriers for the delivery and release of drugs in a cell-specific manner [17,30–33]. Such highly functional nanostructures are prime candidates for developing innovative nanomachines, composed of biocompatible materials, and capable of delivering and releasing nucleic acid-based drugs.

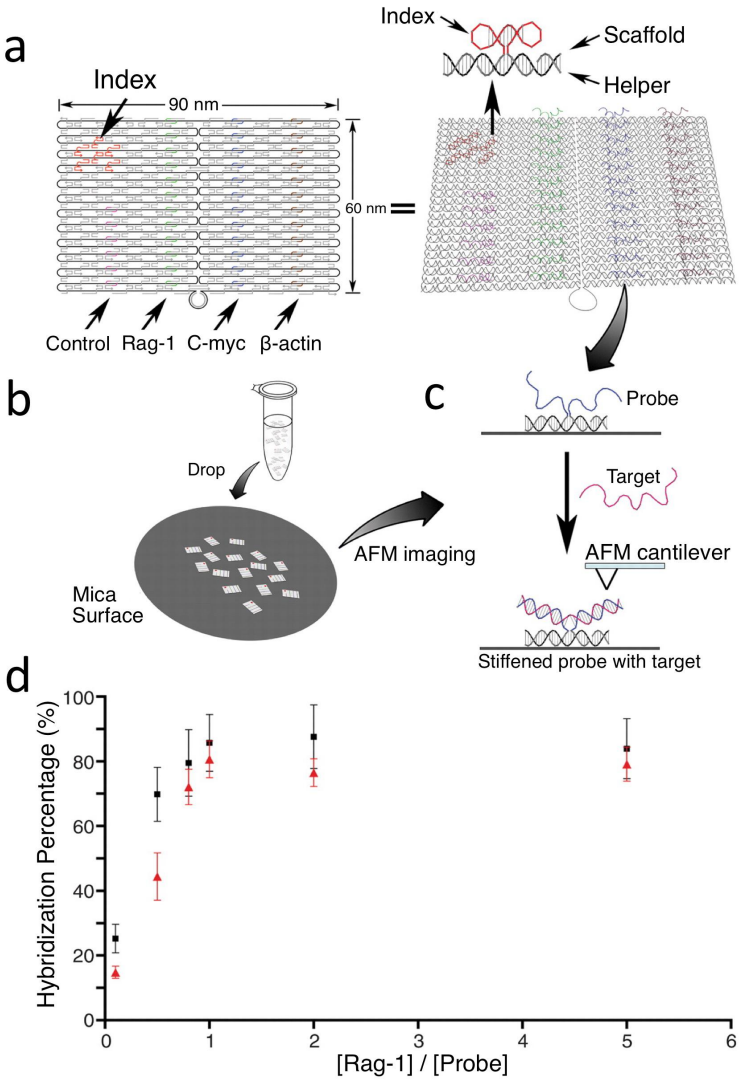

Figure 1.3. DNA origami as nanoarrays for biodetection. (**a**) Schematic representation of DNA origami structure as a DNA-based nanochip for RNA detection. The strands that protrude from the structure core and correspond to three different target probes (Rag-1, C-myc, β-actin) and a control probe. Six dumbbell-shaped bulge loops are used as index spots. Scaffold and unmodified staple strands are grey. (**b**) Scheme for using the DNA-based nanochip to detect RNA. The DNA origami with specific probe is self-assembled and incubated with the target in solution, then placed on a mica surface for AFM imaging. (**c**) Probe design and detection mechanism. Two adjacent staple strands extend from the core structure of the DNA origami, each of which have a half of the probe sequence, respectively. The single-stranded probes are not visible by AFM, due to their flexibility. Following incubation with the target, the half-probes hybridize with the target, forming stiffer double helical structures detectable by AFM. (**d**) Titration of DNA origami probes against the target concentration (Rag-1). Here is shown the plot of hybridization efficiency versus the [target/probe] ratio. The detection is limited only by the concentration of the DNA origami probe: 10 nM (squares) and 200 pM (triangles). Each error bar is the SD calculated from fifty analyzed DNA origami probes. Adapted and reprinted with permission from [2]. Copyright © (2008) American Association for Advancement of the Science.

Obviously, concerns about biostability [34–36] and biocompatibility must be addressed, as nucleic acid-based nanotechnology is still in its infancy [33,37,38]. For instance, Meldrum, Yan and co-workers demonstrated that DNA origami displays enhanced resistance to enzymatic digestion in complex biological mixtures, including cell lysates, and applying a range of incubation times, temperatures and concentrations with respect to the unfolded scaffolds [37] (see Figure 1.4). The authors explain that the enhanced resistance is due to the high charge density and molecular rigidity of the assemblies, which hinders nuclease access and engagement. Very recently, DNA assembly was used to design biocompatible carriers that could deliver a siRNA molecule into a xenografted tumour, with a nearly four-fold increase in siRNA half-life [39]. Also, DNA origami containing intercalated doxorubicin molecules allowed increased doxorubicin internalization in cultured cells, and a strong reversal of drug resistance in doxorubicin resistant cancer cells [33].

We believe that the application of nucleic acid-based nanodevices will greatly benefit from a full understanding of the factors that influence nucleic acid function, reflecting the unique nanoscale environment. Little is known about the effects of crowding, steric hindrance, surface interactions, and molecular order/disorder, which could create unanticipated behaviors, but which also may be exploited to achieve novel functionalities [40–43]. In living cells, nuclear crowding and DNA packing are crucial in the cell cycle and cell differentiation. *In vitro* studies demonstrated that crowding shifts binding reactions towards bound states because of the excluded volume induced by co-solutes [44]. This was confirmed in living cells by Bancaud *et al.* [44] who described crowding as a driving force to maintain functional nuclear compartments at a low cellular energy cost, i.e. without requiring membranes or other additional structural boundaries be involved. DNA packaging is also essential in viral reproductive cycles [45]. Bustamante and coworkers studied viral genome packaging, as catalyzed by the DNA packaging motor of *Bacillus subtilis* phage ϕ29, and showed that it is able to generate the high force needed to pack the 6.6-μm long (19.3 kbp), double-stranded DNA into a 42×54 nm^2 capsid in about 5.5 minutes, reaching near-crystalline density. Also, they demonstrated that the ϕ29 molecular motor is among the strongest known, as it is able to generate a force of 57 pN during DNA packaging and eventually produce an intra-capsid pressure of about 60 atm [46,47]. Such a high pressure likely enables efficient DNA injection into the host cell [45].

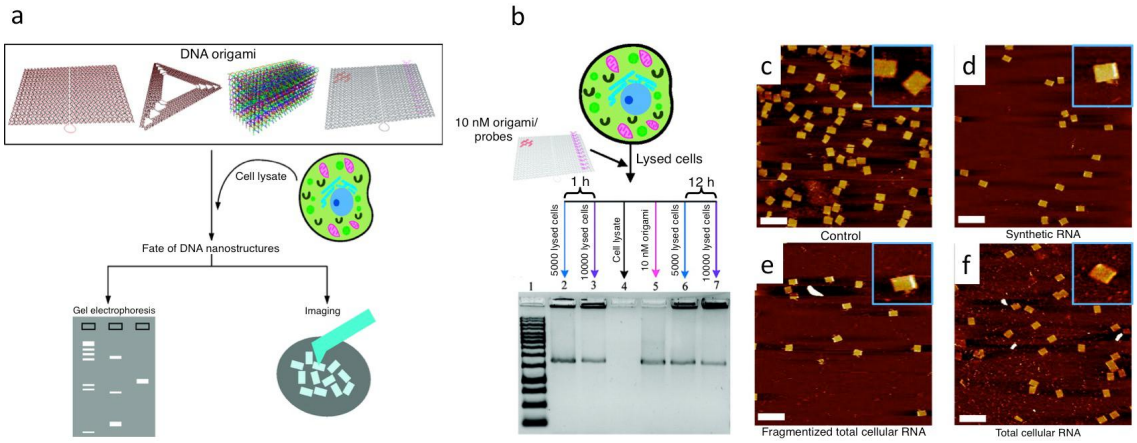

Figure 1.4. Stability of DNA origami nanoarrays in cell lysates. (**a**) Different DNA origami nanostructures are incubated in cell lysates, then analyzed by gel electrophoresis and by AFM to test their stabilities in complex biological mixtures. (**b**) A rectangular DNA origami nanostructure, bearing on one face 20 copies of 40-nucleotide, single-stranded DNA probe complementary to a region of human β-actin gene, is combined with a HeLa cell lysate, then analyzed by agarose gel electrophoresis. The results indicate that the nanostructures are substantially intact after incubation in lysates from 5×10^3 or 10^4 cells for 1h (lanes 2, and 3 respectively), and even after 12h (lanes 5 and 6, respectively). Controls are shown in lane 4 (cell lysate only), and lane 5 (10 nM DNA origami nanostructure). (**c-f**) Topographic AFM imaging allows detection of hybridization of probe-bearing DNA origami nanostructure as a localized height increase on a mica surface, after recovery from the gel. (c) Outcome of incubation of a control DNA origami nanostructure with a synthetic RNA target. The topographic micrographs (scale bar, 300 nm) in (d) (e), and (f) reveal the topographic change following successful hybridization with synthetic, fragmentized total cellular, and total cellular RNA targets, respectively (top-right insets are 250×250 nm^2). A "brighter is higher" grey scale is used for the AFM topographic micrograph. Adapted and reprinted with permission from [37]. Copyright © (2011) American Chemical Society.

In this chapter, that was adapted from a review I co-authored and that was published in Current Medical Chemistry (2013) with title "Effects of nanoscale confinement on the functionality of nucleic acids: implications for nanomedicine, we examine recent studies that address the novel functionality of nucleic acids in highly dense, self-assembled nanostructures. The scope is to address a few cases where the analysis of effects of confinement and crowding on biomolecular function have provided new insight on molecular processes, and how they may aid the development of future nanobiotechnologies.

1.2 Nucleic acid hybridization and dissociation in nanoscale-confined systems

DNA self-assembly permits the generation of highly dense nanostructures comprised of oligonucleotides exhibiting controlled molecular orientations. The close-packing of the molecules in this environment can strongly influence functionality. Understanding the processes associated with the subsequent addition or removal of molecular elements is a prerequisite for ensuring optimal function of the nanostructures and their interaction with external agents. In a recent study, Pinheiro *et al.* [48] used a water-soluble DNA nanostructure, based on 20-nt single-stranded DNA molecules, to analyze the effect of steric crowding on DNA hybridization kinetics. The DNA nanostructure consisted of six parallel double helices, joined by fourteen single-stranded oligonucleotides that cross over from one helix to an adjacent helix, thus providing a planar, rectangular-shaped tile (16 nm long and 14 nm wide) (See Figure 1.5). The six-helix tile has 20-nucleotide-long extensions that generate adjacent single-stranded overhangs. One of the six overhangs is the target probe (TP), while the other overhangs are off-target probes (OTP). The target and off-target strands are fully complementary to target- and off-target probes, respectively. For all experiments, only one of the selected helices displayed the TP overhang, while the remaining five helices were either blunt-ended or displayed the OTP overhang. This design provided precise control of the number of strands surrounding the hybridization site. In particular, the steric factors that were evaluated included (i) the position of the target probe relative to the tile; (ii) the presence/absence of DNA surrounding the hybridization site; and (iii) the formation of a double-helical secondary structure between the target probe and other components of the tile.

The kinetics of hybridization of a target to the six-helix tile was studied by means of real-time fluorescence spectroscopy. For each TP, a reporter fluorophore (5-carboxyfluorescein, FAM) was introduced at the interface between the core and the single-stranded TP. The authors found that duplex formation at the TP overhang caused enhanced FAM fluorescence. The proposed mechanism involves the newly formed double helix displacing the dye from its intercalated (stacked) state within the core of the tile structure. In fact, dye intercalation is likely to enhance photo-induced electron transfer, resulting in a low fluorescence quantum yield.

More efficient hybridization occurs when the TP is surrounded by blunt-end chains, or when located at the outermost position (i.e. adjacent to only a single OTP).

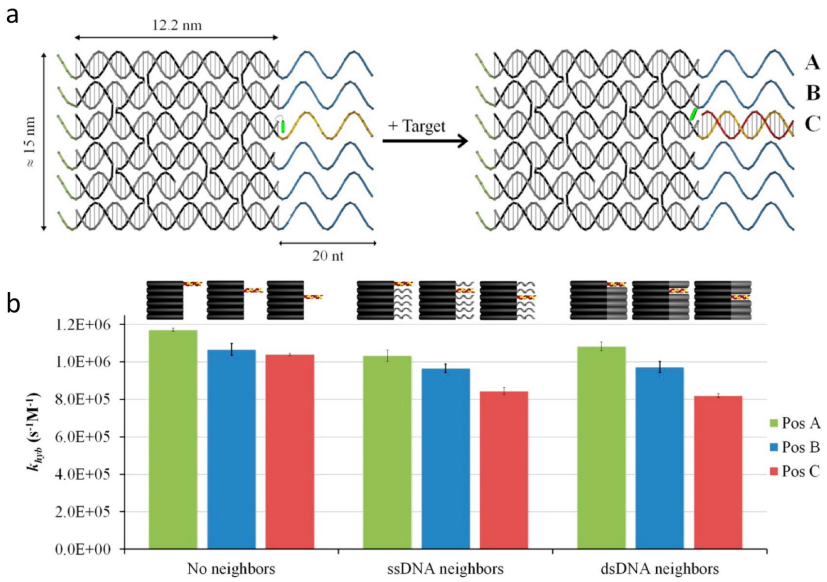

Figure 1.5. The effect of steric crowding on the kinetics of DNA hybridization within a water-soluble DNA nanostructure. **(a)** DNA nanostructure used to analyze the effect of steric crowding on DNA hybridization kinetics. The structure is a rectangular platform consisting of six parallel helices joined by fourteen single-stranded oligonucleotides, thus providing a planar tile, 16 nm long and 14 nm wide. The design provides three unique positions (A, B, C) with intrinsically different characteristics, that can be blunt ends, or functionalized with single- or double-stranded DNA. In the figure all helices are functionalized with a 20 nt extension of single-stranded DNA but only one (C) is as probe for a specific ssDNA sequence in solution. By positioning a fluorophore (5-carboxyfluorescein, FAM) at the edge of the tile in one of the three positions, it is possible to follow hybridization by time-correlated, single photon counting. In the absence of the target probe, the FAM is retained inside the core structure, where interaction with DNA at the base of the tail reduces the fluorescence decay time. The newly formed double helix displaces the dye from its intercalated (stacked) state, thereby enhancing the fluorescent signal. **(b)** By real-time fluorescence microscopy the reaction rate was evaluated as a function of hybridization rate constant for nine different crowding conditions, in which the target probe is in the A, B, or C position, and flanked by dsDNA, ssDNA or blunt ends. More efficient hybridization occurs when the TP is surrounded by blunt ends ("No neighbors" condition), or is located at the outermost position (Pos A). Furthermore, when the TP is located at inner positions (Pos B, Pos C) the hybridization kinetics do not significantly vary between "ssDNA neighbors" or "dsDNA neighbors" condition. Adapted and reprinted with permission from [48]. Copyright © 2012 American Chemical Society.

Furthermore, when the TP is located at inner positions, the hybridization kinetics are largely insensitive to whether the flanking OTPS are single- or double-stranded (see Figure 1.5). Additional experiments using a TP partially hybridized to an adjacent OTP showed that the hybridization rate dramatically decreases when the target probe

bends, rendering its end less accessible from solution. The authors suggest that the observed differences in kinetics are mainly due to differences in the frequency of productive collisions between target and probe, and that the slower hybridization kinetics therefore reflects a less efficient nucleation step. However, following nucleation, the spatial confinement does not significantly inhibit strand alignment and "zippering" of the remaining nucleotides to create the duplex structure [48]. In summary, the work of Pinheiro *et al.* has probed the role of molecular accessibility in highly dense DNA tiles using an unprecedented, quantitative approach.

Bombelli *et al.* grafted hexagonal DNA nanostructures, comprised of short DNA sequences, on phospholipid membranes [49]. They showed that changing the grafting density could affect hybridization kinetics. Hybridization on phospholipid membranes grafted at low density was faster than in bulk, but was slower on densely grafted membranes, due to molecular crowding on the membranes.

Other studies have addressed the effect of crowding on DNA hybridization on self-assembled monolayers on gold surfaces. Ricci and co-workers investigated the effect of molecular crowding on the response of an electrochemical DNA sensor [50]. They used an E-DNA probe, which is an electrochemical equivalent of a molecular beacon, for detecting the hybridization of oligonucleotides on surfaces. The E-DNA sensor was formed by a self-assembled monolayer (SAM) of a redox-modified, 27-nt stem-loop DNA that also carried a thiol, allowing covalent attachment to a gold surface that also functioned as the interrogating electrode. The electrode measures the faradic current that depends on the density and conformation of the stem-loop probe. The current is large when the stem-loop holds the redox moiety in close proximity to the electrode, but decreases upon target hybridization, which opens up the stem and moves the redox moiety away from the electrode surface. Because E-DNA signaling is dependent upon conformational changes in the stem-loop structure, it is also likely to be sensitive to the nature of the molecular packing on the electrode surface. By varying the concentration of the E-DNA probe during SAM formation, the authors were able to vary the density from 3.9×10^{10} to 2.1×10^{12} molecules/cm^2. The authors investigated the faradic suppression upon hybridization as a function of probe density, and observed non–monotonic behavior. When the E-DNA SAM density is $<10^{12}$ molecules/cm^2, signal suppression decreases with a substantially monotonic behavior. This is consistent with previous observations of ssDNA SAM hybridization, which noted that hybridization efficiency is inversely proportional to the probe density on the capturing surface [51–53].

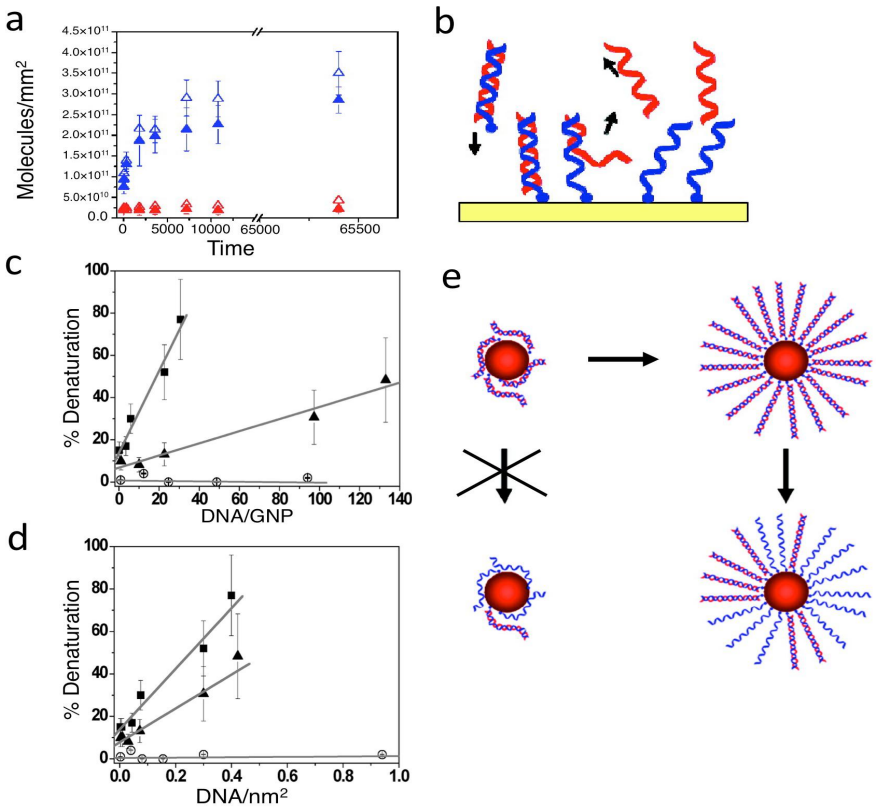

Figure 1.6. Packing-induced DNA denaturation within self-assembled monolayers. (**a**) Density of radiolabeled, thiolated DNA molecules adsorbed (from a 10 μM solution) on a gold surface as a function of adsorption time. Molecules in solution are either thiol-ssDNA or thiol-dsDNA. Solid triangles quantify the surface density (in molecules/mm^2) of radiolabelled, thiolated strands comprised in a preformed duplex, while open triangles quantify the surface density of, radiolabelled, thiolated, single-stranded molecules. The solid triangles below 5.0×10^{10} molecules/mm^2 quantify the surface density of radiolabeled, non-thiolated strands comprised of a preformed duplex, while the open triangles below 5.0×10^{10} molecules/mm^2 quantify the surface density of radiolabeled, non-thiolated strands (from a 10 μM solution) incorporated in a preformed ssDNA monolayer after *in situ* overnight hybridization. The data demonstrate that adsorbed duplexes undergo denaturation, likely due to close molecular packing. (**b**) Schematics of packing-induced denaturation. (**c**) Duplex denaturation on gold nanoparticles (GNP) as a function of the molar ratio. Solid squares quantify the denaturation of a 26 bp thio-DNAs on GNP with a 5 nm diameter, while solid triangles (relative to 26 bp thio-DNAs) and open circles (relative to 50 bp thio-DNAs) describe the phenomenon with GNP of 10 nm diameter. (**d**) Duplex denaturation on GNP as a function of DNA density, relative to the data shown in (a). The results demonstrate that denaturation is minimal for 50 bp thio-DNAs, and exclusively depends on surface density as schematically shown in (**e**). Denaturation is < 20% for DNA surface densities < 1×10^{13} molecules/cm^2 and reaches 80% for densities > 4×10^{13} molecules/cm^2. (**a-b**) Adapted and reprinted with permission from [54]. Copyright © (2008) American Chemical Society. (**c-e**) Adapted and reprinted with permission from [55]. Copyright © (2010) American Chemical Society.

For densities higher than 10^{12} molecules/cm^2 (i.e. for mean probe-to-probe spatial separations less than 10 nm) Ricci and co-workers found the faradic suppression increases dramatically, reaching a saturation value of about 70% of the initial faradic current [50]. Under these conditions, however, the measured equilibration time is ~ 40 min, which is 2- to 8-fold higher than the equilibration times measured with medium and low E-DNA densities, respectively.

This result is consistent with the findings of Pinheiro and co-workers (see above)[48], wherein the bending of the E-DNA probe molecule leads to a reduction in nucleation capability of the initial probe-target interaction. The same study [50] also showed that by varying the AC voltage applied to the electrode that supports the E-DNA SAM, the surface-bound probes oscillate within a self-assembled monolayer. The authors explain that the largest signal suppression observed for high-density sensors is presumably due to the fact that the densely packed probe layer prevents collisions after target hybridization, with the latter result in turn suggesting that densely-packed molecules spend more time in a vertical conformation. The above-described behavior of hybridization-induced suppression of the faradic current at low and medium E-DNA surface densities is largely consistent with independent observations that densely-packed DNA SAMs exhibit a limited hybridization capability [51,53], which reaches >50% in ssDNA SAMs with densities ~ 2-3 ×10^{12} molecules/cm^2.

While it is likely that the surface collision rate decreases for hybridized probes, since hybridization efficiency depends on probe density in a monotonic manner, it is not clear why the measured faradic current suppression reaches 70% in a near step-wise fashion. These observations suggest that for highly dense E-DNA SAMs, faradic current suppression reflects the intrinsic conformational structure of the E-DNA probe as a function of surface density.

This interpretation is supported by the work of Peled and co-workers [54,55], who observed and quantified the crowding-induced dissociation of short (15 or 26 bp) thiolated DNA duplexes on gold surfaces. The authors also investigated DNA self-assembly on flat gold surfaces [54] and on gold nanoparticles [55] (see Figure 1.6). The change in density of surface-bound ssDNA molecules involved in the self-assembly process was monitored using radiolabeled ssDNA molecules, followed by phosphorimaging. In contrast to other widely used approaches such as spectroscopy and electrochemistry, which are indirect and require nonroutine interpretation, the approach of Peled and co-workers allows direct measurement of the absolute density of surface-bound DNA strands. The use of radiolabeled, thiolated ssDNA allowed assessment of surface crowding, while, in parallel, the use of radiolabeled

complementary ssDNA allowed monitoring of duplex denaturation. In a second study, the same group measured duplex dissociation as a function of DNA density on gold nanoparticles [55]. The use of gold nanoparticles served to avoid nonhomogeneity in monolayer formation, which would occur on the flat surfaces used in the first study. As a consequence, the averaged molecular density may not accurately reflect the microscopic environment of individual DNA molecules. The results of the two studies, however, are consistent with each other. The denaturation of dsDNA on the surface is dependent upon formation of a dense layer (>10^{13} molecules/cm^2), as it permits more thiolated DNA molecules to adsorb and additional gold-thiol bonds to be formed in the vacant spaces created upon double-strand dissociation (see Figure 1.6). Peled and coworkers proposed that the area occupied by ssDNA on the surface is smaller than that of a dsDNA, possibly due to the higher flexibility of the ssDNA oligomers, compared with the rigid rod structure of the dsDNAs. In addition, ssDNA oligomers may undergo stretching and extension due to steric and electrostatic repulsion in highly dense monolayers. The results show that, for 15 bp and 26 bp dsDNAs on flat surfaces, or 26 bp dsDNA on gold nanoparticles of differing diameter (5 and 10 nm), DNA duplex denaturation is linearly related to thiol-DNA density on the gold surface, and for the gold nanoparticles is shown to reach 80% at maximum density (~ 4×10^{13} molecules/cm^2) (see Figure 1.6). Denaturation of the 50 bp DNA does not occur to a significant extent (see Figure 1.6). The authors explain that, according to their model, the gain in energy from formation of an additional thiol-gold bond is insufficient to compensate for the energy required to separate the 50 nt strands. The authors also argue that the results exclude the possibility that duplex denaturation is promoted by favorable interactions between the surface and the ssDNA bases. If this were so, the resulting denaturation would be favored at low densities where, according to the mechanism, the adsorption energy between the substrate and dissociated ssDNA would more easily compensate for the energy required for duplex dissociation [56].

The range of DNA densities measured in the experiments of Peled and coworkers [54] (1-4 ×10^{13} molecules/cm^2) is ~ 10-fold higher than the range measured by Ricci and coworkers, even though the experimental conditions used to form the DNA monolayers were very similar. Such differences may be due to the different conformations (ssDNA vs. stem-loop) of the DNA probes used by the two groups, and/or the different methodologies followed for determining DNA density. Crowding-induced denaturation, however, may occur even at densities < 10^{13} molecules/cm^2 for shorter duplexes [54]. For instance, in the work of Ricci et al. [50], a 5 bp stem unzips upon hybridization to form a ≥27 bp duplex. In such conditions, the stepwise change in

faradic suppression may be due to several stems per unit area changing their conformation so as to favor hybridization with fewer, much longer complementary strands. The model of Peled and coworkers also suggests that the stretching of the surface-bound ssDNA within a monolayer can facilitate access of additional DNA molecules to the monolayer.

Recent experiments performed by Scoles and coworkers investigated the functionality of nucleic acids in spatially-confined, self-assembled monolayers created by an AFM-based nanomanipulation technique termed nanografting [57–65]. Originally described by Liu and co-workers in 1997 [66–68], nanografting can create, with unprecedented spatial control, patterns that consist of a homogeneous monolayer phase on flat gold (111) surfaces that are covered by a protective, self-assembled monolayer (SAM) [69–71]. Nanografting is performed by an AFM tip that is scanned at a relatively high load (a few to several tens of nN) over the desired area in a solution containing the thiolated nucleic acid (see Figure 1.7). Due to tip-induced mechanical perturbations, the preadsorbed thiol molecules in the protective SAM undergo local exchange with the thiolated molecules in solution. Patterns can be generated with different shapes and lateral widths, ranging between a few tens of nm to several microns. After resetting the value of the perpendicular applied force to ~ 1 nN or less, the same AFM tip can be used for imaging the newly formed structures.

Our group conducted side-by-side AFM topographic imaging of ssDNA patches nanografted within an oligoethylene-glycol-terminated alkylthiol (TOEG) SAM, and side-by-side AFM topographic imaging of nanografted patches of TOEG within a ssDNA SAM [57]. In this way they were able to show that the topographic height of a nanografted patch of a highly dense ssDNA monolayer is greater than that of the corresponding monolayer obtained by self-assembly. The authors explain that, at the same ssDNA concentration, ssDNA molecules are incorporated in a nanografted patch more efficiently than in the corresponding, spontaneously formed self-assembled monolayer. Thus, in the nanopatch, ssDNAs acquire a mostly stretched conformation as they weakly interact with the gold surface.

The Authors also demonstrated that the hybridization behavior and efficiency in nanografted patches is different than that for ssDNA SAMs. An 18 nt thiolated ssDNA and the corresponding 18 bp thiolated duplex were nanografted in the form of a-few-hundred-nm-wide, square patches, and the mechanical resistance of the inherent molecules was measured by side-by-side topographic imaging of the patches, using different forces applied by the contacting AFM tip (see Figure 1.8). The mechanical resistance on patches obtained using ssDNA was significantly lower than that of

patches created using dsDNA (see Figure 1.8). After *in situ* hybridization, the mechanical resistance of the ssDNA patch increased homogenously within the patch area, and the height *vs.* applied force curve substantially matched the curve measured on the dsDNA patch (see Figure 1.8). As there are only a small number of molecules (~ 10) directly under the contact area of the AFM tip, the authors concluded that the observed change in mechanical resistance reflected the formation of a significant number of duplexes. Specifically, the data demonstrate that, at high density, the maximum amount of duplexes in a nanografted patch is approximately 50% (see Figure 1.8). The results of this study suggest that denaturation is less pronounced in a nanopatch than in the self-assembled monolayer studied by Peled and co-workers. The AFM study provided a maximum density estimation for nanopatches of about ~ 10^{13} molecules/cm^2.

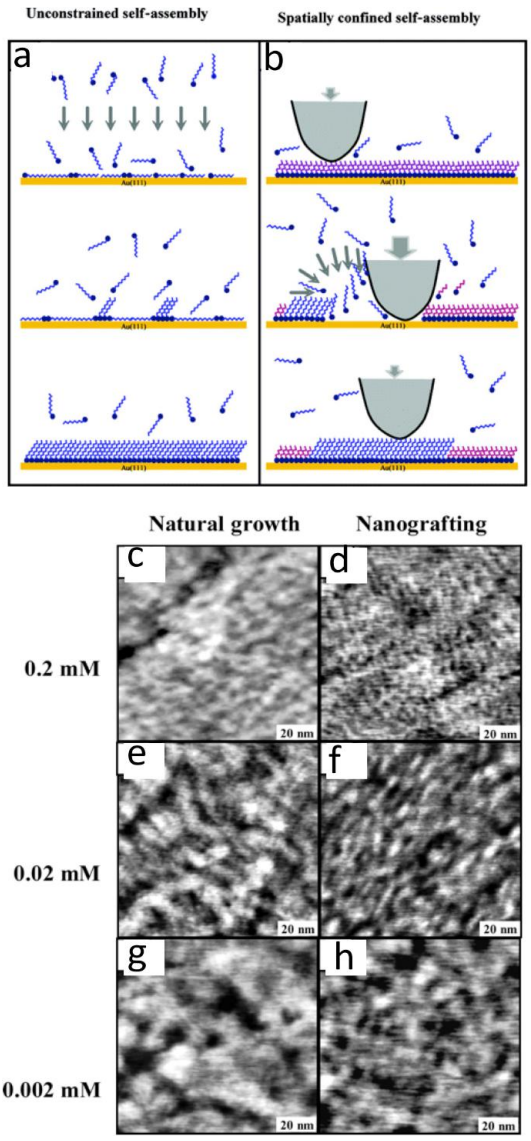

Figure 1.7. Methods of assembly of surface monolayers of nucleic acids. The scheme in (**a**) depicts the unconstrained self-assembly of alkylthiols on a flat gold surface, while the one in (**b**) depicts the AFM tip-assisted, nanolithographic process termed nanografting, which allows formation of laterally-constrained monolayer patches. Here, a highly loading AFM tip (applied force ~ 100 nN) displaces molecules from the surface, that are immediately replaced by the thiol-nucleic acids in solution. (**c-i**) AFM topographic micrographs (100×100 nm^2) of mixed monolayers of SH–$(CH_2)_{17}$–CH_3 (C18) and SH–$(CH_2)_9$–CH_3 (C10), formed either by self-assembly (**c, e,** and **h**) or by nanografting (**d, f,** and **i**), and using C18:C10 = 1:1 solutions at different concentrations: 0.2 mM (c, d); 0.02mM (e, f); 0.002 mM (g, i). At lower thiol concentrations, self-assembled monolayers form thermodynamically favored products, i.e., larger domains. Nanografted patches are less affected by the thiol concentration, and the resulting mixed monolayer is more homogeneous than the corresponding self-assembled monolayer. A "brighter is higher" grey scale is used for the AFM topographic micrograph. Reprinted with permission from [65]. Copyright © (2006) American Chemical Society.

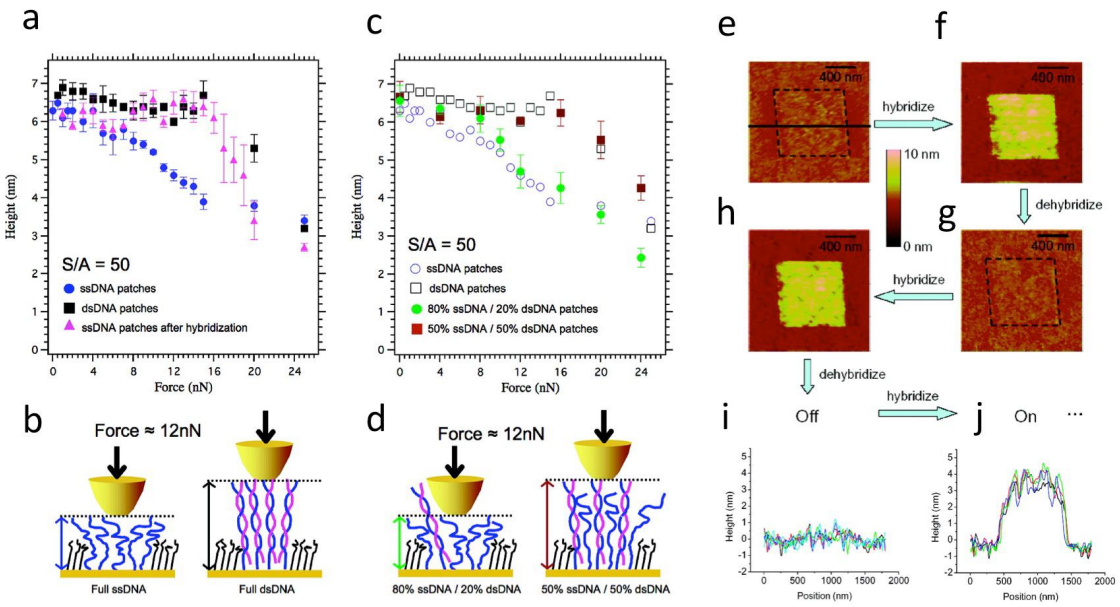

Figure 1.8. Properties of nanografted DNA surface matrices as revealed by atomic force microscopy. (**a**) Compressibility curves, generated by topographic AFM imaging of highly-dense, nanografted DNA patches as a function of the AFM-applied load. The mechanical resistance of a DNA patch significantly changes before (solid circles) and after (solid triangles) *in situ* hybridization. The latter result is similar to the curve obtained with patches of nanografted, preformed dsDNA molecules (black squares). The scheme in (**b**) depicts the result reported in panel (a) for ssDNA and dsDNA nanografted monolayers patches, under an applied force of 12 nN. (**c**) Compressibility curves obtained from high-density patches with mixed composition: ssDNA:dsDNA = 4:1 (solid circles) and 1:1 (solid squares). The mechanical resistance of a patch comprised of ~ 50% dsDNA molecules is similar to that of a patch following *in situ* hybridization. The scheme in (**d**) depicts the result shown in panel (a) for mixed DNA patches, under an applied force of 12 nN. (**e**) An AFM topographic micrograph in which a "nearly invisible" nanografted ssDNA patch is surrounded by a SAM of the same molecule. (**f**) Following hybridization, the height of the nanografted patch is greater than that of the background SAM. The result suggests that ssDNA molecules within the nanografted patch behave differently than those within the SAM, even though the two ssDNA phases are indistinguishable by AFM topographic imaging. An explanation is that a better packing order in the grafted patch provides greater hybridization efficiency. (**g**) By lowering the ionic strength of the solution, surface-bound duplexes can dissociate, and the resulting image is similar to the one in (e). The cycle can be repeated several times (**h-j**). (**i-j**) are line profiles across the pattern. A "brighter is higher" grey scale is used for the AFM topographic micrograph. (**a-d**) Reprinted from [57]. Copyright © (2008) American Chemical Society. (**e-j**) Reprinted from [59]. Copyright © (2012) American Chemical Society.

A subsequent study by Bosco and coworkers [72] combined AFM nanografting and compressibility experiments with coarse-grain numerical simulations in order to establish a density vs. compressibility dependence for ssDNA and dsDNA, which, in turn, was used to account for DNA reactivity within nanografted patches. The study confirmed as well as added additional insight on previous observations, and also provided for the first time calibrated AFM-based and numerical tools for characterizing DNA nanostructures that are too small for accurate examination using optical and spectroscopic methods. The AFM studies suggest that the combing action of the AFM tip during nanografting provides ssDNA matrices with a homogeneous spatial distribution. Moreover, the level of "crosstalk" between adjacent DNA molecules is reduced, compared to spontaneously formed self-assembled monolayers. In the latter case, the structural mobility of ssDNA molecules is reduced, and there is perhaps a greater interaction with the surface.

A recent study by Josephs and coworkers [[73]] examined the level of crowding and homogeneity of DNA monolayers using high-resolution AFM microscopy. In particular, they performed single-molecule-imaging of DNA probes tethered by a hexanethiol linker ($HS–(CH_2)_6–$, also utilized in most of the aforementioned monolayer-related studies) within self-assembled monolayers obtained by alternative methods, and using freshly prepared, ultra-flat gold surfaces. In the first method (also termed Insertion method), the gold surface is initially passivated by a 6-mercaptohexanol ($HS–(CH_2)_6–OH$; MCH) monolayer, then exposed to thiolated DNA, which preferentially attaches to the surface at defect sites in the preformed MCH monolayer. In the second method (also termed "Backfilling," and utilized in most of the aforementioned monolayer-related studies), the gold surface is first exposed to thiolated DNA, then immersed in a solution of MCH, which lifts the DNA off the surface [[74,75]]. The achieved single-molecule sensitivity allowed the investigators to apply spatial statistics to the study of the DNA monolayer, and provided direct evidence that the DNA molecules on the surface, as prepared by backfilling, have a tendency to form aggregates. By contrast, the insertion method yields surfaces that are more uniform at the molecular scale. Although Josephs and coworkers focused on low-density DNA monolayers on gold surfaces, their findings also provided a rationale for the power of nanografting (which is, in effect, an AFM tip-induced "Insertion" process [[68,69]]) as it permits the formation of highly dense monolayer patches in which the spatial distribution of thiolated DNA molecules is more homogenous than that of DNA SAMs, formed by a process similar to "backfilling" (see Figure 1.7). Furthermore, this effect seems to be independent of the presence of a backfilling alkylthiol SAM surrounding the thiolated DNA. Our group [[59]] found that

highly dense SAMs of a thiol ssDNA on a gold surface, and nanografted patches of the same molecule share the same AFM-measured height in the absence of MCH or other backfilling thiol, rendering the patch practically invisible by AFM topographic imaging. Surprisingly, the hybridization-induced height change on a nanopatch is ~ 4-fold greater than that of the corresponding SAM. The height change is reversible upon dehybridization, and the hybridization can be repeated to provide the same topographic change, thus indicating that the structural distinction of the patch and the SAM is conserved (Figure 1.8).

1.3. Enzymatic reactions within nanoscale-confined systems

Enzymatic reactions of surface-attached nucleic acids have been extensively investigated and applied to biosensing and biotechnology [76–79]. For instance, the enzymatic processing of DNA *in situ* has been utilized for cloning and sequencing on solid supports with unprecedented high-throughput capability [76]. Such applications typically require a reaction environment that is engineered to provide maximal reaction efficiency, allowing enzymes to process their substrates in bulk, while avoiding undesirable crowding and steric hindrance-induced side effects [80–82].

Restriction endonucleases are a class of enzymes including thousands of different molecules that are found in prokaryotes. Due to their inherent capacity of digesting DNA, these enzymes contribute to the bacterial defensive mechanisms against foreign genetic elements (e.g. bacteriophages) [83]. The restriction enzymes belong to the restriction and modification system that comprise methyltransferase and endonuclease enzymatic activity [84].

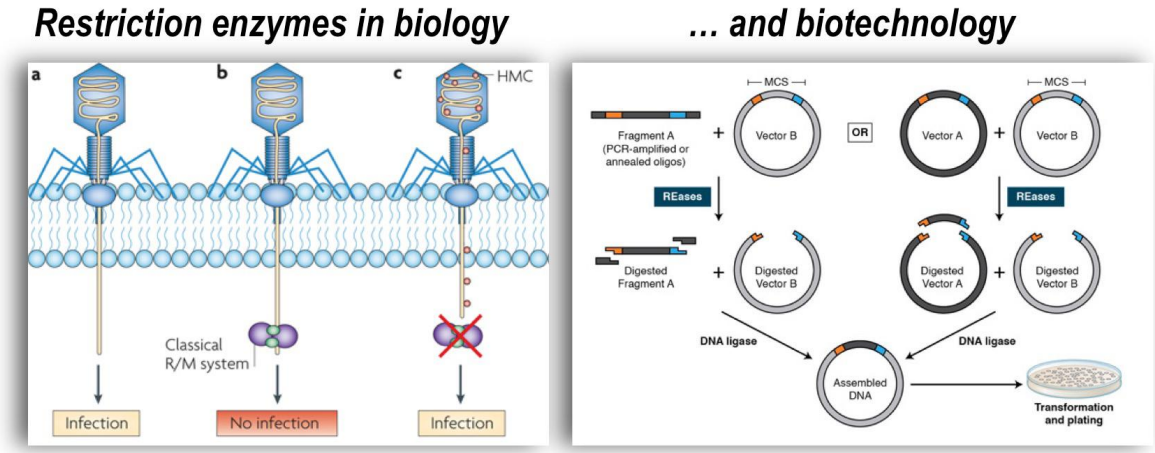

Figure 1.9. Restriction enzymes are major contributors to the bacterial defensive mechanisms against foreign genetic elements (e.g. bacteriophages), and are essential tools for and gene cloning and synthetic biology.

The methyltransferases protect the bacterial DNA against the restriction enzymes by modifying DNA bases with methyl groups (see Figure 1.9). Figure 1.10 shows that type II restriction enzymes specifically recognize and bind DNA sequences termed restriction sites, and cleave either within those sites or in proximity. The DNA sequence of a restriction site is typically between 4 and 8 bases and is typically palindromic [84]. A type II restriction enzyme, which usually acts in homodimeric form, cleave the DNA by breaking the sugar-phosphate backbone (phosphodiester bond) on both helical strands, thus generating blunt or staggered ends with the DNA products [84]. Restriction

enzymes offer the possibility to cut the DNA in nearly any desired location, and allow DNA editing and engineering of synthetic DNA constructs that are extensively utilized in biotechnology and other applications to the life sciences.

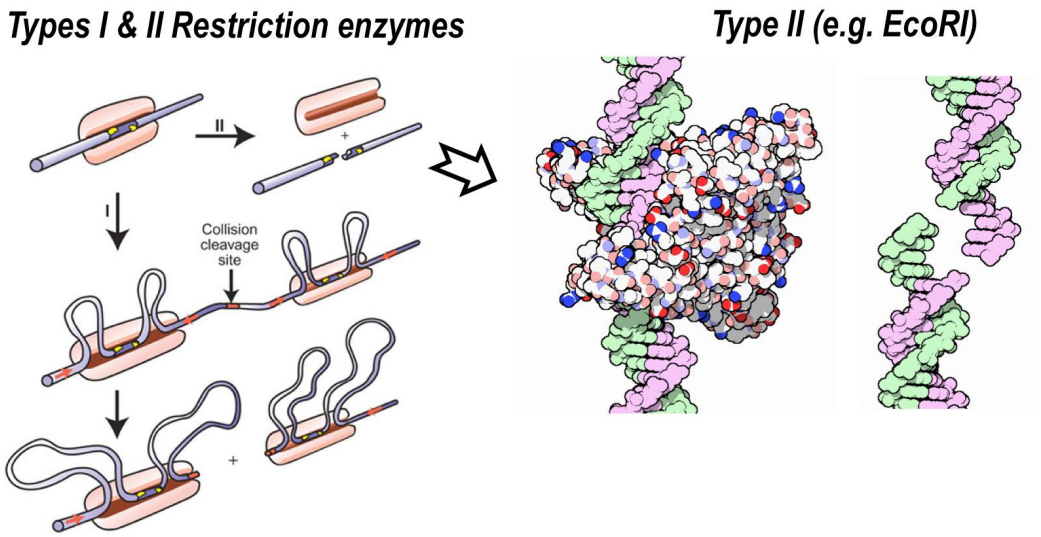

Figure 1.10. Schematic mechanism of action of type I and II restriction enzymes. Type II are highly interesting in DNA nanotechnology because they cleave phosphodiester bonds right inside the their recognition site.

Our group studied the action of the restriction enzyme *Dpn*II, that cleaves dsDNA at a specific sequence (5'–GATC–3'), on surface-bound dsDNA nanopatches obtained by nanografting [58]. By measuring cleavage as a function of packing density of a 44 bp dsDNA, they demonstrated the existence of a threshold, above which the reaction is inhibited essentially in a stepwise fashion (see Figure 1.11). The dsDNA density was estimated by means of topographic height imaging [57,85,86] before the reaction, and the cleavage reaction was observed as a 50% height decrease in the dsDNA patch, which is consistent with the position of the restriction site within the dsDNA probe. The investigators showed that access of *Dpn*II (which acts as homodimer) to the monolayer is fully inhibited when the average dsDNA-dsDNA distance in the patch is less than ~ 10 nm (density ~ 1×10^{12} molecules/cm^2), which also corresponds to the overall width of the enzyme. This result, confirmed in part by other groups [81,87,88], suggests that the accessibility of cleavage sites of dsDNA molecules that are confined in self-assembled nanostructures critically depends on the inherent steric hindrance imposed by the molecular density (see Figure 1.11).

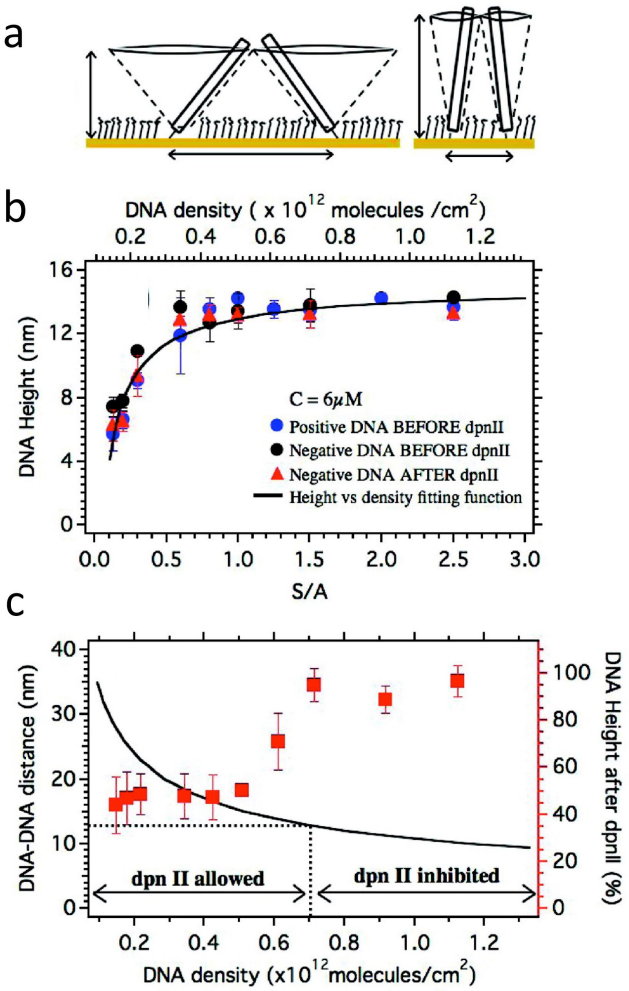

Figure 1.11. Control of steric hindrance on restriction enzyme reactions within nanografted DNA surface matrices, as revealed by atomic force microscopy. (**a**) Illustration of simplified geometrical model to estimate the average dsDNA-dsDNA distance in a monolayer, on the basis of topographic thickness, that can be derived from the measured topographic height of a nanografted patch. During nanografting, the DNA density increases as a function of AFM tip coverage (i.e., the number of "sweeps" of the AFM tip within the same area [S/A]). (**b**) Graph of the patch height for a 44 bp dsDNA molecule as a function of tip coverage. The model proposed in (a) fits well the behaviour of the height vs. S/A, and thus an estimated density can be calculated. (**c**) The percentage height decrease of dsDNA patches after restriction enzymatic reaction (with *Dpn*II endonuclease) as a function of DNA density. The restriction site is located in the middle of the dsDNA molecule, and therefore a ~ 50% height decrease is expected for a successful reaction. The reaction is allowed for densities lower than a certain critical threshold estimated as 0.7×10^{12} molecules/cm^2, which corresponds to an average DNA-DNA separation of ~ 12 nm. The action of the enzyme is therefore steric-dependent, and the stepwise behaviour of its action suggests that enzyme access is inhibited when the spatial separation between DNA molecules is smaller than the size of the enzyme. A "brighter is higher" grey scale is used for the AFM topographic micrograph. Reprinted from [58]. Copyright © (2008) American Chemical Society.

Biagiotti and coworkers investigated the accessibility of ssDNA and dsDNA towards the sequence nonspecific nuclease DNase I, using an electrochemical biosensor [89]. The enzymatic processing of the DNA probes labeled with an electrochemical reporter is 100% efficient at lower probe densities (~ 1×10^{11} molecules/cm^2), but monotonically decreases at higher densities (2.5×10^{12} molecules/cm^2), down to 50% efficiency. However, with dsDNA probes the faradic current suppression resulting from enzymatic digestion of the surface-bound probes was limited to 60% even at the lowest densities investigated ($<1\times10^{11}$ molecules/cm^2), demonstrating that a significant fraction of the immobilized probe is inaccessible to nuclease digestion, regardless of surface density. The current suppression dropped to 30% in a step-wise fashion for densities > 3×10^{11} molecules/cm^2, similar to the enzyme behavior observed in our lab [58]. The latter group further investigated enzymatic reactivity within specific nanografted patterns of dsDNA probes, and unequivocally demonstrated that dsDNA confinement exerts a quantifiable effect on enzyme diffusion within the surface-bound nanostructures [61]. Specifically, they found that an endonuclease has essentially no access to a low-density dsDNA nanopatch that is surrounded by a nanografted “fence” of highly dense dsDNA, regardless of the contact area between the low-density patch and the solution, which can be as large as several square microns (see Figure 1.12). It was indirectly established that the enzyme gains access to its target sites only from the sidewalls of the patch, which are several nm in height, rather than from the larger, topmost face. The enzyme then can diffuse within the two-dimensional matrix and locate its target sites. The “roughness” of the patch, the length of surface-bound DNA, and the type of linker used for attachment are additional factors that influence enzyme action [80,88].

The group of Bar-Ziv developed cell-free transcription/translation molecular circuits in an attempt to demonstrate the bottoms-up construction of synthetic biochemical systems [88]. They designed a biochip with localized “brushes” of 220-bp or 1130-bp dsDNA molecules by a single-step photolithographic approach, allowing control of DNA density by attaching the probes to a chemically engineered surface via UV light-dependent deprotection. The investigators used dsDNA molecules provided with restriction sites for *Bam*HI and/or *Eco*RV in proximity to the two molecular ends, and a fluorescent label at the end more distant from the surface. In this manner, DNA brushes with surface density gradients were formed and their enzymatic processing followed in real time and with spatial resolution by fluorescent optical microscopy (see

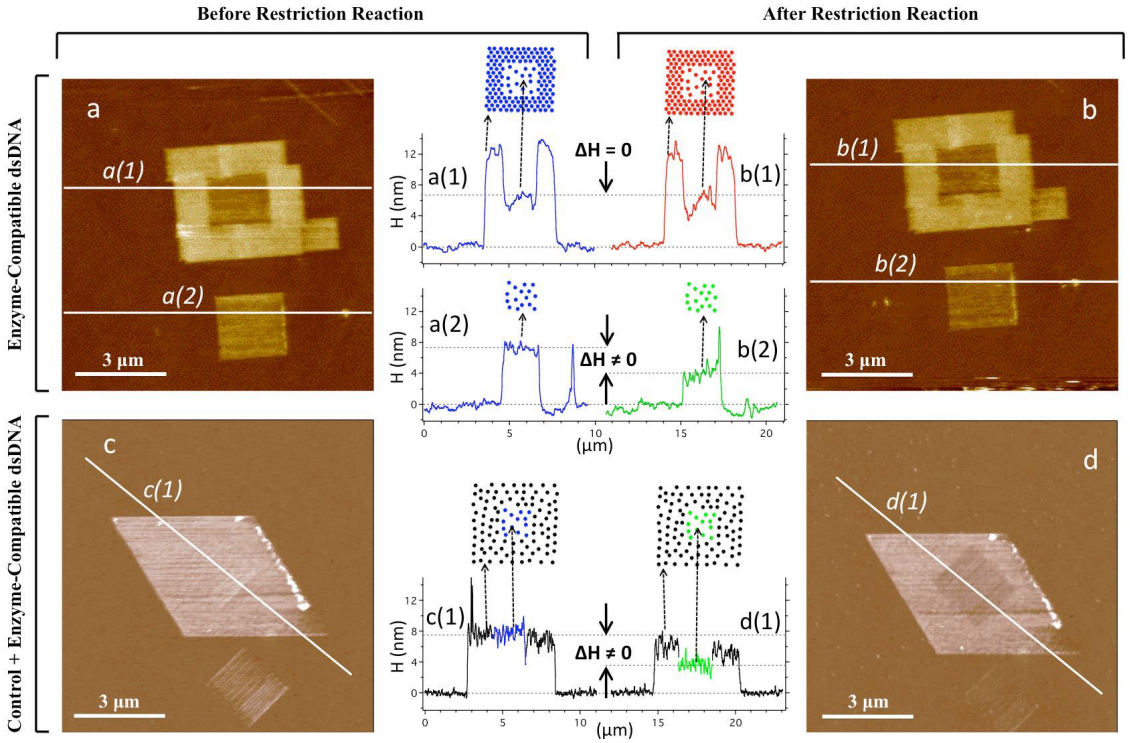

Figure 1.12. Two-dimensional enzyme diffusion in nanografted DNA surface matrices, as revealed by atomic force microscopy. The top figure (**a-b**) shows AFM topographic data, elucidating the effect of a high-density dsDNA patch (fence) surrounding a low-density patch (both obtained by means of nanografting) on the accessibility of dsDNA molecules incorporated within the central, low-density patch, towards an endonuclease (*Dpn*II) in solution. The AFM topographic micrographs in (**a**) and (**b**) display two low-density patches, with (top) and without (bottom) the high-density fence. Graphs (**a1**) and (**a2**) are line profiles relative to the micrograph in (a), while (**b1**) and (**b2**) are profiles relative to the same nanostructures after enzymatic reaction (**b**). The structures are formed with the same 44-bp thiol-dsDNA molecule, having a restriction site in the middle. The dense fence results have higher topographic heights, as packed molecules tend to have a near-vertical orientation (see Figure 1.11). Lines profiles **(a1)** and (**b1**) show that the endonuclease has no access to the dsDNA in the central patch, as the topographic height does not change after enzymatic treatment. Lines (a2) and (b2) instead show that the same low-density patch is accessible to enzyme when there is no high-density fence surrounding the sidewalls (see the ~ 50% height decrease after treatment). AFM micrographs (**c**) and (**d**) depict, before and after the enzymatic reaction, respectively a low-density dsDNA patch surrounded by a larger low-density patch consisting of a control dsDNA molecule lacking restriction sites. Line profiles (**c1**) and (**d1**) show that the dsDNAs within the central patch are accessible to the endonuclease. In turn, enzyme molecules two-dimensionally diffuse within the inert low-density dsDNA matrix and retain their enzymatic activity. Graphical schemes represent the DNA density underlying topographic profiles. Scale bar, 3 µm. A "brighter is higher" grey scale is used for the AFM topographic micrograph. Reprinted from [61].

Figure 1.13). The minimum average distance between dsDNA molecules was estimated to be between 10-20 nm. While the digestion of the 200 bp DNA brush by *Eco*RV at a site near the surface was complete by 10 min, and showed no clear evidence of an effect of density on enzyme efficiency, the 1130 bp brushes revealed a density effect on the function of both *Eco*RV and *Bam*HI. When the *Eco*RV recognition site was located at the top, the relative reaction was complete in 10 min, while a 3-fold increase in reaction time was necessary to attain complete digestion when the restriction site was located at the bottom of the brush (see Figure 1.13) [88]. Restriction enzymes therefore can be controlled even in low-density, disordered systems.

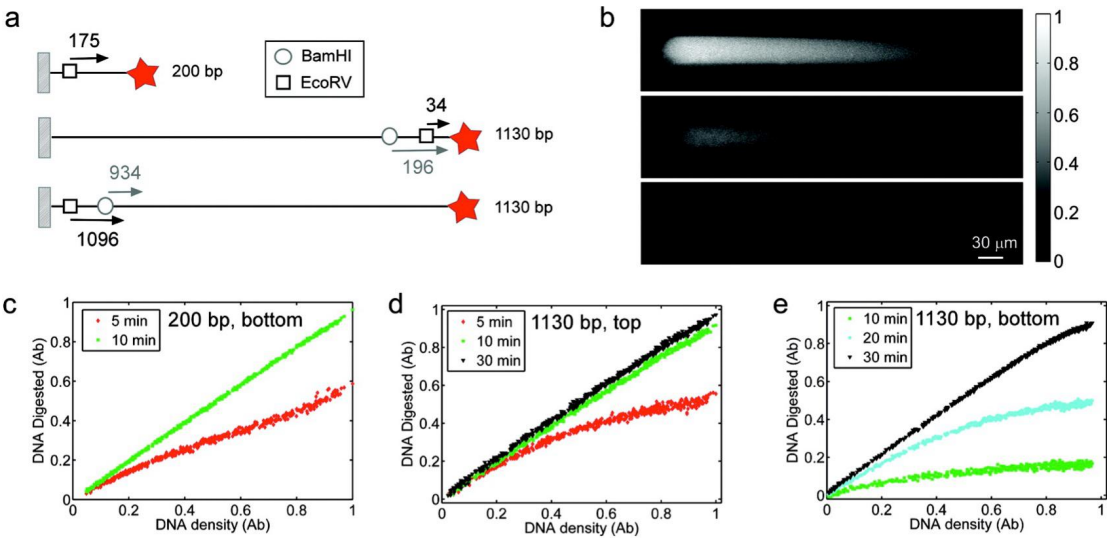

Figure 1.13. The effect of steric hindrance on the kinetics of restriction enzyme reactions in spatially resolved DNA brushes on a chip. (**a**) The scheme depicts representative DNA fragments, functionalized with a fluorescent dye at one terminus, and a surface linker at the other terminus, utilized to form brushes with a spatial density gradient provided by a photolithographic approach. The 200-bp and one 1130 bp sequences have restriction sites in proximity of the surface, while one 1130 bp sequence has restriction sites located on top. (**b**) The action of restriction enzyme is monitored in real-time by means of fluorescent imaging, as the cleaved, surface-bound molecules release the fluorescent dye. Shown are the florescence images of a 1130 bp brush with restriction site at the top, during *Eco*RV restriction reaction at different times: t=0 min (top), t=5 min (middle), and t=10 min (bottom). Panels (**c-e**) plot the fraction of DNA cleaved by *Eco*RV as a function of DNA density and time for a 200 bp brush (**c**) (restriction site at the bottom), and 1130 bp brushes with restriction site on top (**d**), and at the bottom (**e**). The results show that in the latter case, the enzyme reaction is much slower that in the other conditions, and that the reaction rate is negatively affected by DNA density. Therefore, *Eco*RV action in the longer brush is sterically regulated. Reprinted with permission from [88]. Copyright © (2009) American Chemical Society.

Compared to surface-bound monolayers of nucleic acids, water-soluble DNA nanostructures, either consisting of only a few, short sequences, or larger 2D or 3D shapes comprising several thousands of base pairs, are highly ordered systems. There have only been a few reported studies of the enzymatic reactivity of such structures. Keum and co-workers investigated the reactivity of a DNA tetrahedron (prototypical DNA origami) toward specific and non-specific endonucleases [90]. In particular, the authors studied the action of *Dde*I endonuclease as a function of the position of the cleavage site within the DNA tetrahedron. Two variants of the same structure were used, which have, respectively, one restriction site located in the center of one of the edges (T1), or adjacent to one of the vertexes (T2). The two variants were incubated with the endonuclease and the products were analyzed by denaturing gel electrophoresis. The authors found a significant digestion pattern for both the T1 and T2 nanostructures. The DNA tetrahedron has several nicks along the DNA-duplex segments, which provide flexibility to the nanostructure. After treatment with a DNA ligase, the rigidity of the nanostructure increases, and by subsequently reacting the ligated nanostructures with *Dde*I, the authors found that the action of the endonuclease is inhibited only for the ligated T2 nanostructure [90]. Other experiments showed that DNA tetrahedron are more resistant than molecular dsDNA when exposed either to a non-specific nuclease (i.e. DNase I) in solution, or to complex biomolecular mixtures such as fetal bovine serum [90]. Anderson and co-workers carried out experiments *in vivo* (by using a mouse model), and demonstrated that the half-life in the blood system for a DNA tetrahedron linked to a short interfering (si) RNA is longer ($t_{1/2}$ ~ 24 min) than the half-life of the siRNA molecule itself ($t_{1/2}$ ~ 6 min) [39] (see Figure 1.14).

The stability of several DNA origami in the presence of nucleases has been investigated by several groups, using transmission electron microscopy and electrophoretic separation in agarose gels. Castro *et al.* found that the incubation of different 3D DNA nanostructures with exo- or endonucleases provide contrasting results [91]. However the DNA nanostructures appear to be less affected by DNase I than a conventional dsDNA plasmid. In particular, using 1 unit of DNase I, they found that it takes 60 minutes to degrade 2 ng of a DNA nanorod, while only 5 minutes to degrade 65 ng of the dsDNA plasmid. Meldrum & Yan and co-workers used AFM, agarose gel electrophoresis and electron microscopy to study the stability, at different temperatures, of triangular, rectangular and cuboidal DNA nanostructures in cell lysates (see Figure 1.4). They incubated (up to 12 h) DNA origami, single-stranded and double-stranded circular DNA molecules in lysates obtained from different cell lines [37]. While the DNA origami were apparently unaffected by the incubation, the gel

electrophoretic mobility of the dsDNA greatly decreased after treatment, suggesting that, in contrast to the DNA origami, circular dsDNA strongly interacts with proteins in the lysates. Furthermore, a rectangular DNA nanostructure, functionalized with ssDNA overhangs that bind a short ssRNA, was shown to retain its functionality after treatment.

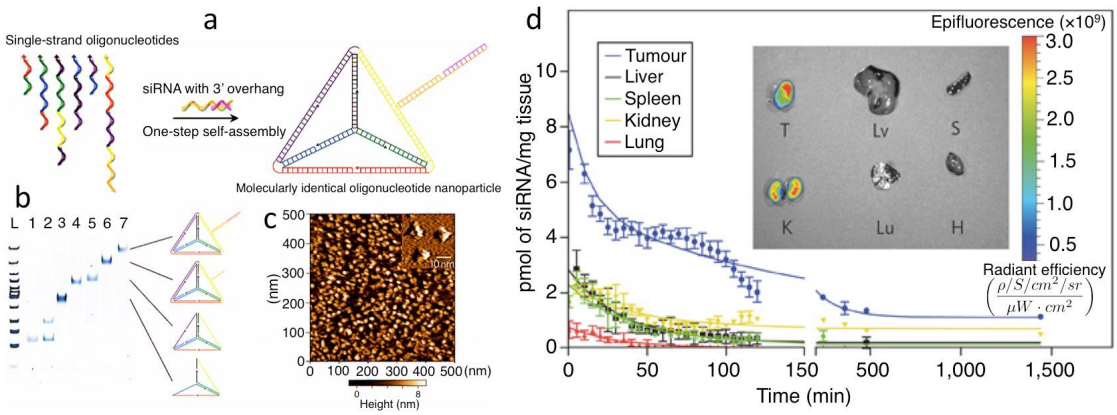

Figure 1.14. Molecularly self-assembled nucleic acid nanoparticles for targeted in vivo siRNA delivery. (**a**) Schematic representation of the composite strands and structure of DNA tetrahedral, linked to a short interfering(si) RNA, forming an siRNA-DNA tetrahedra. This structure was used as a targeted siRNA delivery system. (**b**) Gel electrophoretic characterization of the assembly of DNA tetrahedra linked to siRNA (Lane 1, strand 1; Lane 2, strands 1 and 2; Lane 3, strands 1-3; Lane 4, strands 1-4; Lane 5, strands 1-5; Lane 6, strands 1-6; Lane 7, strands 1-6 and siRNA and Lane L, DNA ladder). (**c**) AFM image of DNA tetrahedra linked to siRNA. The grey scale indicates height. Inset: high resolution AFM image. (**d**) Pharmacokinetics profile and organ biodistribution of an siRNA-DNA tetrahedra delivered in a mouse model. In this experiment the structure was combined with a targeting molecule (folic acid) and Cy5 fluorescent dye for tracking purposes. A nude mouse, bearing KB carcinoma cells as a xenografted tumor, with high expression of folate receptor was used as experimental model. Inset: *ex vivo* fluorescence images of the tumor (T), liver (Lv), spleen (S), kidney (K), heart (H) and lung (L), 12 h after injection. Note the high levels of siRNA in the tumor tissue. Adapted and reprinted with permission from [39]. Copyright © 2012, Rights Managed by Nature Publishing Group.

Within nanostructured systems, enzyme processing was also shown to depend on salt concentration. Seferos *et al.* showed that, although high salt concentrations can be responsible for DNA denaturation, it also can promote resistance to enzymatic cleavage. The group compared the effect of DNase I on dsDNA in solution, and on dsDNA attached to AuNPs, and found that the latter showed a ~ 4-fold greater half-life than the former [92]. The results also showed that the overall cleavage kinetics were slower, although enzyme association was faster with the AuNPs. This effect was due to

high local salt concentration, as monovalent cations can inhibit DNase I by displacing Mg^{2+} and Ca^{2+} ions. In presence of a salt-tolerant mutant of DNase I, the enzymatic action on molecular DNA was recovered.

1.4 Effect of crowding on nucleic acid-nucleic acid and nucleic acid-protein interactions

The application of nucleic acid-based nanostructures to complex biological problems will require an in-depth understanding of nucleic acid behavior in crowded, highly inhomogeneous systems. While the effect of crowding on dsDNA dissociation has been investigated [[55]], little is known of the effect of crowding on DNA-based nanoparticles or related systems. For instance, the theoretical work of Liu *et al.* [[93]] rationalizes that the melting temperature (T_m) increases with molecular density, since the crowding reduces the excluded volume and limits the entropy increase that occurs during DNA melting. In contrast, the T_m can decrease if the crowded molecules in ss form exhibit stronger interactions, compared to the corresponding dsDNA molecules [[93]]. Interactions between ssDNA molecules in crowded systems also have been investigated using gold nanoparticles carrying bound ssDNA. Mirkin and co-workers studied the interactions between nanoparticles coated with two short ssDNA molecules with limited complementarity (3 nucleotides) [[94]]. They demonstrated that multiple, weak interactions between very short complementary sequences bound to nanoparticles can provide a net contact force strong enough to stabilize nanoparticle aggregates. They also determined the melting temperatures of the aggregates as a function of the length of the complementary sequence and the diameter of the nanoparticles. They found that either increasing the salt concentration or the size of the nanoparticle favors aggregation, as indicated by an increase in melting temperature. Also, in high salt conditions (1M NaCl), a single-nt-long complementarity was able to stabilize the aggregation of nanoparticles 150 nm in diameter [[94]]. Mirkin and co-workers proposed three-dimensional hybridization as an explanation of the effect: while single DNA strands can only form a single duplex, molecules bound to nanoparticles can interact in three dimensions, such that base pairing can simultaneously involve multiple strands. 3D hybridization enables AuNP aggregation, and is the cause of the increased melting temperatures observed in these systems.

While the stability of the 3D nanostructures studied by Mirkin and co-workers increases with the number of bp formed for each nanoparticle [[94]], the formation of highly dense, ordered, self-assembled 3D DNA origami nanostructures is hindered by an excessive amount of inter-helix connections, also termed crossovers, which are formed by the hybridization of short ssDNA staples with multiple segments of the long ssDNA scaffold. The amount of inter-helix connections inevitably increases with nanostructure complexity and size, and is related to the effects of molecular crowding on self-assembly of DNA origami nanostructures (see Figure 1.15). The results from

Yan, Shi and coworkers suggest that crossovers introduce repulsive forces and steric hindrance experienced by the ssDNA staples during self-assembly on the ssDNA scaffold [95]. The authors demonstrated that the yield of self-assembling a 3D DNA cuboid structure (with DNA duplexes arranged in a square lattice) increases by diminishing the number of cross-overs only within the core of the cuboid, thus preserving the desired shape.

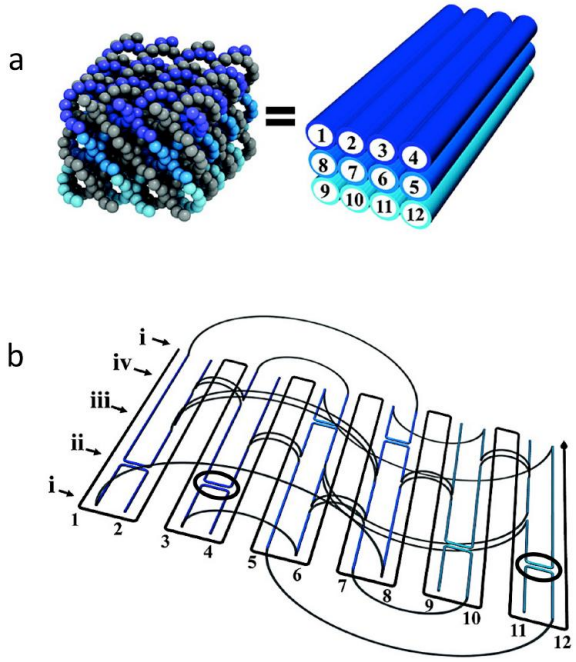

Figure 1.15. Multilayer DNA origami packed on a square lattice. **(a)** DNA nanostructures are formed via Watson-Crick base-paring of several, short single-strand (ss)DNA sequences (termed "staples") with a long circular ssDNA molecule (the "scaffold"). The 12 DNA helices in the figure are therefore formed by the ssDNA of the scaffold (dark grey) and the ssDNAs of the staples (light grey). The helices can be schematically represented as cylinders with different colors that correspond to the staple pattern used to fold the helices (i.e. dark cylinders in C match with helices number 1, 2, 3, 4 in B). Each helix is in contact with four other helices, as in a square lattice fashion. **(b)** The path of the helices inside the nanostructure is represented in a 2D scheme, where the black line is the scaffold and the light grey lines are the staples. Staples join two separated scaffold sequences (1-12) forming crossovers (highlighted with circles) that are periodically distributed inside the structure. Adapted and reprinted with permission from [95]. Copyright © (2009) American Chemical Society.

Macromolecular crowding and excluded volume effects hold importance for *in vitro* enzymatic reactions. Lareu and co-workers showed that reverse transcription (RT) and the polymerase chain reaction (PCR) can be significantly improved in all aspects, including sensitivity, specificity, processivity, yield and thermal stability of Taq DNA polymerase, by adding inert macromolecules such as Ficoll (70 kDa and 400 kDa) to

the reaction volume [96]. The introduced fractional volume occupancies are between 5% and 15%, which is in the accepted range of biological crowding, and thus simulates intracellular environments. The investigators were able to reduce the amount of enzyme by 75% and still attain a good product yield, due to faster reaction kinetics. The investigators explained that the macromolecular crowding-induced, excluded-volume effect lowers the reaction entropy, thus increasing the free energy of the reactants due to enhanced enzyme thermal stability, more efficient primer annealing to its target, greater specificity, and enhanced enzyme-nucleic acid complex formation and stability.

Sugimoto and co-workers [97] have systemically investigated the effect of molecular crowding on the stability of DNA duplexes consisting of Hoogsteen or Watson-Crick base pairs, by adding different concentrations of PEG200 (polyethylene glycol with an average molecular weight of 200 g/mol) as a crowding agent. Interestingly, the free energy of Hoogsteen base pair formation in an intramolecular duplex and a triplex decreases from +1.45±0.15 to +1.09±0.13 kcal mol^{-1}, and from -1.89±0.13 to -2.71±0.11 kcal mol^{-1}, respectively, with increasing concentration of PEG200 from 0 to 20 wt%, while for the formation of Watson-Crick base pairs in the duplex and triplex, the addition of PEG200 increases the free energy from -10.2±0.2 to -8.7± 0.1 kcal mol^{-1}, and from -10.8 ±0.2 to -9.2±0.2 kcal mol^{-1}, respectively. The contrasting effect of molecular crowding on the Hoogsteen and Watson-Crick base pair stability has been rationalized by the differences in the manner of binding of water molecules to the DNA strands. Thermodynamic calculations indicate that stabilization of Hoogsteen base pairs and destabilization of Watson-Crick base pairs reflects a favorable change in enthalpy over an unfavorable change in entropy. Calculation of the number of water molecules associated with the DNA structural changes under conditions of molecular crowding reveal that 1.9±0.1 and 0.8±0.1 water molecules per nucleotide are released upon formation of duplex and triplex Hoogsteen base pairs, respectively, and that 3.4 ±0.2 and 3.3±0.1 water molecules are taken up per nucleotide upon formation of duplex and triplex Watson-Crick base pairs, respectively. Stabilization of Hoogsteen base pairs and destabilization of Watson-Crick base pairs is attributed to the dehydration and hydration, respectively, in the duplex and triplex structures. Kan *et al.* have demonstrated that under salt-deficient conditions, molecular crowding induces the formation of telomeric G-quadruplexes, and increased its competition with duplex formation [98]. A separate study by Miyoshi *et al*. [99] showed that an altered hydration state is responsible for stabilization of quadruplex structures

and destabilization of duplex structures under molecular crowding conditions [99]. Thus, the hydration state is a key determinant of DNA structure formation and stability.

Hancock and co-workers showed how the assembled/disassembled state of protein complexes depends upon the manner of spatial confinement and dilution within the cellular compartments within which the complexes are located [100]. Using immunofluorescence and immunoelectron microscopy, nuclear protein complexes were detected in nucleoli and promyelocytic leukemia bodies (complexes present in the specified disease, but with poorly understood function). Nucleolar complexes were detected by co-localization of the major protein components, including nucleolin, which participates in pre-rRNA processing, and the 194 kDa subunit of RNA pol I, while nucleolar function was confirmed by quantification of rRNA transcript elongation. When the nuclear volume is expanded with an isotonic cationic solution, the complexes cannot be detected. The investigators explain that the disassembly of compartments upon nuclear expansion is provoked by a reduction of the internal concentration of macromolecules. Following subsequent reduction of the nuclear volume, the protein complexes reappeared, and nucleolar function recovered as monitored by rRNA transcript elongation. The authors show that assembly and disassembly of the complex are dependent upon steric crowding. In particular, the addition of inert molecules such as PEG or dextran to the expanded nuclei, in which the complexes are not visible, leads to recovery of the complexes with well-defined shapes and functions, comparable to those of the unperturbed complexes. The latter show a concentration-dependent response to the addition of inert macromolecules used in studies of macromolecular crowding *in vitro*. Crowding agents induce the reassembly phenomenon as an effect of volume exclusion, because they restore the normal intranuclear macromolecular concentration.

Molecular crowding also affects RNA structure, stability and function. Nakano *et al.* investigated the effect of molecular crowding on hammerhead ribozyme catalytic activity, using polyethylene glycols (PEGs) of different molecular weights [101]. Hammerhead ribozyme catalytic activity was enhanced under the molecular crowding conditions, and this facilitation suggested that the active form of the ribozyme is stabilized under crowded conditions, possibly due to dehydration. Very recently, Kumar *et al.* have demonstrated that the molecular crowding conditions of PEG200 favor the formation of the functional tertiary structure of an adenine-specific riboswitch, by promoting the dehydration of stem regions during the conformational change induced by ligand binding [102]. In a theoretical study, Denesyuk and coworkers have shown, using coarse-grained Langevin dynamic simulations, that crowding enhances the

stability of a pseudoknot (PK) relative to hairpin duplex (HP), both in the wild-type and in a mutant associated with dyskeratosis congenital [103].

1.5 Conclusions and goal of this thesis

Nucleic acid nanotechnology is now an established, interdisciplinary field of research that is supported by highly productive collaborations involving researchers in the physical sciences, materials science, computer science, biotechnology, biology, and medicine. Self-assembled nanosystems are highly informative in examining the basic functions of nucleic acids, as they can be immobilized at varying densities, repetitively processed or functionally probed, and ultimately analyzed with single molecule resolution. Several unanticipated properties of nucleic acids and their ability to interact with proteins arise from nanoscale confinement. In particular, the functionality of nucleic acid-based nanosystems is highly dependent on the local density, molecular flexibility, and the network of weak interactions between adjacent nucleic acid molecules. These significantly affect steric accessibility, molecular crowding and hydration to determine nucleic acid hybridization, denaturation, conformation, and enzyme accessibility. We believe that an in-depth understanding of these behaviors and properties will allow significant advances in the field of structural DNA and RNA nanotechnology. Specifically, this knowledge will enable the design of nucleic acid-based nanostructures with unprecedented functionalities, for effective applications in nanomedicine, including diagnostics and drug delivery, which will require that the nanostructures function in a robust, reproducible manner in a variety of complex biomolecular environments.

The goal of this experimental thesis is to carry out a pilot, quantitative, unprecedented study of the peculiar properties associated with nanoscale confinement in water-soluble, nucleic acid nanostructures that influence protein-nucleic acid interactions. In this work, we mostly focused on restriction enzymatic reactions of DNA molecules confined within two-dimensional DNA origami that are most established, self-assembled nanostructures. In fact, as discussed above, restriction enzymes recognize and process DNA with very high sequence-specificity, and introduce permanent modifications to the nucleic acid structure that are key for the implementation of accurate, quantitative experimental approaches for their analysis, as I will explain in the following chapter.

1.6 Bibliography of Chap. 1

1. Gifford, L. K., Sendroiu, I. E., Corn, R. M. & Lupták, A. Attomole Detection of Mesophilic DNA Polymerase Products by Nanoparticle-Enhanced Surface Plasmon Resonance Imaging on Glassified Gold Surfaces. *J. Am. Chem. Soc.* **132,** 9265–9267 (2010).
2. Ke, Y. G., Lindsay, S., Chang, Y., Liu, Y. & Yan, H. Self-assembled water-soluble nucleic acid probe tiles for label-free RNA hybridization assays. *Science* **319,** 180–183 (2008).
3. Niemeyer, C. M. Semisynthetic DNA-Protein Conjugates for Biosensing and Nanofabrication. *Angew. Chem.-Int. Ed.* **49,** 1200–1216 (2010).
4. Akbulut, O., Yu, A. A. & Stellacci, F. Fabrication of biomolecular devices via supramolecular contact-based approaches. *Chem. Soc. Rev.* **39,** 30–37 (2010).
5. Lund, K. *et al.* Molecular robots guided by prescriptive landscapes. *Nature* **465,** 206–210 (2010).
6. Liu, Q. H. *et al.* DNA computing on surfaces. *Nature* **403,** 175–179 (2000).
7. Franco, E. *et al.* Timing molecular motion and production with a synthetic transcriptional clock. *Proc. Natl. Acad. Sci.* **108,** E784–E793 (2011).
8. Seelig, G., Soloveichik, D., Zhang, D. Y. & Winfree, E. Enzyme-Free Nucleic Acid Logic Circuits. *Science* **314,** 1585–1588 (2006).
9. Feldkamp, U. & Niemeyer, C. M. Rational Design of DNA Nanoarchitectures. *Angew. Chem. Int. Ed.* **45,** 1856–1876 (2006).
10. Rothemund, P. W. K. Folding DNA to create nanoscale shapes and patterns. *Nature* **440,** 297–302 (2006).
11. Woo, S. & Rothemund, P. W. K. Programmable molecular recognition based on the geometry of DNA nanostructures. *Nat Chem* **3,** 620–627 (2011).
12. Ke, Y., Ong, L. L., Shih, W. M. & Yin, P. Three-Dimensional Structures Self-Assembled from DNA Bricks. *Science* **338,** 1177–1183 (2012).
13. Jonkheijm, P., Weinrich, D., Schröder, H., Niemeyer, C. & Waldmann, H. Chemical Strategies for Generating Protein Biochips. *Angew. Chem. Int. Ed.* **47,** 9618–9647 (2008).
14. Meyer, R. & Niemeyer, C. M. Orthogonal Protein Decoration of DNA Nanostructures. *Small* **7,** 3211–3218 (2011).
15. Lavella, G. J., Jadhav, A. D. & Maharbiz, M. M. A Synthetic Chemomechanical Machine Driven by Ligand–Receptor Bonding. *Nano Lett.* **12,** 4983–4987 (2012).
16. Voigt, N. V *et al.* Single-molecule chemical reactions on DNA origami. *Nat Nano* **5,** 200–203 (2010).

17. Douglas, S. M., Bachelet, I. & Church, G. M. A Logic-Gated Nanorobot for Targeted Transport of Molecular Payloads. *Science* **335,** 831–834 (2012).
18. Rinker, S., Ke, Y., Liu, Y., Chhabra, R. & Yan, H. Self-assembled DNA nanostructures for distance-dependent multivalent ligand-protein binding. *Nat Nano* **3,** 418–422 (2008).
19. Kuzyk, A., Laitinen, K. T. & Torma, P. DNA origami as a nanoscale template for protein assembly. *Nanotechnology* **20,** 1–5 (2009).
20. Ghosh, D. *et al.* M13-templated magnetic nanoparticles for targeted in vivo imaging of prostate cancer. *Nat Nano* **7,** 677–682 (2012).
21. Sacca, B. & Niemeyer, C. M. DNA Origami: The Art of Folding DNA. *Angew. Chem.-Int. Ed.* **51,** 58–66 (2012).
22. Jabbari, H., Aminpour, M. & Montemagno, C. Computational Approaches to Nucleic Acid Origami. *ACS Comb. Sci.* **17,** 535–547 (2015).
23. Kuzyk, A. *et al.* DNA-based self-assembly of chiral plasmonic nanostructures with tailored optical response. *Nature* **483,** 311–314 (2012).
24. Acuna, G. P. *et al.* Fluorescence Enhancement at Docking Sites of DNA-Directed Self-Assembled Nanoantennas. *Science* **338,** 506–510 (2012).
25. Kukolka, F., Schoeps, O., Woggon, U. & Niemeyer, C. M. DNA-Directed Assembly of Supramolecular Fluorescent Protein Energy Transfer Systems. *Bioconjug. Chem.* **18,** 621–627 (2007).
26. Stein, I. H., Schueller, V., Boehm, P., Tinnefeld, P. & Liedl, T. Single-Molecule FRET Ruler Based on Rigid DNA Origami Blocks. *Chemphyschem* **12,** 689–695 (2011).
27. Stein, I. H., Steinhauer, C. & Tinnefeld, P. Single-Molecule Four-Color FRET Visualizes Energy-Transfer Paths on DNA Origami. *J. Am. Chem. Soc.* **133,** 4193–4195 (2011).
28. Krishnan, Y. & Simmel, F. C. Nucleic Acid Based Molecular Devices. *Angew. Chem.-Int. Ed.* **50,** 3124–3156 (2011).
29. Pinheiro, A. V, Han, D., Shih, W. M. & Yan, H. Challenges and opportunities for structural DNA nanotechnology. *Nat Nano* **6,** 763–772 (2011).
30. Hubbell, J. A. & Chilkoti, A. Nanomaterials for Drug Delivery. *Science* **337,** 303–305 (2012).
31. Zhao, Y.-X. *et al.* DNA Origami Delivery System for Cancer Therapy with Tunable Release Properties. *ACS Nano* **6,** 8684–8691 (2012).
32. Walsh, A. S., Yin, H., Erben, C. M., Wood, M. J. A. & Turberfield, A. J. DNA Cage Delivery to Mammalian Cells. *ACS Nano* **5,** 5427–5432 (2011).

33. Jiang, Q. *et al.* DNA Origami as a Carrier for Circumvention of Drug Resistance. *J. Am. Chem. Soc.* **134,** 13396–13403 (2012).
34. Hahn, J., Wickham, S. F. J., Shih, W. M. & Perrault, S. D. Addressing the Instability of DNA Nanostructures in Tissue Culture. *ACS Nano* **8,** 8765–8775 (2014).
35. Goltry, S. *et al.* DNA topology influences molecular machine lifetime in human serum. *Nanoscale* **7,** 10382–10390 (2015).
36. Chen, Y.-J., Groves, B., Muscat, R. A. & Seelig, G. DNA nanotechnology from the test tube to the cell. *Nat Nano* **10,** 748–760 (2015).
37. Mei, Q. *et al.* Stability of DNA Origami Nanoarrays in Cell Lysate. *Nano Lett.* **11,** 1477–1482 (2011).
38. Nishikawa, M., Rattanakiat, S. & Takakura, Y. DNA-based nano-sized systems for pharmaceutical and biomedical applications. *Biol. Mater. Eng. DNA RNA Drug Deliv. Nanomedicine* **62,** 626–632 (2010).
39. Lee, H. *et al.* Molecularly self-assembled nucleic acid nanoparticles for targeted in vivo siRNA delivery. *Nat. Nanotechnol.* **7,** 389–393 (2012).
40. Miyoshi, D. & Sugimoto, N. Molecular crowding effects on structure and stability of DNA. *Target. DNA Part 1* **90,** 1040–1051 (2008).
41. Minton, A. P. How can biochemical reactions within cells differ from those in test tubes? *J. Cell Sci.* **119,** 2863–2869 (2006).
42. McGuffee, S. R. & Elcock, A. H. Diffusion, Crowding & Protein Stability in a Dynamic Molecular Model of the Bacterial Cytoplasm. *PLOS Comput. Biol.* **6,** 1–18 (2010).
43. Lizana, L., Konkoli, Z., Bauer, B., Jesorka, A. & Orwar, O. Controlling Chemistry by Geometry in Nanoscale Systems. *Annu. Rev. Phys. Chem.* **60,** 449–468 (2009).
44. Bancaud, A. *et al.* Molecular crowding affects diffusion and binding of nuclear proteins in heterochromatin and reveals the fractal organization of chromatin. *Embo J.* **28,** 3785–3798 (2009).
45. Teif, V. B. & Bohinc, K. Condensed DNA: Condensing the concepts. *Prog. Biophys. Mol. Biol.* **105,** 208–222 (2011).
46. Smith, D. E. *et al.* The bacteriophage &phis; 29 portal motor can package DNA against a large internal force. *Nature* **413,** 748–752 (2001).
47. Chemla, Y. R. *et al.* Mechanism of Force Generation of a Viral DNA Packaging Motor. *Cell* **122,** 683–692 (2005).
48. Pinheiro, A. V, Nangreave, J., Jiang, S., Yan, H. & Liu, Y. Steric Crowding and the Kinetics of DNA Hybridization within a DNA Nanostructure System. *ACS Nano* **6,** 5521–5530 (2012).

49. Bombelli, F. B. *et al.* Closed nanoconstructs assembled by step-by-step ss-DNA coupling assisted by phospholipid membranes. *Soft Matter* **5,** 1639–1645 (2009).
50. Ricci, F., Lai, R. Y., Heeger, A. J., Plaxco, K. W. & Sumner, J. J. Effect of Molecular Crowding on the Response of an Electrochemical DNA Sensor. *Langmuir* **23,** 6827–6834 (2007).
51. Peterson, A. W., Heaton, R. J. & Georgiadis, R. M. The effect of surface probe density on DNA hybridization. *Nucl Acids Res* **29,** 5163–5168 (2001).
52. Steel, A. B., Levicky, R. L., Herne, T. M. & Tarlov, M. J. Immobilization of nucleic acids at solid surfaces: Effect of oligonucleotide length on layer assembly. *Biophys. J.* **79,** 975–981 (2000).
53. Castelino, K., Kannan, B. & Majumdar, A. Characterization of Grafting Density and Binding Efficiency of DNA and Proteins on Gold Surfaces. *Langmuir* **21,** 1956–1961 (2005).
54. Peled, D., Daube, S. S. & Naaman, R. Selective Enzymatic Labeling To Detect Packing-Induced Denaturation of Double-Stranded DNA at Interfaces. *Langmuir* **24,** 11842–11846 (2008).
55. Peled, D., Naaman, R. & Daube, S. S. Packed DNA Denatures on Gold Nanoparticles. *J. Phys. Chem. B* **114,** 8581–8584 (2010).
56. Chen, C., Wang, W., Ge, J. & Zhao, X. S. Kinetics and thermodynamics of DNA hybridization on gold nanoparticles. *Nucleic Acids Res.* **37,** 3756–3765 (2009).
57. Mirmomtaz, E. *et al.* Quantitative Study of the Effect of Coverage on the Hybridization Efficiency of Surface-Bound DNA Nanostructures. *Nano Lett.* **8,** 4134–4139 (2008).
58. Castronovo, M. *et al.* Control of Steric Hindrance on Restriction Enzyme Reactions with Surface-Bound DNA Nanostructures. *Nano Lett.* **8,** 4140–4145 (2008).
59. Liang, J., Castronovo, M. & Scoles, G. DNA as Invisible Ink for AFM Nanolithography. *J. Am. Chem. Soc.* **134,** 39–42 (2011).
60. Bano, F. *et al.* Toward Multiprotein Nanoarrays Using Nanografting and DNA Directed Immobilization of Proteins. *Nano Lett.* **9,** 2614–2618 (2009).
61. Castronovo, M. *et al.* Two-dimensional enzyme diffusion in laterally confined DNA monolayers. *Nat. Commun.* **2,** 1–10 (2011).
62. Parisse, P., Vindigni, A., Scoles, G. & Casalis, L. In Vitro Enzyme Comparative Kinetics: Unwinding of Surface-Bound DNA Nanostructures by RecQ and RecQ1. *J. Phys. Chem. Lett.* **3,** 3532–3537 (2012).
63. Sanavio, B. *et al.* Oriented Immobilization of Prion Protein Demonstrated via Precise Interfacial Nanostructure Measurements. *Acs Nano* **4,** 6607–6616 (2010).

64. Staii, C., Wood, D. W. & Scoles, G. Ligand-induced structural changes in maltose binding proteins measured by atomic force microscopy. *Nano Lett.* **8,** 2503–2509 (2008).
65. Hu, Y., Das, A., Hecht, M. H. & Scoles, G. Nanografting de novo proteins onto gold surfaces. *Langmuir* **21,** 9103–9109 (2005).
66. Xu, S. & Liu, G. y. Nanometer-Scale Fabrication by Simultaneous Nanoshaving and Molecular Self-Assembly. *Langmuir* **13,** 127–129 (1997).
67. Xu, S., Miller, S., Laibinis, P. E. & Liu, G. Fabrication of Nanometer Scale Patterns within Self-Assembled Monolayers by Nanografting. *Langmuir* **15,** 7244–7251 (1999).
68. Liu, M., Amro, N. A. & Liu, G. Nanografting for surface physical chemistry. *Annu. Rev. Phys. Chem.* **59,** 367–386 (2008).
69. Yu, J., Tan, Y. H., Li, X., Kuo, P.-K. & Liu, G. A Nanoengineering Approach to Regulate the Lateral Heterogeneity of Self-Assembled Monolayers. *J. Am. Chem. Soc.* **128,** 11574–11581 (2006).
70. Castronovo, M. *et al.* Mechanical Stabilization Effect of Water on a Membrane-like System. *J. Am. Chem. Soc.* **129,** 2636–2641 (2007).
71. Scaini, D., Castronovo, M., Casalis, L. & Scoles, G. Electron Transfer Mediating Properties of Hydrocarbons as a Function of Chain Length: A Differential Scanning Conductive Tip Atomic Force Microscopy Investigation. *ACS Nano* **2,** 507–515 (2008).
72. Bosco, A. *et al.* Hybridization in nanostructured DNA monolayers probed by AFM: theory versus experiment. *Nanoscale* **4,** 1734–1741 (2012).
73. Josephs, E. A. & Ye, T. Nanoscale Spatial Distribution of Thiolated DNA on Model Nucleic Acid Sensor Surfaces. *ACS Nano* **7,** 3653–3660 (2013).
74. Park, S., Brown, K. A. & Hamad-Schifferli, K. Changes in Oligonucleotide Conformation on Nanoparticle Surfaces by Modification with Mercaptohexanol. *Nano Lett.* **4,** 1925–1929 (2004).
75. Levicky, R., Herne, T. M., Tarlov, M. J. & Satija, S. K. Using Self-Assembly To Control the Structure of DNA Monolayers on Gold: A Neutron Reflectivity Study. *J. Am. Chem. Soc.* **120,** 9787–9792 (1998).
76. Metzker, M. L. Sequencing technologies - the next generation. *Nat Rev Genet* **11,** 31–46 (2010).
77. Eid, J. *et al.* Real-Time DNA Sequencing from Single Polymerase Molecules. *Science* **323,** 133–138 (2009).

78. Zhou, W.-J., Chen, Y. & Corn, R. M. Ultrasensitive Microarray Detection of Short RNA Sequences with Enzymatically Modified Nanoparticles and Surface Plasmon Resonance Imaging Measurements. *Anal. Chem.* **83,** 3897–3902 (2011).
79. Heyman, Y., Buxboim, A., Wolf, S. G., Daube, S. S. & Bar-Ziv, R. H. Cell-free protein synthesis and assembly on a biochip. *Nat Nano* **7,** 374–378 (2012).
80. Carmon, A. *et al.* Solid-phase PCR in microwells: Effects of linker length and composition on tethering hybridization, and extension. *Biotechniques* **32,** 410–420 (2002).
81. McCalla, S. E., Luryi, A. L. & Tripathi, A. Steric Effects and Mass-Transfer Limitations Surrounding Amplification Reactions on Immobilized Long and Clinically Relevant DNA Templates. *Langmuir* **25,** 6168–6175 (2009).
82. Buxboim, A., Daube, S. S. & Bar-Ziv, R. Synthetic gene brushes: a structure-function relationship. *Mol Syst Biol* **4,** 1–8 (2008).
83. Labrie, S. J., Samson, J. E. & Moineau, S. Bacteriophage resistance mechanisms. *Nat Rev Micro* **8,** 317–327 (2010).
84. Pingoud, A. & Jeltsch, A. Structure and function of type II restriction endonucleases. *Nucleic Acids Res.* **29,** 3705–3727 (2001).
85. Zhou, D., Sinniah, K., Abell, C. & Rayment, T. Label-Free Detection of DNA Hybridization at the Nanoscale: A Highly Sensitive and Selective Approach Using Atomic-Force Microscopy13. *Angew. Chem. Int. Ed.* **42,** 4934–4937 (2003).
86. Zhou, D., Sinniah, K., Abell, C. & Rayment, T. Use of Atomic Force Microscopy for Making Addresses in DNA Coatings. *Langmuir* **18,** 8278–8281 (2002).
87. Palanisamy, R., Connolly, A. R. & Trau, M. Considerations of Solid-Phase DNA Amplification. *Bioconjug. Chem.* **21,** 690–695 (2010).
88. Bar, M. & Bar-Ziv, R. H. Spatially Resolved DNA Brushes on a Chip: Gene Activation by Enzymatic Cascade. *Nano Lett.* **9,** 4462–4466 (2009).
89. Biagiotti, V. *et al.* Probe accessibility effects on the performance of electrochemical biosensors employing DNA monolayers. *Anal. Bioanal. Chem.* **402,** 413–421 (2012).
90. Keum, J.-W. & Bermudez, H. Enhanced resistance of DNA nanostructures to enzymatic digestion. *Chem. Commun. Camb. Engl.* 7036–7038 (2009). doi:10.1039/b917661f
91. Castro, C. E. *et al.* A primer to scaffolded DNA origami. *Nat Meth* **8,** 221–229 (2011).
92. Seferos, D. S., Prigodich, A. E., Giljohann, D. A., Patel, P. C. & Mirkin, C. A. Polyvalent DNA Nanoparticle Conjugates Stabilize Nucleic Acids. *Nano Lett.* **9,** 308–311 (2009).

93. Liu, Y., Shang, Y., Liu, H., Hu, Y. & Jiang, J. Crowding effect on DNA melting: a molecular thermodynamic model with explicit solvent. *Phys. Chem. Chem. Phys.* **14,** 15400–15405 (2012).
94. Hurst, S. J., Hill, H. D. & Mirkin, C. A. 'Three-Dimensional Hybridization' with Polyvalent DNA−Gold Nanoparticle Conjugates. *J. Am. Chem. Soc.* **130,** 12192–12200 (2008).
95. Ke, Y. *et al.* Multilayer DNA Origami Packed on a Square Lattice. *J. Am. Chem. Soc.* **131,** 15903–15908 (2009).
96. Lareu, R. R., Harve, K. S. & Raghunath, M. Emulating a crowded intracellular environment in vitro dramatically improves RT-PCR performance. *Biochem. Biophys. Res. Commun.* **363,** 171–177 (2007).
97. Miyoshi, D., Nakamura, K., Tateishi-Karimata, H., Ohmichi, T. & Sugimoto, N. Hydration of Watson−Crick Base Pairs and Dehydration of Hoogsteen Base Pairs Inducing Structural Polymorphism under Molecular Crowding Conditions. *J. Am. Chem. Soc.* **131,** 3522–3531 (2009).
98. Kan, Z. *et al.* Molecular Crowding Induces Telomere G-Quadruplex Formation under Salt-Deficient Conditions and Enhances its Competition with Duplex Formation. *Angew. Chem. Int. Ed.* **45,** 1629–1632 (2006).
99. Miyoshi, D., Karimata, H. & Sugimoto, N. Hydration Regulates Thermodynamics of G-Quadruplex Formation under Molecular Crowding Conditions. *J. Am. Chem. Soc.* **128,** 7957–7963 (2006).
100. Hancock, R. A role for macromolecular crowding effects in the assembly and function of compartments in the nucleus. *J. Struct. Biol.* **146,** 281–290 (2004).
101. Nakano, S., Karimata, H. T., Kitagawa, Y. & Sugimoto, N. Facilitation of RNA Enzyme Activity in the Molecular Crowding Media of Cosolutes. *J. Am. Chem. Soc.* **131,** 16881–16888 (2009).
102. Kumar, V., Endoh, T., Murakami, K. & Sugimoto, N. Dehydration from conserved stem regions is fundamental for ligand-dependent conformational transition of the adenine-specific riboswitch. *Chem. Commun.* **48,** 9693–9695 (2012).
103. Denesyuk, N. A. & Thirumalai, D. Crowding Promotes the Switch from Hairpin to Pseudoknot Conformation in Human Telomerase RNA. *J. Am. Chem. Soc.* **133,** 11858–11861 (2011).

Chapter 2 – Results and discussion

2.1 The action of nucleases in two-dimensional DNA origami objects – a study of DNaseI

Following our fundamental interest in studying protein-DNA interactions over DNA segments that are integrated within DNA origami objects, we started with an investigation of the stability of DNA origami against the action of Deoxyribonuclease I (DNaseI). DNaseI is an endonuclease that catalyzes the hydrolytic cleavage of phosphodiester linkages in the DNA backbone, and can cut the double-stranded DNA (dsDNA), and also the single-stranded DNA (ssDNA) with a lower cut rate [1]. DNaseI cuts DNA without relative sequence specificity [1]. Importantly for our study, the presence of cleavages in the DNA is a permanent signature of DNaseI successful interaction with DNA. Therefore, we plan to measure the progression of endonuclease reactions by measuring the composition of DNA origami-products as obtained from the degradation of an initial complete structure. A similar approach involving DNaseI has been extensively applied to profile genomic expression by mapping the regions of genomic DNA that are accessible to transcription factors [2].

We designed a comparative experiment of DNAaseI action with three forms of DNA: a triangular DNA origami, the M13mp18 ssDNA (M13 ssDNA), and the genomic dsDNA from calf thymus (genomic dsDNA). These DNA forms, were selected because are representative of different levels of molecular packaging and molecular order in solution. The M13 ssDNA is a circular DNA forms a random coil with a high level of molecular accessibility and disorder. The genomic dsDNA extract is likely to be comprised of longer DNA fragments than M13 ssDNA, but will share similar properties in terms of accessibility and molecular order. For simplicity, we selected the triangular DNA origami because it is the most rigid 2D DNA origami, and very well characterized by other groups in terms of physical properties and applications (as discussed in the Introduction).

We incubated the different DNA forms with DNaseI for 30 minutes, at 37˚C, at different enzyme concentrations (hereafter expressed in Kunitz Units, KU) in 50 µL of reaction volume. The reaction products were analyzed with Agarose Gel Electrophoresis (AGE), and the results are showed in Figure 2.1.

As expected, M13 ssDNA is highly accessible to DNaseI as it was completely degraded already with 0.5 mKU of enzyme.

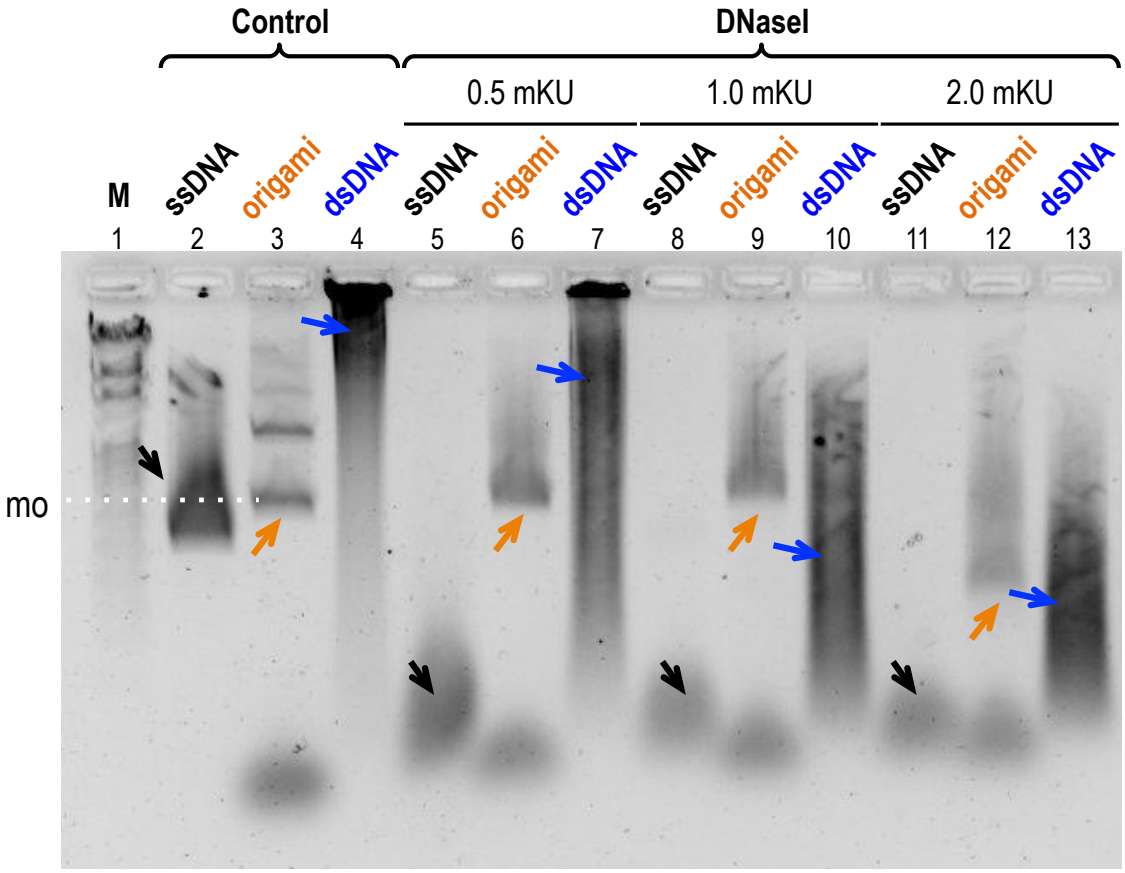

Figure 2.1. Stability of three DNA forms against DNAseI: triangular DNA origami, M13 ssDNA, and genomic dsDNA. The three DNA forms were mixed with the enzyme (see the indicated enzymatic units in the figure) and incubated for 30 minutes at 37˚C. DNaseI reaction products were analyzed with native agarose gel electrophoresis. Lane 1: DNA Molecular Weight Marker IV; lanes 2, 5, 8, 11: 10 µg of M13mp18 ssDNA. Lanes 3, 6, 9, 12: 3.76 µg of triangular DNA origami. Lanes 4, 7, 10, 13: 40 µg genomic dsDNA (calf thymus). Lanes 2, 3, 4 are control experiments performed with solutions lacking the DNaseI. Lanes 5, 6, 7 were incubated with 0.5 mKU of DNAseI. Lanes 8, 9, 10 were incubated with 1.0 mKU of DNAseI. Lanes 11, 12, 13 were incubated with 2.0 mKU of DNAseI. ssDNA = M13mp18 ssDNA, origami = triangular DNA origami, dsDNA = genomic dsDNA, mo = monomeric form of triangular DNA origami.

In contrast, genomic dsDNA displayed a lower accessibility to DNaseI as evidenced by a progressive degradation as a function of enzyme concentration. Since the DNAseI cleaves without sequence specificity [1], the product of genomic dsDNA

digestion is a distribution of fragments with the average length that progressively decreases as a function of enzymatic concentration. The triangular DNA origami is the most robust among the three investigated DNA forms. The band relative to the intact monomeric form of DNA origami can be found after incubation with 0.5 mKU and 1.0 mKU of enzyme, and remains a major component of the fragmentation pattern in the gel. With 2.0 mKU of DNaseI the triangle is compromised as is shown by a smeared band that reaches a molecular mass compatible with fractions of the intact DNA origami. In the gel of Figure 2.1, a gel band at a very low molecular mass is shown together with the triangular DNA origami. This band corresponds to the short staples that are in 5x excess of the M13 scaffold (during the folding reaction), and which remain in solution during the enzymatic reaction. Due to their presence, such staples could help increase the stability of the DNA origami objects as they provide a suitable substrate for the enzyme.

In conclusion, triangular DNA origami showed a higher resistance to the action of DNaseI with respect to both genomic dsDNA and ssDNA. What factors control enzymatic reaction in such DNA nanostructures?

Previous results of our group demonstrated that the activity of restriction enzymes is sterically hindered within surface-bound DNA nanostructures with densities ranging 0.5-10 x 10^12 molecules/cm2 [3,4]. Since the density of DNA helices across a section of any 2D DNA origami reaches a value of ~ 1.5 x 10^13 molecules/cm2, steric inhibition could play a role in the stability of DNA origami against DNaseI. DNA stability experiments performed with complex, three-dimensional (3D) DNA origami objects, using AGE and cryo-electron microscopy (cryo-EM) for analysis, was recently reported by Dietz and co-workers in a study published on Nature Methods [5]. The authors showed that 3D DNA origami objects had a greater resistance to DNAseI action as compared to plasmid dsDNA. They explained that DNA origami objects were shielded from DNAseI action because of the high level of packing of short dsDNA segments within the DNA origami structure. In a previous work, the Yan's group studied the stability of 2D and 3D DNA origami objects, and found results that are in substantial agreement with the results of our and Dietz's labs. In their experiments, Yan and co-workers incubated 2D DNA origami object and the dsDNA and ssDNA forms of the M13 scaffold with cellular lysates (that are rich of nucleases among other DNA-processing enzymes), and analyzed the results with AGE, atomic force microscopy (AFM), and electron microscopy. Interestingly, the results show that 1 h and 12 h long incubations leaves unaltered the DNA origami object, which migrate in gels very

similarly to control experiments. In contrast, they found that the unfolded DNA forms are highly affected by the lysates, and more easily degraded than the DNA origami [6].

Besides the high molecular packaging, DNAseI action was previously shown to depend on to the structure [7,8] and the mechanical properties[1] of the substrate DNA. In particular, the DNaseI action within 2D DNA origami could be inhibited by the structural motifs associated with the fact that each DNA duplex is linked to the adjacent by crossover junctions that occur every 16 base pairs. Crossovers are tertiary DNA structural motifs formed by branched DNA junctions with four-arms. Such motif as well as three-arms junctions have been shown to protect DNA from DNAseI digestion [7]. In addition, a recent study demonstrated that a DNA tetrahedron nanostructure, which is formed by the hybridization of 4 ssDNA sequences and with the vertexes consisting of three-arms branched junctions, showed dramatically enhanced resistance to DNAseI as compared to the distinct dsDNA components [9].

In addition to the high molecular packing and the complex structural motifs inside a DNA origami objects, it is remarkable that the persistence length of compact, 3D DNA origami is much higher than the one of dsDNA in the linear form, leading to a 15 to 38 folds increase of bending rigidity [10]. Such an increase of rigidity is achieved regardless the fact that the inner structure of 3D DNA origami objects is rich of defects because it is typically comprised of consecutive dsDNA segments of 16 bp. In turn, the distribution of mechanical stress or torsion on the dsDNA segments within a DNA origami may be an additional relevant factor affecting the action of nucleases.

Another aspect that may have some relevance in this regard is the presence of contours in 2D DNA origami or surfaces in 3D objects. These are likely to be the most accessible components of the inherent structures, and could introduce spatial hierarchies in enzymatic reactions.

In conclusion, many are the physical factors that could influence enzyme access, binding, and processing in large DNA nanostructures. Most of the studies addressing this problem however do not allow a quantitative characterization of such factors. A useful approach here would be to accurately analyze enzymatic reaction products as a function of their spatial coordinates within a DNA origami object. To achieve this, we decided to take advantage of the site-specific action of several type II endonucleases on the M13 scaffold sequence, as described in the following sections.

2.2 The action of endonuclease in two-dimensional DNA origami objects – a study of several type II restriction enzymes

Type II endonucleases, also termed type II restriction enzymes (REs), recognize and cleave a DNA sequence termed restriction site, with exquisite high specificity, mostly acting as homodimers. Many restriction enzymes has been resolved and characterized [11,12], and their biochemical activity has been deeply studied [1,13]. With the DNA origami technology it is possible to introduce a well-defined correspondence between a DNA sequence and its position(s) within the shape. In addition, the restriction sites available for each specific enzyme can be easily mapped in the file that contains path and sequence map, which is typically outputted by DNA origami design software (in our case Cadnano), using a simple text finder tool. In turn, REs are ideal workbench for studying protein-DNA interactions in dense DNA nanostructures.

In addition, REs are well established tools for DNA modification and are therefore essential tools for biotechnology with over 600 restriction enzymes being commercially available [14]. Therefore, understanding the action of REs on DNA origami objects will enlarge implementable functionalities of DNA nanostructures with the potential of opening the door to unprecedented biotechnology applications of DNA nanotechnology.

The circular M13mp18 ssDNA (M13 ssDNA) utilized to form DNA in this thesis is the common scaffold used to assemble DNA origami by folding different shapes by varying only the pool of staple strands [15–17]. To study the action of restriction enzymes on a DNA origami, we selected a set of 11 REs, namely BamHI, DraI, Hin1II, NlaIII, HaeIII, BsuRI, MspI, RsaI, Hpy4CHIV, HhaI and AluI, because they have several restriction sites along the M13 DNA sequence (see Appendix). The corresponding restriction sites are GGATCC, TTTAAA, CATG (for both Hin1II and NlaIII), GGCC (for both HaeIII and BsuRI), CCGG, GTAC, ACGT, GCGC and AGCT, respectively. Eight of the investigated REs and the corresponding number of sites in the M13 sequence are listed in Figure 2.2A. BamHI has only one site in M13, and mostly serves as control (not shown in Figure 2.2). NlaIII and Hin1II, HaeIII and BsuRI are two couples of isoschizomers, which means that the enzymes cleave the same restriction site. In turn, in principle, isoschizomers fragment the DNA scaffold folded in a DNA origami object in the same way, and only one of the enzymes for each couple is shown in Figure 2.2A.

We examined the action of such 11 REs on the M13 scaffold folded in three different forms, i.e., the triangular and rectangular DNA origami (chosen because they are two different, very well-characterized, two-dimensional DNA nanostructures) and

the circular M13 dsDNA. Since the latter has minimum packing level compared to DNA origami, it serves as control. The colored circles depicted in Figure 2.2B-D schematically indicate for each restriction enzyme the positions of all the corresponding, available restriction sites within the three DNA forms. Figure 2.2E depicts the fragments typically expected from the complete enzymatic digestion of the circular M13 dsDNA shown in Figure 2.2D.

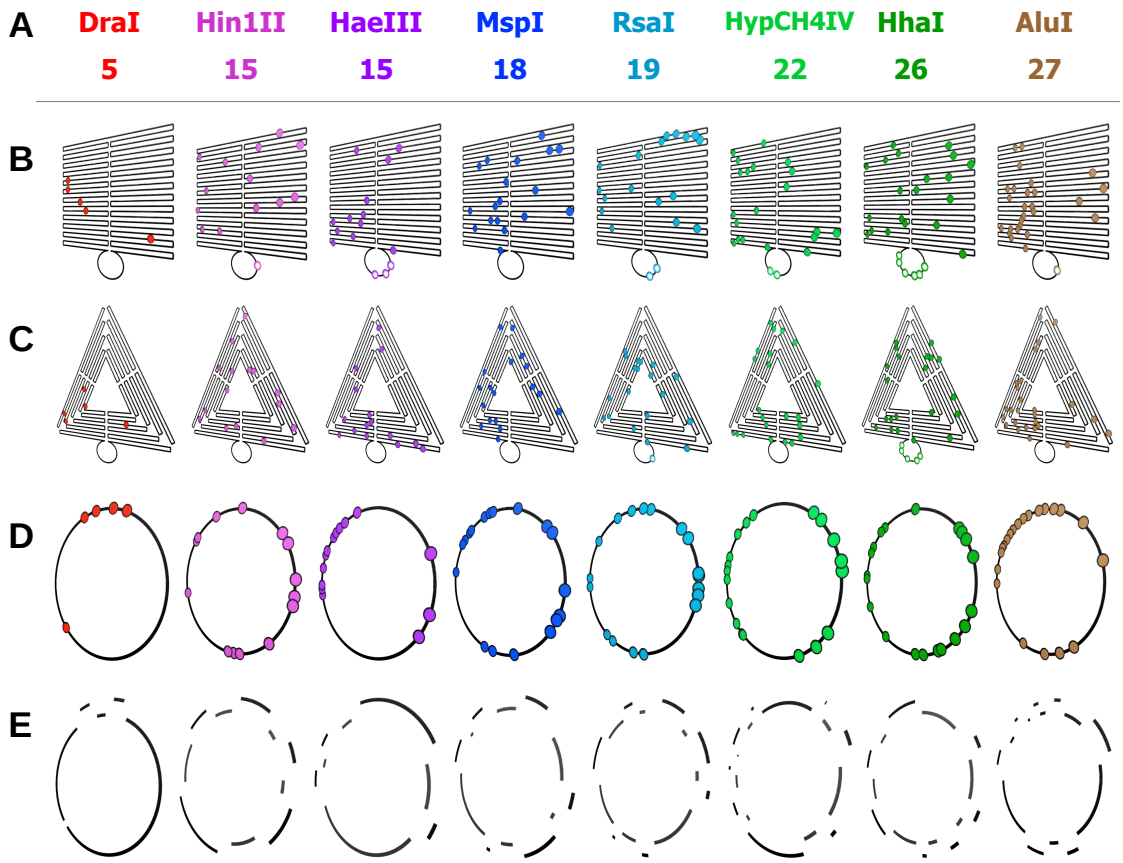

Figure 2.2. The restriction sites within the M13 DNA sequence have specific spatial distributions in the DNA origami objects. A) The list of investigated restriction enzymes and the number of corresponding sites within the M13 DNA sequence. B) Shows the spatial distributions of restriction sites in the rectangular DNA origami for each enzyme in A), C) is for the triangular DNA origami, and D) is for the circular M13 dsDNA. E) Schematically shows the complete fragmentation products for the M13 DNA.

Such sets of fragments can be obtained from the enzymatic reaction of a DNA origami only if the enzymes can successfully recognize and cleave all the inherent sites. Of note, the spatial distribution of restriction sites in the rectangular and triangular nanostructures depicted in Figure 2.2B-C, respectively, is not the only possible. In fact, several different sets of staples can be designed to obtain the same shape starting

from the same DNA scaffold. Each set corresponds to a different shift of the M13 sequence along the spatial coordinates of the folded scaffold (represented by the folded black line in each shape in Figure 2.2B-C), and in turn uniquely determines the spatial distribution of all restriction sites.

Triangular and rectangular DNA origami were synthetized according to previously reported protocols [15] and were purified from the excess of staples that was used to form them with a PEG-based method [18]. Figure 2.3 shows the limits of a microscopy-based approach in the analysis of our system. Here, the triangular DNA origami was treated with 10 units of MspI enzyme, for 1 hour at 37˚C. The reaction was stopped by quickly cooling the reaction through placing the tube in ice, while the analysis of the reaction products was performed immediately after reaction stopping. The results of topographic imaging by atomic force microscopy (AFM) shown in Figure 2.3 show that triangular DNA origami treated with MspI and untreated controls have indistinguishable shapes. Structural differences that could be attributed to specific enzymatic cleavage on the DNA origami cannot be detected by imaging the topography of the DNA origami at small scan size (Figure 2.3D).

The successful action of a restriction enzyme over a restriction site in a DNA origami leads to the local fragmentation of the ssDNA scaffold without alteration of the local folding. This because the scaffold fragments are kept incorporated within the nanostructure by the presence of unmodified, surrounding staple strands. Therefore, the inherent alteration of the DNA structure must be only near the restriction site, which has a typical length of 2 - 6 bp (i.e. 0.7 - 2 nm) depending on the enzyme. In turn, the accurate investigation of the behavior of restriction reactions within DNA origami would require sub-nanometer spatial resolution, which is very challenging even with state-of-the-art AFM. In addition, the scanning probe of the AFM can damage the DNA origami during imaging, and such structural changes could be erroneously interpreted as effects of enzymatic modifications.

In turn, due to the lack of spatial resolution, our AFM results are unable to inform on the behavior of MspI on the triangular DNA origami. Our AFM data however are in apparent agreement with AFM or other microscopy data previously reported by other groups that supported the conclusion that DNA origami display enhanced DNA stability against the action of several endonucleases and exonucleases in purified solutions, in cell lysates, or in fetal bovine serum [5,6,19].

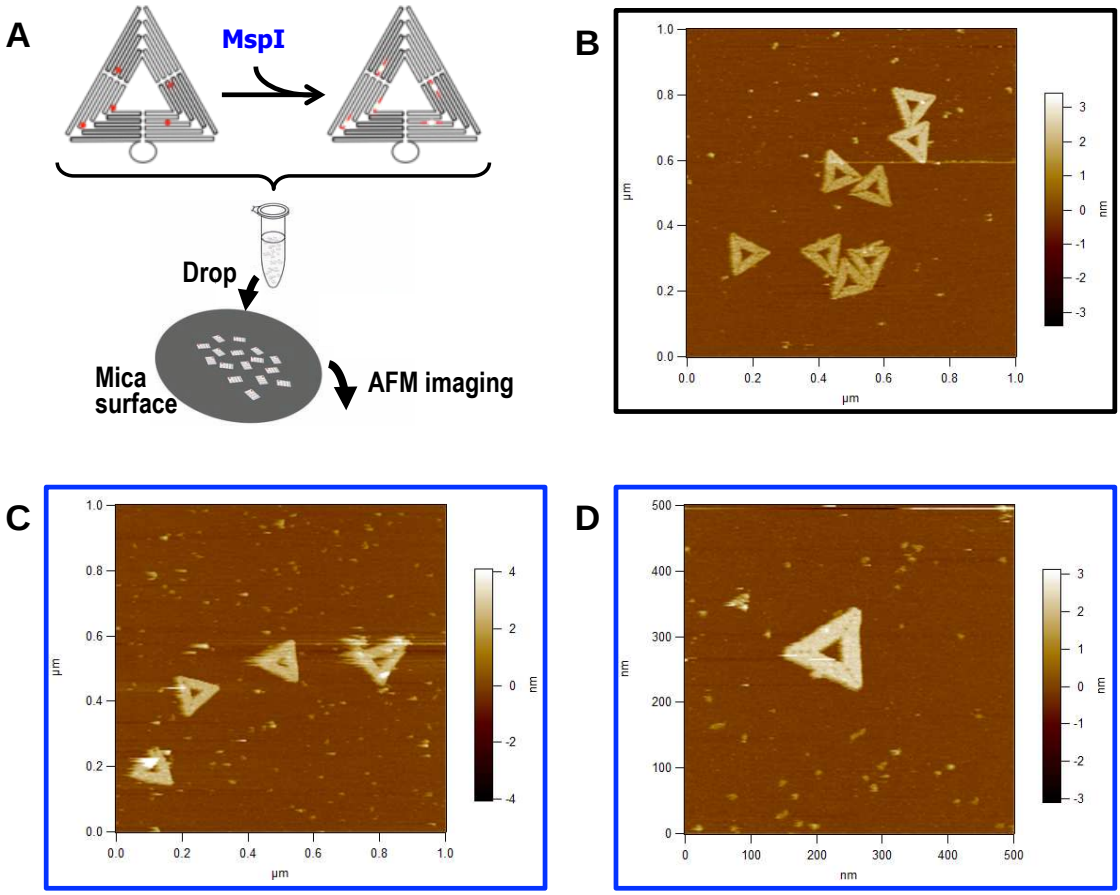

Figure 2.3. Triangular DNA origami treated with the MspI restriction enzyme and analyzed with atomic force microscopy (AFM). A) Schematically, the triangular DNA origami is self-assembled and purified from the DNA staples in excess (by centrifugation following addition of PEG in solution). Then the purified nanostructures are incubated with 10 units of MspI for 1 hour at 37˚C. Finally, 10 µL of treated DNA origami are loaded on a freshly-cleaved Mica surface to permit topographic imaging of the DNA origami with AFM. B) AFM micrograph of purified triangular DNA origami (control). C) and D) AFM micrographs of triangular DNA origami treated with MspI enzyme and acquired at different scan sizes. Color code: the brighter is higher. The results show no evident structural defects caused by the enzymatic reaction.

Similarly, also the use of native gel electrophoresis (e.g. AGE.), which has been extensively applied to characterize the synthesis quality and yield of DNA nanostructures [15,16], would unlikely permit the detection of such highly spatially localized, enzymatic modifications of the DNA scaffold backbone. So, the visualization of nanometric structural changes in DNA origami objects is a challenging task. For instance, the Dietz's group has developed a hybridization assay based on the use of fluorescently labeled, de-Bruijin probes aimed at quantifying the incorporation efficiency of DNA staples within DNA origami objects. Their primary scope was apparently to establish a general tool to assess the quality of synthesis of DNA

nanostructures for design optimization and mass production [20]. Remarkably, the lack of a staple in a DNA origami is likely to introduce a stronger structural defect than the cleavage of two phosphodiester bonds, which we need to detect in this work in order to study the action of restriction enzymes.

Therefore, we seek an optimized, high-throughput methodology to accurately study the behavior of eleven restriction enzymes in DNA origami that display several restriction sites for each enzyme. The approach followed in this work is to melt the enzyme-reacted DNA origami to separate its ssDNA components and detect the fragments of the M13 scaffold as depicted in Figure 2.4A. In fact, since the selected restriction enzymes can find less than 30 sites distributed over the >7000-nt-long M13 scaffold, the fragments are quite long (as graphically anticipated in Figure 2.2E), and therefore can be detected with gel electrophoresis (see Methods). For example, a single cleavage would transform the circular M13 scaffold into a linear strand; two cleavage events on the same DNA origami would produce two distinct fragments of the scaffold, and finally a complete digestion of the inherent sites would fragment the scaffold as it occurs in a fully unfolded dsDNA form.

Of note, following a similar approach, one could chose to analyze restriction reactions in DNA origami by detecting fragments of the inherent staples rather than scaffold. In fact, in DNA origami all restriction sites are formed by the hybridization of the scaffold with one or two staples. By following such an approach however, it requires to cope with the fact that the length of such staples is in the narrow range of 32 - 42 nt. This brings primary limitations in the use of gel electrophoresis for detecting staple fragments. In fact, gel electrophoresis is inaccurate for detecting DNAs that differ in sequence and have the identical length, and in addition, staples modified by enzymes would likely be as short as other unmodified staples in the background. An optimized approach to detect staple fragments produced by restriction reactions is underway in our laboratory, primarily involving polymerase chain reactions (PCR) or DNA sequencing, but will not be discussed in this thesis.

Figure 2.4B shows the results of a set of pilot experiments involving the structures depicted in Figure 2.2, which was carried out to explore the possibility of studying an enzymatic restriction reaction by detecting the inherent M13 scaffold fragments. After the self-assembly of both triangular and rectangular DNA origami objects with the standard protocol, the structures were purified from the staple excess used for promoting their formation as described above (see Methods). Such purification step is essential as it permits to remove background DNA molecules that contain restriction sites and which would therefore participate to the enzymatic reactions. The

enzymatic reactions were performed in solution at 37˚C, with the DNA substrate at 10 nM concentration and 10 units of enzyme (one at a time among BamHI, DraI, Hin1II, NlaIII, BsuRI, HaeIII, MspI, RsaI, Hyp4CHIV, HhaI and AluI) in 50 µL of reaction volume. The reactions were stopped after 1 hour with freezing obtained by incubating the reaction solution at -80˚C for 20 minutes. After stopping the reaction, all the DNA nanostructures were thermally denatured at 95°C for 3 min, followed by thermal shock obtained by incubating the sample into ice for at least 5 min to permit the irreversible dissociation of scaffold fragments from the initial, folded conformation. The enzymatic reactions products were analyzed with agarose gel electrophoresis. The use of dsDNA molecular weight markers allows estimating the molecular weight of the M13 dsDNA fragments.

Figure 2.4B shows that for each enzyme, the fragmentation pattern relative to the circular M13 dsDNA coincides with the expected pattern that was calculated from the M13 sequence using the open access software NEBcutter V.20 (http://nc2.neb.com/NEBcutter2/) that are not shown in this thesis. This finding demonstrates that reaction conditions permit the complete enzymatic degradation of the circular dsDNA, and that the inherent restriction sites are fully accessible. In turn, this dsDNA molecule serves as accurate control. Figure 2.4B also shows that for each enzyme we obtain different fragmentation patterns depending on the DNA origami shape. For both DNA origami objects, certain enzymes can reach and process several restriction sites of the M13 scaffold, as it is evidenced by the presence of multiple bands in the gels in Figure 2.4B. In particular, the range of molecular weights of the M13 fragments produced by the action of Hin1II on the rectangle, and of HaeIII, BsuRI, MspI, RsaI, HhaI and AluI on both shapes is higher than of the fragments generated by the action of the same enzymes on the circular M13 dsDNA. This observation suggests that several restriction sites within both DNA origami objects are inaccessible to the corresponding enzymes. In certain cases all sites are inaccessible as evidenced by the fact that the action of Hin1II on the triangle, BsuRI on the rectangle, and BamHI, DraI, and NlaIII on both shapes produces single gel bands that coincide with the results of the control experiments lacking the enzymes during reactions.

In turn, the results shown in Figure 2.4B demonstrate that the stability of DNA nanostructures to the action of endonucleases cannot be established univocally. In fact, although the length of the fragments associated with fully restricted M13 can be estimated from the gel bands, an accurate determination of which sites are enzyme-accessible in a background of non-accessible sites is a challenging task to achieve with gel analysis. In fact, the gel analysis demonstrates that several of such fragments

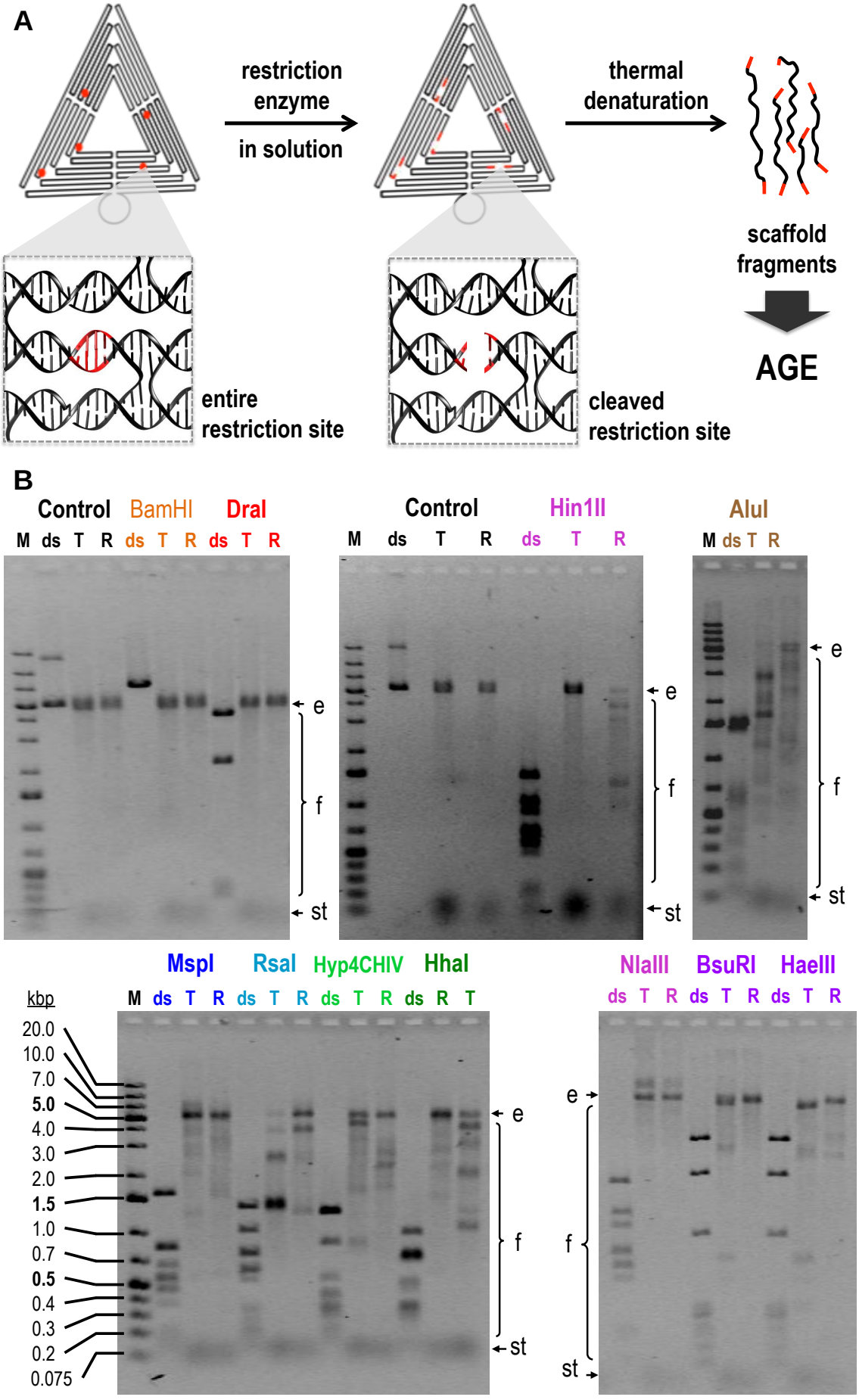
A
restriction
enzyme
in solution
thermal
denaturation
scaffold
fragments
AGE
entire
restriction site
cleaved
restriction site
B
Control
BamHI
DraI
M ds T R ds T R ds T R
e
f
st
Control
Hin1II
M ds T R ds T R
AluI
M ds T R
MspI
RsaI
Hyp4CHIV
HhaI
kbp
M ds T R ds T R ds T R ds R T
20.0
10.0
7.0
5.0
4.0
3.0
2.0
1.5
1.0
0.7
0.5
0.4
0.3
0.2
0.075
NlaIII
BsuRI
HaeIII
ds T R ds T R ds T R

Figure 2.4. Effects of restriction reactions on two-dimensional DNA origami. A) Schematic illustration of the approach adopted to detect enzymatic modifications within DNA origami objects. The self-assembled DNA origami objects were treated with the different enzymes at 37˚C for 1 hour, following purification of the DNA origami-containing solutions from background DNA molecules. The solution is then thermally treated to dissociate the DNA origami objects in their single-stranded DNA components. The sample is then analyzed with electrophoresis on a 1% agarose gel (AGE). B) The AGE analysis of reaction products for the triangular and rectangular DNA origami, and the circular M13 dsDNA for each of the 11 enzymes investigated in this study. For each case, the control experiments are carried out under identical conditions and lacking the enzyme. In this case, the reactions produce a constant migration pattern that is compatible with the unmodified scaffold. In particular, for the triangle and the rectangle there is a single gel band, while for the M13 dsDNA two distinct bands are seen. Here, the lower mobility band (top) corresponds to the relaxed circular dsDNA, while the higher gel mobility band (bottom) corresponds to the supercoiled form of the M13 dsDNA. For each enzyme, the fragmentation pattern of the circular M13 dsDNA coincides with the pattern expected for the cleavage of all the inherent restriction sites, indicating no stable folding of this form of the M13 DNA, which in turn can be used as control. Surprisingly, the effects of restriction reactions are changing between the triangular and the rectangular DNA origami. For the triangle, BamHI, DraI, Hin1II and NlaIII cannot generate multiple M13 fragments, while BsuRI, HaeIII, MspI, RsaI, Hyp4CHIV, HhaI and AluI generate several fragments. For the rectangle, a single fragment is found for BamHI and DraI, while Hin1II, BsuRI, HaeIII, MspI, RsaI, Hyp4CHIV, HhaI and AluI, demonstrate extended digestion of the inherent restriction sites. e = entire scaffold; f = fragments of the scaffold; st = staples involved in DNA origami self-assembly.

are >1000 bases in length and therefore they could derive from the cleavage of different combinations of restriction sites. Accurate sequencing of the enzyme products would allow mapping the fragments, although the task cannot be easily approached with current sequencing platforms. In fact, the available technologies allow sequencing DNA fragments of only a few hundreds nucleotides in length. In turn, the M13 segments should be further fragmented and complex bioinformatics analysis should be performed to reconstruct the sequence of the enzyme-produce segments by alignment of the shorter reads. In addition, validating such a method would require the generation of several M13 fragments with different lengths. A valid alternative could be the sequencing of the DNA scaffold fragments produced with nanopore technology.

Regardless the limitation described above, the gel electrophoresis results shown in Figure 2.4B provide qualitative information on enzyme-DNA interactions in the DNA origami. Almost all investigated enzymes having a 4-bp-long restriction site (i.e. Hin1II, BsuRI, HaeIII, MspI, RsaI, Hyp4CHIV, HhaI and AluI) are able to fragment the DNA scaffold, while the action of the two only enzymes having 6-bp-long sites is fully

inhibited in both nanostructures. In turn, Figure 2.4B suggests that the length of the site could affect the enzyme interaction with DNA origami objects. Restriction enzymes require the formation of a stable complex with dsDNA, and, in turn, the internal structure of the investigated 2D DNA origami objects comprised of 16-bp-long dsDNA segments could strongly affect enzyme's action. For example, structural studies of MspI and BamHI restriction enzymes in complex with DNA substrates revealed that the DNA region interacting with the enzyme is longer than the site length, i.e. 7 bp for MspI and and 11 bp BamHI [11,12]. In addition, a study on HindIII suggested that the enzyme binds at least two uninterrupted turns of the DNA helix to carry out the cleavage (i.e. 21 bp) including its 6-bp site [13]. Therefore, it is likely that presence of 16-bp-long DNA segments within DNA origami (corresponding to approx. 1.5 helical turns) challenges the inherent action of the two investigated enzymes with restriction sites of 6 bp (BamHI and DraI).

Figure 2.4B also illustrates differences in the action of isoschizomers, i.e. REs, which recognize and cleave the same sequence. BsuRI and HaeIII apparently produced the same fragmentation pattern in the triangle, with a slightly lower intensity of the gel bands relative to BsuRI. The action of the two enzymes, however, changes dramatically in the rectangle. In this case, HaeIII is able to cleave several restriction sites that are unaffected by BsuRI. The conclusions of a study on the behaviors of the isoschizomers HaeIII and BsuRI published by Wolfes and co-workers [21] suggest a possible interpretation of our results. They explain that the two enzymes have different binding mechanisms, as HaeIII would interact with both major and minor groove of the DNA duplex, while BsuRI would mainly bind in major groove [21]. Within DNA origami objects, therefore, it seems that enzymes that strongly interact with their sites are favored in cleaving them.

The second couple of investigated isoschizomers is Hin1II and NlaIII. Figure 2.4B shows that NlaIII can cleave none of the shapes, while the action of Hin1II can be successful only in the rectangular DNA origami. To our knowledge, there are not published studies of the mechanism of action of Hin1II and NlaIII. Following our analysis for HaeIII and BsuRI isoschizomers, it seems that Hin1II interacts with higher number of interactions (e.g. major and minor groove of DNA) while NlaIII could interact with fewer numbers of interactions (e.g. minor groove or major groove of DNA).

In conclusion, the analysis of the fragmentation pattern of the circular M13 scaffold as a function of the shape of the DNA origami objects treated with the same enzyme reveals that within DNA origami, restriction site accessibility for Hin1II, BsuRI, HaeIII, MspI, RsaI, Hyp4CHIV, HhaI and AluI depends on structural factors that are

inherent to the nucleic acid nanosystems. Thus, the same site along the primary DNA sequence of the scaffold could be accessible in one 2D DNA origami object and inaccessible in the other. Based on the fact that 1) overall structural properties such as DNA planar density, and regularity of the DNA texture is substantially shape-independent, while 2) the spatial distribution of sites can greatly vary from shape to shape, it is likely that the underlying differences in restriction site accessibility are associated with (small?) changes in the DNA folding within and near restriction sites.

2.3 The action of HhaI restriction enzyme in the DNA origami triangle – a study with single-site resolution

To examine which factors are involved in controlling site accessibility we designed an approach aimed at simplifying the number of variables involved in restriction reactions. Given the similar behavior of restriction enzymes with 4-bp-long sites, we focused on a single enzyme and one DNA origami shape (i.e. HhaI and the triangle, as it will be explained below). In the following paragraphs I will discuss the results and the motivations that led to our strategy.

It is known that restriction enzymes can possess the ability to process the single stranded DNA. This however is typically associated with a reaction rate much lower than that of dsDNA processing [22,23]. However, this ability could introduce a fraction of DNA origami objects that contain a few restriction sites in which only the staple strand is fragmented, while the site sequence on the scaffold is unmodified. Such a cleavage event, although unlikely, could not be detected with our method. We examined therefore the action of our investigated enzymes on the circular M13 ssDNA scaffold. We added the DpnII enzyme as control. Figure 2.5 shows the results obtained by incubating the M13 ssDNA with each enzyme for 1 hour at 37˚C. Reaction products were denatured with thermal treatment as described above, and immediately analyzed in 4% polyacrylamide gel electrophoresis in denaturing conditions with 8 M urea.

The gel shows that BsuRI, HaeIII, AluI, MspI, RsaI and Hyp4CHIV are able to cleave ssDNA into several fragments. HhaI, DraI, Hin1II, DpnII, BamHI and NlaIII instead produce a single gel band with electrophoretic mobility similar to that found in the control experiment, indicating that such enzymes substantially lack the ability to cleave ssDNA. Our findings are in agreement with previous studies of HaeIII [22,24], MspI [25] and HhaI [26]. Restriction enzymes framed in black in Figure 2.5 are those that can cleave at least one of the two DNA origami objects. HhaI and Hin1II are the only enzymes that can exclusively process dsDNA and also can process restriction sites in the DNA origami objects.

The action of HhaI and CfoI isoschizomers on GCGC site was investigated in a previous study [26]. The Authors utilized and designed single stranded DNA oligomers to contain the GCGC site and to inhibit the formation of stable duplex DNA segments in solution during enzymatic reactions. They found that both enzymes are unable to cleave the ssDNA substrates. Interestingly, they also demonstrated that HhaI can cleave long ssDNA substrates containing multiple sites with a reaction rate higher than its isoschizomer CfoI. They argue that such enhanced activity of HhaI is likely

associated with its ability to complex with transient duplex sites that form as a consequence of the presence of several restriction sites on the same long ssDNA molecule [26]. In fact, the sequence of a type II restriction site is palindromic, i.e. it coincides with its complementary sequence [13].

In Figure 2.5 however HhaI has a negligible activity on ssDNA M13 scaffold compared to others and looks a good candidate for our experiments. In addition, compared to other investigated restriction enzymes that are unable to process the circular M13 ssDNA scaffold, 1) HhaI has the highest number of restriction sites (26, see Figure 2.2) in the M13 sequence, and 2) its action is particularly effective on triangular DNA origami as it produces a major fragmentation pattern (see Figure 2.4B).

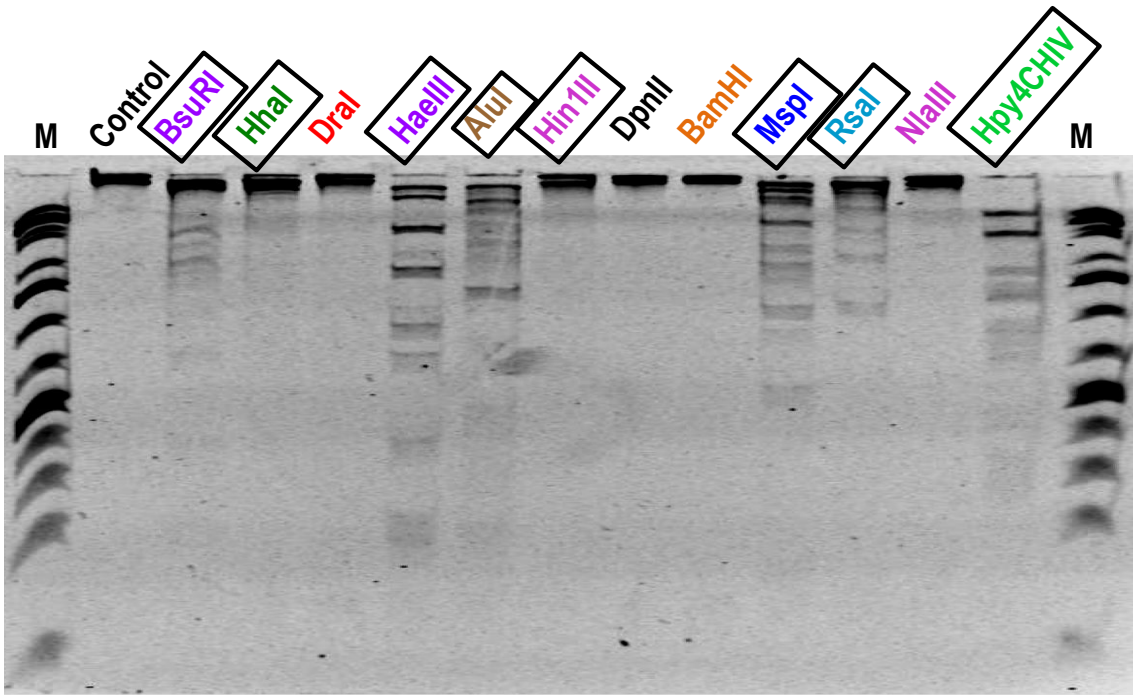

Figure 2.5. The action of the investigated REs on the circular M13 ssDNA scaffold alone. The circular M13mp18 ssDNA was incubated for 1 hour at 37˚C with 10 units of BsuRI, HhaI, DraI, HaeIII, AluI, Hin1II, DpnII, BamHI, MspI, RsaI, NlaIII and HpyCH4IV. Control experiments were carried out by incubating M13 ssDNA under identical conditions but lacking enzymes. The reaction products were analyzed with 4% polyacrylamide gel electrophoresis in denaturing conditions (8M Urea). BsuRI, HaeIII, AluI, Hin1II, MspI, RsaI, Hyp4CHIV (framed in black) are able to fragment the DNA origami objects , while HhaI, DraI, DpnII, BamHI and NlaIII are not.

We utilized HhaI to study the stability of restriction sites as a function of time. The results on HhaI kinetics are shown in Figure 2.6. The experiments were performed incubating 10 units of HhaI enzyme with M13 dsDNA, triangular DNA origami and rectangular DNA origami. The experiments were carried out following our established

protocol. This includes thermal denaturation of the DNA origami objects after stopping the enzymatic treatment, and the analysis of DNA scaffold fragments performed with electrophoresis in 1% agarose gel. The fragmentation of the circular M13 dsDNA was analyzed in gel immediately after stopping the enzymatic treatment, i.e. without thermal denaturation of the reaction products. Figure 2.6A shows that M13 dsDNA is degraded after 15 minutes of incubation, and the fragmentation pattern is constant for all the investigated incubation times. Figure 2.6B-C show that, similarly to Figure 2.6A, 15 minutes of incubation time are sufficient to produce the fragmentation patterns of the two DNA origami objects found in Figure 2.4B. For the rectangle in Figure 2.6C, the intensities of the inherent gel bands weakly depend on the incubation time, with the gel bands corresponding to lower molecular weights that become more intense as a function of time.

For the triangle in Figure 2.6B, and incubation time between 15 minutes and 2 hours, the gel displays very similar fragmentation patterns comprised of all the 5 major gel bands found in Figure 2.4B. Like for the rectangle, the gel bands corresponding to lower molecular weights become more intense as a function of time. Overnight incubation (14 hours) yields three distinct gel bands (with lower molecular weights) that partially overlap with the fragmentation pattern found for shorter incubations. In particular, one band appears at 2 h and becomes very intense after 14 h.

In the triangle the enzyme-accessible sites are mostly digested already after with 15 minutes. In turn, for those sites, the enzyme processivity in the DNA origami must be as high as in the M13 dsDNA. In contrast, the results shown in Figure 2.6 demonstrate that several restriction sites are irreversibly protected during the enzymatic reaction. This directly derives from the great difference between the saturated fragmentation patterns relative to the two DNA origami objects and that of the dsDNA control. In turn, our results indicate protein-nucleic acid interaction involved in the enzymatic reaction of HhaI digitally depends on structural constrains. As the enzymatic reaction proceeds, the occurrence of multiple cleavage events on the same M13 molecule (regardless its type of folding) leads to depletion of the fragments with higher molecular masses, towards the formation of the fragmentation pattern relative to overnight incubation. The reaction on the M13 dsDNA, however, reaches completion in 15 minutes, whereas in DNA origami objects it takes several hours to reach saturation.

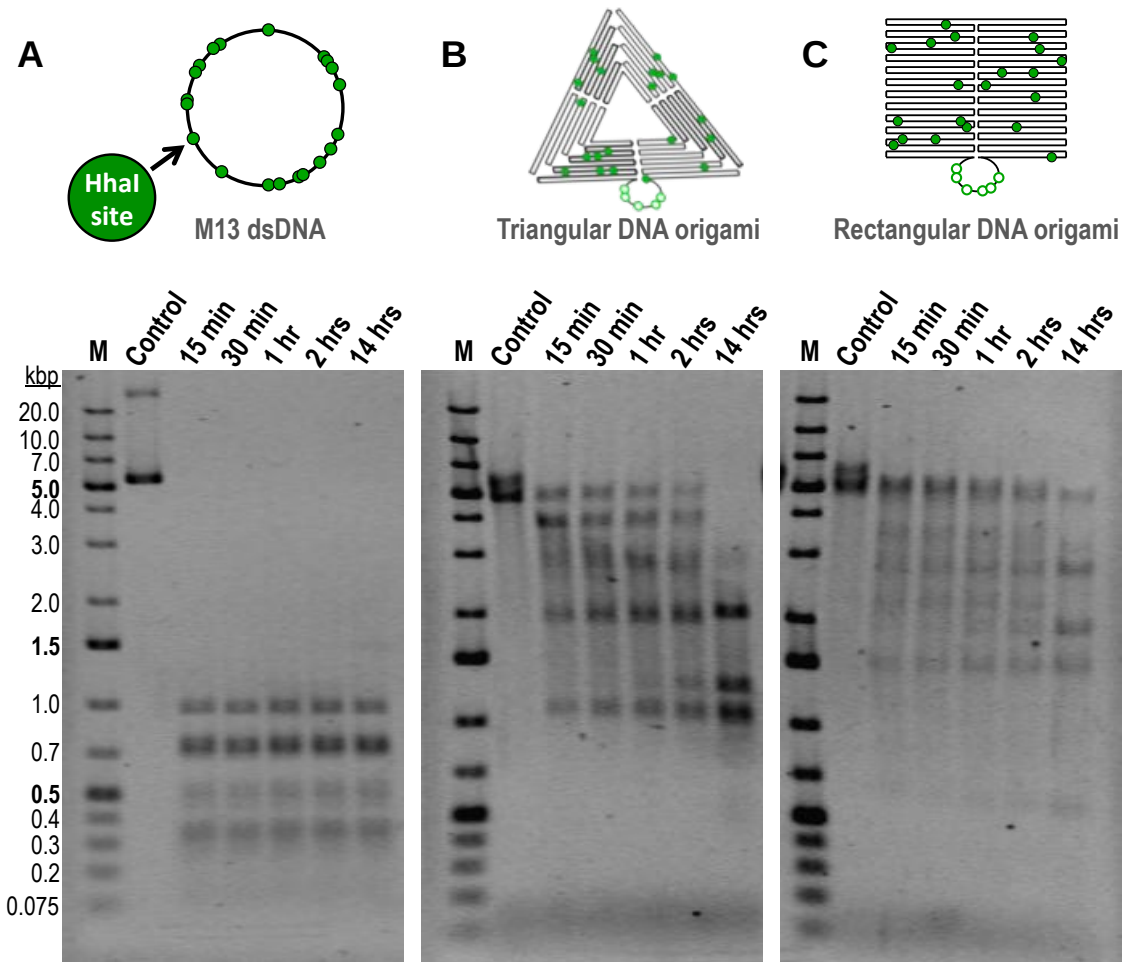

Figure 2.6. HhaI kinetics with DNA origami objects. (A) (top) Schematics of the M13 dsDNA and the inherent HhaI sites. (bottom) M13 dsDNA was incubated for the indicated amount of time at 37˚C with HhaI. The reaction products were separated in a 1% agarose gel. Control experiment was performed under identical conditions, but lacking the enzyme. (B-C) (top) Schematics of the triangular and rectangular DNA origami, and their inherent HhaI sites. The objects were incubated for indicated amount of times at 37˚C with 10 units of HhaI. After the reaction, the structures were melted by thermal denaturation and the reaction products were separated in a 1% agarose gel.

Restriction enzymes find their targets through two different mechanisms, i.e. either *via* three-dimensional enzyme diffusion in the reaction volume, or *via* one-dimensional diffusion (sliding) along the DNA molecule that contains the target sequence. In addition, short-range intramolecular “hopping” can contribute to the facilitated diffusion [[27]]. In this way restriction enzyme can sample many sites within the same dsDNA molecule, and an optimal length of approximately 100 bp was estimated to maximize enzyme performance [[27]]. These mechanisms explain the fast HhaI restriction on M13 dsDNA in our experiments, but do not explain our results with DNA origami objects. On the other hand, as discussed before, the internal structure of a 2D

DNA origami object is comprised of several 16 bp long dsDNA segments, which are expected to strongly inhibit the 1D enzyme diffusion. In turn, restriction enzymes interacting with DNA origami objects spend a significant amount of time in associating with and dissociating from DNA. In addition the cross-section of a M13 dsDNA molecule is likely bigger than that of a DNA origami objects because the DNA density in a DNA origami is the highest possible. In turn, an enzyme molecule may need too much time to find and bind to a DNA origami object.

To determine which sites are cleavable in the DNA origami objects we started from mapping the exact position of each HhaI site within the DNA origami objects as previously shown in Figure 2.2. Such an analysis was carried out using the graphical model of the nano-objects generated with the software that we used to design DNA origami objects, Cadnano [[28]]. This will permit a straightforward evaluation of the structural constrains that may have a role in determining the accessibility of restriction sites. The obtained map of HhaI restriction sites within the triangular DNA origami is schematically shown in Figure 2.7. For a high-resolution version that includes the explicit sequences of scaffold and staples see the appendix. Here, the HhaI sites were indexed in ascending order along the scaffold starting from its 5' end. The starting point for the enumeration is indicated in Figure 2.7. According to such indexing, sites 1 to 20 are located within the triangular shape, whereas sites 22 to 26 are located in the single-stranded, unstructured segment of the scaffold depicted as a loop in Figure 2.7. Site 21 is half within the structure and half unstructured.

Second, we generated simple, two-dimensional diagram depicting a region comprising three adjacent DNA duplexes of 32 bp (i.e. approx. 6nm x 11nm, respectively), as shown in Figure 2.8. Each diagram has one restriction site nearly in the center, and includes DNA origami objects structural features such as nicks, and crossover junctions along the inherent duplexes. Figure 2.8B shows that site 7 is involved in a crossover junction in the rectangle, while the same site is located within a duplex segment in the triangle. Since holiday junctions are known to inhibit the action of endonucleases, the diagrams described in Figure 2.8 suggest that restriction sites affected by major structural constrains are likely inaccessible to restriction enzymes. Similarly, other structural constrains may emerge within DNA origami objects that contribute to the shape-dependent fragmentations patterns shown in Figures 2.4 and 2.6.

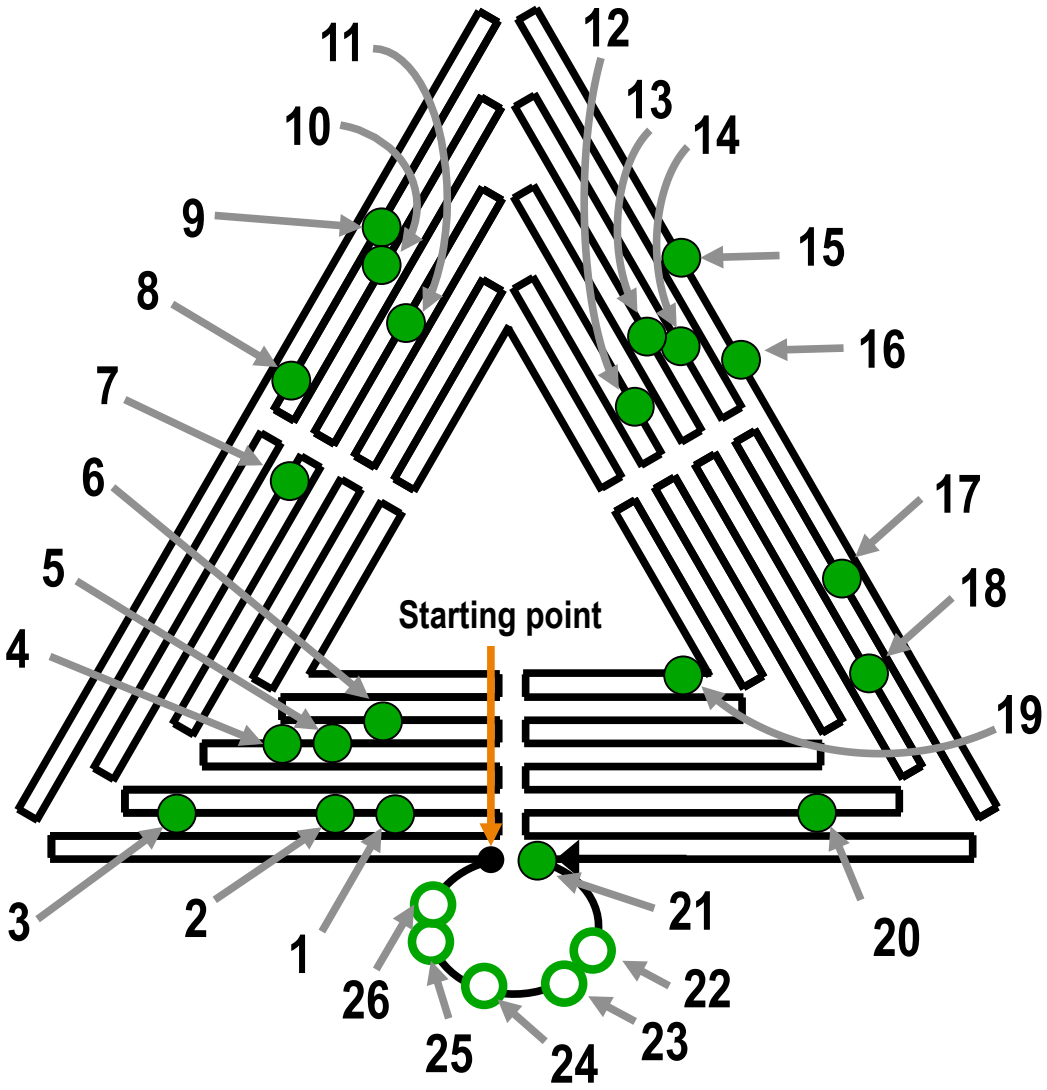

Figure 2.7. Schematic map of HhaI restriction sites in the triangular DNA origami. The sites are indexed in ascending order from 5' to 3', starting from the first nucleotide incorporated within the triangular shape (see the black dot). Solid green circles indicate restriction sites in which the scaffold is hybridized to one or more staples, while open green circles indicated sites located on the single-stranded region of the M13 scaffold.

In the following paragraph I will describe the experimental approach that we designed to analyze the enzyme-accessibility of restriction sites with single-site resolution. In addition, I will focus on the triangular structure because it provides clearer results with the agarose gel analysis shown in Figures 2.4 and 2.5. We anticipate that the approach consists in systematically turning off all but one the restriction sites within a DNA origami. This is achieved by 1) introducing a mismatch in the sequence of the restriction site in the staple strand that participates in forming the dsDNA site,

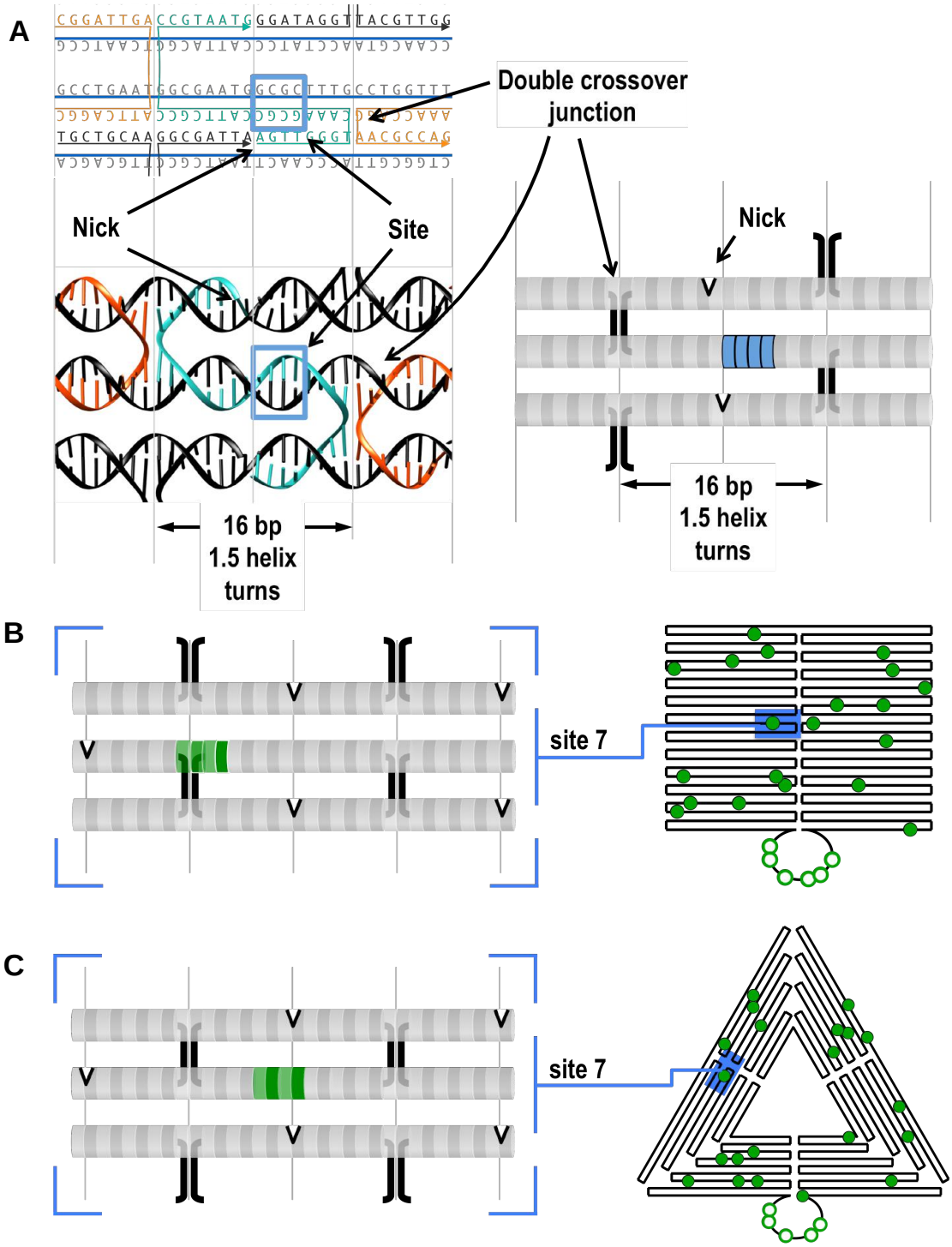

Figure 2.8. Diagrams representing the regions surrounding HhaI restriction sites within the investigated DNA origami objects. (A) On the left is shown a molecular illustration of a region of approximately 6nm x 11nm within a DNA origami object, obtained with DNA origami builder (Cadnano, top) and with a most established software tool for predicting the structure of DNA origami objects (CanDO, bottom) (see Methods). The restriction site (framed in blue) is nearly in the center of a duplex segment of 16 bp (1.5 helix turns) between two crossover junctions with opposite directions. The corresponding diagram is shown on the right. Here, dsDNA segments are shown as tubes, while the short segments with alternate brighter and darker grey represent

the inherent base pairs. Crossover junctions are illustrated as black lines connecting two adjacent dsDNA segments. Nicks are indicated by the indentations along dsDNA segments. (B) Diagram corresponding to site 7 (highlighted in green) in the rectangular DNA origami. Here, site 7 is formed by three DNA strands. Two are staples involved in a crossover junction. (C) Diagram corresponding to the same site 7 (highlighted in green) in the triangular DNA origami. Here, the site is located in a dsDNA segment.

and 2) exploiting the specificity of HhaI for dsDNA restriction sites. A prior analysis was dedicated to study the effect of changing one or two central nucleotides in the site of short duplexes using this approach. The results of the experiments are not show in this thesis, because we straightforwardly found that changing one nucleotide within the site is sufficient to inhibit HhaI enzyme action. Unpublished data from our group, however, revealed that the restriction enzyme BamHI is able to cleave a mutated, 6-bp-long site in surface-bound, densely packed DNA nanostructures. Similarly, triangular and rectangular DNA origami objects are comprised of dsDNA molecules that are densely packed, although only in two dimensions. To make sure that HhaI enzyme is fully inhibited within our modified restriction sites, we mutated two inherent nucleotides.

Figure 2.9A shows that we generated a modified version of the triangular DNA origami object that we termed “all-OFF”, and which has all HhaI sites turned off. We mutated the HhaI site from the native form 5’-**GCGC**-3’ by changing the sequence into 5’-**GATC**-3’ on the staple strand. Also, we turned off all the HhaI sites within the loop using opportunely designed complementary strands (see Appendix) with mutated sites. Figure 2.9B shows the unmodified version of the triangular DNA origami that we termed “ON”. The all-OFF triangle was assembled by incubating a mixture containing (i) the mutated DNA staple strands that hybridize to a site, (ii) all the other, unmodified strands not involved in the formation of HhaI sites, and (iii) the circular M13 ssDNA scaffold. The all-OFF and all-ON DNA origami objects were self-assembled and purified with established protocols (see Methods). Next, the objects were incubated with HhaI enzyme for 1 hour at 37˚. The reacted DNA origami objects were melted with thermal treatment and were separated and analyzed with AGE. The results in Figure 2.9C show that the reaction with the all-OFF triangular DNA origami produces a single gel band that is identical to the one obtained in the control experiment (lacking the enzyme), while with the all-ON version we obtained results comparable to those in Figure 2.4 and 2.6. These findings demonstrated that we found a consistent approach to turn off site reactivity within DNA origami objects.

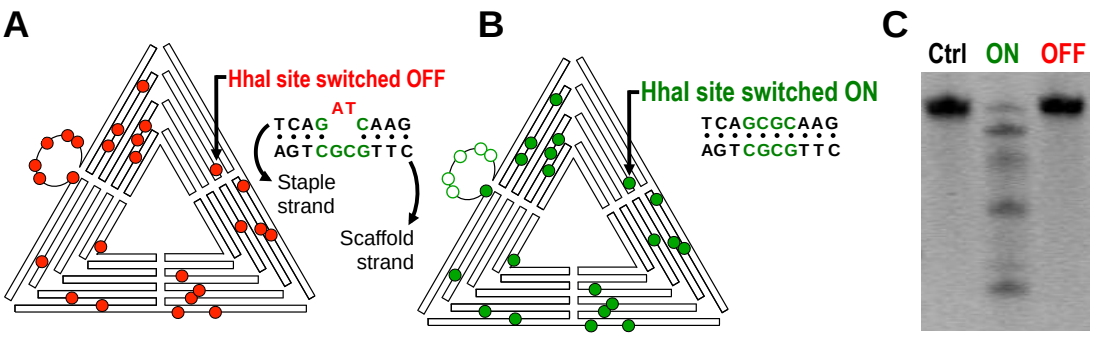

Figure 2.9. Methodology adopted to silence HhaI sites within DNA origami objects towards examining one site at a time. (A) Schematic illustration of the all-OFF triangular DNA origami that has all the inherent HhaI sites tuned off. The inset shows the mismatch introduced in the site within the staple strand to inhibit HhaI action. (B) Schematic illustration of the all-ON triangular DNA origami that has all HhaI sites correctly formed, while the sites within the loop are left in the single stranded form (and can hybridize with each other). The inset shows the unmodified HhaI site. (C) The picture shows the results for all-ON and all-OFF versions of the triangular DNA origami treated with HhaI enzyme. The enzymatic reactions were performed with 10 units of HhaI for 1 hour and at 37˚C. Afterwards, the structures were melted and than analyzed with 1% agarose gel. The control experiment was treated under identical reaction conditions but lacking the enzyme.

Following the approach introduced in Figure 2.9, we probed one by one the accessibility of all the HhaI sites within the triangle. Figure 2.10A shows the modified DNA triangle designed to test the accessibility of site 7. Here, only site 7 is correctly formed while the other sites are mismatched. In addition we activated a single site within the loop for reference. Such DNA origami was self-assembled by incubating a mixture containing (i) the staple strand carrying the correct sequence that hybridize to site 7 in the scaffold, (ii) all the other staple strands carrying the mismatched sequence to turn off all the other HhaI sites, (iii) all the unmodified strands not involved in forming HhaI sites, (iv) a set of additional DNA strands designed to hybridize in the loop to form the reference active site (site 24) and turn off the remaining sites (i.e. 22, 23, 25, and 26, see Figure 2.7), and (v) the circular M13 ssDNA scaffold. By varying the composition of the staples in such mixture, we selectively turned on and off the reactivity of HhaI restriction sites one by one.

Following this approach, any unreactive site cannot be cleaved (even when it is accessible to the enzyme), while the cleavage of a reactive site depends only on its intrinsic accessibility to HhaI enzyme. In turn, we generated modified DNA origami versions enabling a systematic analysis of HhaI sites accessibility within triangular DNA origami.

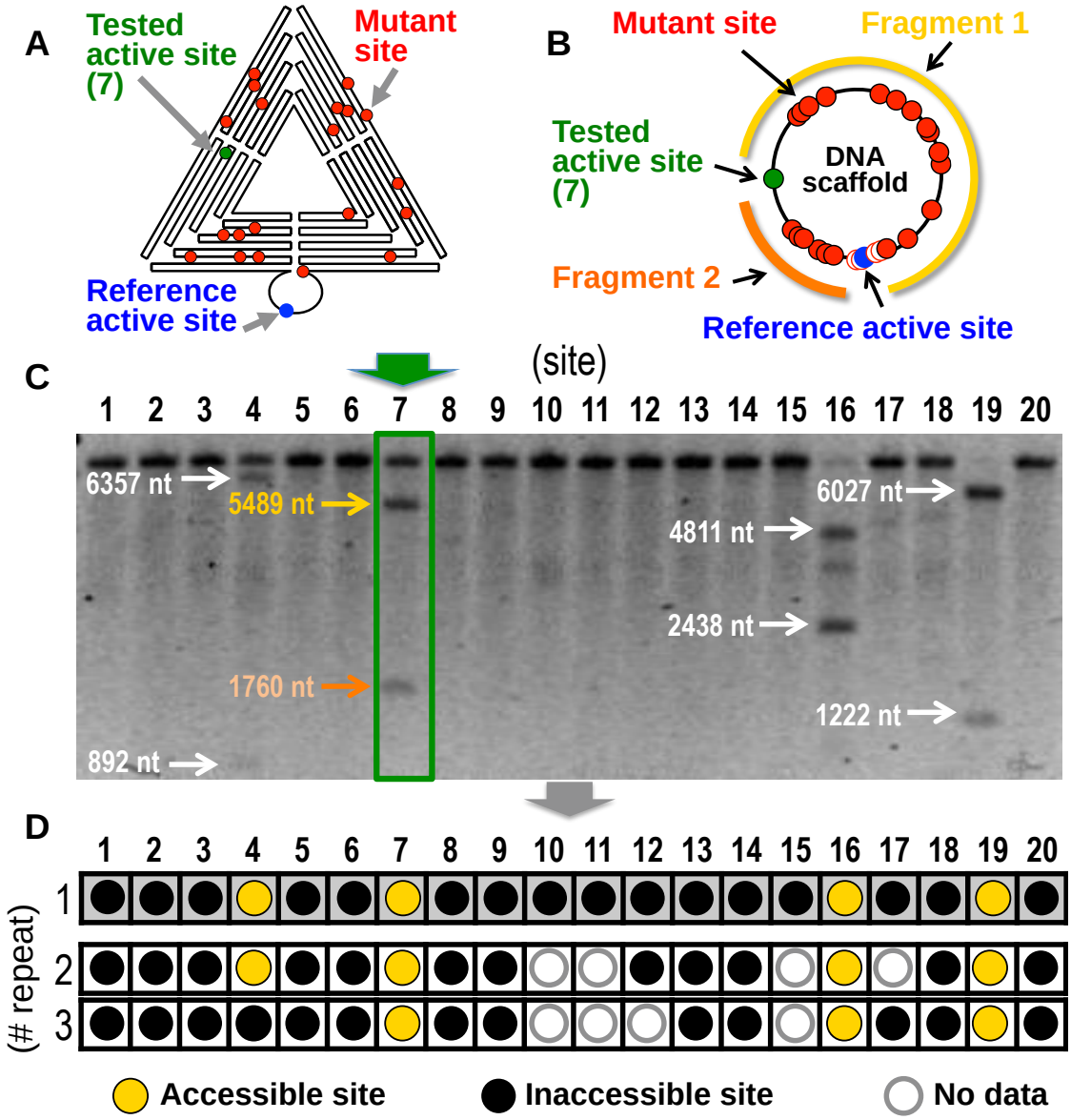

Figure 2.10. Measuring site accessibility of HhaI sites in triangular DNA origami with single-site resolution. (A) Schematics of the modified DNA triangle with a single, active HhaI site (i.e. site 7, green-filled circle) in the structure along with the reference in the loop (site 24, blue-filled circle). The other HhaI sites are silenced (red filled circles). (B) Schematic representation of the circular DNA scaffold used to form DNA origami with superposed HhaI sites with color code defined as in (A). The cleavage of sites 7 and reference produces two fragments with complementary lengths. (C) Results of the experiments for determining the site accessibility of HhaI sites within the DNA origami triangle with single-site resolution. For each lane, the activated site is indicated on the top of the gel. Near each band in the gel, the expected lengths of the fragments are indicated. The modified triangular DNA origami objects were incubated with 10 units of HhaI enzyme for 1 hour and at 37˚C. After the reaction, the structures were melted by thermal denaturation and the reaction products were separated in a 1% agarose gel. (D) The table shows the results of three repeats of the same array of experiments. The darker row depicts the results shown in (C).

The detection principle is described in Figure 2.10B. Here, the DNA scaffold is represented as a circular strand, and the HhaI sites are represented by circles with the same color code of Figure 2.10A. During the reaction, HhaI enzyme cleaves the reference site and introduces the first discontinuity in the scaffold, which linearize its sequence. If the tested site is accessible a second cleavage occurs that splits the scaffold in two fragments of complementary lengths that are visible in the gel.

The modified triangular DNA origami objects were self-assembled and purified with established protocols (see Methods). The purified DNA origami objects were incubated with 10 unit of HhaI for 1 hour and at 37˚C. The reactions were stopped by incubating samples for 20 minutes at -80˚C. The reacted DNA origami objects were denatured with thermal treatment, and analyzed by agarose gel electrophoresis.

Figure 2.10C shows the results of our site-by-site examination of DNA accessibility in the triangle. The gel in the figure shows that only sites 4, 7, 16 and 19 are clearly cleaved, while all the others are clearly unmodified by HhaI enzyme. Also, the bands relative to longer fragments generated by the enzymatic fragmentation of the M13 scaffold have different intensities, suggesting that different levels of accessibility may occur. A qualitative analysis based on band intensities allows ordering the restriction sites as a function of the enzyme product: site 4, site 7, site 16 and site 19.

We checked the specificity of the detected bands using the linear map of the HhaI sites shown in Figure 2.11. Using this tool, we calculated the length of the two M13 fragments that should be produced by cleaving site 24 (i.e. the reference) and each of the accessible sites indicated in Figure 2.10C. The results are listed below:

- site 4: 892 nt and 6357 nt;
- site 7: 1760 nt and 5489 nt;
- site 16: 2438 nt and 4811 nt;
- site 19: 1222 nt and 6027 nt.

A comparison of the expected fragments lengths and the height of the gel bands for each accessible site shown in Figure 2.10C indicates that the M13 fragments produced by HhaI enzyme match our expectations in each experiment.

Figure 2.10D shows schematically the results of three repeats of the array of experiments associated with the gel in Figure 2.10C. We obtained reproducible results except for the site 4. In addition, in the two positive experiments for the site 4, it showed two gel bands that had very low intensities.

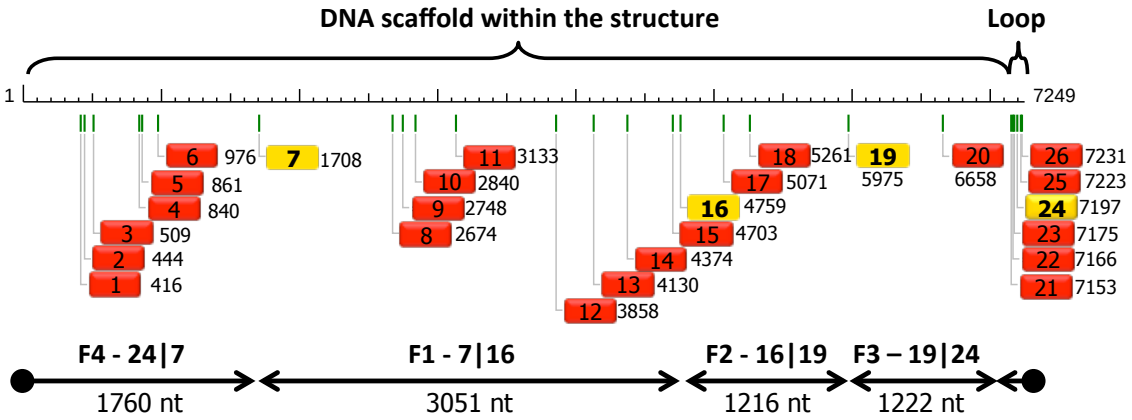

Figure 2.11. Mapping HhaI sites on a linear representation of the M13 DNA scaffold of the DNA origami triangle. For each site the map reports its index, and the distance from the starting point according to the criterion established in Figure 2.7. Shown on top are the portions of scaffold included within the structure and in the eternal loop. The sites identified in Figure 2.10 are highlighted in yellow. Below, are shown the fragments produced by cleaving all sites 7, 16, 19 and 24 together with the corresponding length for each M13 fragment. Our nomenclature: F1-7|16 indicates that fragment 1 is the fragment between sites 7 and 16.

Figure 2.12 shows a comparison of the results of HhaI kinetics on the triangular DNA origami (Figure 2.6B) with the results obtained with single site resolution (Figure 2.10C). The gel on the right in Figure 2.12, shows the fragments produced when a single site can be cleaved in the triangle. These bands serve as reference to estimate the lengths of the fragments associated with the 6 major gel bands that are produced by the HhaI reaction with the all-ON DNA origami triangle, shown on the left in the same gel. These bands are:

- Band 1, ~1200 nt;
- Band 2, ~1700 nt;
- Band 3, ~ 3000 nt;
- Band 4, ~ 4800 nt;
- Band 5, ~ 6000 nt;
- Band 6, ~ 7200 nt, corresponding to the linear or circular M13 ssDNA.

In the gel on the left in Figure 2.12, the products of the 1-hour-long HhaI reaction with the all-ON DNA triangle are consistent with those found in the other gel (see right) in terms of gel bands number and intensities. Also, the three gel bands found after overnight incubation (see gel on the left) are already present after 1 hour of reaction.

In turn, we were able to estimate the lengths of such stable products:

- Band 1, ~1200 nt;
- Band 2, ~1700 nt;
- Band 3, ~ 3000 nt.

Figure 2.11 shows that the single stranded DNA loop of the all-ON triangle contains 5 HhaI sites (22, 23, 24, 25, 26), which are very close. We calculated the secondary structures of the loop with the computation tool Mfold [29]. The results predict two possible foldings with ΔG of -24.62 kcal/mol and -23.47 kcal/mol, respectively. Furthermore, in both foldings, 2 fully duplex HhaI sites are formed (see Appendix). The formation of such secondary structures can be promoted by prolonging the incubation. In turn, the overnight incubation of the all-ON DNA triangle likely leads to a complete digestion of the restriction sites in the loop.

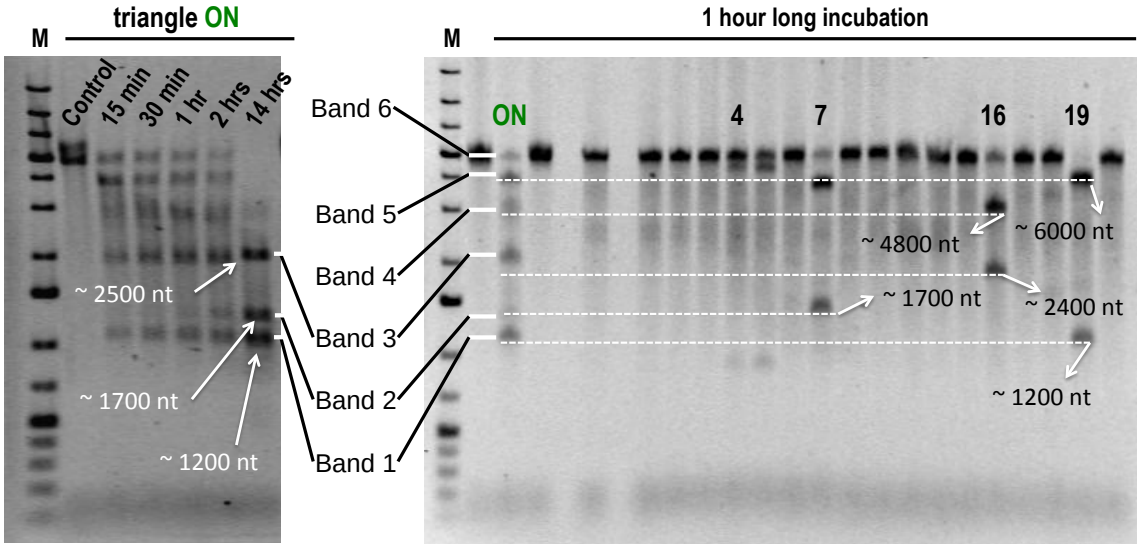

Figure 2.12. Comparative analysis of the results obtained on the kinetics of HhaI and its site-specific action in the triangular DNA origami. The experiments shown here are those described in Figures 2.6 and 2.10. On the right are shown the results from our investigation of HhaI site accessibility at single-site resolution. Here, the length of each fragment associated with gel bands for sites 7, 16 and 19 were calculated and displayed on the gel. The all-ON triangle incubated for 1 hour with HhaI leads to the six bands shown on the right in the same gel. The length of the fragment for each of such bands was estimated from the bands on the left, which correspond to fragments of known length. On the left are shown the results relative to the kinetics of HhaI on the all-ON triangle. The length of the stable fragments that emerge after overnight incubation were estimated from the gel on the left and coincide with the inherent bands labeled as 1, 2 and 3 in the figure, and which are already present after an incubation of 1 hour.

Figure 2.11 shows the calculated number of fragments and their lengths in the case that sites 7, 16, 19 and 24 (in the loop) of the all-ON DNA triangle are fully cleaved by HhaI (adding more cleaved sites in the loop would lead to negligible differences in the calculation):

- Fragment 1 from 3' end of site 7 to the 5' end of site 16 (hereafter termed as F1 7|16) = 3051 nt;
- F2 16|19, 1216 nt;
- F3 19|24, 1222 nt;
- F4 24|7, 1760 nt.

We compared these numbers with the estimated lengths of the fragments relative to the all-ON DNA triangle after overnight incubation, and found a good match with the fragments generated by cleaving sites 7, 16, and 19. In fact, Band 1 in Figure 2.12 has an estimated length of 1200 nt and is compatible with fragments F2 and F3 that have calculated lengths of 1216 nt and 1222 nt, respectively. Similarly, Bands 2 and 3 in Figure 2.12, with estimated lengths of 1700 nt and 3000 nt respectively, are compatible with fragments F4 and F1 that have calculated lengths of 1760 and 3051, respectively.

These results indicate that sites 7, 16 and 19 are accessible in the unmodified triangular DNA origami, while site 4 is not (see Figure 2.13), although the single-site analysis shown in Figure 2.10 seems to suggest that it is. Figure 2.7 shows that the site 4 is located nearby the site 5 and 6. So it could be that the accessibility of site 4 increases in our experiments with mismatched sites. In fact, the mismatches in sites 5 and 6 introduce flexible DNA motifs that are absent in the unmodified DNA triangle, and which could contribute to a mechanical relaxation over or near site 4.

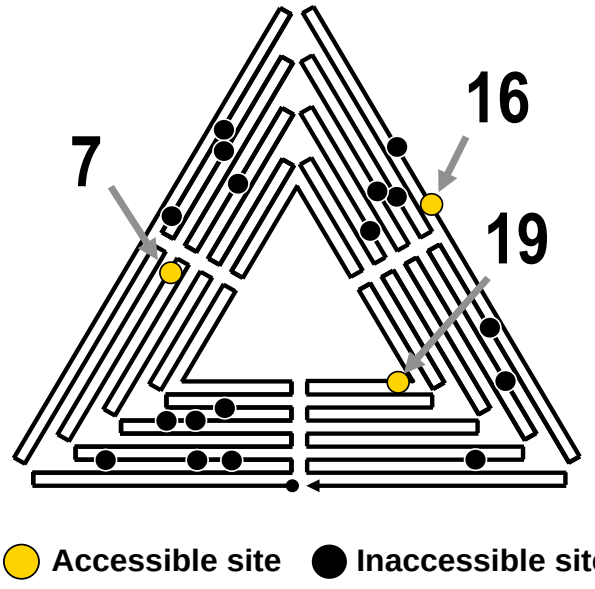

Figure 2.13. Schematic map of the DNA origami triangle with all the HhaI restriction sites.

With our experimental approach we unequivocally found that only sites 7, 16, and 19 are fully accessible by the HhaI enzyme. Strikingly, our results demonstrate that in the nanostructure, the HhaI reaction behaves in a step-wise fashion with certain sites that are cleaved mostly after a few minutes of incubation and the others that remain stable for several hours. These results indicate that protein-nucleic acid interaction involved in the enzymatic reaction of HhaI digitally depends on structural constrains, and could be fine tuned by design.

2.4 Towards a predictive model of restriction enzyme action in two-dimensional DNA origami objects

The results discussed in the previous sections substantially demonstrate that a DNA sequence within a 2D DNA origami object unless fully accessible to endonucleases is stable against their action. We found that site accessibility depends on the shape of the inherent DNA origami object, thus suggesting that site accessibility depends on merely structural properties inherent the DNA. We believe therefore that our results introduce the unprecedented possibility to digitally control a biochemical reaction in a DNA origami exclusively based on the inherent DNA structural features.

DNA origami technology has led to an impressive progression of software tools to design and evaluate the physical properties of DNA origami objects. So far however, little information on the reactivity of DNA origami has been encoded in such tools. So, in the following section I will describe a model that was developed in our laboratory, and that consistently explains our results on the action of HhaI on the triangular DNA origami, as obtained with single-site resolution. The long-range goal is to develop a predictive model that allows designing DNA nanostructures with desired functional properties based on its stability against nucleases.

Figure 2.14 depicts our approach based on the application of the simple diagrams already introduced in Figure 2.8 that schematically represent DNA molecules near restriction sites, including the inherent crossover junctions between adjacent dsDNA segments, and the nicks within such dsDNA segments. Such diagrams allow measuring the distance between each nucleotide of a restriction site and the nearest structural features (Figure 2.14A and B), and the spatial distribution of structural constrains and features with respect restriction sites (Figure 2.14C and see also Figure 2.15) as well as the relative distance between these elements (Figure 15C). In addition, the diagrams allow detecting the presence of “unit cells” comprised of adjacent dsDNA segments that are joined by two consecutive crossover junctions. As shown in Figure 2.15D, the width of such unit cell is of 32 bp (i.e. 3 helix turns) and is consistent with the structure of the B-DNA form. Within a unit cell, the orientation with respect to the plan of the 2D DNA origami of the nucleotides that form a restriction site can be easily calculated, as shown in Figure 2.14E.

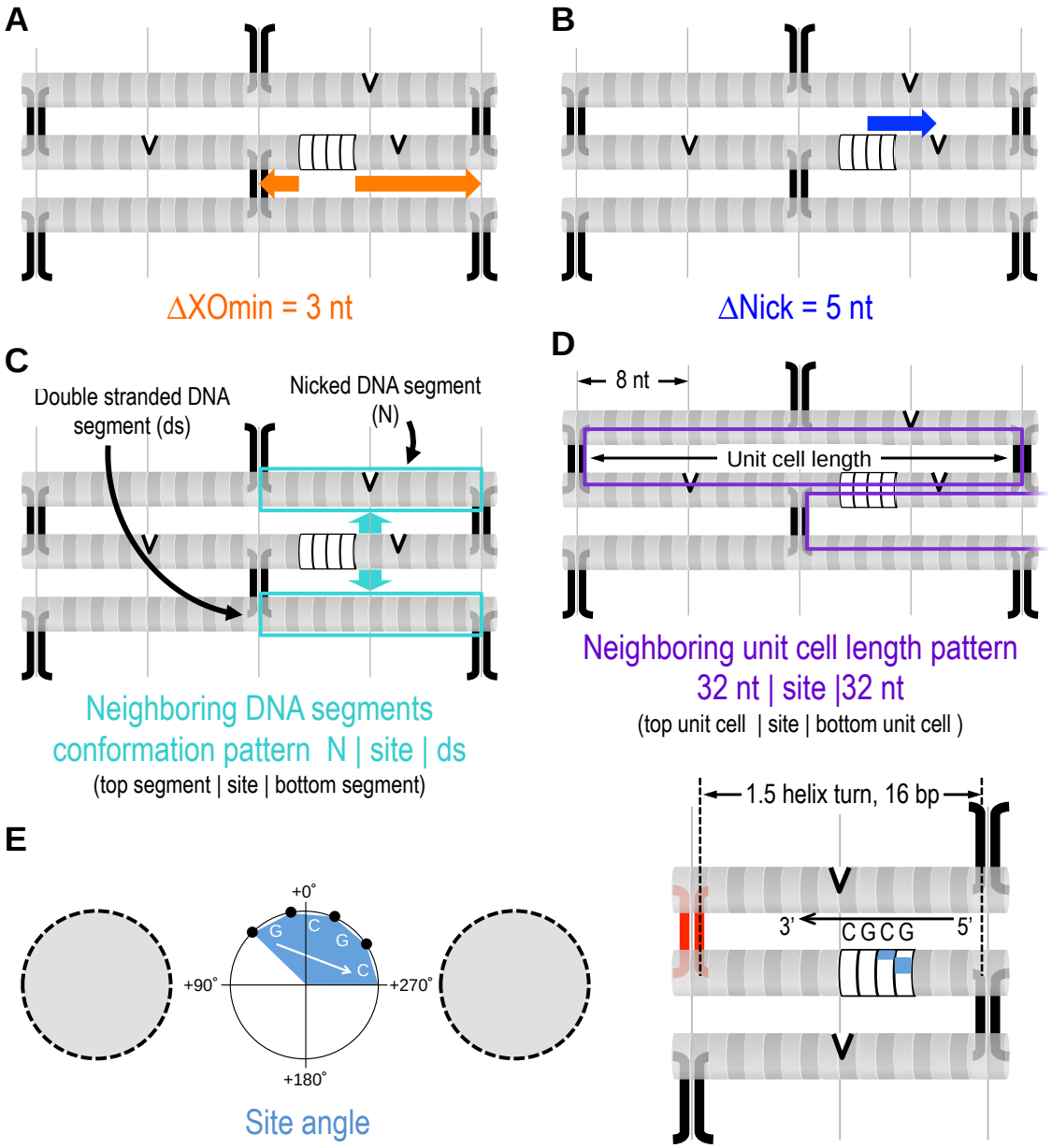

Figure 2.14. Use of diagrams for studying the effect of local structural constrains on the reactivity of restriction sites in 2D DNA origami. This figure shows major structural parameters associated with restriction sites, using the diagram described in Figure 2.8. (A) Distance measured in bp between a restriction site and the nearest crossover junctions. For each restriction site, ΔXOmin is the minimum distance between each crossover and a starting or ending nucleotide of its 4-nt-long sequence. (B) Distance measured in bp between the center of a restriction site and the nearest nick along the site-containing dsDNA segment (ΔNick). (C) Conformation of the DNA segments adjacent to the site. Shown is a site flanked by a nick-containing DNA segment and a fully formed dsDNA segment. In our nomenclature, this configuration is termed “N | site | ds”. (D) Size of the unit cells that contains a restriction site. Each site belongs to two adjacent cells with width of 32 bp (the cell at the bottom is shown in part). (E) Determination of restriction site orientation with the diagram representing the site. In 2D DNA origami used in this study, the rotation angle between two consecutive base pairs (i.e.

two bars in the ladder model) is $3\pi/16$. In addition, the base pairs near crossover junctions are nearly parallel to the nanostructure surface (see also Figure 2.8A). The diagram on the right in panel E shows a dsDNA segment of 16 bp located between two consecutive crossovers, which correspond to 1.5 helix turns. An HhaI restriction site (5'-GCGC-3') starts at 9 bp from the crossover on the left (in red). The blue squares in the schematic site are the phosphate groups over the inherent staple strand, and an arrow indicates their 5'→3' direction. On the left, three circles depict the section of the adjacent DNA duplexes in the diagram on the right. A polar graph in the center shows (with black dots) the angles of the DNA base pairs forming the HhaI site with respect to the orientation of the crossover in red (right). The arrow indicates the 5'→3' direction of the staple strand. The blue-filled area in polar graph depicts the position of the major groove of the restriction site with respect to the flanking DNA duplexes (grey-filled circles).

Following our approach, we generated a diagram for each HhaI site as shown in Figure 2.15.

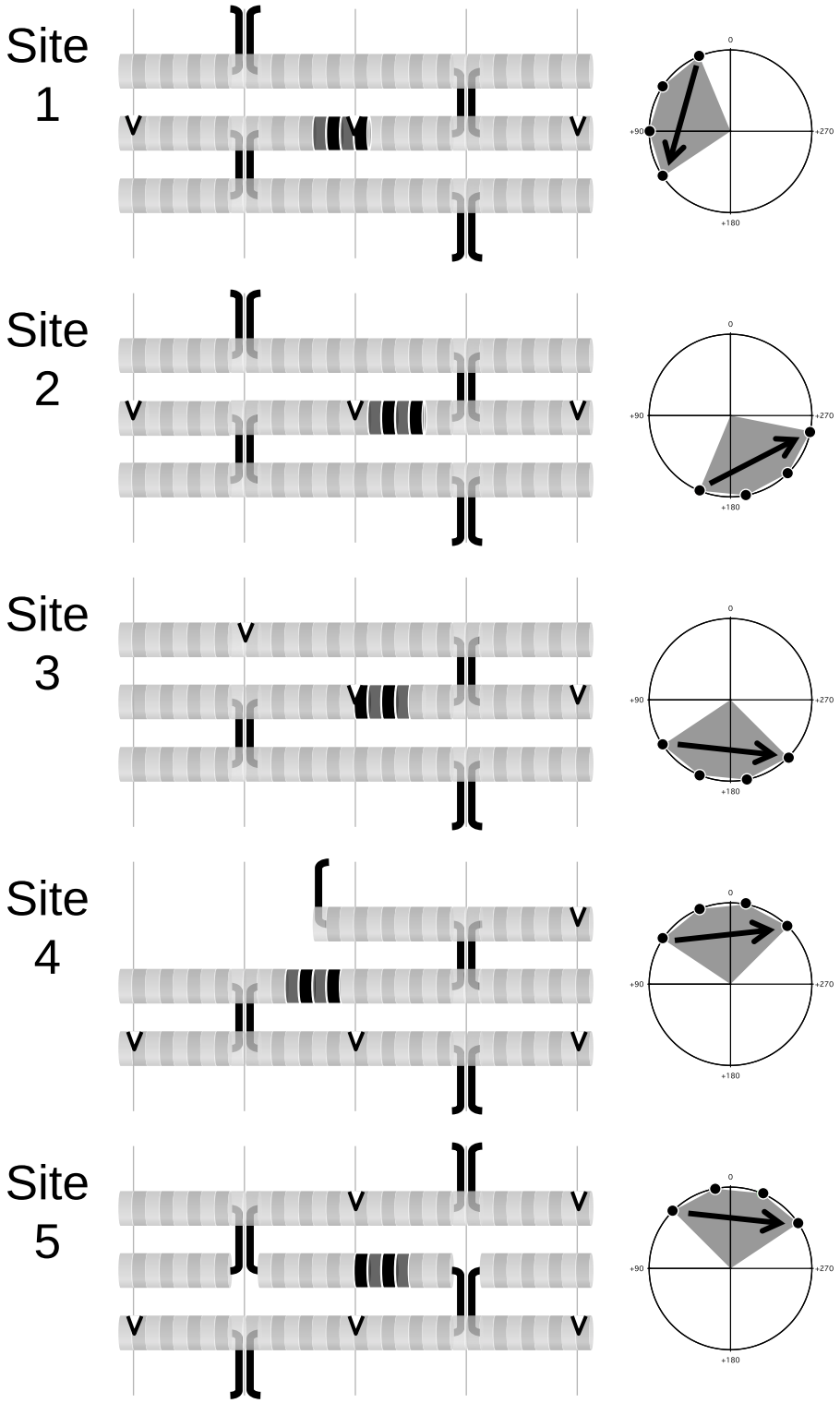
Site 1
Site 2
Site 3
Site 4
Site 5
0
+90
+270
+180

Site 6

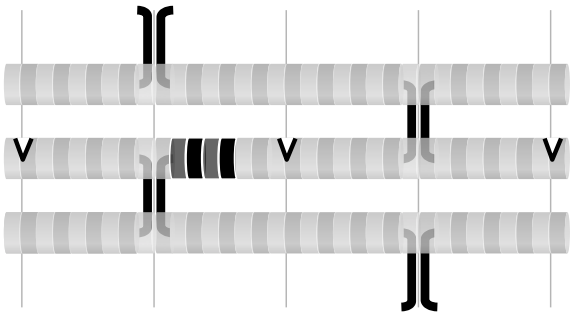

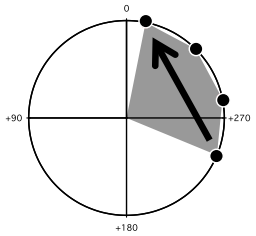

Site 7

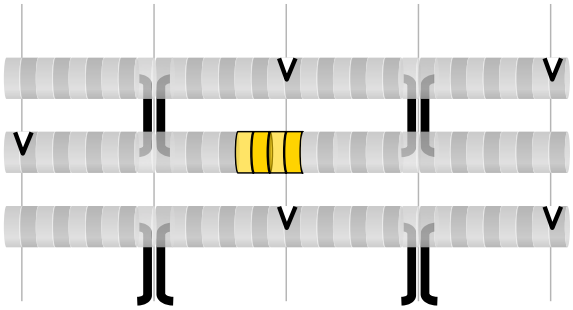

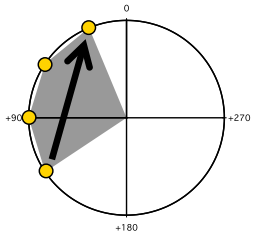

Site 8

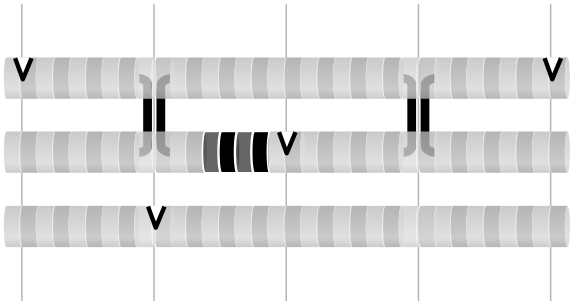

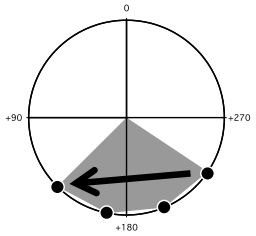

Site 9

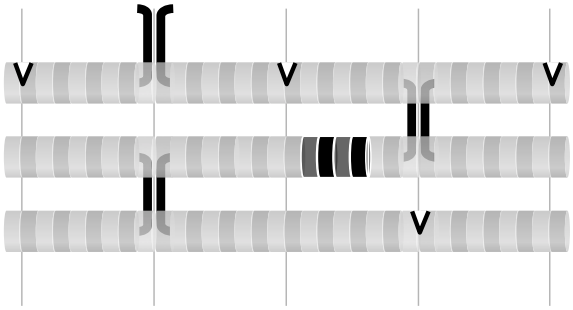

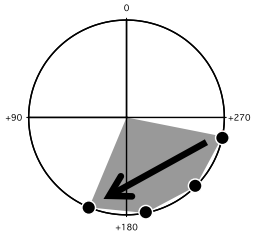

Site 10

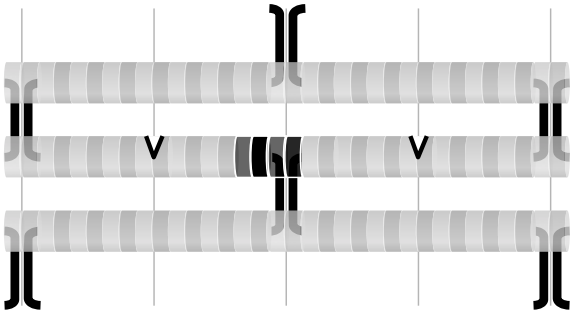

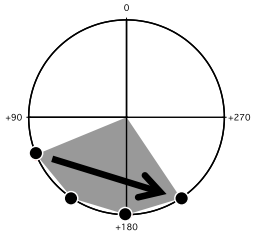

Site 11

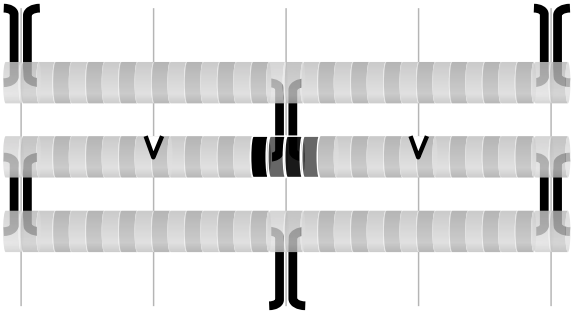

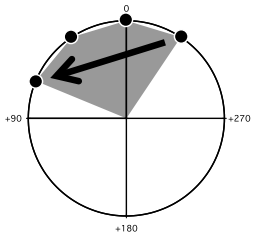

Site 12

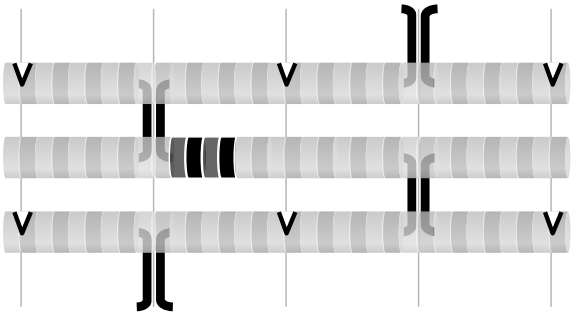

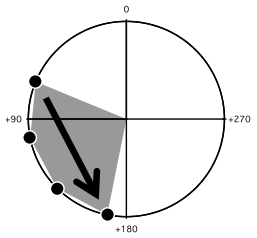

Site 13

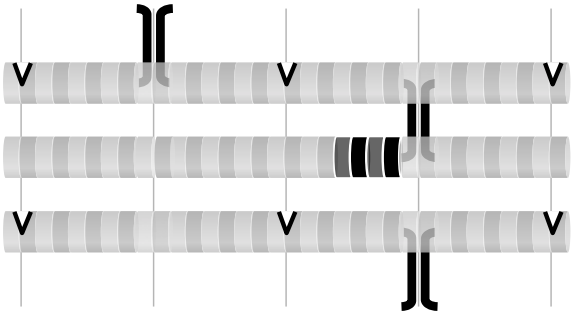

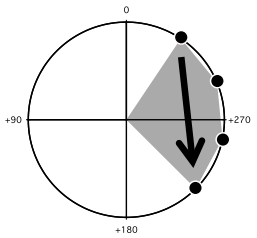

Site 14

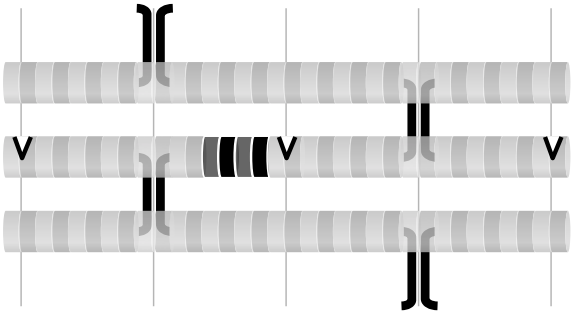

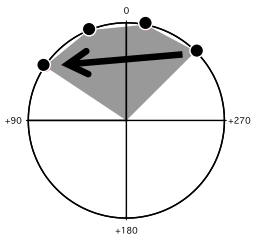

Site 15

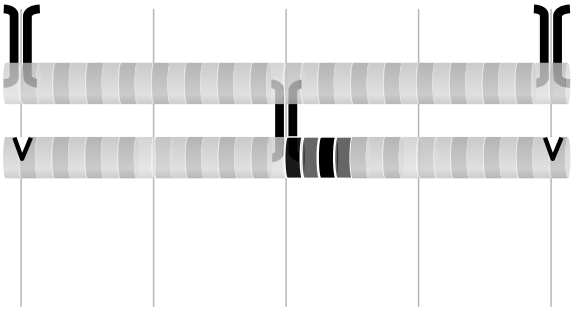

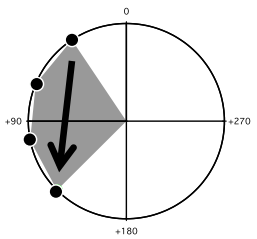

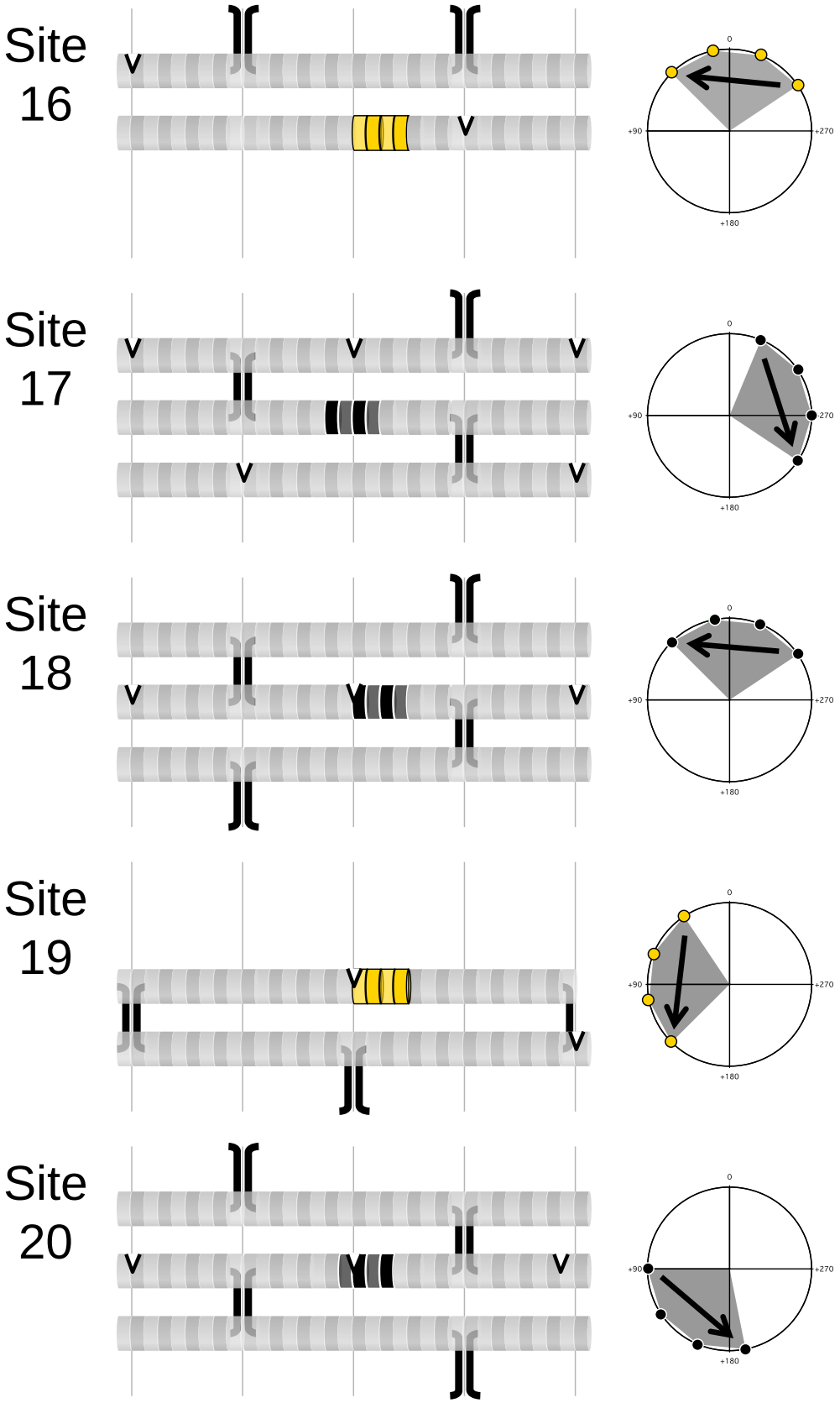

Figure 2.15. Diagrams are generated for each HhaI restriction site within the investigated triangular DNA origami. In particular, sites 4, 15, 16, and 19 are located on the edge of the DNA origami triangle, and in turn their corresponding diagrams lack one dsDNA segment. For each diagram on the left, we derived a polar graph on the right that shows the angle of each base

pair in the site (dots). According to Figure 2.14E, in each polar graph, an arrow indicates the 5'-3' direction of the inherent staple strand, while the grey-filled area indicates the position of the major groove of the restriction site with respect to the flanking DNA duplexes. The sites are colored in black if inaccessible to HhaI, and in yellow if accessible to the restriction enzyme (see Figure 2.10).

2.4.1 Presence of a crossover junction that overlaps with a restriction site

The experiments shown in Figures 2.10 and 2.12 demonstrate that all the sites that overlap with a crossover junction cannot be cleaved by HhaI, regardless their position in the triangular nanostructure (namely sites 10, 11 and 15, as schematically shown with diagrams in Figures 2.13 and 2.15). This finding is consistent with former studies showing the ability of secondary and tertiary DNA structures to inhibit the site-specific action of endonucleases [13]. In addition, Lu and co-workers demonstrated that nucleotides close to 3 and 4 arms branched DNA motifs inhibit the nuclease activity of DNaseI that lack site-specificity [7]. The tertiary structures investigated in their study are very similar to crossover junctions present in our DNA nanostructures. We can conclude that a site overlapping with a crossover junction is inaccessible, however, beyond the crossover itself, also the proximity to the crossover junction could be involved in controlling site accessibility.

2.4.2 Presence of a crossover junction located near a restriction site

Crossover junctions are essential components of any DNA origami object. Consistently with our results discussed above and of others, the presence of such tertiary structures in DNA origami is likely to positively contribute to the stability of the nucleic acid to the action of endonucleases. In our experiments with the triangular DNA origami, however, only 3 restriction sites overlap such a junction.

In turn, the proximity between a crossover junction and a restriction site may influence its reactivity. So, we measured the distance between each site and the nearest crossover, termed $\Delta XOmin$ and defined in Figure 2.14A, using the diagrams in Figure 2.15. The use of such value permits to introduce a quantitative criterion for scoring restriction sites as a function of their vicinity to a crossover junction as shown on the left in Figure 2.16. Because of the periodicity of the internal structure in a DNA origami objects, a restriction site is typically located between two crossover junctions (see Figures 2.14 and 2.15). For several sites, the inter-crossover distance is 16 nucleotides (1.5 helix turns), and thus according to our definition the maximum value of $\Delta XOmin$ is 6 bp. Higher values of $\Delta XOmin$ are associated with the presence of larger unit cells that are mostly found near the edges of the nanostructure (see Appendix).

The two tables in Figure 2.16 show that enzyme-cleavable sites 7, 19, and 16 have $\Delta XOmin$= 5, 12, and 20 bp, respectively, while if $\Delta XOmin$ < 5 bp no sites are accessible by the enzyme.

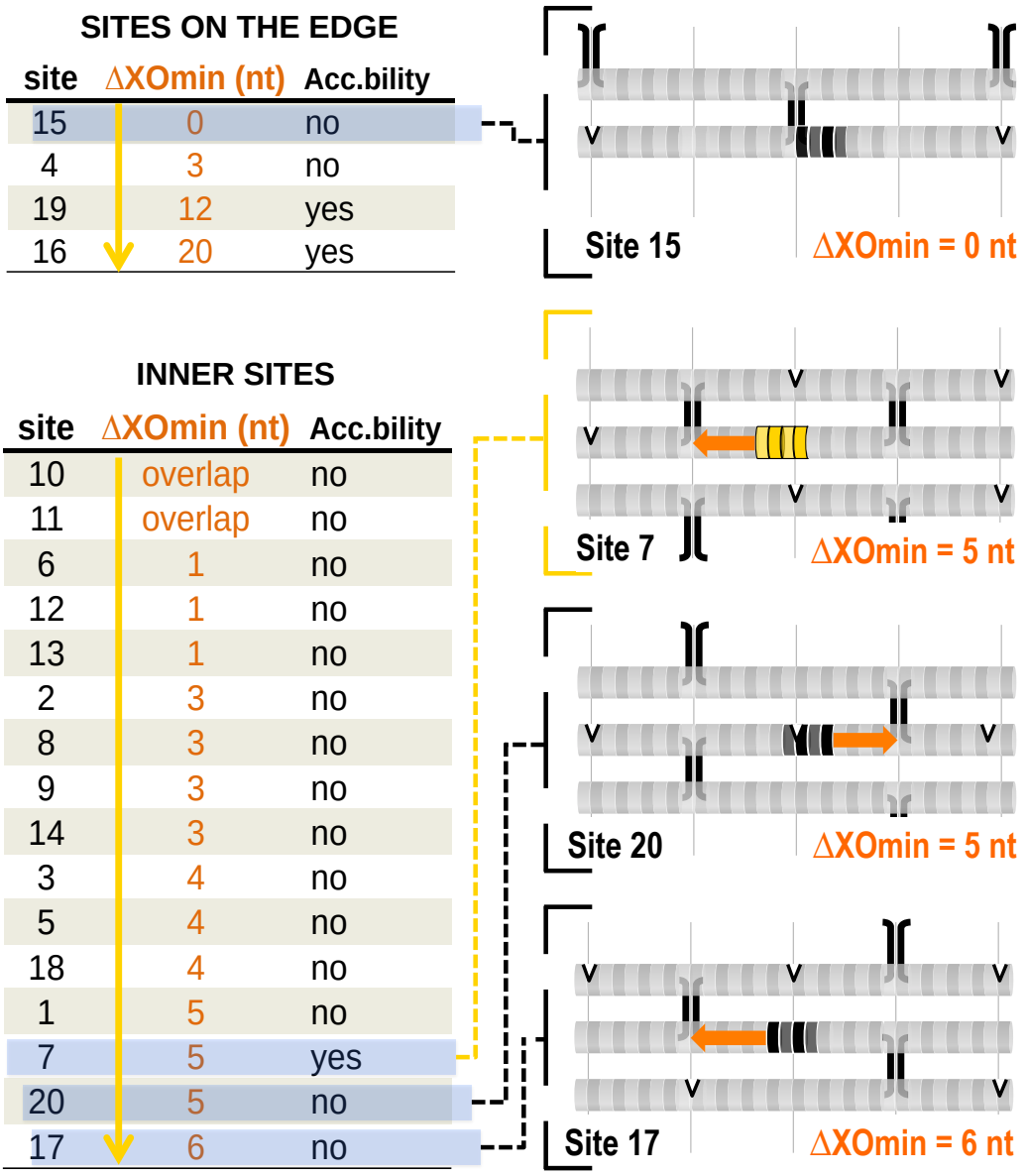

Figure 2.16. Analyzing the effect of the distance of a restriction site to the nearest crossover junction along the same DNA segment on the accessibility to HhaI (termed ΔXOmin, see Figure 2.14A). Two tables on the left list the value of ΔXOmin for all the HhaI restriction sites in the triangular DNA origami. Sites located on a nanostructure edge are analyzed separately (on top). (left) Selected diagrams showing that site 15 overlaps with a crossover, while sites 7, 20 and 17 are located near the center of dsDNA duplex segments. The tables show that restriction sites can be processed by HhaI enzyme only if ΔXOmin >5 bp. In addition, diagrams for sites 7, 17, and 20 suggest that site accessibility depends on the presence of nick within the dsDNA segments that flank a restriction site.

In addition, in spite of the similarity of diagrams relative to sites 7, 17, and 20, with corresponding $\Delta XOmin$ values varying between 5 and 6 bp, only site 7 ($\Delta XOmin$= 5) is cleaved by HhaI enzyme. Figure 2.16 evidences that cleaved sites either located on an edge of the nanostructure or flanked by DNA segments provided with nicks, are likely to increase the flexibility of the segments. Accessible sites therefore, seem to have less physical constrains than the others. In the following paragraph I will address this aspect in details.

2.4.3 Presence and conformation of DNA segments that flank a restriction site

The diagrams in Figure 2.15 show that the investigated HhaI sites are typically flanked by at least one 16-bp-long dsDNA segment, each one containing one nick at most. A nick is a discontinuity of the phosphate backbone of one of the two strands forming a DNA duplex segment, and typically increases the inherent flexibility [30]. In turn, with two flanking segments, there are three configurations as depicted in the diagrams relative to sites 7, 17, and 20 in Figure 2.16. Here below I introduce a convenient labeling method for such configurations that will serve in the analysis of our experimental results. The three, adjacent DNA segments (with the restriction site

located in the central element) can be associated with a state “A | B | C”, in which the value of A and C is either “nicked” (N) or duplex (ds), and the value of the B is always “site”, as depicted in Figure 2.17A. In turn, sites 7, 17 and 20 correspond to the three states N|site|N, N|site|ds, ds|site|ds, respectively. Following this approach, if a site is located on a nanostructure edge only two states are defined. These are N|site and ds|site and correspond to site 4 and sites 16 or 19, respectively (see Figures 2.15 and 2.17B).

Figure 2.17B and C collect the information obtained so far on each restriction site in terms of distance from crossover junctions, configuration of the flanking DNA segments, and accessibility to HhaI enzyme. The two tables list the results for the sites located on an edge (B) and within the nanostructure bulk (C). The table in Figure 2.17C shows that in our DNA triangle there are eight sites of ds|site|ds type (with ΔXOmin=1, 3, 4, and 5 bp), four sites of N|site|N type (with ΔXOmin=1, 4, and 5 bp), and two sites of N|site|ds type (with ΔXOmin=3 and 6 bp, respectively). The table clearly shows that restriction sites of ds|site|ds type are never cleaved by HhaI enzyme, regardless the value of ΔXOmin. In contrast, the only enzyme-accessible restriction sites with ΔXOmin $\geq$ 5 bp are either of N|site|N type or are located on a nanostructure edge.

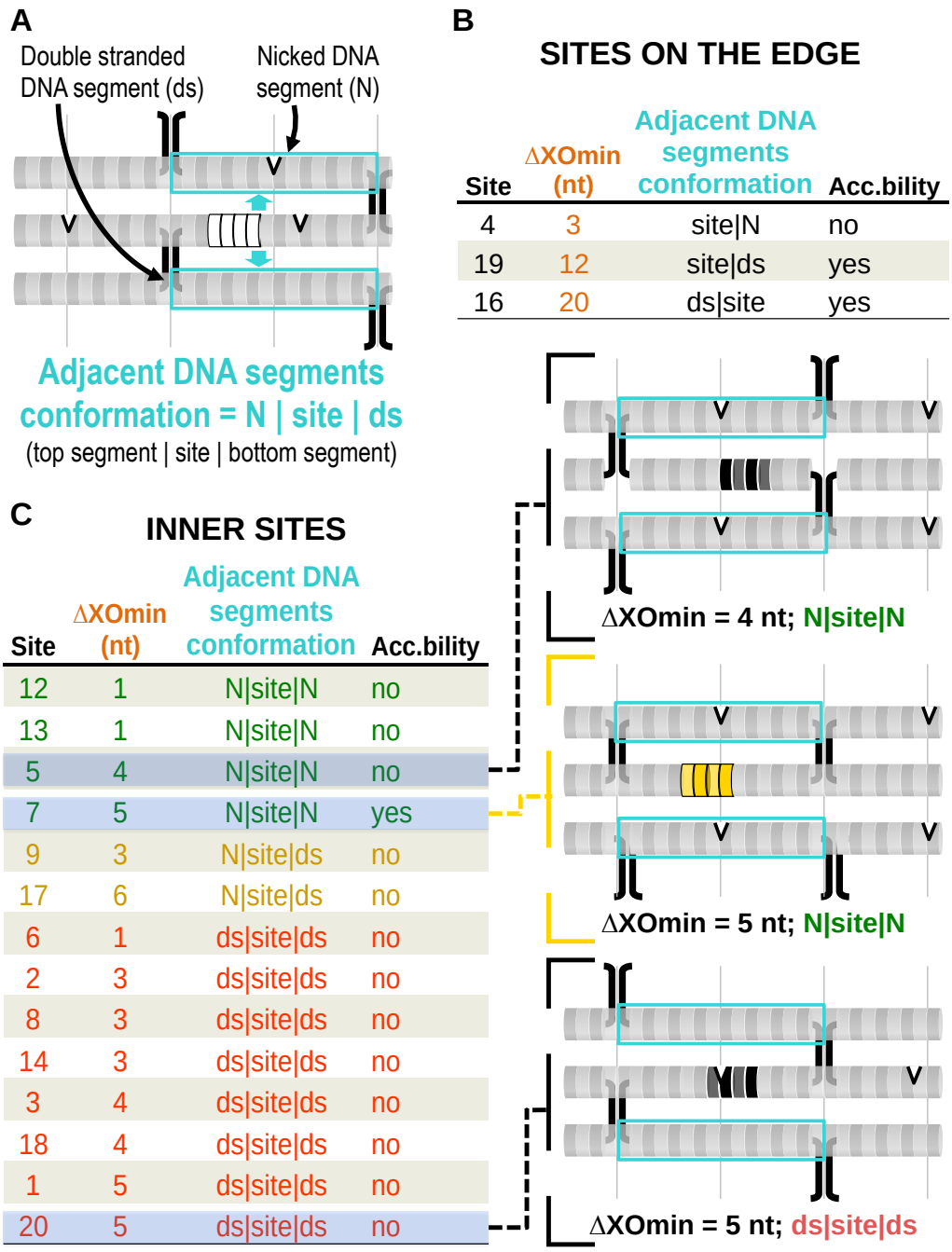

Figure 2.17. The conformation of the DNA segments flanking an HhaI site influences enzyme action. (A) The dsDNA segments that flank a restriction site are framed in the diagram. The segment on top has a nick in the center, while the segment at the bottom is formed by two, fully complementary DNA sequences. Such configuration of the restriction site is labeled as "N | site | ds", where "N" and "ds" indicate the nicked dsDNA segment, and the nick-free dsDNA segment, respectively. The table in (B) Lists the configuration for each site located on a nanostructure edge. The table in (C) groups the other sites in three different configurations, for each of which sites are listed in ascending order of ΔXOmin. On the right are shown the diagrams of sites 5, 7 and 20. Site 5 and 7 share the configuration of the flanking DNA segments but have 1-bp ΔXOmin difference. Sites 7 and 20 have the same ΔXOmin value, but different configurations of the flanking DNA segments.

The analysis shown in Figure 2.17 leads to a relatively simple interpretation of the experimental results discussed so far. It seems that the HhaI restriction enzyme requires that the physical flexibility of the region surrounding a restriction site is higher that a certain critical threshold. In fact, the presence of nicks is likely to relax the DNA duplexes flanking a restriction site [30,31], thus introducing more space around the site and allowing enzyme-DNA binding. Similarly, restriction sites located on a nanostructure edge are less constrained than in the bulk.

In addition, the analysis in Figure 2.17C suggests that in certain cases, simple criteria could be used to design DNA nanostructures with predictable accessibility to endonucleases. Specifically, for restriction sites flanked by two DNA segments, the action of HhaI correlates with the presence of nicks within the site-flanking DNA segments, and the distance between the site and the nearest crossover junction (ΔXOmin). The data shown in Figure 2.17C relative to sites 5, 7, and 20 demonstrate that very small structural changes near a restriction site can be reflected by dramatic changes on its accessibility (see the diagrams on the right). For instance, site 7 is accessible by HhaI although its distance with respect to the adjacent crossover is just a single base higher than that of site 5, which is inaccessible to HhaI.

2.4.4 Presence of nicks near or within a restriction site

Based on the high sensitivity of the HhaI reaction upon structural constrains in a DNA origami, in this section I will examine the effect of the presence of a nick within or in proximity to a restriction site. The nick is a lacking phosphodiester bond between two consecutive nucleotides in a double helix. The restriction enzyme initially binds its cognate site on the dsDNA backbone [27] and crystallographic analysis established that the length of the DNA segment involved in protein-DNA interactions with a restriction enzyme is slightly longer than in the typical B-DNA form [32]. This indicates mechanical stress of the DNA upon enzyme binding. In turn, the presence of a nick could inhibit enzyme-DNA complex formation regardless the steric constrains discussed in the previous section. In DNA origami objects, nicks are typically generated by couples of staple strands binding over consecutive sequences of the scaffold, with one staple having its 3' end next to the 5' end of the other.

We designed nine 64-bp-long, nicked DNA duplexes starting from a common sequence of 64 nt and shifting the nick along the other strand one base at a time, as shown in the representative scheme on top in Figure 2.18A. Each nicked dsDNA molecule is formed upon the hybridization of three strands. One strand (the longer, with 64 nt) is the common scaffold, while the other two strands hybridize over two consecutive parts of the scaffolds, whose lengths depend on the position of the nick.

The nicked duplexes were formed by incubating the three inherent ssDNA strands at equimolar concentration for 1 hour at 37°C. Each molecule was then treated with HhaI enzyme for 1 hour at 37˚C, and the reaction products were analyzed with native, polyacrylamide gel electrophoresis. For each molecule a control experiment is conducted under identical conditions, but lacking the enzyme. As positive control we used a nick-free DNA duplex with the same sequence. Figure 2.18A, shows the enzyme products of the different molecules indexed from I to IX according to the position of the nick (see schematics on top).

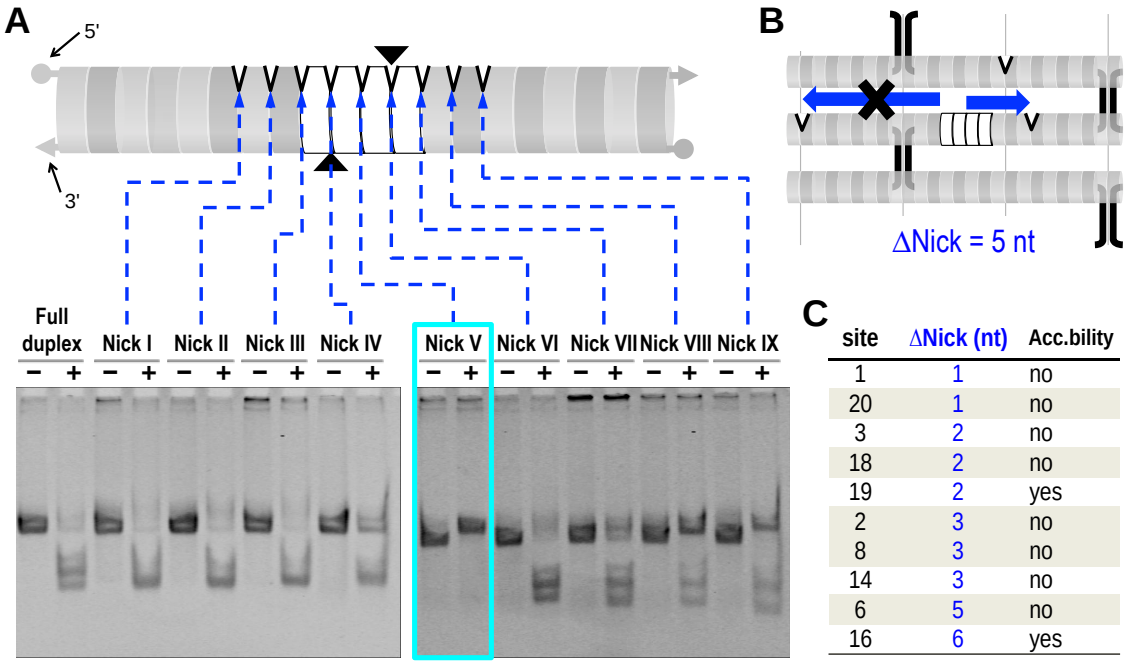

site	ΔNick (nt)	Acc.bility
1	1	no
20	1	no
3	2	no
18	2	no
19	2	yes
2	3	no
8	3	no
14	3	no
6	5	no
16	6	yes

Figure 2.18. Influence of a nick near or within an HhaI restriction site in a short dsDNA molecule. (A) Schematic representation of DNA molecules used in this experiment. Each one consists of a nicked DNA duplex, and has the nick in a different position. Two black triangles indicate the phosphodiester bonds that are cleaved by HhaI enzyme within the 4-bp-long restriction site that is positioned in the center of all the investigated molecules. In this way, we studied the effect of the nick in nine positions (Nick I – Nick IX) within a range of 9 bp centered within the DNA molecules. The so-formed DNA molecules were incubated with 10 units of HhaI for 1 hour at 37˚C and the reaction products were analyzed with electrophoresis in 18% polyacrylamide gel. The gel image shows that HhaI successfully digested the restriction site in all the configurations, except for Nick V (framed in cyan), in what case the enzyme is fully inhibited. The gel also shows incomplete digestion for the configurations termed Nick IV, VII, VIII, and IX. (B) Definition of distance between a restriction site and the nearest nick (ΔNick) using our diagrams. (C) Table listing all the HhaI restriction sites in the investigated, triangular DNA origami, in ascending order of ΔNick and with ΔNick ≤6.

The results in Figure 2.18A demonstrate that HhaI successfully cleaves its site in most cases with a single exception, i.e. when the nick is positioned right in the center (experiment V). In this case we define that the distance between the site and the nick is ΔNick=0 (see definition in Figure 2.18B). In addition, gel bands compatible with an incomplete restriction reaction are found when the nick is near the 3' end of the site (experiments VII, VIII and IX).

The results shown in Figure 2.18A demonstrates that a nick has a weak influence on the action of HhaI. To match these findings with our results on the action of HhaI in a triangular DNA origami (shown in Figures 2.10 and 2.12), using our diagrams we screened all HhaI sites in the triangle and selected those with a nick in the same 16-bp-long dsDNA segment (see Figure 2.18B). The selection is listed in Figure 2.18C in ascending order of ΔNick. The table show that none of such restriction sites has ΔNick=0. Interestingly, site 19 is accessible to HhaI and has a nick at ΔNick=2, which is consistent with the results shown in Figure 2.18A. These results therefore support the conclusion that the presence of nicks near HhaI restriction sites has little direct influence on enzyme action in a 2D DNA origami.

2.5 The effect of flexibility and structural defects in DNA origami triangle on the action of HhaI restriction enzyme – a study with single-site resolution

The topographic AFM image in Figure 2.19A shows a rectangular DNA origami rolled up on itself. Also, a prediction of the mechanical properties of a DNA origami can be achieved with the CanDo software [5], and is illustrated in Figure 2.19B for the rectangle. The model predicts the bending of the rectangle from different perspectives. These findings suggest that the rectangular DNA origami is a very flexible structure. On the other hand, the well-formed triangular DNA origami is always detected by AFM as a planar structure on the surface (see Figure 2.3B-D). Figure 2.19D shows the prediction of the mechanical properties of the triangular DNA origami computed with Cando [5], which show that the triangle is more rigid than the rectangle. Therefore, different 2D DNA origami objects can have very different mechanical properties in terms of flexibility and rigidity.

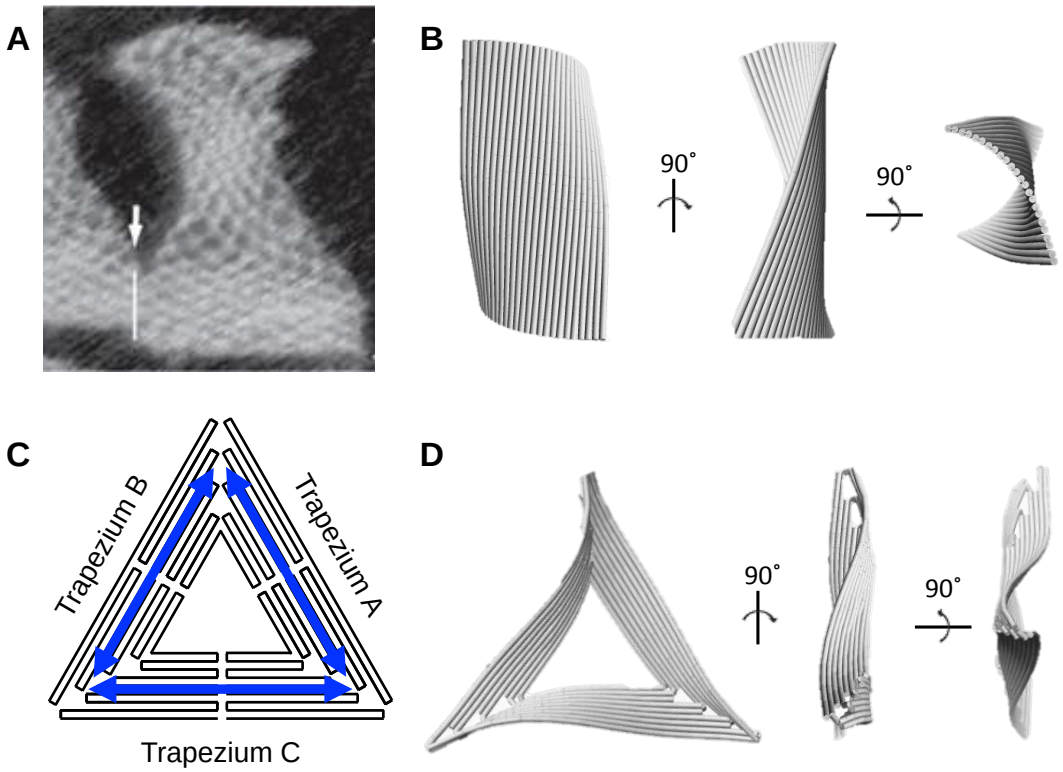

Figure 2.19. Mechanical properties of 2D DNA origami objects. (A) Atomic Force microscopy image of rectangular DNA origami rolled up on itself. The image was adapted from [15]. (B) Prediction of the mechanical behavior computed with Cando for the rectangular DNA origami along three different perspectives. (C) Schematic representation of the folding of the DNA scaffold into the triangular DNA origami, and the trapezoidal elements TA, TB, and TC. (D) Prediction of the mechanical behavior computed with Cando for the triangular DNA origami along three different perspectives.

Figure 2.19C shows that the triangular DNA origami is comprised of three trapezia joined together (termed TA, TB and TC, see Figure 2.19C). If we damage by design the integrity of one of the axis, it is likely that entire structure becomes less rigid. The inset in Figure 2.20 shows the molecular design of a hole in TA. The defect was created with a size that should be small enough to not affect the formation of the DNA origami objects. The defect is located right on the middle area of such trapezium and is obtained by removing few staples from the pool used to self-assemble the triangular DNA origami. The defect was designed not to subtract staples that are involved in the formation of HhaI restriction sites. With the same approach, we generated three triangular DNA origami variants, each one having a defect in a single trapezium of the three available. In addition, we followed the approach adopted in the previous experiments, by which we generated a number of fully formed, triangular DNA origami with a single, active HhaI site per structure. Figure 2.20 depicts a triangular DNA origami with a single active site in TB along with the structural defect in TA. Since the spatial position of the hole can be varied within the triangular shape, we expect this combined approach will allow exploring how the global mechanical properties of a DNA origami objects would affect the enzyme-accessibility of restriction sites.

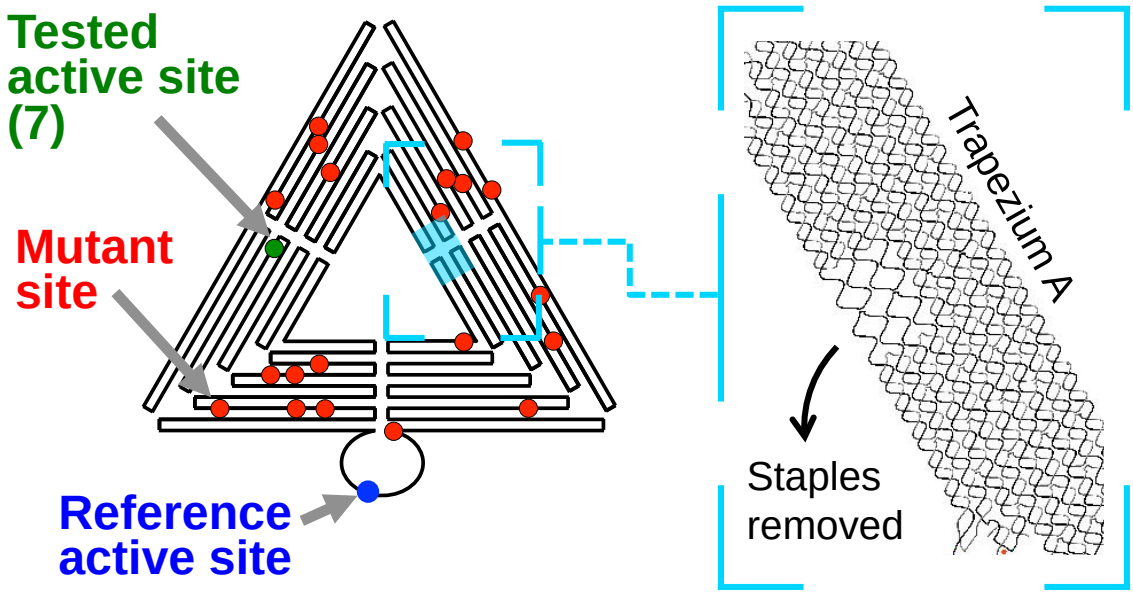

Figure 2.20. Experimental approach used to probe sites accessibility within a triangular DNA origami provided with a major structural defect. On the left, it is shown schematically the triangular DNA origami with a defect on the trapezium A (TA), and with and an active HhaI site (site 7) in trapezium B (TB). The inset on the right shows that the defect in TA is generated by removial of 4 staples, none of which is involved in the formation of the restriction site as evident by the lack of active restriction sites in the region (see left).

The triangular DNA origami variants were synthetized and purified as described above (see Methods). The purified DNA origami objects were incubated with HhaI enzyme for 1 hour at 37˚C. The reacted DNA origami objects were melted by a thermal treatment, and the scaffold fragments were analyzed with agarose gel electrophoresis as previously described (see Methods). Figure 2.21 shows the obtained results with the structural modification localized in trapezium A (TA). Gel analysis at the bottom shows that only sites 4, 7, 8, 12, 16 and 19 are consistently found digested (see both gels), and their position in the triangle is shown in the schematics on top. Figure 2.22 shows the results of the experiments performed with the structural defect in trapezium B (TB). Gel analysis at the bottom shows that only sites 4, 7, 8, 12, 16 and 19 are consistently found digested (see both gels), and their position in the triangle is shown in the schematics on top. The patterns of enzyme-accessible sites coincide if the hole is in TA or TB. Figure 2.23 shows the results of the experiments performed with the structural defect in trapezium C (TC). Gel analysis at the bottom shows that only sites 7, 8, 12, 13, 16 and 19 are consistently found digested (see both gels), and their position in the triangle is shown in the schematics on top. The TC-modified, triangular DNA origami provides a slightly different pattern of sites accessibility with respect to TA- and TB-modified triangles.

The table in Figure 2.24 collects the results illustrated in Figures 2.21-23 regarding HhaI sites accessibility as a function of the position of the structural defect in the triangular DNA origami. The number of restriction sites that are cleaved by HhaI in this experiment is always higher than in the unmodified triangle (shown in Figure 2.10). Sites 7, 16 and 19 that are already accessible in the unmodified triangular DNA origami remain accessible in the presence of the holes. Sites 4, 8, 12 and 13, however, are turned-on by the presence of a hole as detailed in the table in Figure 2.24. Likely, a triangular DNA origami objects carrying a major structural defect is more flexible then without. Therefore, the results collected in the table of Figure 2.24 suggest that the higher the flexibility of a DNA origami object, the higher is the number of inherently accessible restriction sites.

Furthermore, the table in Figure 2.24 allows the analysis of the relationship between the location of turned-on sites and the location of the hole. Site 8 and 12 are located on the TB, and TA respectively, are both turned-off in the unmodified triangle, and are always turned-on for all modified triangles investigated in Figures 2.21-23. Surprisingly, the response of sites 8 and 12 is independent on their location in the triangle as well as the location of the structural modifications.

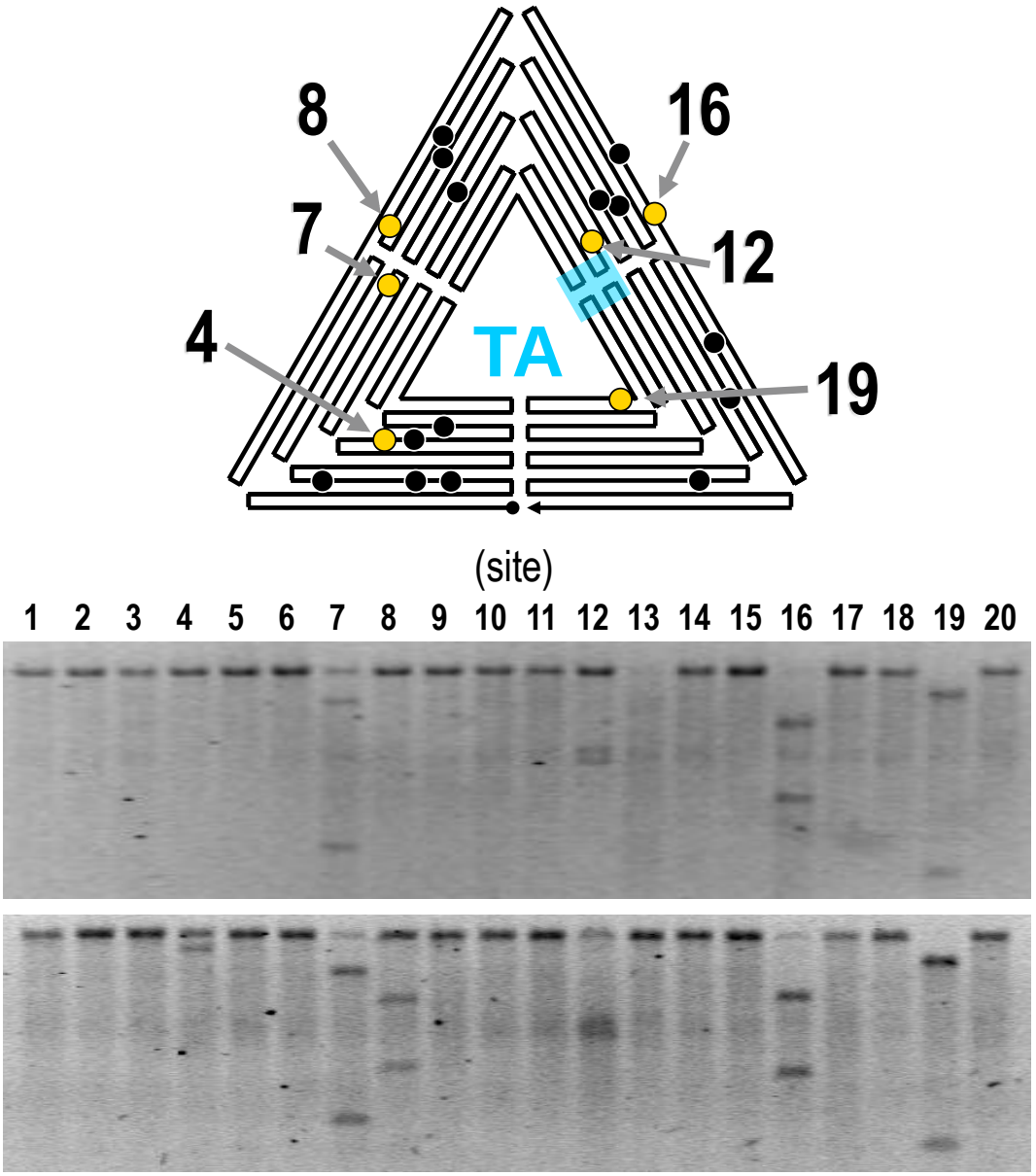

Figure 2.21. HhaI site accessibility within triangular DNA origami with modified trapezium A (TA). A schematic representation of the TA-modified, triangle is shown on top. The "hole" is highlighted in cyan. The yellow-filled circles depict the accessible sites (see gels below), while the black-filled circles depict the enzyme-inaccessible sites. Two gels at the bottom show the result of the HhaI enzymatic reaction with TA-modified triangular DNA origami objects, which have a single active HhaI site (for sites 1-20). The modified triangular DNA origami objects were incubated for 1 hour, at 37˚C with 10 units of HhaI. After the reaction, the nanostructures were melted and the DNA scaffold fragments were analyzed in 1% agarose gel electrophoresis.

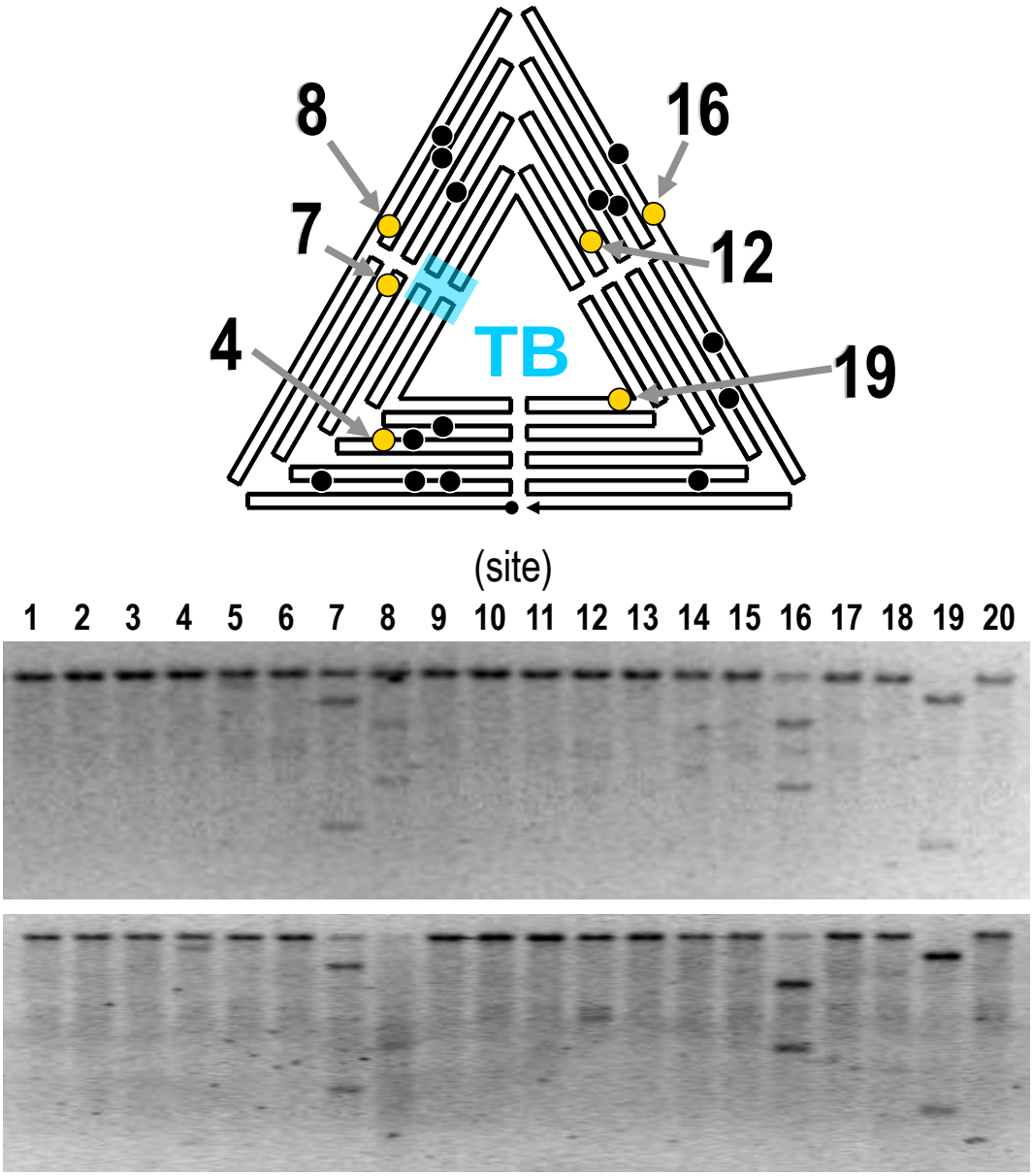

Figure 2.22. HhaI site accessibility within triangular DNA origami with modified trapezium B (TB). A schematic representation of the TB-modified, triangle is shown on top. The "hole" is highlighted in cyan. The yellow-filled circles depict the accessible sites (see gels below), while the black-filled circles depict the enzyme-inaccessible sites. Two gels at the bottom show the result of the HhaI enzymatic reaction with TB-modified triangular DNA origami objects, which have a single active HhaI site (for sites 1-20). The modified triangular DNA origami objects were incubated for 1 hour, at 37˚C with 10 units of HhaI. After the reaction, the nanostructures were melted and the DNA scaffold fragments were analyzed in 1% agarose gel electrophoresis.

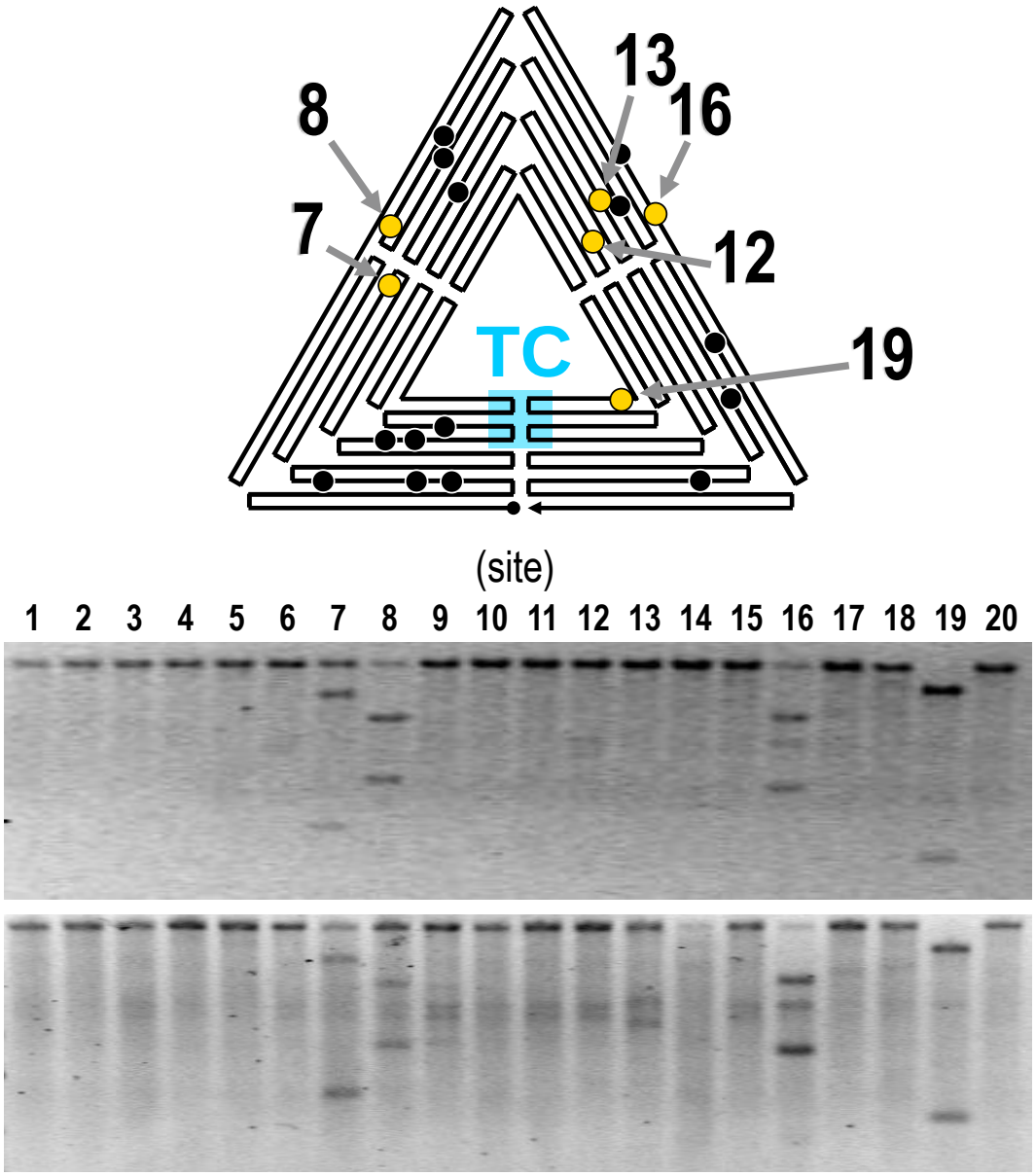

Figure 2.23. HhaI site accessibility within triangular DNA origami with modified trapezium C (TC). A schematic representation of the TC-modified, triangle is shown on top. The "hole" is highlighted in cyan. The yellow-filled circles depict the accessible sites (see gels below), while the black-filled circles depict the enzyme-inaccessible sites. Two gels at the bottom show the result of the HhaI enzymatic reaction with TC-modified triangular DNA origami objects, which have a single active HhaI site (for sites 1-20). The modified triangular DNA origami objects were incubated for 1 hour, at 37˚C with 10 units of HhaI. After the reaction, the nanostructures were melted and the DNA scaffold fragments were analyzed in 1% agarose gel electrophoresis.

In contrast, sites 4, and 13 are located on TC, and TA respectively, are both turned-off in the unmodified triangle, and turn on in the TA- or TB-modified triangle, and TC-modified triangle, respectively. Also in this case, site activation does not require spatial vicinity between restriction site and structural defect (i.e. the hole in the trapezium). Moreover, Figure 2.24 demonstrates that the distance between such a hole and the consequentially turned-on sites varies from a few nanometers to several tens of nanometers. The triangle in Figure 2.24 shows that turned-on sites tend to accumulate within two regions (highlighted in yellow) over TB and TA, and near two major junctions. The latter are the edges of hemi-trapezoidal DNA tiles and likely introduce higher flexibility. Interestingly, however, several sites in proximity to structural defects in TA, TB, and TC remain turned-off in all the experiments.

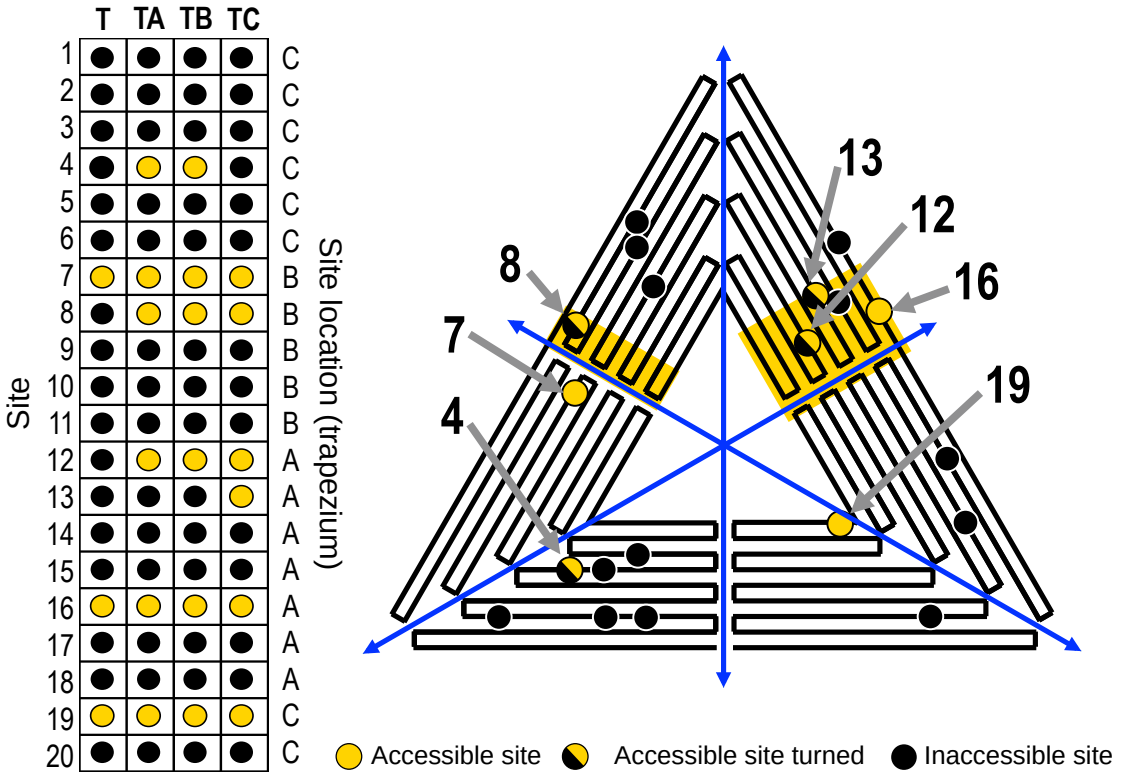

Figure 2.24. The flexibility of a 2D DNA origami affects site accessibility to HhaI enzyme. On the left, the table displays the accessibility of HhaI sites within the triangular DNA origami in native form (T) and with a structural modification in trapezium A (TA), trapezium B (TB) or trapezium C (TC). Accessible sites are indicated as yellow-filled circles, while inaccessible site are indicated with black-filled circles. On the right, the schematic, triangular DNA origami carries a map of the HhaI sites. Sites that always turned-on are indicated with yellow-filled circles; sites that are turned-on in presence of a hole in any of the trapezia are indicated with yellow/black-filled circles. The blue arrows highlight the axes that follow the junctions between trapezia. In yellow is highlighted the areas in which turned-on sites accumulate.

In addition, we note that, depending on the position of the site between two consecutive crossovers, the major and minor grooves of a restriction site are differently exposed on the surface of the DNA nanostructure, as described in Figure 2.14E. For instance, the major groove of site 7 faces to the flanking DNA segments, and is systematically cleaved by HhaI enzyme. In addition, the width of the unit cells neighboring a site could influence the flexibility and the steric hindrance of the DNA duplexes in the vicinity, and in turn affect site accessibility. Figure 2.25 combines the results shown in Figure 2.24 with the characteristics of the restriction sites according to our analysis, and in particular in terms of 1) the configuration of the site-flanking DNA segments (as shown in Figure 2.17), 2) the width of the unit cell that contains the restriction site (as defined in Figure 2.14), and 3) the orientation of the base pairs in the restriction site with respect to the nanostructure surface (as defined in Figure 2.14). The table in Figure 2.25 shows that HhaI enzyme can cleave restriction sites regardless their orientation, as well as the width of the inherent unit cell. A striking aspect that emerges in Figure 2.25 is a strong correlation between the configurations of the site-flanking DNA segments and the accessibility of the inherent sites. In fact, six of the seven sites that were found to be cleavable by HhaI enzyme in at least one of the investigated modified triangles are of N|site|N type (see also Figure 2.17), or are located on a nanostructure edge. In addition, from the tables shown in Figures 2.17, 2.24, and 2.25, it emerges that a restriction site is consistently cleaved by HhaI enzyme in all the investigated triangular nanostructures only if sufficiently distant from the adjacent crossovers (i.e. ΔXOmin $\geq$ 5 bp, according to Figure 2.17). With such an interpretation, however, the behavior of site 8 is not clear. In fact, this site is turned-on by the presence of any of the structural defects in the trapezia (TA, TB, and TC) although according to our model it should be highly constrained because it is of ds|site|ds type and has ΔXOmin = 3 bp.

In conclusion, the results shown in Figures 2.21-25 strongly suggest that the ability of HhaI restriction enzyme to access and process a restriction site in a 2D DNA origami depends upon the mechanical flexibility of DNA near the site, which can increase in the presence of large and distant defects in the DNA origami structure.

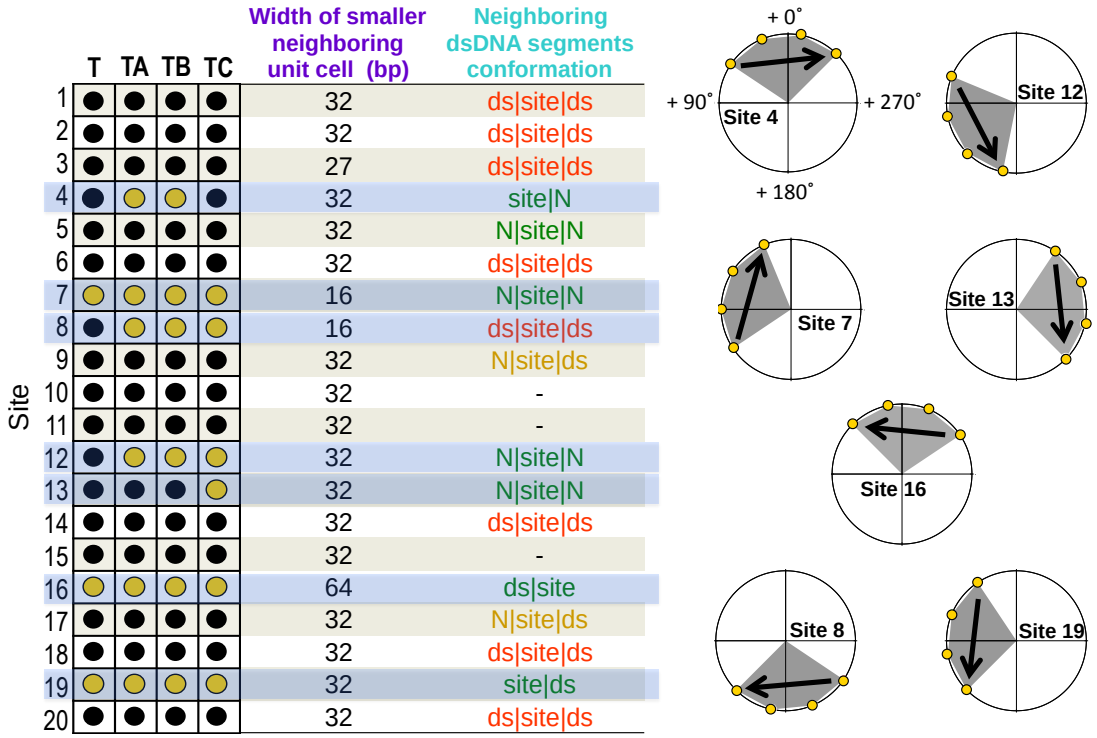

Figure 2.25. Towards a rationalization of the action of endonucleases on 2D DNA origami objects. On the left, the table displays the accessibility of HhaI sites within the triangular DNA origami in the native form (T) and with a structural modification in trapezium A (TA), trapezium B (TB) or trapezium C (TC). Accessible sites are indicated with yellow-filled circles, while inaccessible sites are indicated with black-filled circles. The other columns list several site-specific parameters derived from the diagrams in Figure 2.15, including the width of the smallest unit cell containing the site and the configuration of the dsDNA segments adjacent to the site. On the right, the polar graphs show that the sites that are accessible to HhaI enzyme in the defective triangular DNA origami are found with different orientations. The yellow dots indicate the angle of each base pair with respect to the nanostructure surface.

2.6 The action of Hin1II restriction enzyme in the DNA origami triangle – a study with single-site resolution

A complex aspect of this study is in the fact that type II restriction enzymes recognize and cleave DNA sequences with very high specificity involving different mechanisms of DNA recognition and of DNA processing [12,32,33]. In the previous sections, we identified major structural factors that influence the action of HhaI restriction enzyme in the triangular DNA origami. These factors however may reflect the specific reaction mechanism of HhaI enzyme. This investigated enzyme however processes a 4-bp-long restriction site as the majority of type II restriction enzymes, and, in addition, the results in Figure 2.4 shows that the DNA origami objects scaffold fragments generated by HhaI are in the same range of those produced by most of the investigated enzymes. In turn, we applied our experimental and analytical approaches to study the action of another restriction enzyme, namely Hin1II, on the DNA triangle. Figure 2.5 (ssDNA cleavage) showed that both HhaI and Hin1II enzymes have high specificity for restriction sites in the dsDNA form. As discussed in the previous sections, this aspect is essential for the implementation of our experimental approach aimed at studying the enzyme-accessibility of restriction sites within DNA origami objects with single-site resolution.

Figure 2.26A schematically shows the triangular DNA origami with its Hin1II sites indexed in ascending order from 5' to 3' according to the rule depicted in Figure 2.7. Also, the map shows that there are 15 Hin1II sites inside the triangle. To probe their accessibility with single site resolution, for each of such sites we generated a modified triangle in which all but one the inherent Hin1II sites are turned-off. This operation was achieved by using staple strands containing the sequence 5'-CGCG-3' that hybridizes to the Hin1II site 5'-CATG-3' in the scaffold. Figure 2.26B schematically depicts a modified triangle in which the 6th site is the only active site that can be recognized by Hin1II. The external loop on the triangle investigated so far (hereafter termed "loop 1") does not contain any Hin1II site that can serve for reference. The DNA origami technology, however, allows shifting the scaffold sequence along its folding path within the object by opportunely changing the set of staples utilized. This, in turn, offers a simple solution to our problem. We introduced an additional loop (hereafter termed "loop 2") that contains an always on Hin1II site as shown in Figure 2.26A and B. Here, loop 2 is formed by a 50 nt sequence of the scaffold, protrudes from the surface of the triangle, and includes site 15 in its center (see Figure 2.26C). In contrast, loop 1 is 50 nt shorter than in the unmodified triangle. In addition, such solution is most convenient. In fact, site 15 is nearest to loop 1 in the unmodified triangle (see Figure 2.25C), and in

turn, to pull site 15 outside the nanostructure, we had to recalculate the sequences of only twelve staples and add a DNA strand that hybridizes to site 15 within loop 2. Of note, the modified nanostructure is equivalent to the unmodified version, except that site 15 overlaps with a crossover junction (see the inset in Figure 2.26A), and therefore would be highly unlikely accessible to Hin1II.

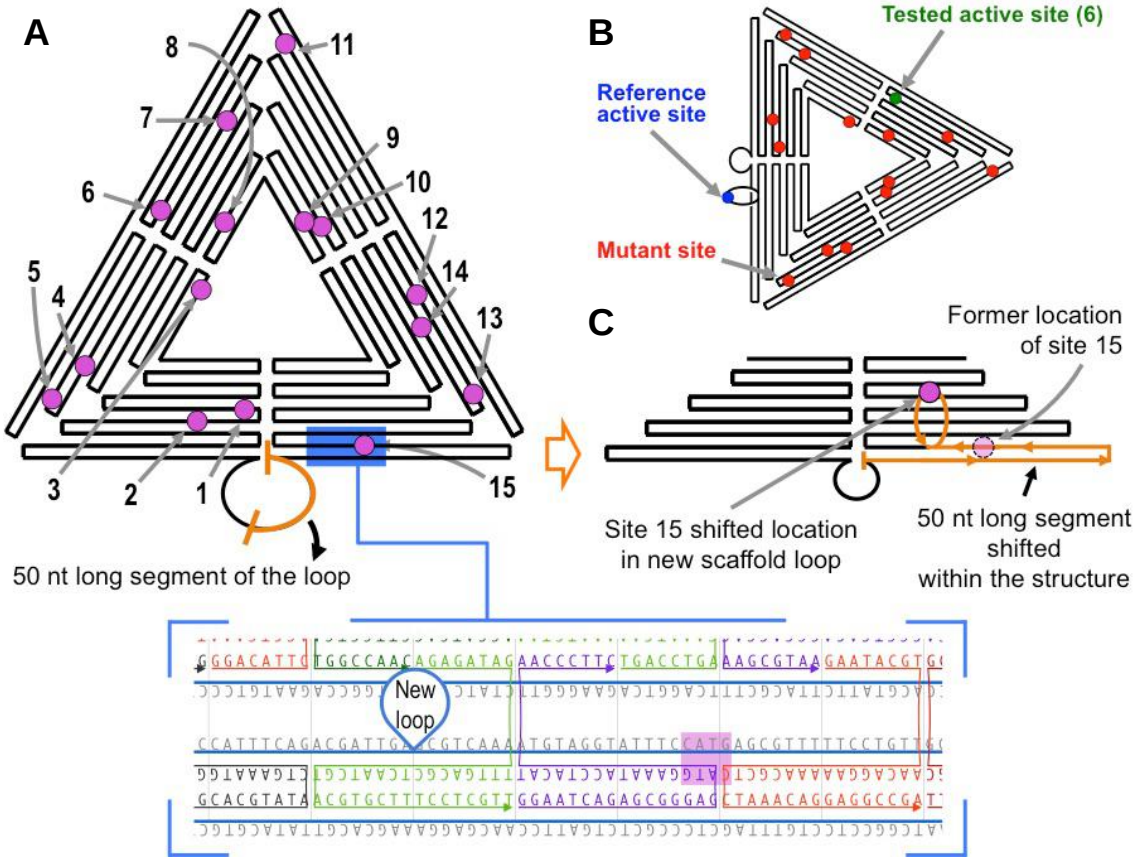

Figure 2.26. Designing a strategy to probe accessibility of Hin1II sites within the triangular DNA origami. (A) Schematically Hin1II sites superimposed on triangular DNA origami. The inset at the bottom shows a DNA origami design near site 15 (highlighted in magenta). (B) Schematics of an example of modified triangular DNA origami with site 6 being the only activated. Here is also shown a newly designed loop 2 that protrudes from the nanostructure surface and contains a reference, active site. (C) Schematic representation of loop 2 that is obtained by shifting a 50-nt-long segment of scaffold from loop 1 into the triangle, and pulling a segment of the same length in the indicated position. The scaffold shift was designed in order to move site 15 in the newly formed structure. Since it protrudes from the structure the inherent Hin1II site becomes enzyme-accessible.

The modified triangular DNA origami objects were synthetized and purified with established protocols (see Methods). The purified triangles were incubated with for 1 hour at 37˚C with 10 units of Hin1II enzyme as done previously (Figure 2.4). The

reacted triangles were then melted with a thermal treatment, and the scaffold fragments were analyzed with agarose gel electrophoresis as previously described (se Methods). The gel analysis in Figure 2.27 shows that only the site 7 was accessible in our modified triangle. The position of site 7 in the triangle is shown schematically on the right along the positions of all the other (inaccessible) sites.

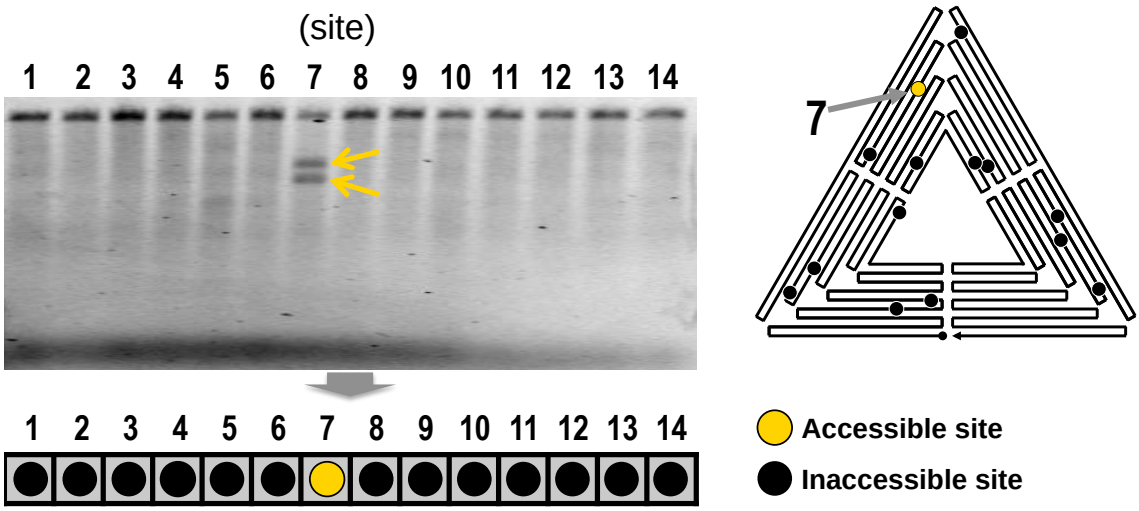

Figure 2.27. Probing site accessibility for Hin1II within the triangular DNA origami, and with single site resolution. DNA origami objects were incubated with 10 units of Hin1II for 1 hour and at 37°C. After the reaction the DNA origami objects were melted and the obtained scaffold fragments were analyzed with 1% agarose gel electrophoresis (left). The gel shows that Hin1II cleaves only site 7. On the right, the accessibility and the position of all the Hin1II sites is schematically shown in the triangle.

Figure 2.28B illustrates schematically the structure surrounding the site 7, which is the only accessible site for Hin1II in triangular DNA origami. For each Hin1II site, the table in Figure 2.28A displays the relative parameters obtained with our analysis. Site 7 is of N|site|N type, has ΔXOmin = 4 bp and is located within a unit cell of 32 bp in width. According to our results for HhaI, Hin1II enzyme needs that the DNA structure near a restriction site is relatively flexible. In fact, all sites of ds|site|ds or ds|site|N types are found to be enzyme-inaccessible. The only exception is site 14 that is clearly inaccessible to Hin1II although, according to our analysis, it is very similar to site 7. Evident differences between these two sites are the distance from the crossover junctions that is 1 bp higher for site 14 (see Figure 2.28B), and the orientation of the major groove with respect to the nanostructure surface (see Figure 2.28C).

A

Site	ΔXOmin (nt)	Adjacent DNA segments conformation	Width of the smallest unit cell (bp)	Accessibility
1	overlap	-	32	no
2	4	N|site|ds	16	no
3	0	site|ds	16	no
4	overlap	-	32	no
5	2	ds|site	27	no
6	3	N|site|N	16	no
7	4	N|site|N	32	yes
8	1	ds|site|N	32	no
9	6	ds|site|N	32	no
10	1	ds|site|ds	32	no
11	3	N|site|ds	32	no
12	2	ds|site|ds	32	no
13	3	ds|site|ds	27	no
14	6	N|site|N	32	no

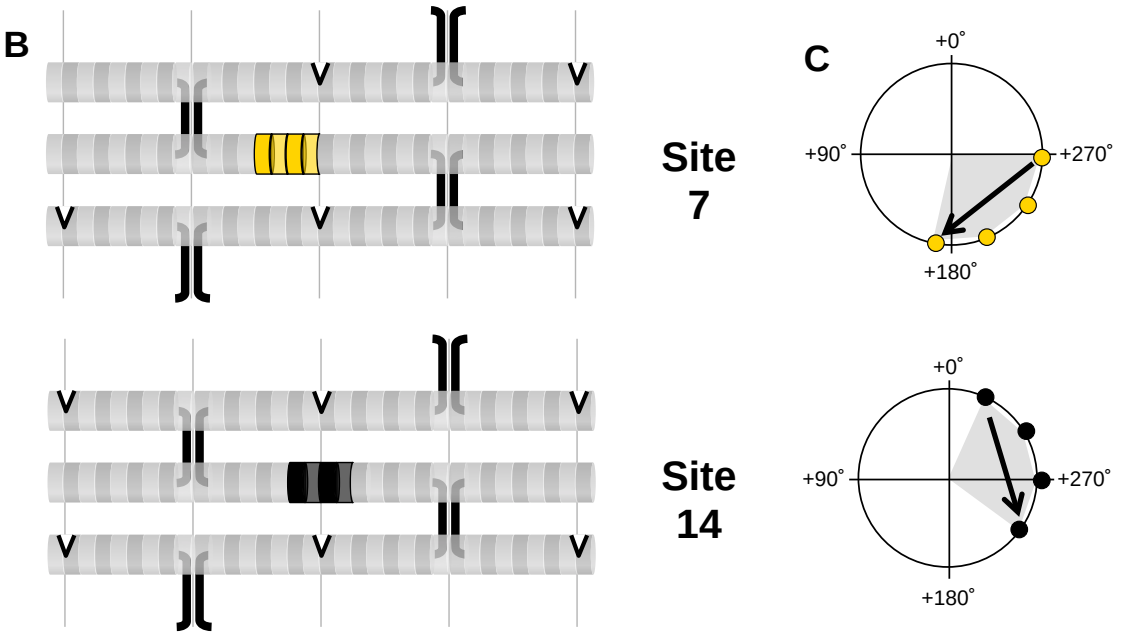

Figure 2.28. Analyzing the results of Hin1II action on triangular DNA origami. (A) For each Hin1II site, the table lists the distance between the site and the nearest crossover junction (ΔXOmin, as defined in Figure 2.14A), the conformation of the site-flanking DNA segments (modeled as A | site | B, as defined in Figure 2.14C), and the width of the smallest unit cell containing the site (see Figure 2.14D) as obtained from diagrams similar to those shown in Figure 2.15 for HhaI. Two examples are shown in (B) for sites 7 and 14, respectively. (C) Polar graphs for sites 7 and 14 according Figure 2.14E. Here, the circles are the nucleotides of the site on the staple, and an arrow indicates its 5'→3' direction. The accessible site is depicted in yellow and the inaccessible site is depicted in black.

In conclusion, from our comparative analysis of the behavior of HhaI and Hin1II with triangular DNA origami, it emerges that the results obtained for the two enzymes are in good agreement. Our results strongly suggest that several structural properties of DNA nanostructures concur to determine the accessibility of a DNA sequence to an endonuclease. In particular, in the triangles, most relevant factors are the distance between a restriction site and the adjacent crossover junctions, and the presence and conformation of site-flanking DNA segments. For both enzymes, the accessible sites share the presence of nicks in such flanking DNA segments. These and the other observations discussed in this chapter are consistent with our interpretation that the DNA rigidity inhibits enzyme action, and, conversely, enzyme-accessible sites are located over relatively flexible regions of the investigated DNA nanostructures.

2.6 Bibliography for Chap. 2

1. Suck, D. DNA recognition by structure-selective nucleases. *Biopolymers* **44,** 405–421 (1997).
2. Mundade, R., Ozer, H. G., Wei, H., Prabhu, L. & Lu, T. Role of ChIP-seq in the discovery of transcription factor binding sites, differential gene regulation mechanism, epigenetic marks and beyond. *Cell Cycle* **13,** 2847–2852 (2014).
3. Castronovo, M. *et al.* Control of steric hindrance on restriction enzyme reactions with surface-bound DNA nanostructures. *Nano Lett.* **8,** 4140–5 (2008).
4. Castronovo, M. *et al.* Two-dimensional enzyme diffusion in laterally confined DNA monolayers. *Nat. Commun.* **2,** 210–297 (2011).
5. Castro, C. E. *et al.* A primer to scaffolded DNA origami. *Nat. Methods* (2011). doi:10.1038/NMETH.1570
6. Mei, Q. *et al.* Stability of DNA Origami Nanoarrays in Cell Lysate. *Nano Lett.* **11,** 1477–1482 (2011).
7. Lu, M., Guo, Q., Seeman, N. C. & Kallenbach, N. R. DNase I cleavage of branched DNA molecules. *J. Biol. Chem.* **264,** 20851–4 (1989).
8. Drew, H. R. & Travers, A. A. DNA structural variations in the E. coli tyrT promoter. *Cell* **37,** 491–502 (1984).
9. Keum, J.-W. & Bermudez, H. Enhanced resistance of DNA nanostructures to enzymatic digestion. *Chem. Commun. (Camb).* 7036–8 (2009). doi:10.1039/b917661f
10. Kauert, D. J., Kurth, T., Liedl, T. & Seidel, R. Direct mechanical measurements reveal the material properties of three-dimensional DNA origami. *Nano Lett.* **11,** 5558–5563 (2011).
11. Newman, M., Strzelecka, T., Dorner, L. F., Schildkraut, I. & Aggarwal, a K. Structure of Bam HI endonuclease bound to DNA: partial folding and unfolding on DNA binding. *Science* **269,** 656–663 (1995).
12. Xu, Q., Roberts, R. & Guo, H. Two crystal forms of the restriction enzyme MspI–DNA complex show the same novel structure. *Protein Sci.* 2590–2600 (2005). doi:10.1110/ps.051565105.son
13. Fuchs, R. & Blakesley, R. *Guide to the Use of Type II Restriction Endonucleases*. **100,** (Elsevier, 1983).
14. Roberts, R. J., Vincze, T., Posfai, J. & Macelis, D. REBASE--a database for DNA restriction and modification: enzymes, genes and genomes. *Nucleic Acids Res* **43,** D298–9 (2015).
15. Rothemund, P. W. K. Folding DNA to create nanoscale shapes and patterns.

Nature **440,** 297–302 (2006).

16. Douglas, S. M. *et al.* Self-assembly of DNA into nanoscale three-dimensional shapes. *Nature* **459,** 414–418 (2009).
17. Dietz, H., Douglas, S. M. & Shih, W. M. Folding DNA into Twisted and Curved Nanoscale Shapes. *Science (80-.).* **325,** 725–730 (2009).
18. Stahl, E., Martin, T. G., Praetorius, F. & Dietz, H. Facile and Scalable Preparation of Pure and Dense DNA Origami Solutions. *Angew. Chemie* n/a–n/a (2014). doi:10.1002/ange.201405991
19. Hahn, J., Wickham, S. F. J., Shih, W. M. & Perrault, S. D. Addressing the instability of DNA nanostructures in tissue culture. *ACS Nano* **8,** 8765–75 (2014).
20. Wagenbauer, K. F., Wachauf, C. H. & Dietz, H. Quantifying quality in DNA self-assembly. *Nat. Commun.* **5,** 1–7 (2014).
21. Wolfes, H., Fliess, a & Pingoud, a. A comparison of the structural requirements for DNA cleavage by the isoschizomers HaeIII, BspRI and BsuRI. *Eur. J. Biochem.* **150,** 105–10 (1985).
22. Blakesley, R. & Wells, R. 'Single-stranded'DNA from φX174 and M13 is cleaved by certain restriction endonucleases. *Nature* **257,** 421–422 (1975).
23. Nishigaki, K., Kaneko, Y., Wakuda, H., Husimi, Y. & Tanaka, T. Type II restriction endonucleases cleave single-stranded DNAs in general. *Nucleic Acids Res.* **13,** 5747–60 (1985).
24. Horiuchi, K. & Zinder, N. D. Site-specific cleavage of single-stranded DNA by a Hemophilus restriction endonuclease. *Proc. Natl. Acad. Sci. U. S. A.* **72,** 2555–8 (1975).
25. Yoo, O. J. & Agarwal, K. L. Cleavage of single strand oligonucleotides and bacteriophage phi X174 DNA by Msp I endonuclease. *J. Biol. Chem.* **255,** 10559–62 (1980).
26. Reckmann, B. & Krauss, G. The cleavage of single-stranded DNA by the isoschizomeric restriction endonuclease HhaI and CfoI. *Biochim. Biophys. Acta - Gene Struct. Expr.* **908,** 90–96 (1987).
27. Halford, S. E. How do site-specific DNA-binding proteins find their targets? *Nucleic Acids Res.* **32,** 3040–3052 (2004).
28. Douglas, S. M. *et al.* Rapid prototyping of 3D DNA-origami shapes with caDNAno. *Nucleic Acids Res.* **37,** 5001–5006 (2009).
29. Zuker, M. Mfold web server for nucleic acid folding and hybridization prediction. *Nucleic Acids Res.* **31,** 3406–3415 (2003).
30. Protozanova, E., Yakovchuk, P. & Frank-Kamenetskii, M. D. Stacked–

Unstacked Equilibrium at the Nick Site of DNA. *J. Mol. Biol.* **342,** 775–785 (2004).

31. Pan, K. *et al.* Lattice-free prediction of three-dimensional structure of programmed DNA assemblies. *Nat. Commun.* **5,** 5578 (2014).
32. Viadiu, H. & Aggarwal, a K. The role of metals in catalysis by the restriction endonuclease BamHI. *Nat. Struct. Biol.* **5,** 910–916 (1998).
33. Horton, J. R. *et al.* DNA nicking by HinP1I endonuclease: Bending, base flipping and minor groove expansion. *Nucleic Acids Res.* **34,** 939–948 (2006).

Chapter 3 – Conclusions and future perspectives

Recent studies already reported on the enhanced stability of DNA origami objects of different shapes against different nucleases, in purified solutions and in complex biological mixture. There is, however, a lack of information on the structural factors that determine enzymatic reactions in such highly dense DNA nanostructures.

In this PhD work, I have carried out an unprecedented investigation of the action of >10 type II restriction enzymes on two-dimensional DNA origami objects. For two enzymes in particular (HhaI and Hin1II) we mapped their action with single-site resolution using gel electrophoresis analysis of the enzyme-generated fragments of DNA molecules contained in the nanostructures.

We found the action of such restriction enzymes can be spatially controlled on the nanostructures in a digital fashion, in the sense that the reaction is either fully inhibited or allowed to proceed with high efficiency. Our results strongly suggest that several structural properties of DNA nanostructures concur to determine such an unprecedented behavior. In particular, in the investigated nanosystems, the most relevant factors are (i) the distance between a restriction site and the adjacent crossover junctions, and (ii) the presence and conformation of site-flanking DNA segments. For both enzymes, the accessible sites share the presence of nicks in such flanking DNA segments. These and the other observations detailed and discussed in this thesis are consistent with our interpretation that DNA rigidity within a DNA nanostructure is mostly responsible for such spatially controlled enzyme inhibition.

We plan to use a two-dimensional DNA origami object as a nanochips for detecting short nucleic acids such as micro (mi)RNA, as captured with a probe protruding from the nanochip surface. Following previous results of our group on

surface-bound nucleic acids monolayers, we plan to use an ancillary, HhaI restriction enzyme for site-specifically imprinting the presence of captured miRNAs on the DNA origami scaffold, in solution. With such detection approach, the nanochip serves as a matrix for imprinting and storing biological information that is present in the probed sample. In addition, the control over the nanochip stability against nucleases allows applying such detection approach directly in aggressive environments, as can be the cell lysate, inside that biomolecules as miRNAs are subjected to alterations of their content due to its rapid degradation.

The results of this thesis are essential towards developing the imprinting-based sensor described above. In particular, we plan to modify two staples near one restriction site. In turn, two ssDNA overhangs will be bridged only upon target binding, thus leading to the formation of a double helix segment, which will cover the surface of the restriction site, thus protecting it from the action of the enzyme. Another (control) site will be located within an unstructured region of the DNA nanochips, as to have maximum accessibility. Successful enzymatic reaction on both sites (i.e. no target present on the DNA nanochips' surface during the enzyme reaction) will lead, after melting the DNA self-assemblies, to the formation of two distinct fragments of the scaffold. On the contrarily, in the case that a copy of the target binds to the DNA nanochips, the scaffold will be enzyme-cleaved over a single site, and thus linearized. In this way, we plan to quantify miRNA targets by measuring the molar ratio between the linearized scaffold and its miRNA-specific fragments, by means of low-cost tools for DNA separation.

Chapter 4 – Materials and methods

4.1 Design of DNA origami objects

We used Cadnano 1.0 software [1] that was downloaded from http://cadnano.org, to generate and reproduce the design of the triangular and rectangular DNA origami published by Rothemund P.W.K. [2]. Next, we populated the scaffold path with template sequence (showed in Appendix) that allows the software providing the complementary sequences of staples.

From Cadnano we obtained an .svg file that shows the schematic representation of the design with scaffold sequence (blue) and staple sequences (multi-color). The .svg file was converted in a .pdf file with Adobe Illustrator (http://www.adobe.com/it/products/illustrator.html). We generated modified .pdf files that show the sites positions for each investigated enzyme on triangular and rectangular DNA origami schemes (see Appendix). The restriction sites were mapped by highlighting them (yellow) on the design schemes by using the find and the highlighting text tools of Adobe Acrobat Reader (https://acrobat.adobe.com/it/it/products/pdf-reader.html).

With Cando[3] we generated the molecular views of tiles of the DNA origami. The procedure consists in submitting the structure design generated with Cadnano to the online Cando website (http://cando-dna-origami.org), and therefore we obtained the .pdb file that we manipulated and viewed with rendering software Chimera (https://www.cgl.ucsf.edu/chimera/).

4.2 Design of staple with mutant site

We identified the staples containing a site for HhaI or Hin1II on the scheme of the triangular DNA origami that highlight their sites shown in appendix. The complete sequence of identified staples was obtained by searching in the list of staples of the triangle (staples names are highlighted in bold) a short piece of their sequences copied from the scheme. The staple sequences were mutated within the site sequence, for

HhaI the site was mutated from 5'-G**CG**C-3' to 5'-G**AT**C-3', while for Hin1II the site was mutated from 5'-C**AT**G-3' to 5'-C**CG**G-3'. The modified sequences are showed in appendix.

4.3 Design of the modified version of the loop

To implement the approach for studying Hin1II sites accessibility at single-site resolution within the triangle we created a second loop that was termed loop 2 (see Figure 2.26). To do so, we modified the DNA scaffold sequence of the triangle that is shown in appendix by removing 50 nt between the positions 6818 and 6868. The sequence that was removed will form the loop 2 sequence that contains the Hin1II 15th site as showed below:

5'-GCGTCAAAATGTAGGTATTTC**CATG**AGCGTTTTTCCTGTTGCAATGGCTG-3'

The modified scaffold sequence that was obtained is shown in appendix. This sequence was used to populate the design of the unmodified triangular DNA origami in Cadnano, permitting to recalculate the sequence of the 12 staples complementary to the region with shifted scaffold, which are shown in appendix.

4.4 Reagents

Circular single-stranded M13mp18 DNA (M13 ssDNA), circular double-stranded M13mp18 DNA (M13 dsDNA), and DpnII, BamHI, HaeIII, NlaIII and HypCH4IV enzymes were purchased from New England Biolabs, Ipswich, USA.

NiCl2, Tris, MgCl2, PEG8000, EDTA, NaCl, HCl, NaOH, DNaseI enzyme, CaCl2, Glycerol, Calf Thymus DNA, Agarose, Glacial acetic acid, Boric acid and Urea were purchased from Sigma-Aldrich, Saint Louis, Missouri, USA.

GeneRuler 1 kb Plus DNA Ladder, TriTrack DNA Loading Dye (6X), Acrylamide: Bis-Acrylamide 29:1 40% solution, AluI, BsuRI, DraI, Hin1II, HhaI, MspI and RsaI enzymes were purchased from Thermo Fisher Scientific, Waltham, Massachusetts, USA.

DNA Molecular Weight Marker IV was purchased from Hoffmann-La Roche AG, Basel, Switzerland.

MICA (clear ruby muscovite) was purchased from Mica Corporation, New York, USA.

DNA oligonucleotides that served as staple strands or other complementary strands were purchased unpurified from Sigma-Aldrich, Saint Louis, Missouri, USA or Biomers.net GmbH, Ulm, Germany at 100 μM diluted in water and was stored at -20˚C.

4.5 Assembly of DNA origami objects

We followed the protocol published by Rothemund P.W.K. [2]. For assembling the desired DNA origami object the specific pool of staples strands and the complementary strands were mixed with M13 ssDNA, at final concentrations of 50 nM and 10 nM or 100 nM and 20 nM, respectively, to a final volume of 50 µL in 40 mM Tris at pH 8.5 and 12.5 mM MgCl2. The self-assembly of the structures was performed by heating the reaction solution at 95˚C for 3 minutes, than decreasing the temperature from 95˚C to 20˚C at a rate of 1˚C/minute in a thermal cycler (Bio-rad, Hercules, California, USA).

4.6 Purification of DNA origami objects

We followed the protocol published by Stahl and co-workers[4]. The self-assembled DNA nanostructures were mixed 1:1 (v/v) with the precipitation solution that contains 15% PEG8000 (w/v), 5 mM Tris, 1 mM EDTA and 500 mM NaCl. The obtained solution is mixed by inversion and centrifuged at 16'000 g for 25 minutes at 4˚C with table top microcentrifuge (Thermo Fisher Scientific, Waltham, Massachusetts, USA). The supernatant was removed using a micropipette. The pellet was resuspended with a solution that contains 40 mM Tris at pH 8.5 with a volume equivalent to the initial solution of DNA origami for ~14 hours at RT.

4.7 DNaseI reactions

DNaseI enzyme was dissolved in solution containing 10 mM Tris-HCl at pH 7.5, 10 mM CaCl2, 10 mM MgCl2 and 50% Glycerol (v/v). Calf Thymus DNA was dissolved in TE 1X solution to final concentration of 1 mg/mL. The enzymatic reaction solution contains 3.76 µg of triangular DNA origami or 40 µg of Calf thymus DNA or 10 µg of M13 ssDNA, and DNAseI enzymatic units was added according to the experiment in Figure 2.1, in a volume of 50 µL in 10 mM Tris-HCl at pH 7.5, 2.5 mM MgCl2, 0.1 mM CaCl2. The reaction was incubated at 37˚C for 30 minutes in water bath (Julabo GmbH, Seelbach, Germany) and the reaction was stopped with 10 µL of 500 mM EDTA at pH 8.5.

4.8 Restriction enzymes reactions

The reaction mixture contains 5 nM of the purified DNA nanostructures or of M13 ssDNA or of M13 dsDNA, 10 units of enzyme, in Tango Buffer for enzymes obtained from Thermo-Fisher Scientific or in CutSmart Buffer for enzymes obtained from New England Biolabs to a final volume of 50 µL. The reaction was incubated at 37˚C for 1 hour or indicated times in kinetics experiments in water bath (Julabo GmbH, Seelbach, Germany) and was stopped with 20 minutes incubation at -80˚C.

4.9 HhaI reactions on DNA with nick

For annealing the desired DNA duplex with the specific nick position the appropriate combination of DNA strands (see Appendix) were mixed to a final concentration of 1 μM, in 25 μL in 40 mM Tris at pH 8.5 and 12.5 mM MgCl2 and was incubated with a thermocyler. The solution was subjected to a thermal treatment from 80˚C to 20˚C by a decrease temperature rate -1˚C/30 sec.

The enzymatic reaction was performed in solution that contains 100 nM of annealed DNA, 10 units of HhaI enzyme in Tango Buffer to a final volume of 50 μL. The solution was incubated for 1 hour at 37˚C in water bath. The reaction was stopped by placing the reaction in ice and adding the TriTrack loading Buffer.

4.10 Analysis of enzymatic reaction products

For the analysis of DNA sample in native conditions, the DNA sample was added to TriTrack DNA Loading Dye and was loaded on 1% agarose gel in TAE 1X or on 18% polyacrylamide gel and electrophoresed at 80V or 100V and 10 mA, respectively.

For the analysis of DNA sample in denaturing conditions, the DNA sample was added to TriTrack DNA Loading Dye and was subject to a thermal shock treatment incubating the sample at 95˚C for 3 minutes in a thermal cycler and then immediately placing the sample in ice for at least 5 minutes. The denatured sample was loaded on 1% agarose gel in TAE 1X and electrophoresed at 60V or 80V, or in 4% polyacrylamide gel in urea 8M and TBE 1X and electrophoresed at 10 mA.

The nanoscopic characterization of DNA nanostructures was done with Atomic Force Microscope MF3PD (Asylum research, Santa Barbara, USA) and using Tip BL-AC40TS-C2 (Olympus, Tokyo, Japan) with resonance frequency of ~110 kHz and of spring constant 0.09 N/m. The sample was prepared by a solution that contains 0.33 nM of purified DNA origami in 10 mM NiCl2, 40 mM Tris at pH 8.5 and 12.5 mM MgCl2 to a final volume of 30 μL. The 30 μL of the sample was dropped on freshly cleaved MICA and incubated for 10 minutes. Next, the MICA was washed very gently with distilled water (18.2 MΩ) and was positioned under AFM and was added with 100 μL of solution containing 40 mM Tris at pH 8.5 and 12.5 mM MgCl2. The imaging was preformed in liquid and in tapping mode.

4.11 Bibliography of Chap. 3

1. Douglas, S. M. *et al.* Rapid prototyping of 3D DNA-origami shapes with caDNAno. *Nucleic Acids Res.* **37,** 5001–5006 (2009).
2. Rothemund, P. W. K. Folding DNA to create nanoscale shapes and patterns. *Nature* **440,** 297–302 (2006).
3. Pan, K. *et al.* Lattice-free prediction of three-dimensional structure of programmed DNA assemblies. *Nat. Commun.* **5,** 5578 (2014).
4. Stahl, E., Martin, T. G., Praetorius, F. & Dietz, H. Facile and Scalable Preparation of Pure and Dense DNA Origami Solutions. *Angew. Chemie* n/a–n/a (2014). doi:10.1002/ange.201405991

Appendix

M13mp18 sequence used to design the staples for all DNA origami objects used in this thesis.

TTCCCTTCCTTTCTCGCCACGTTCGCCGGCTTTCCCCGTCAAGCTCTAAATCGGGGGCTCC
CTTTAGGGTTCCGATTTAGTGCTTTACGGCACCTCGACCCCAAAAAACTTGATTTGGGTGA
TGGTTCACGTAGTGGGCCATCGCCCTGATAGACGGTTTTTCGCCCTTTGACGTTGGAGTC
CACGTTCTTTAATAGTGGACTCTTGTTCCAAACTGGAACAACACTCAACCCTATCTCGGGCT
ATTCTTTTGATTTATAAGGGATTTTGCCGATTTCGGAACCACCATCAAACAGGATTTTCGCC
TGCTGGGGCAAACCAGCGTGGACCGCTTGCTGCAACTCTCTCAGGGCCAGGCGGTGAAG
GGCAATCAGCTGTTGCCCGTCTCGCTGGTGAAAAGAAAAACCACCCTGGCGCCCAATACG
CAAACCGCCTCTCCCCGCGCGTTGGCCGATTCATTAATGCAGCTGGCACGACAGGTTTCC
CGACTGGAAAGCGGGCAGTGAGCGCAACGCAATTAATGTGAGTTAGCTCACTCATTAGGC
ACCCCAGGCTTTACACTTTATGCTTCCGGCTCGTATGTTGTGTGGAATTGTGAGCGGATAA
CAATTTCACACAGGAAACAGCTATGACCATGATTACGAATTCGAGCTCGGTACCCGGGGAT
CCTCTAGAGTCGACCTGCAGGCATGCAAGCTTGGCACTGGCCGTCGTTTTACAACGTCGT
GACTGGGAAAACCCTGGCGTTACCCAACTTAATCGCCTTGCAGCACATCCCCCTTTCGCCA
GCTGGCGTAATAGCGAAGAGGCCCGCACCGATCGCCCTTCCCAACAGTTGCGCAGCCTG
AATGGCGAATGGCGCTTTGCCTGGTTTCCGGCACCAGAAGCGGTGCCGGAAAGCTGGCT
GGAGTGCGATCTTCCTGAGGCCGATACGGTCGTCGTCCCCTCAAACTGGCAGATGCACGG
TTACGATGCGCCCATCTACACCAACGTAACCTATCCCATTACGGTCAATCCGCCGTTTGTT
CCCACGGAGAATCCGACGGGTTGTTACTCGCTCACATTTAATGTTGATGAAAGCTGGCTAC
AGGAAGGCCAGACGCGAATTATTTTTGATGGCGTTCCTATTGGTTAAAAAATGAGCTGATTT
AACAAAAATTTAACGCGAATTTTAACAAAATATTAACGTTTACAATTTAAATATTTGCTTATAC
AATCTTCCTGTTTTTGGGGCTTTTCTGATTATCAACCGGGGTACATATGATTGACATGCTAG
TTTTACGATTACCGTTCATCGATTCTCTTGTTTGCTCCAGACTCTCAGGCAATGACCTGATA
GCCTTTGTAGATCTCTCAAAAATAGCTACCCTCTCCGGCATTAATTTATCAGCTAGAACGGT
TGAATATCATATTGATGGTGATTTGACTGTCTCCGGCCTTTCTCACCCTTTTGAATCTTTAC
CTACACATTACTCAGGCATTGCATTTAAAATATATGAGGGTTCTAAAAATTTTTATCCTTGCG
TTGAAATAAAGGCTTCTCCCGCAAAAGTATTACAGGGTCATAATGTTTTTGGTACAACCGAT
TTAGCTTTATGCTCTGAGGCTTTATTGCTTAATTTTGCTAATTCTTTGCCTTGCCTGTATGAT
TTATTGGATGTTAATGCTACTACTATTAGTAGAATTGATGCCACCTTTTCAGCTCGCGCCCC
AAATGAAAATATAGCTAAACAGGTTATTGACCATTTGCGAAATGTATCTAATGGTCAAACTA
AATCTACTCGTTCGCAGAATTGGGAATCAACTGTTACATGGAATGAAACTTCCAGACACCG
TACTTTAGTTGCATATTTAAAACATGTTGAGCTACAGCACCAGATTCAGCAATTAAGCTCTA
AGCCATCCGCAAAAATGACCTCTTATCAAAAGGAGCAATTAAAGGTACTCTCTAATCCTGAC
CTGTTGGAGTTTGCTTCCGGTCTGGTTCGCTTTGAAGCTCGAATTAAAACGCGATATTTGA
AGTCTTTCGGGCTTCCTCTTAATCTTTTTGATGCAATCCGCTTTGCTTCTGACTATAATAGTC
AGGGTAAAGACCTGATTTTTGATTTATGGTCATTCTCGTTTTCTGAACTGTTTAAAGCATTTG
AGGGGGATTCAATGAATATTTATGACGATTCCGCAGTATTGGACGCTATCCAGTCTAAACA
TTTTACTATTACCCCCTCTGGCAAAACTTCTTTTGCAAAAGCCTCTCGCTATTTTGGTTTTTA
TCGTCGTCTGGTAAACGAGGGTTATGATAGTGTTGCTCTTACTATGCCTCGTAATTCCTTTT
GGCGTTATGTATCTGCATTAGTTGAATGTGGTATTCCTAAATCTCAACTGATGAATCTTTCT
ACCTGTAATAATGTTGTTCCGTTAGTTCGTTTTATTAACGTAGATTTTTCTTCCCAACGTCCT
GACTGGTATAATGAGCCAGTTCTTAAAATCGCATAAGGTAATTCACAATGATTAAAGTTGAA
ATTAAACCATCTCAAGCCCAATTTACTACTCGTTCTGGTGTTCTCGTCAGGGCAAGCCTTAT
TCACTGAATGAGCAGCTTTGTTACGTTGATTTGGGTAATGAATATCCGGTTCTTGTCAAGAT
TACTCTTGATGAAGGTCAGCCAGCCTATGCGCCTGGTCTGTACACCGTTCATCTGTCCTCT
TTCAAAGTTGGTCAGTTCGGTTCCCTTATGATTGACCGTCTGCGCCTCGTTCCGGCTAAGT
AACATGGAGCAGGTCGCGGATTTCGACACAATTTATCAGGCGATGATACAAATCTCCGTTG
TACTTTGTTTCGCGCTTGGTATAATCGCTGGGGGTCAAAGATGAGTGTTTTAGTGTATTCTT
TCGCCTCTTTCGTTTTAGGTTGGTGCCTTCGTAGTGGCATTACGTATTTTACCCGTTTAATG
GAAACTTCCTCATGAAAAAGTCTTTAGTCCTCAAAGCCTCTGTAGCCGTTGCTACCCTCGTT
CCGATGCTGTCTTTCGCTGCTGAGGGTGACGATCCCGCAAAAGCGGCCTTTAACTCCCTG
CAAGCCTCAGCGACCGAATATATCGGTTATGCGTGGGCGATGGTTGTTGTCATTGTCGGC
GCAACTATCGGTATCAAGCTGTTTAAGAAATTCACCTCGAAAGCAAGCTGATAAACCGATA
CAATTAAAGGCTCCTTTTGGAGCCTTTTTTTTTGGAGATTTTCAACGTGAAAAAATTATTATT
CGCAATTCCTTTAGTTGTTCCTTTCTATTCTCACTCCGCTGAAACTGTTGAAAGTTGTTTAG
CAAAACCCCATACAGAAAATTCATTTACTAACGTCTGGAAAGACGACAAAACTTTAGATCGT
TACGCTAACTATGAGGGTTGTCTGTGGAATGCTACAGGCGTTGTAGTTTGTACTGGTGACG
AAACTCAGTGTTACGGTACATGGGTTCCTATTGGGCTTGCTATCCCTGAAAATGAGGGTGG

TGGCTCTGAGGGTGGCGGTTCTGAGGGTGGCGGTTCTGAGGGTGGCGGTACTAAACCTC
CTGAGTACGGTGATACACCTATTCCGGGCTATACTTATATCAACCCTCTCGACGGCACTTA
TCCGCCTGGTACTGAGCAAAACCCCGCTAATCCTAATCCTTCTCTTGAGGAGTCTCAGCCT
CTTAATACTTTCATGTTTCAGAATAATAGGTTCCGAAATAGGCAGGGGGCATTAACTGTTTA
TACGGGCACTGTTACTCAAGGCACTGACCCCGTTAAAACTTATTACCAGTACACTCCTGTA
TCATCAAAAGCCATGTATGACGCTTACTGGAACGGTAAATTCAGAGACTGCGCTTTCCATT
CTGGCTTTAATGAAGATCCATTCGTTTGTGAATATCAAGGCCAATCGTCTGACCTGCCTCAA
CCTCCTGTCAATGCTGGCGGCGGCTCTGGTGGTGGTTCTGGTGGCGGCTCTGAGGGTGG
TGGCTCTGAGGGTGGCGGTTCTGAGGGTGGCGGCTCTGAGGGAGGCGGTTCCGGTGGT
GGCTCTGGTTCCGGTGATTTTGATTATGAAAAGATGGCAAACGCTAATAAGGGGGCTATGA
CCGAAAATGCCGATGAAAACGCGCTACAGTCTGACGCTAAAGGCAAACTTGATTCTGTCGC
TACTGATTACGGTGCTGCTATCGATGGTTTCATTGGTGACGTTTCCGGCCTTGCTAATGGT
AATGGTGCTACTGGTGATTTTGCTGGCTCTAATTCCCAAATGGCTCAAGTCGGTGACGGTG
ATAATTCACCTTTAATGAATAATTTCCGTCAATATTTACCTTCCCTCCCTCAATCGGTTGAAT
GTCGCCCTTTTGTCTTTAGCGCTGGTAAACCATATGAATTTTCTATTGATTGTGACAAAATA
AACTTATTCCGTGGTGTCTTTGCGTTTCTTTTATATGTTGCCACCTTTATGTATGTATTTTCT
ACGTTTGCTAACATACTGCGTAATAAGGAGTCTTAATCATGCCAGTTCTTTTGGGTATTCCG
TTATTATTGCGTTTCCTCGGTTTCCTTCTGGTAACTTTGTTCGGCTATCTGCTTACTTTTCTT
AAAAAGGGCTTCGGTAAGATAGCTATTGCTATTTCATTGTTTCTTGCTCTTATTATTGGGCTT
AACTCAATTCTTGTGGGTTATCTCTCTGATATTAGCGCTCAATTACCCTCTGACTTTGTTCA
GGGTGTTCAGTTAATTCTCCCGTCTAATGCGCTTCCCTGTTTTTATGTTATTCTCTCTGTAAA
GGCTGCTATTTTCATTTTTGACGTTAAACAAAAAATCGTTTCTTATTTGGATTGGGATAAATA
ATATGGCTGTTTATTTTGTAACTGGCAAATTAGGCTCTGGAAAGACGCTCGTTAGCGTTGG
TAAGATTCAGGATAAAATTGTAGCTGGGTGCAAAATAGCAACTAATCTTGATTTAAGGCTTC
AAAACCTCCCGCAAGTCGGGAGGTTCGCTAAAACGCCTCGCGTTCTTAGAATACCGGATA
AGCCTTCTATATCTGATTTGCTTGCTATTGGGCGCGGTAATGATTCCTACGATGAAAATAAA
AACGGCTTGCTTGTTCTCGATGAGTGCGGTACTTGGTTTAATACCCGTTCTTGGAATGATA
AGGAAAGACAGCCGATTATTGATTGGTTTCTACATGCTCGTAAATTAGGATGGGATATTATT
TTTCTTGTTCAGGACTTATCTATTGTTGATAAACAGGCGCGTTCTGCATTAGCTGAACATGT
TGTTTATTGTCGTCGTCTGGACAGAATTACTTTACCTTTTGTCGGTACTTTATATTCTCTTAT
TACTGGCTCGAAAATGCCTCTGCCTAAATTACATGTTGGCGTTGTTAAATATGGCGATTCTC
AATTAAGCCCTACTGTTGAGCGTTGGCTTTATACTGGTAAGAATTTGTATAACGCATATGAT
ACTAAACAGGCTTTTTCTAGTAATTATGATTCCGGTGTTTATTCTTATTTAACGCCTTATTTAT
CACACGGTCGGTATTTCAAACCATTAAATTTAGGTCAGAAGATGAAATTAACTAAAATATATT
TGAAAAAGTTTTCTCGCGTTCTTTGTCTTGCGATTGGATTTGCATCAGCATTTACATATAGTT
ATATAACCCAACCTAAGCCGGAGGTTAAAAAGGTAGTCTCTCAGACCTATGATTTTGATAAA
TTCACTATTGACTCTTCTCAGCGTCTTAATCTAAGCTATCGCTATGTTTTCAAGGATTCTAAG
GGAAAATTAATTAATAGCGACGATTTACAGAAGCAAGGTTATTCACTCACATATATTGATTTA
TGTACTGTTTCCATTAAAAAAGGTAATTCAAATGAAATTGTTAAATGTAATTAATTTTGTTTTC
TTGATGTTTGTTTCATCATCTTCTTTTGCTCAGGTAATTGAAATGAATAATTCGCCTCTGCGC
GATTTTGTAACTTGGTATTCAAAGCAATCAGGCGAATCCGTTATTGTTTCTCCCGATGTAAA
AGGTACTGTTACTGTATATTCATCTGACGTTAAACCTGAAAATCTACGCAATTTCTTTATTTC
TGTTTTACGTGCTAATAATTTTGATATGGTTGGTTCAATTCCTTCCATAATTCAGAAGTATAA
TCCAAACAATCAGGATTATATTGATGAATTGCCATCATCTGATAATCAGGAATATGATGATA
ATTCCGCTCCTTCTGGTGGTTTCTTTGTTCCGCAAAATGATAATGTTACTCAAACTTTTAAAA
TTAATAACGTTCGGGCAAAGGATTTAATACGAGTTGTCGAATTGTTTGTAAAGTCTAATACT
TCTAAATCCTCAAATGTATTATCTATTGACGGCTCTAATCTATTAGTTGTTAGTGCACCTAAA
GATATTTTAGATAACCTTCCTCAATTCCTTTCTACTGTTGATTTGCCAACTGACCAGATATTG
ATTGAGGGTTTGATATTTGAGGTTCAGCAAGGTGATGCTTTAGATTTTTCATTTGCTGCTGG
CTCTCAGCGTGGCACTGTTGCAGGCGGTGTTAATACTGACCGCCTCACCTCTGTTTTATCT
TCTGCTGGTGGTTCGTTCGGTATTTTTAATGGCGATGTTTTAGGGCTATCAGTTCGCGCATT
AAAGACTAATAGCCATTCAAAAATATTGTCTGTGCCACGTATTCTTACGCTTTCAGGTCAGA
AGGGTTCTATCTCTGTTGGCCAGAATGTCCCTTTTATTACTGGTCGTGTGACTGGTGAATCT
GCCAATGTAAATAATCCATTTCAGACGATTGAGCGTCAAAATGTAGGTATTTCCATGAGCGT
TTTTCCTGTTGCAATGGCTGGCGGTAATATTGTTCTGGATATTACCAGCAAGGCCGATAGT
TTGAGTTCTTCTACTCAGGCAAGTGATGTTATTACTAATCAAAGAAGTATTGCTACAACGGT
TAATTTGCGTGATGGACAGACTCTTTTACTCGGTGGCCTCACTGATTATAAAAACACTTCTC
AAGATTCTGGCGTACCGTTCCTGTCTAAAATCCCTTTAATCGGCCTCCTGTTTAGCTCCCG
CTCTGATTCCAACGAGGAAAGCACGTTATACGTGCTCGTCAAAGCAACCATAGTACGCGCC

CTGTAGCGGCGCATTAAGCGCGGCGGGTGTGGTGGTTACGCGCAGCGTGACCGCTACAC
TTGCCAGCGCCCTAGCGCCCGCTCCTTTCGCTTTC

Modified scaffold sequence used to design the staples for Hin1II triangle with two loops.

TTCCCTTCCTTTCTCGCCACGTTCGCCGGCTTTCCCCGTCAAGCTCTAAATCGGGGGCTCC
CTTTAGGGTTCCGATTTAGTGCTTTACGGCACCTCGACCCCAAAAAACTTGATTTGGGTGA
TGGTTCACGTAGTGGGCCATCGCCCTGATAGACGGTTTTTCGCCCTTTGACGTTGGAGTC
CACGTTCTTTAATAGTGGACTCTTGTTCCAAACTGGAACAACACTCAACCCTATCTCGGGCT
ATTCTTTTGATTTATAAGGGATTTTGCCGATTTCGGAACCACCATCAAACAGGATTTTCGCC
TGCTGGGGCAAACCAGCGTGGACCGCTTGCTGCAACTCTCTCAGGGCCAGGCGGTGAAG
GGCAATCAGCTGTTGCCCGTCTCGCTGGTGAAAAGAAAAACCACCCTGGCGCCCAATACG
CAAACCGCCTCTCCCCGCGCGTTGGCCGATTCATTAATGCAGCTGGCACGACAGGTTTCC
CGACTGGAAAGCGGGCAGTGAGCGCAACGCAATTAATGTGAGTTAGCTCACTCATTAGGC
ACCCCAGGCTTTACACTTTATGCTTCCGGCTCGTATGTTGTGTGGAATTGTGAGCGGATAA
CAATTTCACACAGGAAACAGCTATGACCATGATTACGAATTCGAGCTCGGTACCCGGGGAT
CCTCTAGAGTCGACCTGCAGGCATGCAAGCTTGGCACTGGCCGTCGTTTTACAACGTCGT
GACTGGGAAAACCCTGGCGTTACCCAACTTAATCGCCTTGCAGCACATCCCCCTTTCGCCA
GCTGGCGTAATAGCGAAGAGGCCCGCACCGATCGCCCTTCCCAACAGTTGCGCAGCCTG
AATGGCGAATGGCGCTTTGCCTGGTTTCCGGCACCAGAAGCGGTGCCGGAAAGCTGGCT
GGAGTGCGATCTTCCTGAGGCCGATACGGTCGTCGTCCCCTCAAACTGGCAGATGCACGG
TTACGATGCGCCCATCTACACCAACGTAACCTATCCCATTACGGTCAATCCGCCGTTTGTT
CCCACGGAGAATCCGACGGGTTGTTACTCGCTCACATTTAATGTTGATGAAAGCTGGCTAC
AGGAAGGCCAGACGCGAATTATTTTTGATGGCGTTCCTATTGGTTAAAAAATGAGCTGATTT
AACAAAAATTTAACGCGAATTTTAACAAAATATTAACGTTTACAATTTAAATATTTGCTTATAC
AATCTTCCTGTTTTTGGGGCTTTTCTGATTATCAACCGGGGTACATATGATTGACATGCTAG
TTTTACGATTACCGTTCATCGATTCTCTTGTTTGCTCCAGACTCTCAGGCAATGACCTGATA
GCCTTTGTAGATCTCTCAAAAATAGCTACCCTCTCCGGCATTAATTTATCAGCTAGAACGGT
TGAATATCATATTGATGGTGATTTGACTGTCTCCGGCCTTTCTCACCCTTTTGAATCTTTAC
CTACACATTACTCAGGCATTGCATTTAAAATATATGAGGGTTCTAAAAATTTTTATCCTTGCG
TTGAAATAAAGGCTTCTCCCGCAAAAGTATTACAGGGTCATAATGTTTTTGGTACAACCGAT
TTAGCTTTATGCTCTGAGGCTTTATTGCTTAATTTTGCTAATTCTTTGCCTTGCCTGTATGAT
TTATTGGATGTTAATGCTACTACTATTAGTAGAATTGATGCCACCTTTTCAGCTCGCGCCCC
AAATGAAAATATAGCTAAACAGGTTATTGACCATTTGCGAAATGTATCTAATGGTCAAACTA
AATCTACTCGTTCGCAGAATTGGGAATCAACTGTTACATGGAATGAAACTTCCAGACACCG
TACTTTAGTTGCATATTTAAAACATGTTGAGCTACAGCACCAGATTCAGCAATTAAGCTCTA
AGCCATCCGCAAAAATGACCTCTTATCAAAAGGAGCAATTAAAGGTACTCTCTAATCCTGAC
CTGTTGGAGTTTGCTTCCGGTCTGGTTCGCTTTGAAGCTCGAATTAAAACGCGATATTTGA
AGTCTTTCGGGCTTCCTCTTAATCTTTTTGATGCAATCCGCTTTGCTTCTGACTATAATAGTC
AGGGTAAAGACCTGATTTTTGATTTATGGTCATTCTCGTTTTCTGAACTGTTTAAAGCATTTG
AGGGGGATTCAATGAATATTTATGACGATTCCGCAGTATTGGACGCTATCCAGTCTAAACA
TTTTACTATTACCCCCTCTGGCAAAACTTCTTTTGCAAAAGCCTCTCGCTATTTTGGTTTTTA
TCGTCGTCTGGTAAACGAGGGTTATGATAGTGTTGCTCTTACTATGCCTCGTAATTCCTTTT
GGCGTTATGTATCTGCATTAGTTGAATGTGGTATTCCTAAATCTCAACTGATGAATCTTTCT
ACCTGTAATAATGTTGTTCCGTTAGTTCGTTTTATTAACGTAGATTTTTCTTCCCAACGTCCT
GACTGGTATAATGAGCCAGTTCTTAAAATCGCATAAGGTAATTCACAATGATTAAAGTTGAA
ATTAAACCATCTCAAGCCCAATTTACTACTCGTTCTGGTGTTCTCGTCAGGGCAAGCCTTAT
TCACTGAATGAGCAGCTTTGTTACGTTGATTTGGGTAATGAATATCCGGTTCTTGTCAAGAT
TACTCTTGATGAAGGTCAGCCAGCCTATGCGCCTGGTCTGTACACCGTTCATCTGTCCTCT
TTCAAAGTTGGTCAGTTCGGTTCCCTTATGATTGACCGTCTGCGCCTCGTTCCGGCTAAGT
AACATGGAGCAGGTCGCGGATTTCGACACAATTTATCAGGCGATGATACAAATCTCCGTTG
TACTTTGTTTCGCGCTTGGTATAATCGCTGGGGGTCAAAGATGAGTGTTTTAGTGTATTCTT
TCGCCTCTTTCGTTTTAGGTTGGTGCCTTCGTAGTGGCATTACGTATTTTACCCGTTTAATG
GAAACTTCCTCATGAAAAAGTCTTTAGTCCTCAAAGCCTCTGTAGCCGTTGCTACCCTCGTT
CCGATGCTGTCTTTCGCTGCTGAGGGTGACGATCCCGCAAAAGCGGCCTTTAACTCCCTG
CAAGCCTCAGCGACCGAATATATCGGTTATGCGTGGGCGATGGTTGTTGTCATTGTCGGC
GCAACTATCGGTATCAAGCTGTTTAAGAAATTCACCTCGAAAGCAAGCTGATAAACCGATA
CAATTAAAGGCTCCTTTTGGAGCCTTTTTTTTTGGAGATTTTCAACGTGAAAAAATTATTATT

CGCAATTCCTTTAGTTGTTCCTTTCTATTCTCACTCCGCTGAAACTGTTGAAAGTTGTTTAG
CAAAACCCCATACAGAAAATTCATTTACTAACGTCTGGAAAGACGACAAAACTTTAGATCGT
TACGCTAACTATGAGGGTTGTCTGTGGAATGCTACAGGCGTTGTAGTTTGTACTGGTGACG
AAACTCAGTGTTACGGTACATGGGTTCCTATTGGGCTTGCTATCCCTGAAAATGAGGGTGG
TGGCTCTGAGGGTGGCGGTTCTGAGGGTGGCGGTTCTGAGGGTGGCGGTACTAAACCTC
CTGAGTACGGTGATACACCTATTCCGGGCTATACTTATATCAACCCTCTCGACGGCACTTA
TCCGCCTGGTACTGAGCAAAACCCCGCTAATCCTAATCCTTCTCTTGAGGAGTCTCAGCCT
CTTAATACTTTCATGTTTCAGAATAATAGGTTCCGAAATAGGCAGGGGGCATTAACTGTTTA
TACGGGCACTGTTACTCAAGGCACTGACCCCGTTAAAACTTATTACCAGTACACTCCTGTA
TCATCAAAAGCCATGTATGACGCTTACTGGAACGGTAAATTCAGAGACTGCGCTTTCCATT
CTGGCTTTAATGAAGATCCATTCGTTTGTGAATATCAAGGCCAATCGTCTGACCTGCCTCAA
CCTCCTGTCAATGCTGGCGGCGGCTCTGGTGGTGGTTCTGGTGGCGGCTCTGAGGGTGG
TGGCTCTGAGGGTGGCGGTTCTGAGGGTGGCGGCTCTGAGGGAGGCGGTTCCGGTGGT
GGCTCTGGTTCCGGTGATTTTGATTATGAAAAGATGGCAAACGCTAATAAGGGGGCTATGA
CCGAAAATGCCGATGAAAACGCGCTACAGTCTGACGCTAAAGGCAAACTTGATTCTGTCGC
TACTGATTACGGTGCTGCTATCGATGGTTTCATTGGTGACGTTTCCGGCCTTGCTAATGGT
AATGGTGCTACTGGTGATTTTGCTGGCTCTAATTCCCAAATGGCTCAAGTCGGTGACGGTG
ATAATTCACCTTTAATGAATAATTTCCGTCAATATTTACCTTCCCTCCCTCAATCGGTTGAAT
GTCGCCCTTTTGTCTTTAGCGCTGGTAAACCATATGAATTTTCTATTGATTGTGACAAAATA
AACTTATTCCGTGGTGTCTTTGCGTTTCTTTTATATGTTGCCACCTTTATGTATGTATTTTCT
ACGTTTGCTAACATACTGCGTAATAAGGAGTCTTAATCATGCCAGTTCTTTTGGGTATTCCG
TTATTATTGCGTTTCCTCGGTTTCCTTCTGGTAACTTTGTTCGGCTATCTGCTTACTTTTCTT
AAAAAGGGCTTCGGTAAGATAGCTATTGCTATTTCATTGTTTCTTGCTCTTATTATTGGGCTT
AACTCAATTCTTGTGGGTTATCTCTCTGATATTAGCGCTCAATTACCCTCTGACTTTGTTCA
GGGTGTTCAGTTAATTCTCCCGTCTAATGCGCTTCCCTGTTTTTATGTTATTCTCTCTGTAAA
GGCTGCTATTTTCATTTTTGACGTTAAACAAAAAATCGTTTCTTATTTGGATTGGGATAAATA
ATATGGCTGTTTATTTTGTAACTGGCAAATTAGGCTCTGGAAAGACGCTCGTTAGCGTTGG
TAAGATTCAGGATAAAATTGTAGCTGGGTGCAAAATAGCAACTAATCTTGATTTAAGGCTTC
AAAACCTCCCGCAAGTCGGGAGGTTCGCTAAAACGCCTCGCGTTCTTAGAATACCGGATA
AGCCTTCTATATCTGATTTGCTTGCTATTGGGCGCGGTAATGATTCCTACGATGAAAATAAA
AACGGCTTGCTTGTTCTCGATGAGTGCGGTACTTGGTTTAATACCCGTTCTTGGAATGATA
AGGAAAGACAGCCGATTATTGATTGGTTTCTACATGCTCGTAAATTAGGATGGGATATTATT
TTTCTTGTTCAGGACTTATCTATTGTTGATAAACAGGCGCGTTCTGCATTAGCTGAACATGT
TGTTTATTGTCGTCGTCTGGACAGAATTACTTTACCTTTTGTCGGTACTTTATATTCTCTTAT
TACTGGCTCGAAAATGCCTCTGCCTAAATTACATGTTGGCGTTGTTAAATATGGCGATTCTC
AATTAAGCCCTACTGTTGAGCGTTGGCTTTATACTGGTAAGAATTTGTATAACGCATATGAT
ACTAAACAGGCTTTTTCTAGTAATTATGATTCCGGTGTTTATTCTTATTTAACGCCTTATTTAT
CACACGGTCGGTATTTCAAACCATTAAATTTAGGTCAGAAGATGAAATTAACTAAAATATATT
TGAAAAAGTTTTCTCGCGTTCTTTGTCTTGCGATTGGATTTGCATCAGCATTTACATATAGTT
ATATAACCCAACCTAAGCCGGAGGTTAAAAAGGTAGTCTCTCAGACCTATGATTTTGATAAA
TTCACTATTGACTCTTCTCAGCGTCTTAATCTAAGCTATCGCTATGTTTTCAAGGATTCTAAG
GGAAAATTAATTAATAGCGACGATTTACAGAAGCAAGGTTATTCACTCACATATATTGATTTA
TGTACTGTTTCCATTAAAAAAGGTAATTCAAATGAAATTGTTAAATGTAATTAATTTTGTTTTC
TTGATGTTTGTTTCATCATCTTCTTTTGCTCAGGTAATTGAAATGAATAATTCGCCTCTGCGC
GATTTTGTAACTTGGTATTCAAAGCAATCAGGCGAATCCGTTATTGTTTCTCCCGATGTAAA
AGGTACTGTTACTGTATATTCATCTGACGTTAAACCTGAAAATCTACGCAATTTCTTTATTTC
TGTTTTACGTGCTAATAATTTTGATATGGTTGGTTCAATTCCTTCCATAATTCAGAAGTATAA
TCCAAACAATCAGGATTATATTGATGAATTGCCATCATCTGATAATCAGGAATATGATGATA
ATTCCGCTCCTTCTGGTGGTTTCTTTGTTCCGCAAAATGATAATGTTACTCAAACTTTTAAAA
TTAATAACGTTCGGGCAAAGGATTTAATACGAGTTGTCGAATTGTTTGTAAAGTCTAATACT
TCTAAATCCTCAAATGTATTATCTATTGACGGCTCTAATCTATTAGTTGTTAGTGCACCTAAA
GATATTTTAGATAACCTTCCTCAATTCCTTTCTACTGTTGATTTGCCAACTGACCAGATATTG
ATTGAGGGTTTGATATTTGAGGTTCAGCAAGGTGATGCTTTAGATTTTTCATTTGCTGCTGG
CTCTCAGCGTGGCACTGTTGCAGGCGGTGTTAATACTGACCGCCTCACCTCTGTTTTATCT
TCTGCTGGTGGTTCGTTCGGTATTTTTAATGGCGATGTTTTAGGGCTATCAGTTCGCGCATT
AAAGACTAATAGCCATTCAAAAATATTGTCTGTGCCACGTATTCTTACGCTTTCAGGTCAGA
AGGGTTCTATCTCTGTTGGCCAGAATGTCCCTTTTATTACTGGTCGTGTGACTGGTGAATCT
GCCAATGTAAATAATCCATTTCAGACGATTGAGCGGTAATATTGTTCTGGATATTACCAGCA
AGGCCGATAGTTTGAGTTCTTCTACTCAGGCAAGTGATGTTATTACTAATCAAAGAAGTATT
GCTACAACGGTTAATTTGCGTGATGGACAGACTCTTTTACTCGGTGGCCTCACTGATTATA

AAAACACTTCTCAAGATTCTGGCGTACCGTTCCTGTCTAAAATCCCTTTAATCGGCCTCCTG
TTTAGCTCCCGCTCTGATTCCAACGAGGAAAGCACGTTATACGTGCTCGTCAAAGCAACCA
TAGTACGCGCCCTGTAGCGGCGCATTAAGCGCGGCGGGTGTGGTGGTTACGCGCAGCGT
GACCGCTACACTTGCCAGCGCCCTAGCGCCCGCTCCTTTCGCTTTC

Sequence of staples for the triangle. In bold the staples that contain a site for Hin1II or HhaI.

A1 cggggtttcctcaagagaaggattttgaatta
A2 agcgtcatgtctctgaatttaccgactacctt
A3 ttcataatccccttattagcgtttttcttacc
A4 atggtttatgtcacaatcaatagatattaaac
A5 tttgatgattaagaggctgagacttgctcagtaccaggcg
A6 ccggaacccagaatggaaagcgcaacatggct (HhaI) and (Hin1II)
A7 aaagacaacattttcggtcatagccaaaatca
A8 gacgggagaattaactcggaataagtttatttccagcgct (HhaI)
A9 gataagtgccgtcgagctgaaacatgaaagtatacaggag (Hin1II)
A10 tgtactggggatcttcattaaagcagagccac
A11 caccggaaagcgcgttttcatcggaagggcga (HhaI)
A12 cattcaacaaacgcaaagacaccagaacaccctgaacaaa
A13 tttaacggttcggaacctattattagggttgatataagta
A14 ctcagagcatattcacaaacgaattaataagt
A15 ggagggaatttagcgtcagactgtccgcctcc
A16 gtcagagggtaattgatggcaacatataaaagcgattgag
A17 tagcccggaataggtgaatgccccctgcctatggtcagtg
A18 ccttgagtcagacgattggccttgcgccaccc
A19 tcagaacccagaatcaagtttgccggtaaata
A20 ttgacggaaatacatacataaagggcgctaatatcagaga (HhaI)
A21 cagagccaggaggttgaggcaggtaacagtgcccg
A22 attaaaggccgtaatcagtagcgagccaccct
A23 gataacccacaagaatgttagcaaacgtagaaaattattc
A24 gccgccagcattgacaccaccctc
A25 agagccgcaccatcgatagcagcatgaattat
A26 caccgtcaccttattacgcagtattgagttaagcccaata
A27 agccatttaaacgtcaccaatgaacaccagaacca
A28 ataagagcaagaaacatggcatgattaagactccgacttg (Hin1II)
A29 ccattagcaaggccgggggaatta
A30 gagccagcgaatacccaaaagaacatgaaatagcaatagc
A31 tatcttaccgaagcccaaacgcaataataacgaaaatcaccag
A32 cagaaggaaaccgaggtttttaagaaaagtaagcagatagccg
A33 ccttttttcatttaacaatttcataggattag
A34 tttaacctatcataggtctgagagttccagta
A35 agtataaaatatgcgttatacaaagccatctt
A36 caagtacctcattccaagaacgggaaattcat
A37 agagaataacataaaaacagggaagcgcatta (HhaI)
A38 aaaacaaaattaattaaatggaaacagtacattagtgaat
A39 ttatcaaaccggcttaggttgggtaagcctgt
A40 ttagtatcgccaacgctcaacagtcggctgtc
A41 tttccttagcactcatcgagaacaatagcagcctttacag
A42 agagtcaaaaatcaatatatgtgatgaaacaaacatcaag
A43 actagaaatatataactatatgtacgctgaga
A44 tcaataatagggcttaattgagaatcataatt
A45 aacgtcaaaaatgaaaagcaagccgtttttatgaaaccaa
A46 gagcaaaagaagatgagtgaataaccttgcttatagctta
A47 gattaagaaatgctgatgcaaatcagaataaa
A48 caccggaatcgccatatttaacaaaatttacg
A49 agcatgtatttcatcgtaggaatcaaacgatttttttgttt (Hin1II)
A50 acatagcgctgtaaatcgtcgctattcatttcaattacct
A51 gttaaatacaatcgcaagacaaagccttgaaa
A52 cccatcctcgccaacatgtaatttaataaggc (Hin1II)

A53 **tcccaatccaaataagattaccgcgcccaataaataatat (HhaI)**
A54 tcccttagaataacgcgagaaaacttttaccgacc
A55 gtgtgataaggcagaggcattttcagtcctga
A56 acaagaaagcaagcaaatcagataacagccatattattta
A57 gtttgaaattcaaatatattttag
A58 aatagatagagccagtaataagagatttaatg
A59 gccagttacaaaataatagaaggcttatccggttatcaac
A60 ttctgacctaaaatataaagtaccgactgcagaac
A61 **gcgcctgttattctaagaacgcgattccagagcctaattt (HhaI)**
A62 tcagctaaaaaaggtaaagtaatt
A63 **acgctaacgagcgtctggcgttttagcgaacccaacatgt (Hin1II)**
A64 acgacaataaatcccgacttgcgggagatcctgaatcttacca
A65 tgctattttgcacccagctacaattttgttttgaagccttaaa
B1 tcatatgtgtaatcgtaaaactagtcattttc
B2 gtgagaaaatgtgtaggtaaagatacaacttt
B3 **ggcatcaaatttggggcgcgagctgagttaaa (HhaI)**
B4 ttcgagctaagacttcaaatatcgcggaacga
B5 acagtcaaagagaatcgatgaacgaccccggttgataatc
B6 atagtagtatgcaatgcctgagtaggccggag
B7 aaccagacgtttagctatattttcttctacta
B8 gaataccacattcaacttaagaggaagcccgatcaaagcg
B9 agaaaagccccaaaaagagtctggagcaaacaatcaccat
B10 caatatgaccctcatatattttaaagcattaa
B11 catccaataaatggtcaataacctcggaagca
B12 aactccaagattgcatcaaaaagataatgcagatacataa
B13 cgttctagtcaggtcattgcctgacaggaagattgtataa
B14 caggcaagataaaaatttttagaatattcaac
B15 gattagagattagatacatttcgcaaatcata
B16 cgccaaaaggaattacagtcagaagcaaagcgcaggtcag
B17 gcaaatatttaaattgagatctacaaaggctactgataaa
B18 ttaatgccttatttcaacgcaagggcaaagaa
B19 ttagcaaatagatttagtttgaccagtacctt
B20 taattgctttaccctgactattatgaggcatagtaagagc
B21 ataaagcctttgcgggagaagcctggagagggtag
B22 taagaggtcaattctgcgaacgagattaagca
B23 aacactatcataacccatcaaaaatcaggtctccttttga
B24 atgaccctgtaatacttcagagca
B25 **taaagctatgtaacagttgattcccatttttg (Hin1II)**
B26 cggatggcacgagaatgaccataatcgtttaccagacgac
B27 **taattgcttggaagtttcattccaaatcggttgta (Hin1II)**
B28 gataaaaaccaaaatattaaacagttcagaaattagagct
B29 actaaagtacggtgtcgaatctgg
B30 tgctgtagatccccctcaaatgctgcgagaggcttttgca
B31 **aaagaagttttgccagcataaatattcattgactcaacatgtt (Hin1II)**
B32 aatactgcggaatcgtaggggtaatagtaaaatgtttagact
B33 **agggatagctcagagccaccaccccatgtcaa (Hin1II)**
B34 caacagtttatggggttttgctaatcaaaagg
B35 ggccgcttcgctgaggcttgcagggaaaaggt
B36 **ggcgcagactccatgttacttagccgttttaa (HhaI) and (Hin1II)**
B37 acaggtagaaagattcatcagttgagatttag
B38 cctcagaaccgccacccaagcccaataggaacgtaaatga
B39 attttctgtcagcggagtgagaataaccgata
B40 tattcggtttgcgggatcgtcacccgaaatcc
B41 gcgacctgcggtcaatcataagggacggaacaacattatt
B42 **agacgttaccatgtaccgtaacacccctcagaaccgccac (Hin1II)**
B43 ccacgcatagaaaggaacaactaagtctttcc
B44 aattgtgtctcagcagcgaaagacaccatcgc
B45 ttaataaaacgaactaaaccgaactgaccaacgcctgata
B46 aggtttagtaccgccatgagtttcgtcaccaggatctaaa
B47 **gttttgtcaggaattgcgaataatgccgacaa (HhaI)**

B48 tgacaacaagcatcggaacgaggggagattt
B49 gtatcatctttgaaagaggacagaggaagaaaaatctacg
B50 agcgtaactacaaactacaacgcctatcaccgtactcagg
B51 atagttgcaatttttcacgttgatcatagtt (HhaI)
B52 agtacaactagcaacggctacagatgataccg
B53 accagtcaggacgttgtgaacggtgtacagaccgaaacaa
B54 acagacaacccaaatctccaaaaaaaaaatttctt
B55 aaacagctggctttgaggactaaagcgattat
B56 accaagcgcaggcgcataggctggagaactggctcattat (HhaI)
B57 tcgaggtgaggctccaaaaggagc
B58 gacccccagacttttttcatgaggagcttgctt (Hin1II)
B59 accttatgcgattttactgaccttcatcaagatcatcttt
B60 tcggtttatcaagtttccattaaacgggaatacac
B61 taaaacacgtaatcttgacaagaattaatcattgtgaatt
B62 aggcgaaagtaaaatacgtaatgc
B63 tggtttaatttcaactccggatattcattaccaacgaaag
B64 caccaacctaacaaatcaacgtaacaataaattgggcttgaga
B65 ccctgacgagaacaccagaacgagtagagctgctcattcagtg
C1 atcgggagatatacagtaacagtacaaataatt
C2 cctgattaaaggagcggaattatctcggcctc
C3 ggcaaatcacctcaatcaatatctgcaggtcga
C4 cgaccagtacattggcagattcacctgattgc
C5 tggcaatttttaacgtcagatgaaaacaataacggattcg
C6 aaggaattacaaagaaaccaccagtcagatga
C7 ggacattcacctcaaatatcaaacacagtaga
C8 ttgacgagcacgtatactgaaatggattatttaataaaag
C9 cctgattgctttgaattgcgtagattttcaggcatcaata
C10 taatcctgattatcattttgcggagaggaagg
C11 ttatctaaagcatcaccttgctgatggccaac
C12 agagatagtttgacgctcaatcgtacgtgctttcctcgtt
C13 gattatacacagaaataaagaaataccaagttacaaaatc
C14 taggtgcataaaagtttgagtaacattgtttg
C15 tgacctgacaaatgaaaaatctaaaatatctt
C16 ggaatcagagcgggagatggaaatacctacataacccttc
C17 gcgcagaggcgaattaattattagcacgtaaattctgaat (HhaI)
C18 tatggaagcgaacgttattaatttctaacaac
C19 taatagatcgctgagagccagcagaagcgtaa
C20 gaatacgtaacaggaaaaacgctcctaaacaggaggccga
C21 tcaatagatattaaatcctttgccgaattgaacca
C22 caatatttgcctgcaacagtgccatagagccg
C23 ttaaagggattttagataccgccagccattgcggcacaga
C24 acaattcgacaactcgtaatacat
C25 ttgaggatggtcagtattaacaccttgaatgg
C26 ctattagtatatccagaacaatatcaggaacggtacgcca
C27 cgcgaactaaaacagaggtgaggcttagaagtatt (HhaI)
C28 gaatcttgagaagtgtatcggccttgctggtactttaatg
C29 accaccagcagaagatgatagcc
C30 ctaaaacattagaagaactcaaacttttataatcagtgag
C31 gccaccgagtaaaagaacatcacttgcctgagcgccattaaaa
C32 tctttgattagtaatagtctgtccatcacgcaaattaaccgtt
C33 cgcgtctgataggaacgccatcaacttttac
C34 aggaagatggggacgacgaccgtaatcatatt
C35 ctctagagcaagcttgcatgcctggtcagtt (Hin1II)
C36 ccttcaccgcgagacgggcaacagcagtcaca
C37 cgagaaaggaagggaagcgtactatggttgct
C38 gctcatttttaaccagccttcctgtagccaggcatctgc
C39 cagtttgacgcactccagccagctaaacgacg
C40 gccagtgcgatccccgggtaccgagtttttct
C41 tttcaccagcctggccctgagagaaagccggcgaacgtgg
C42 gtaaccgtctttcatcaacattaaaatttttgttaaatca

C43	**acgttgtattccggcaccgcttctggcgcatc (HhaI)**
C44	ccagggtggctcgaattcgtaatccagtcacg
C45	**tagagcttgacggggagttgcagcaagcggtcattgggcg (HhaI)**
C46	gttaaaattcgcgttaatgtgagcgagtaacatacgttgg
C47	tgtagatgggtgccggaaaccaggaacgccag
C48	**ggttttccatggtcatagctgtttgagaggcg (Hin1II)**
C49	gtttgcgtcacgctggtttgccccaagggagcccccgatt
C50	ggataggtacccgtcggattctcctaaacgttaatatttt
C51	**agttgggtcaaagcgccattcgccccgtaatg (HhaI)**
C52	**cgcgcgggcctgtgtgaaattgttggcgatta (HhaI)**
C53	ctaaatcggaaccctaagcaggcgaaaatccttcggccaa
C54	**cggcggattgaattcaggctgcgcaacgggggatg (HhaI)**
C55	tgctgcaaatccgctcacaattcccagctgca
C56	ttaatgaagtttgatggtggttccgaggtgccgtaaagca
C57	tggcgaaatgttgggaagggcgat
C58	tgtcgtgcacacaacatacgagccacgccagc
C59	caagttttttggggtcgaaatcggcaaaatccgggaaacc
C60	tcttcgctattggaagcataaagtgtatgcccgct
C61	ttccagtccttataaatcaaaagagaaccatcacccaaat
C62	**gcgctcacaagcctggggtgccta (HhaI)**
C63	cgatggcccactacgtatagcccgagatagggattgcgtt
C64	aactcacattattgagtgttgttccagaaaccgtctatcaggg
C65	acgtggactccaacgtcaaagggcgaatttggaacaagagtcc
L-B1A	tgtagcattccttttataaacagtt
L-B2A	ctttaattgtattccaccagagcc
L-B3A	cactacgaaggttagcaccatta
L-B4A	aataaggcttgaacaaagttac
L-A1C	ttaattaatttttttaccatatcaaa
L-A2C	ttaatttcatcttagactttacaa
L-A3C	ctgtccagacgtataccgaacga
L-A4C	tcaagattagtgtagcaatact
L-C1B	gtgggaacaaatttctatttttgag
L-C2B	cggtgcgggccttccaaaaacatt
L-C3B	atgagtgagcttttaaatatgca
L-C4B	actattaaagaggatagcgtcc

Sequences of staples for the rectangle.

Rect_1	tcacgttgaaaatctcgcgaataataatttttt
Rect_2	aggaagtttccattaataaagacttttttcatg
Rect_3	caggcgcataggctggtgaacggtgtacagac
Rect_4	ggtagaaagattcatcgaacaacattattaca
Rect_5	tgaccataaatcaaaagttcagaaaacgagaa
Rect_6	gtgtctggaagtttcaatgcaactaaagtacg
Rect_7	ttttgcgggagaagcctatgaccctgtaatac
Rect_8	gtcaatcatatgtaccatcgtaaaactagcat
Rect_9	gtgtagatgggcgcatgggataggtcacgttg
Rect_10	agtgccaagcttgcatttgtaaaacgacggcc
Rect_11	tattgggcgccagggtggagaggcggtttgcg
Rect_12	tggcccactacgtgaaccgtctatcagggcga
Rect_13	tcttttcactcaaagggcgaaaaaccatca
Rect_14	aggtcgacttcggccaacgcgcggggtttt
Rect_15	cgtgcatctttcccagtcacgacggcctgc
Rect_16	gataatcagcggattgaccgtaatcgtaac
Rect_17	tcaacgcaaaatcgatgaacggtaccggtt
Rect_18	ataacagttttgtaccaaaaacattttatt
Rect_19	tctttaccccaacatgttttaaatttccat
Rect_20	gatttaggacaaatgctttaaacaatcagg
Rect_21	ttcatcaagtaaaacgaactaacgagttga
Rect_22	aaaatacgtttgaaagaggacagactgacc

Rect_23	aaaggctccagaggctttgaggacacgggt
Rect_24	agaaaggaacaactaaaggaattcaaaaa
Rect_25	cccaaatcaagttttttggggtcgaaacgtgga
Rect_26	ctccaacgcagtgagacgggcaaccagctgca
Rect_27	ttaatgaactagaggatccccgggggggtaacg
Rect_28	ccagggttgccagtttgaggggacccgtggga
Rect_29	acaaacggaaaagccccaaaaacactggagca
Rect_30	aacaagagggataaaaatttttagcataaagc
Rect_31	taaatcgggattcccaattctgcgatataatg
Rect_32	ctgtagcttgactattatagtcagttcattga
Rect_33	atccccctataccacattcaactagaaaaatc
Rect_34	tacgttaaagtaatcttgacaagaaccgaact
Rect_35	gaccaactaatgccactacgaaggggtagca
Rect_36	acggctacaaaaggagcctttaatgtgagaat
Rect_37	tgcccttcagagtccactattaaagggtgccg
Rect_38	ctcgaattcgggaaacctgtcgtgcagctgat
Rect_39	gtatcggccgcaaggcgattaagtttaccgag
Rect_40	tgtataagccaacccgtcggattctgacgaca
Rect_41	atatattttgtcattgcctgagagtggaagat
Rect_42	agatttagtcaataaagcctcagagaaccctc
Rect_43	gcggattgcagagcttaattgctgaaacgagt
Rect_44	tacataacgggaatcgtcataaataaagcaaa
Rect_45	attcattacgtcaggacgttgggaaatgcaga
Rect_46	ctaaaacgaggtcaatcataagggaaccggat
Rect_47	gtttatcaggacagcatcggaacgacaccaac
Rect_48	caactttcaacagtttcagcggatgtatcg
Rect_49	taaagcactaaatcggaaccctaatccagttt
Rect_50	ggaacaaccgcctggccctgaggcccgctt
Rect_51	tccagtcgtaatcatggtcataaaaggggg
Rect_52	atgtgcttcaggaagatcgcacaatgtgag
Rect_53	cgagtaaaaatatttaaattgttacaaagg
Rect_54	ctatcagaaatgcaatgcctgaattagcaa
Rect_55	aattaagttgaccattagatacttttgcgg
Rect_56	atggcttatcaaaaagattaagagcgtcca
Rect_57	atactgcccaaaaggaattacgtggctcat
Rect_58	tataccaccaaatcaacgtaacgaacgagg
Rect_59	cgcagacaagaggcaaaagaatccctcagc
Rect_60	agcgaaacttgctttcgaggtgttgctaaa
Rect_61	cagcaagcgtagggttgagtgttgtagggagc
Rect_62	cctgtgtgattgcgttgcgctcactagagttg
Rect_63	agctttccgattacgccagctggcggctgttt
Rect_64	aatattttggctttcatcaacattatccagcc
Rect_65	gtaggtaaactatttttgagagatcaaacgtt
Rect_66	aaatggtcaacaggcaaggcaaagagtaatgt
Rect_67	ccgaaagactttgataagaggtcatatttcgc
Rect_68	gtaagagcaaatgtttagactggataggaagc
Rect_69	ctcattcagatgcgattttaagaacaggcata
Rect_70	aacactcatccatgttacttagccgaaagctg
Rect_71	taaacagctttttgcgggatcgtcaacactaa
Rect_72	taaatgaattttctgtatgggattaatttct
Rect_73	ccccgatttagagcttgacggggaaaaagaata
Rect_74	gcccgagagtccacgctggtttgcagctaact
Rect_75	cacattaaaattgttatccgctcatgcgggcc
Rect_76	tcttcgctgcaccgcttctggtgcggccttcc
Rect_77	tgtagccattaaaattcgcattaaatgccgga
Rect_78	gagggtaggattcaaaagggtgagacatccaa
Rect_79	taaatcatataacctgtttagctaacctttaa
Rect_80	ttgctcctttcaaatatcgcgtttgagggggt
Rect_81	aatagtaaacactatcataaccctcattgtga
Rect_82	attacctttgaataaggcttgcccaaatccgc

Rect_83	gacctgctctttgacccccagcgagggagtta
Rect_84	aaggccgctgataccgatagttgcgacgttag
Rect_85	aggcgaaaaatcccttataaatcaagccgg
Rect_86	cacacaacaggtgcctaatgagtgcccagc
Rect_87	ccaggcaaagggaagggcgatcggcaattc
Rect_88	gttaaatcaaaataattcgcgtctcggaaa
Rect_89	cggagacagctagctgataaattaattttt
Rect_90	catttggggatagtagtagcattaaaaggc
Rect_91	gagcttcaatcaggattagagagttatttt
Rect_92	ccagacgacaaagaagttttgccataattc
Rect_93	gaaacaccaaatttcaactttaatcgttta
Rect_94	caagcgcgatgataaattgtgtcgtgacga
Rect_95	aatgacaactcgctgaggcttgcattatac
Rect_96	tctaaagttttgtcgtctttccagccgac
Rect_97	cgaacgtggcgagaaaggaagggaaaccagta
Rect_98	tcggcaaatcctgtttgatggtggaccctca
Rect_99	aagcctggtacgagccggaagcatagatgat
Rect_100	caactgttgcgccattcgccattcaaacatc
Rect_101	gccatcaagctcatttttaaccacaaatcc
Rect_102	caaccgtttcaaatcaccatcaattcgagcc
Rect_103	ttctactacgcgagctgaaaaggttaccgcg
Rect_104	ccaacaggagcgaaccagaccggagccttta
Rect_105	cttttgcagataaaaaccaaaataaagactc
Rect_106	gatggtttgaacgagtagtaaatttaccatt
Rect_107	tcatcgccaacaaagtacaacggacgccagc
Rect_108	atattcggaaccatcgcccacgcagagaagg
Rect_109	atcaatatcgaacctcaaatatcaattccgaaa
Rect_110	ggcaattcacatattcctgattatcaaagtgta
Rect_111	aagaaaacaaagaagatgatgaaacaggctgcg
Rect_112	aatcgcaagtatgtaaatgctgatgataggaac
Rect_113	agtaataagttaggcagaggcatttatgatatt
Rect_114	cccaatagctcatcgtaggaatcatggcatcaa
Rect_115	cagagagaaaaaaatgaaaatagcaagcaaact
Rect_116	cttattacgaagaactggcatgattgcgagagg
Rect_117	agcaaggcctcaccagtagcaccatgggcttga
Rect_118	attgacaggccaccaccagagccgcgatttgta
Rect_119	attaggattggctgagactcctcaataaccgat
Rect_120	tccacagacagccctcatagttagcgtaacga
Rect_121	ataaaagggacattctggccaacaaagcatc
Rect_122	accttgcttggtcagttggcaaagagcgga
Rect_123	attatcattcaatataatcctgacaattac
Rect_124	ctgagcaaaaattaattacattttgggtta
Rect_125	tataactaacaaagaacgcgagaacgccaa
Rect_126	catgtaatagaatataaagtaccaagccgt
Rect_127	ttttatttaagcaaatcagatatttttgt
Rect_128	ttaacgtctaacataaaaacaggtaacgga
Rect_129	atacccaacagtatgttagcaaattagagc
Rect_130	cagcaaaaggaaacgtcaccaatgagccgc
Rect_131	caccagaaaggttgaggcaggtcatgaaag
Rect_132	tattaagaagcggggttttgctcgtagcat
Rect_133	ttgaaaggagcaaatgaaaaatctagagatag
Rect_134	gattatactaagaaaccaccagaagtcaacag
Rect_135	tcatttgaaggcgaattattcatttttgtttg
Rect_136	ttcaaatataacctccggcttaggtaacaatt
Rect_137	ggtaaagtaatcgccatatttaacaaaacttt
Rect_138	ttatccggtctcatcgagaacaagcgacaaaa
Rect_139	attagacggccaaataagaaacgatagaaggc
Rect_140	aatacataccgaggaaacgcaataagaagcgc
Rect_141	tcgatagcattgagccatttgggaacgtagaa
Rect_142	tggccttgaagagccaccaccctcagaaacca

Rect_143	ggcggataacctattattctgaaacagacgat
Rect_144	tcaccagtacaaactacaacgcctagtacca
Rect_145	aacccttctgacctgaaagcgtaagacgctgag
Rect_146	agccagcaattgaggaaggttatcatcatttt
Rect_147	gcggaacatctgaataatggaaggtacaaaat
Rect_148	cgcgcagattacctttttaatgggagagact
Rect_149	acctttttattttagttaatttcatagggctt
Rect_150	aattgagaattctgtccagacgactaaaccaa
Rect_151	gtaccgcaattctaagaacgcgagtattattt
Rect_152	atcccaatgagaattaactgaacagttaccag
Rect_153	aaggaaacataaaggtggcaacattatcaccg
Rect_154	tcaccgacgcaccgtaatcagtagcagaaccg
Rect_155	ccaccctctattcacaaacaaatacctgccta
Rect_156	tttcggaagtgccgtcgagagggtgagtttcg
Rect_157	atctttagggcctgcaacagtgccaatacg
Rect_158	acctaccatagtttgagtaacatttaaaat
Rect_159	tacataaatctttgaataccaagtgttaga
Rect_160	gacctaaatcaaaatcataggtctaaacag
Rect_161	aaacaacatgccaacgctcaacagtcttct
Rect_162	tagcgaacctccaagaacgggtatgacaat
Rect_163	acaaagtcacaaaataaacagccagcgttt
Rect_164	gaaacgcaaagatagccgaacaaaccctga
Rect_165	aatcaagtttcattaaaggtgaatataaaa
Rect_166	cattaaagccagagccgccaccctcgacag
Rect_167	aagtatagcaaacagttaatgcccaatcct
Rect_168	aggaacccatgtaccgtaacacttgatat
Rect_169	tggcacagacaatatttttgaatggggtcagta
Rect_170	ttaacaccagcactaacaactaatcgttatta
Rect_171	attttaaaatcaaaattatttgcacggattcg
Rect_172	cctgattgcaatatatgtgagtgatcaatagt
Rect_173	gaatttatttaatggtttgaaatattcttacc
Rect_174	agtataaagttcagctaatgcagatgtctttc
Rect_175	cttatcattcccgacttgcgggagcctaattt
Rect_176	gccagttagagggtaattgagcgctttaagaa
Rect_177	aagtaagcagacaccacggaataatattgacg
Rect_178	gaaattattgcctttagcgtcagaccggaacc
Rect_179	gcctccctcagaatggaaagcgcagtaacagt
Rect_180	gcccgtatccggaataggtgtatcagcccaat
Rect_181	agccgtcaaaaaacagaggtgaggcctattag
Rect_182	cagaaataaaaatcctttgcccgaaagattag
Rect_183	tgcttctgttcgggagaaacaataacgtaaaa
Rect_184	tgtgataaaaagacgctgagaagagataacct
Rect_185	tgtttatcaatatgcgttatacaaaccgaccg
Rect_186	agccttaaaccaatcaataatcggcacgcgcc
Rect_187	agagagatagagcgtctttccagaggttttga
Rect_188	ttgtcacaatcttaccgaagccctttaatatc
Rect_189	gcgttttcaagggagggaaggtaaagtttatt
Rect_190	aatttaccgggaaccagagccaccactgtagc
Rect_191	tcaggaggtggggtcagtgccttgagtctctg
Rect_192	ccaccctcattttcagggatagcaaccgtac
Rect_193	tctttaatgcgcgaactgatagccccaccag
Rect_194	cagaagattagataatacatttgtcgacaa
Rect_195	ctcgtattagaaattgcgtagatacagtac
Rect_196	cttttacaaaatcgtcgctattagcgatag
Rect_197	cttagatttaaggcgttaaataaagcctgt
Rect_198	ttagtatcacaatagataagtccacgagca
Rect_199	tgtagaaatcaagattagttgctcttacca
Rect_200	acgctaacacccacaagaattgaaaatagc
Rect_201	aatagctatcaatagaaaattcaacattca
Rect_202	accgattgtcggcattttcggtcataatca

Rect_203 aaatcaccttccagtaagcgtcagtaataa
Rect_204 gttttaacttagtaccgccacccagagcca
Rect_205 aaaaataccgaacgaactaaaacatcgccatt
Rect_206 agactttacaaacaataggatttagaagtatt
Rect_207 agatgaatatacagtatttcaggtttaacgtc
Rect_208 aatccttgaaaacataattaattttcccttag
Rect_209 cataattactagaaaagaataaacaccggaat
Rect_210 tatcccatcctaattttgaacaagaaaaataa
Rect_211 caattttatcctgaatattttgcacccagcta
Rect_212 agagcaagaaacaatggttaagcccaataata
Rect_213 caaagacaaaagggcgtatggtttaccagcgc
Rect_214 cgtttgccatcttttcatagccccttattag
Rect_215 atacaggagtgtactgtacatggcttttgatg
Rect_216 cagaaccgccaccctctcagaaccgccaccct

Sequences of staples with mutant HhaI site for triangle.

Site #	Staple name	Sequence of staples with mutat site (5'... 3')
1	**C45_MutS1**	TAGAGCTTGACGGGGAGTTGCAGCAAGCGGTCATTGG**G**A**T**
2	**C52_MutS2**	C**G**A**T**C**G**GGCCTGTGTGAAATTGTTGGCGATTA
3	**C62_MutS3**	**G**A**T**CTCACAAGCCTGGGGTGCCTA
4	**C54_MutS4**	CGGCGGATTGAATTCAGGCT**G**A**T**CAACGGGGGATG
5	**C51_MutS5**	AGTTGGGTCAAA**G**A**T**CCATTCGCCCCGTAATG
6	**C43_MutS6**	ACGTTGTATTCCGGCACCGCTTCTG**G**A**T**CATC
7	**B03_MutS7**	GGCATCAAATTTGGG**G**A**T**CGAGCTGAGTTAAA
8	**B56_MutS8**	ACCAA**GCG**CAG**G**A**T**CATAGGCTGGAGAACTGGCTCATTAT
9	**B36_MutS9**	G**G**A**T**CAGACTCCATGTTACTTAGCCGTTTTAA
10	**B56_MutS10**	ACCAA**G**A**T**CAG**GCGC**ATAGGCTGGAGAACTGGCTCATTAT
8 and 10	**B56_MutS8-10**	ACCAA**G**A**T**CAG**G**A**T**CATAGGCTGGAGAACTGGCTCATTAT
11	**B47_MutS11**	GTTTTGTCAGGAATTGCGAATAAT**T**C**C**GACAA
11	**B51_MutS11**	ATAGTT**G**AAATTTTTTCACGTTGATCATAGTT
12	**A06_MutS12**	CCGGAACCCAGAATGGAAA**G**A**T**CAACATGGCT
13	**A11_MutS13**	CACCGGAAA**G**A**T**CGTTTTCATCGGAAGGGCGA
14	**A08_Muts14**	GACGGGAGAATTAACTCGGAATAAGTTTATTTCCA**G**A**T**CT
15	**A20_MutS15**	CCTTGAGTCAGACGATTGGCCTT**G**A**T**CCACCC
16	**A37_MutS16**	AGAGAATAACATAAAAACAGGGAA**G**A**T**CATTA
17	**A53_MutS17**	TCCCAATCCAAATAAGATTACC**G**A**T**CCCAATAAATAATAT
18	**A61_MutS18**	**G**A**T**CCTGTTATTCTAAGAACGCGATTCCAGAGCCTAATTT
19	**C17_MutS19**	**G**A**T**CAGAGGCGAATTAATTATTAGCACGTAAATTCTGAAT
20	**C27_MutS20**	A**T**CGAACTAAAACAGAGGTGAGGCTTAGAAGTATT
22, 23	**Loop3_MutS22-23**	CCACACCCGCC**G**A**T**CTTAAT**G**A**T**CCGCTACAGG
24	**Loop2_MutS24**	GTAGCGGTCACGCT**G**A**T**CGTAACCA
24	**Loop2_OnS24**	GTAGCGGTCACGCT**GCGC**GTAACCA
25, 26	**Loop1_MutS25-26**	AAGCGAAAGGAGCGG**G**A**T**CTAGG**G**A**T**CTGGCAAGT

Sequences of staples with mutant Hin1II site for triangle.

Site #	staple name	Staple sequence with mutant site ('5...3')
1	**C48_mutHin**	ggttttcc**cgg**gtcatagctgtttgagaggcg
2	**C35_mutHin**	ctctagagcaagcttg**ccgg**cctggtcagtt
3	**B33_mutHin**	agggatagctcagagccaccaccc**ccgg**tcaa
4	**B25_mutHin**	taaagcta**gg**taacagttgattcccatttttg
4	**B27_mutHin**	taattgcttggaagtttcattc**cc**aatcggttgta
5	**B31_mutHin**	aaagaagttttgccagcataaatattcattgactcaa**ccgg**tt
6	**B36_mutHin**	ggcgcagactc**ccgg**ttacttagccgttttaa
7	**B58_mutHin**	gacccccagacttttt**ccgg**aggagcttgctt
8	**B42_mutHin**	agacgttac**ccgg**taccgtaacacccctcagaaccgccac
9	**A09_mutHin**	gataagtgccgtcgagctgaaa**ccgg**aaagtatacaggag
10	**A06_mutHin**	ccggaacccagaatggaaagcgcaa**ccgg**gct
11	**A28_mutHin**	ataagagcaagaaa**ccgg**gcatgattaagactccgacttg
12	**A49_mutHin**	ag**ccgg**tatttcatcgtaggaatcaaacgatttttgttt
13	**A63_mutHin**	acgctaacgagcgtctggcgttttagcgaacccaa**ccgg**t
14	**A52_mutHin**	cccatcctcgccaa**ccgg**taatttaataaggc

Sequences of modified staples for Hin1II triangle with two loops.

C37_shift CGAGAAAGGAAGGGAACGCTGCGCGTAACCAC

C8_shift CACACCCGCCGCGCTTCTGAAATGGATTATTTAATAAAAG

C12_shift AGAGATAGATTACCGCTCAATCGTAATGCGCCGCTACAGG

C16_shift GCGCGTACTATGGTTGTAATATCCAGAACAATAACCCTTC

C20_shift GAATACGTCTATCGGCCTTGCTGGCTTTGACGAGCACGTA

C23_shift TAACGTGCTTTCCTCGAGTAGAAGAACTCAAAGGCACAGA

C26_shift CTATTAGTTAACATCACTTGCCTGTTGGAATCAGAGCGGG

C28_shift AGCTAAACAGGAGGCCCTTCTTTGATTAGTAACTTTAATG

C30_shift CTAAAACATAACCGTTGTAGCAATAGATTAAAGGGATTTTA

C31_shift GACAGGAACGGTACGCGTCCATCACGCAAATTCGCCATTAAAA

C32_shift CCGAGTAAAAGAGTCTCAGAATCTTGAGAAGTGTTTTTATAAT

L-A4C_shift TCAAGATTAGTCAGTGAGGCCA

loop compl_S15_shift AACAGGAAAAACGCTCATGGAAATACCTAC

Sequences that are used for the experiment of the nick effect on HhaI enzymatic activity.

Oligo name	Sequence (5' - … - 3')
dsDNA_Compl	AGGTAATTGAAATGAATAATTCGCCTCTGCGCGATTTTGTAACTTGGTATTCAAAGCAATCAGG
dsDNA	CCTGATTGCTTTGAATACCAAGTTACAAAATCGCGCAGAGGCGAATTATTCATTTCAATTACCT
I-a	CCTGATTGCTTTGAATACCAAGTTACAAAA
I-b	TCGCGCAGAGGCGAATTATTCATTTCAATTACCT
II-a	CCTGATTGCTTTGAATACCAAGTTACAAAAT
II-b	CGCGCAGAGGCGAATTATTCATTTCAATTACCT
III-a	CCTGATTGCTTTGAATACCAAGTTACAAAATC
III-b	GCGCAGAGGCGAATTATTCATTTCAATTACCT
IV-a	CCTGATTGCTTTGAATACCAAGTTACAAAATCG
IV-b	CGCAGAGGCGAATTATTCATTTCAATTACCT
V-a	CCTGATTGCTTTGAATACCAAGTTACAAAATCGC
V-b	GCAGAGGCGAATTATTCATTTCAATTACCT
VI-a	CCTGATTGCTTTGAATACCAAGTTACAAAATCGCG
VI-b	CAGAGGCGAATTATTCATTTCAATTACCT
VII-a	CCTGATTGCTTTGAATACCAAGTTACAAAATCGCGC
VII-b	AGAGGCGAATTATTCATTTCAATTACCT
VIII-a	CCTGATTGCTTTGAATACCAAGTTACAAAATCGCGCA
VIII-b	GAGGCGAATTATTCATTTCAATTACCT
IX-a	CCTGATTGCTTTGAATACCAAGTTACAAAATCGCGCAG
IX-b	AGGCGAATTATTCATTTCAATTACCT

Custom Digest

Circular Sequence: M13

Sequence digested with: AluI

Cleavage code	Enzyme name code
blunt end cut	Available from NEB
5' extension	Has other supplier
3' extension	Not commercially available
cuts 1 strand	*: cleavage affected by CpG methylation #: cleavage affected by other methylation (enz. name): ambiguous site

ORFs:
a: 434 aa
b: 426 aa
c: 410 aa
d: 348 aa
e: 168 aa
f: 112 aa
g: 110 aa

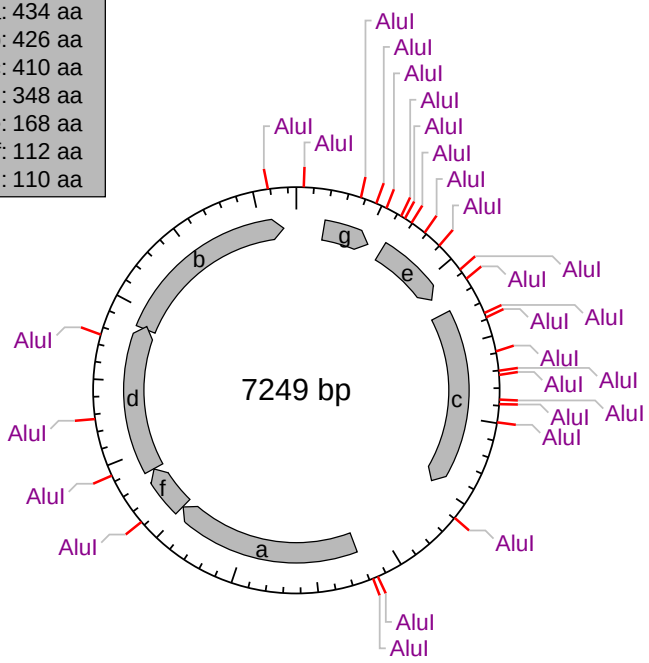

Custom Digest

Circular Sequence: M13

Sequence digested with: BamHI

Cleavage code	Enzyme name code
blunt end cut	Available from NEB
5' extension	Has other supplier
3' extension	Not commercially available
cuts 1 strand	*: cleavage affected by CpG methylation #: cleavage affected by other methylation (enz. name): ambiguous site

ORFs:
a: 434 aa
b: 426 aa
c: 410 aa
d: 348 aa
e: 168 aa
f: 112 aa
g: 110 aa

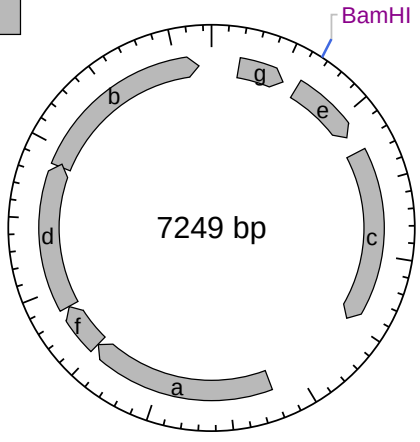

Custom Digest

Circular Sequence: M13

Sequence digested with: HaeIII

Cleavage code	Enzyme name code
blunt end cut	Available from NEB
5' extension	Has other supplier
3' extension	Not commercially available
cuts 1 strand	*: cleavage affected by CpG methylation #: cleavage affected by other methylation (enz. name): ambiguous site

ORFs:
a: 434 aa
b: 426 aa
c: 410 aa
d: 348 aa
e: 168 aa
f: 112 aa
g: 110 aa

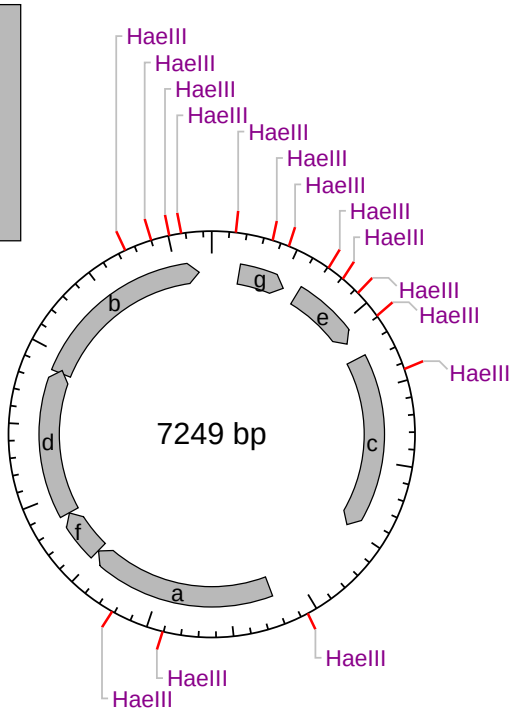

Custom Digest

Circular Sequence: M13

Sequence digested with: DraI

Cleavage code	Enzyme name code
blunt end cut	Available from NEB
5' extension	Has other supplier
3' extension	Not commercially available
cuts 1 strand	*: cleavage affected by CpG methylation #: cleavage affected by other methylation (enz. name): ambiguous site

ORFs:
a: 434 aa
b: 426 aa
c: 410 aa
d: 348 aa
e: 168 aa
f: 112 aa
g: 110 aa

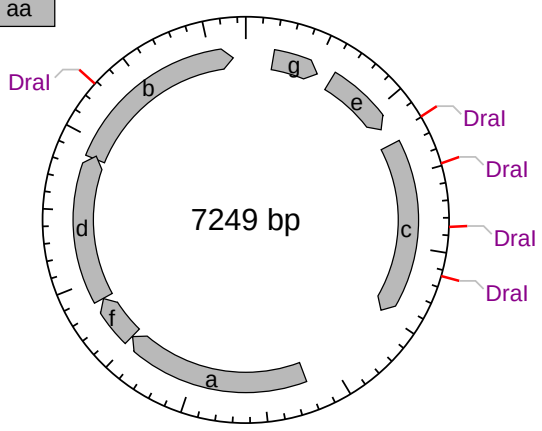

Custom Digest

Circular Sequence: M13

Sequence digested with: HhaI

Cleavage code	Enzyme name code
blunt end cut	Available from NEB
5' extension	Has other supplier
3' extension	Not commercially available
cuts 1 strand	*: cleavage affected by CpG methylation #: cleavage affected by other methylation (enz. name): ambiguous site

ORFs:
a: 434 aa
b: 426 aa
c: 410 aa
d: 348 aa
e: 168 aa
f: 112 aa
g: 110 aa

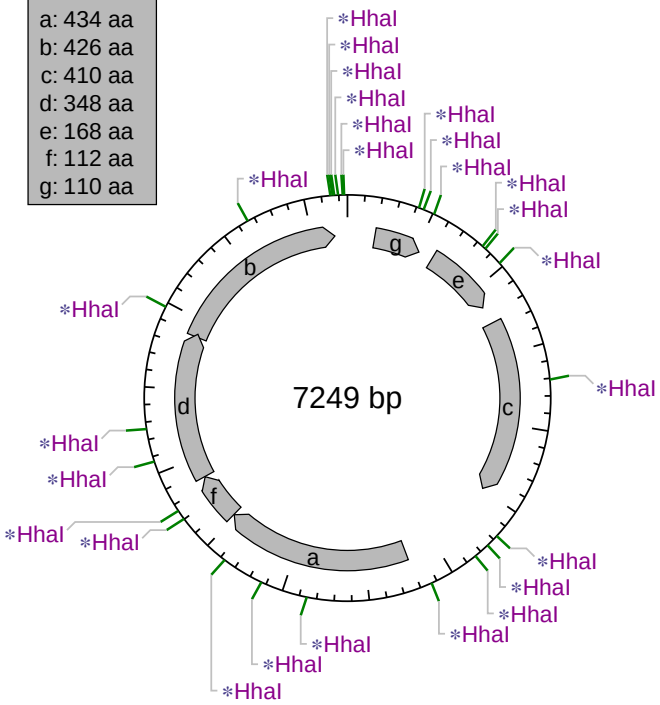

Custom Digest

Circular Sequence: M13

Sequence digested with: NlaIII

Cleavage code	Enzyme name code
blunt end cut	Available from NEB
5' extension	Has other supplier
3' extension	Not commercially available
cuts 1 strand	*: cleavage affected by CpG methylation #: cleavage affected by other methylation (enz. name): ambiguous site

ORFs:
a: 434 aa
b: 426 aa
c: 410 aa
d: 348 aa
e: 168 aa
f: 112 aa
g: 110 aa

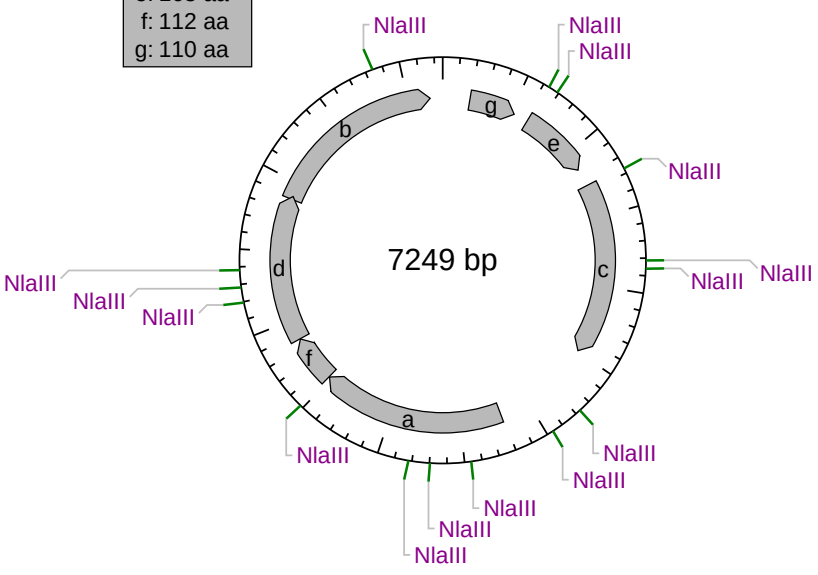

Custom Digest

Circular Sequence: M13

Sequence digested with: HpyCH4IV

Cleavage code	Enzyme name code
blunt end cut	Available from NEB
5' extension	Has other supplier
3' extension	Not commercially available
cuts 1 strand	*: cleavage affected by CpG methylation
	#: cleavage affected by other methylation
	(enz. name): ambiguous site

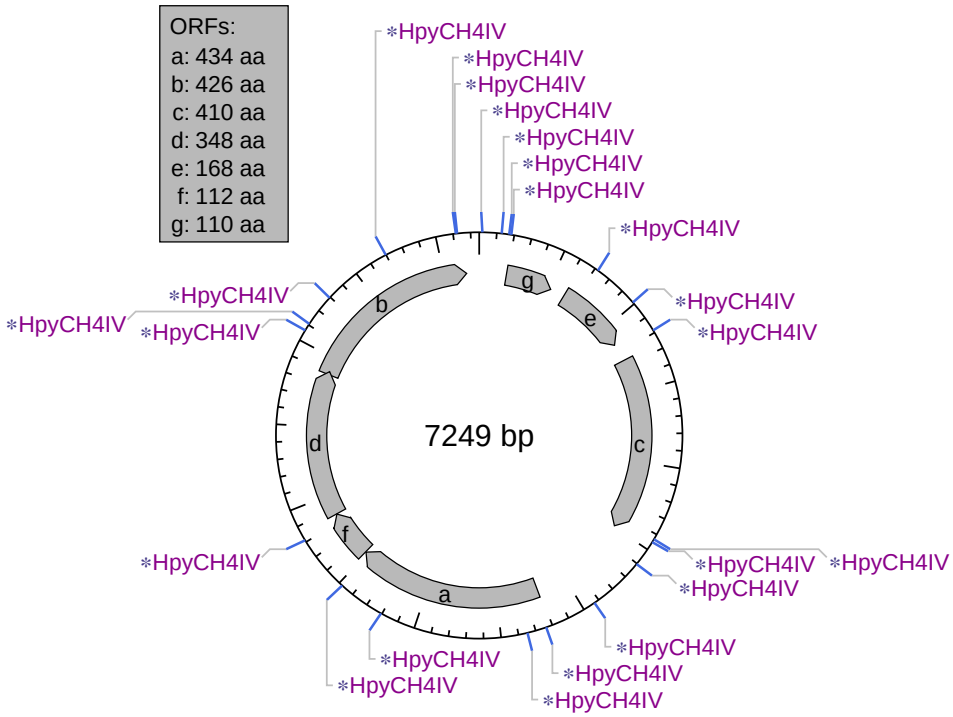

Custom Digest

Circular Sequence: M13

Sequence digested with: MspI

Cleavage code	Enzyme name code
blunt end cut	Available from NEB
5' extension	Has other supplier
3' extension	Not commercially available
cuts 1 strand	*: cleavage affected by CpG methylation
	#: cleavage affected by other methylation
	(enz. name): ambiguous site

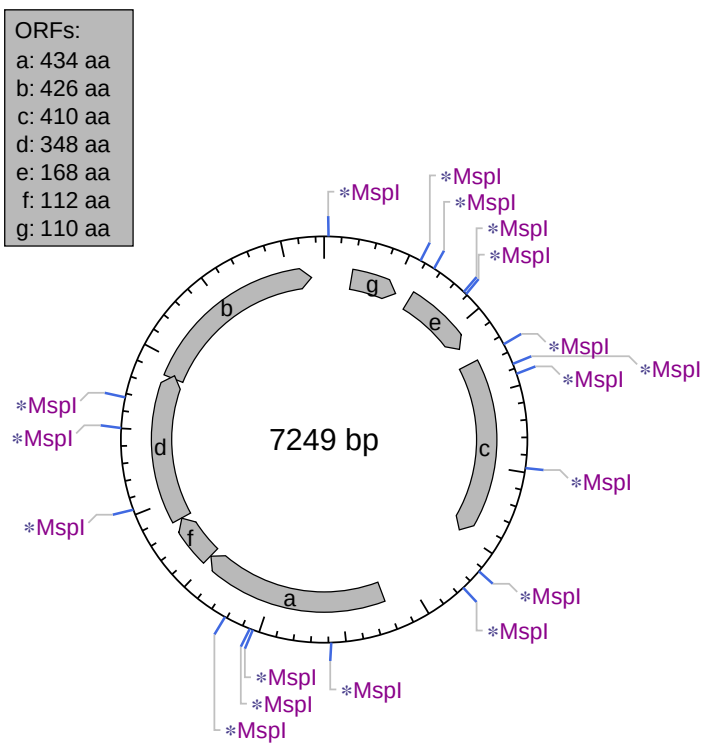

Custom Digest

Circular Sequence: M13

Sequence digested with: RsaI

Cleavage code	Enzyme name code
blunt end cut	Available from NEB
5' extension	Has other supplier
3' extension	Not commercially available
cuts 1 strand	*: cleavage affected by CpG methylation #: cleavage affected by other methylation (enz. name): ambiguous site

ORFs:
a: 434 aa
b: 426 aa
c: 410 aa
d: 348 aa
e: 168 aa
f: 112 aa
g: 110 aa

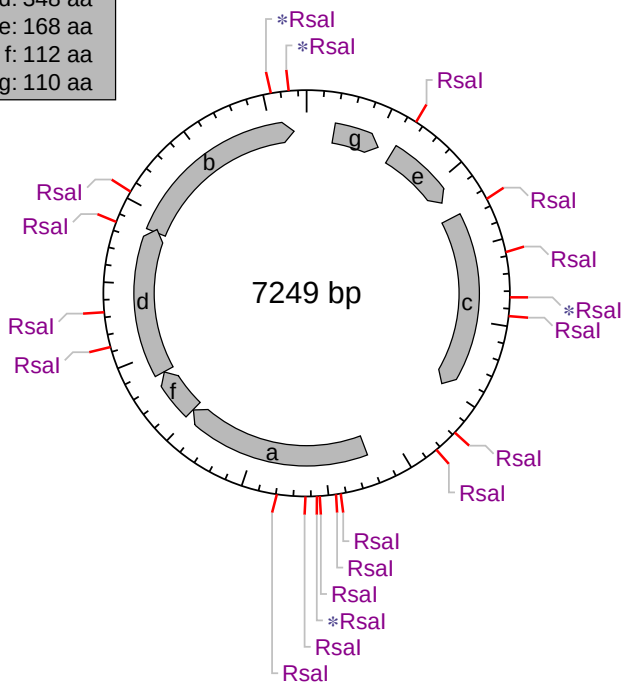

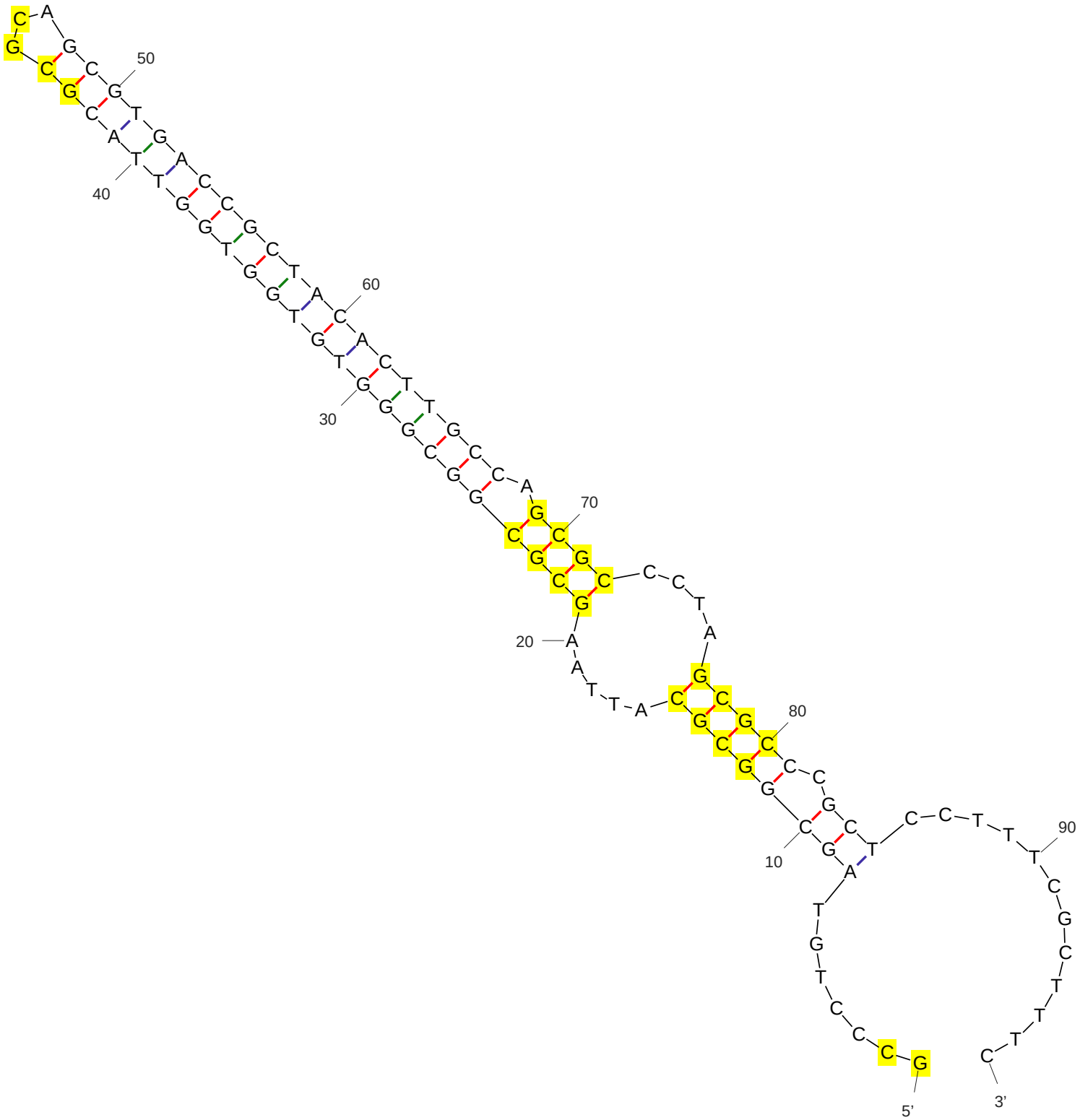

dG = -24.62 loop

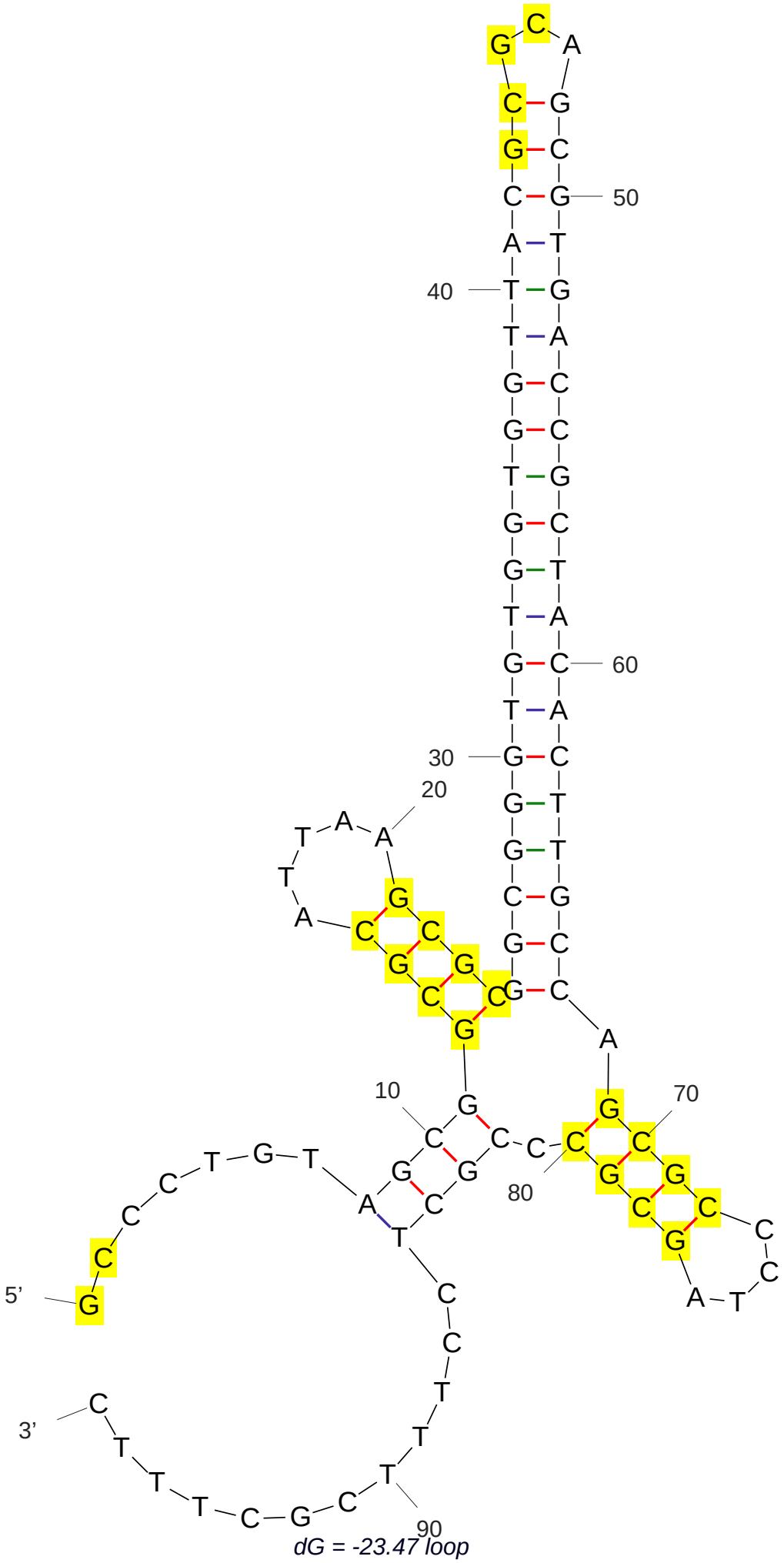
5’
3’
10
20
30
40
50
60
70
80
90
dG = -23.47 loop

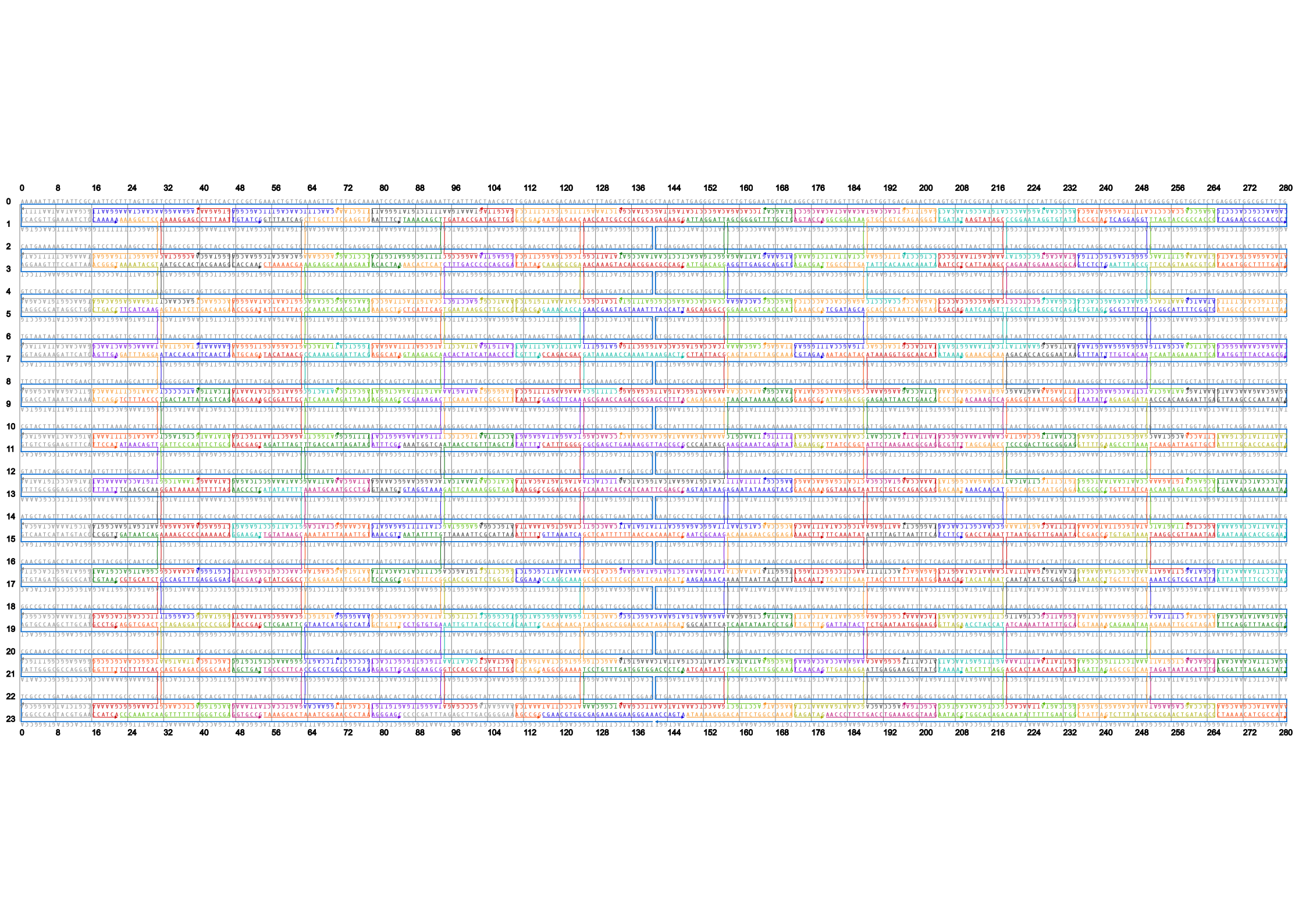

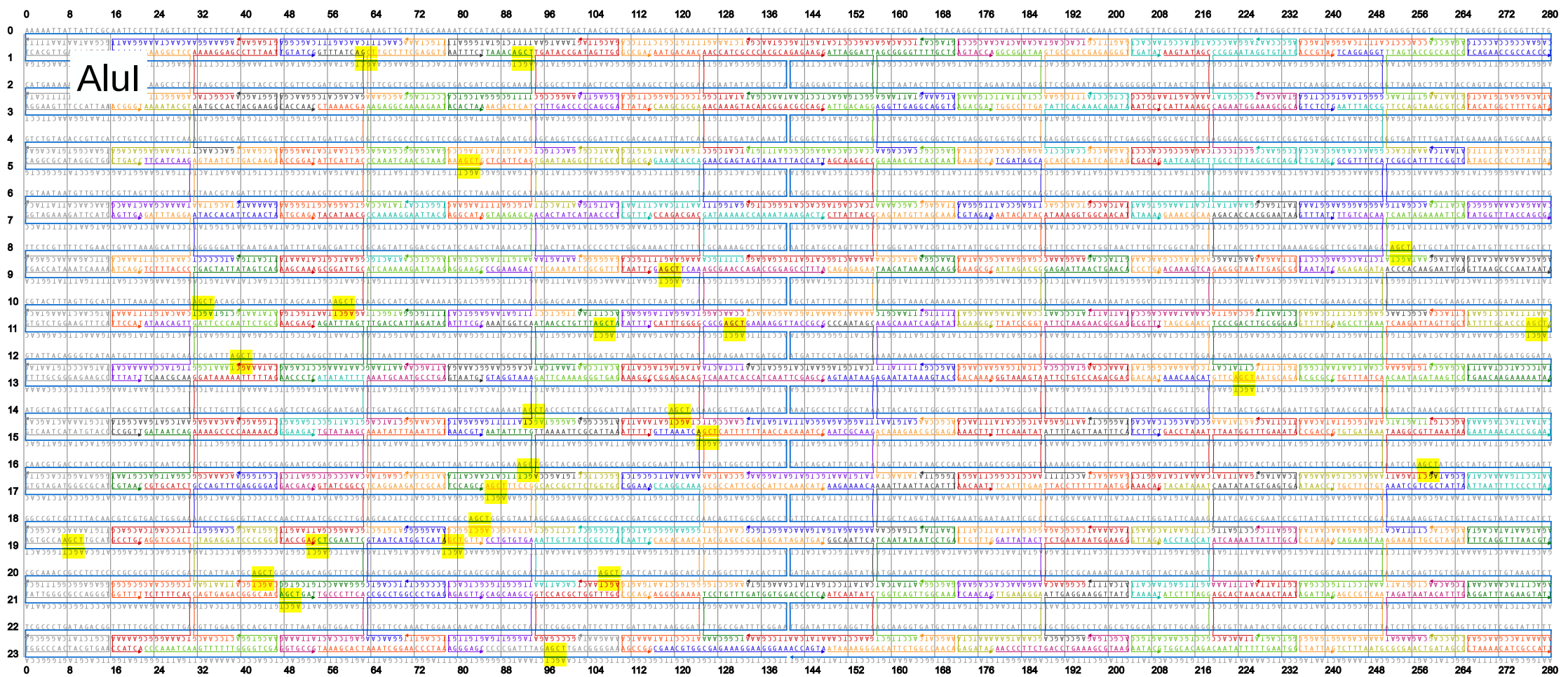
AluI

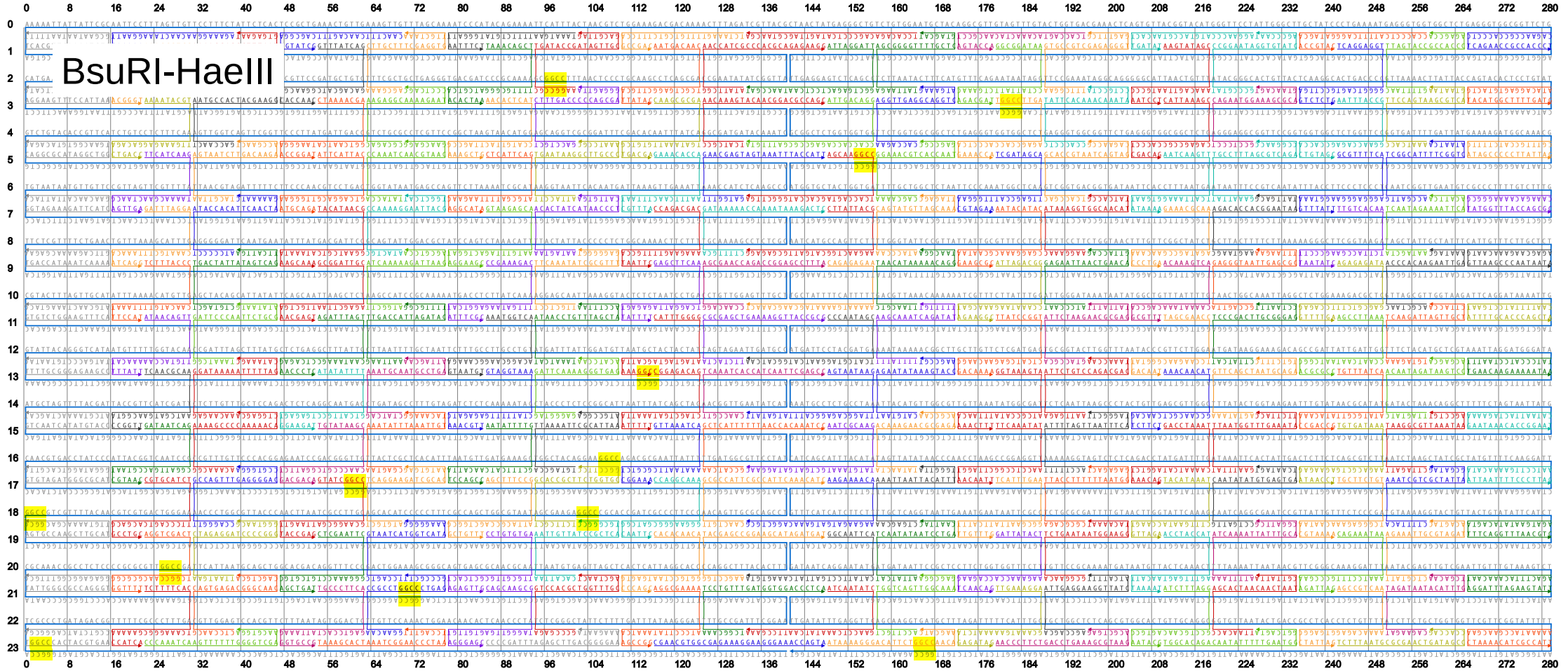
BsuRI-HaeIII

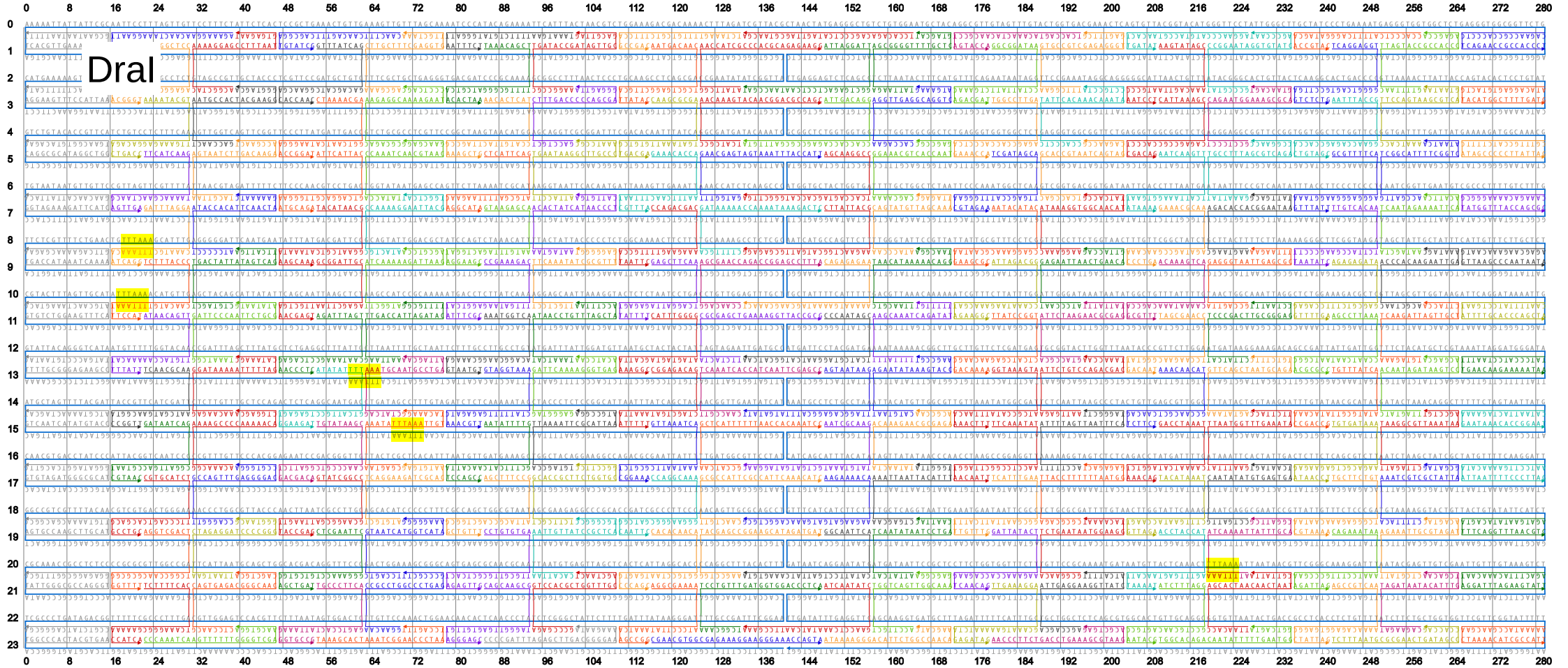
DraI

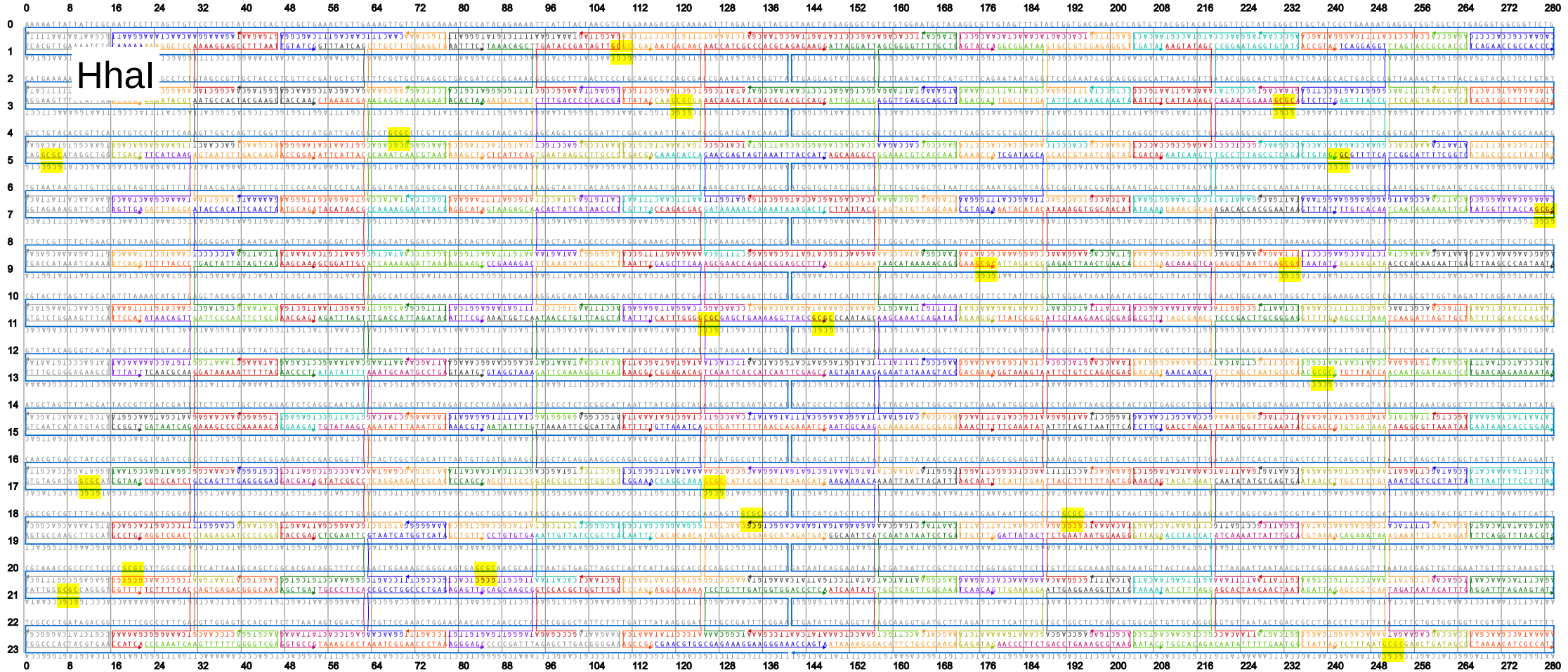
HhaI

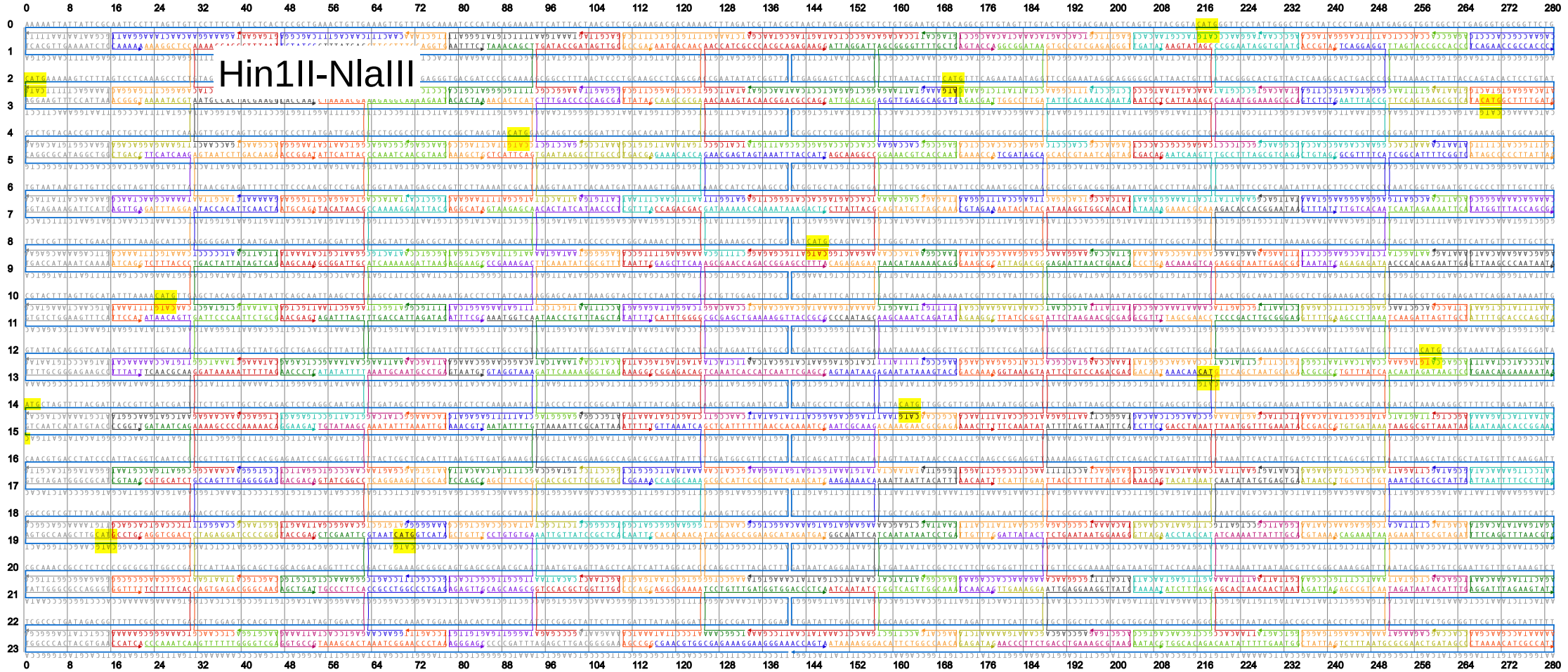
Hin1II-NlaIII

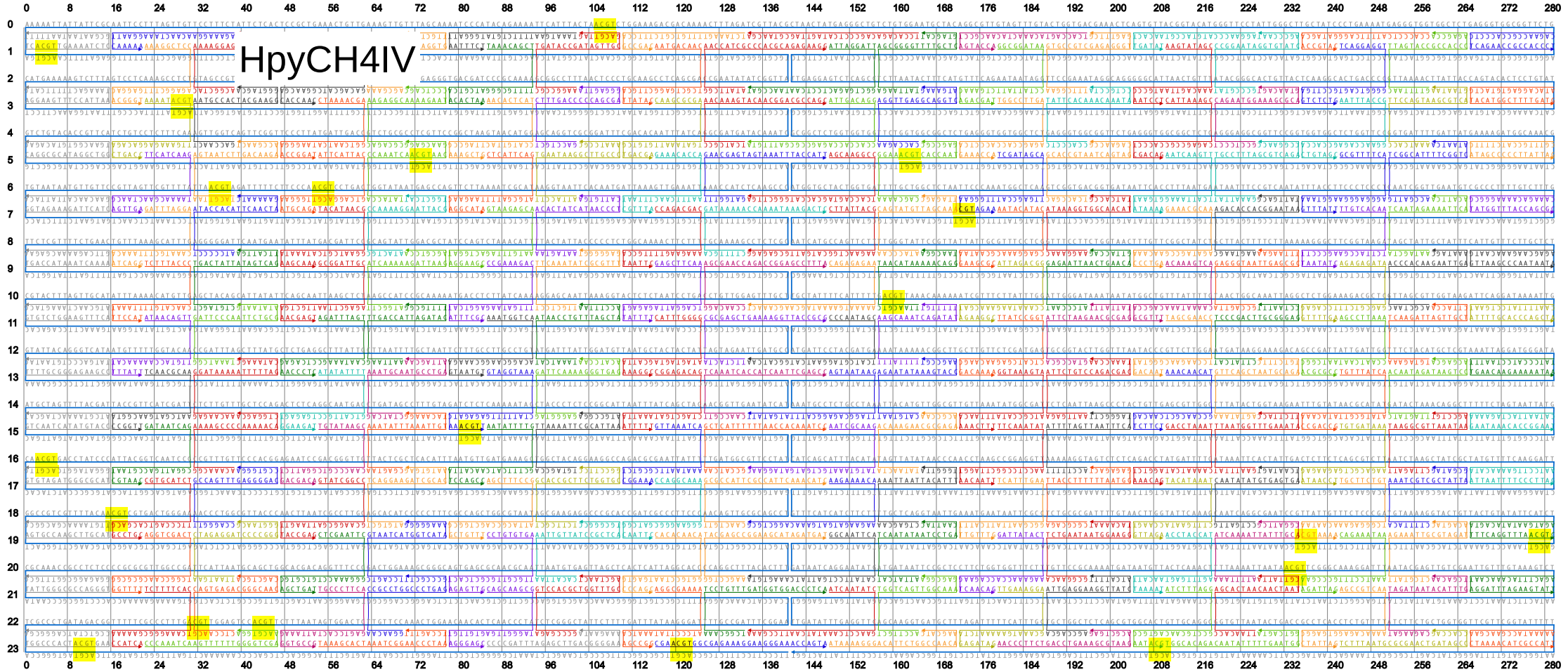
HpyCH4IV

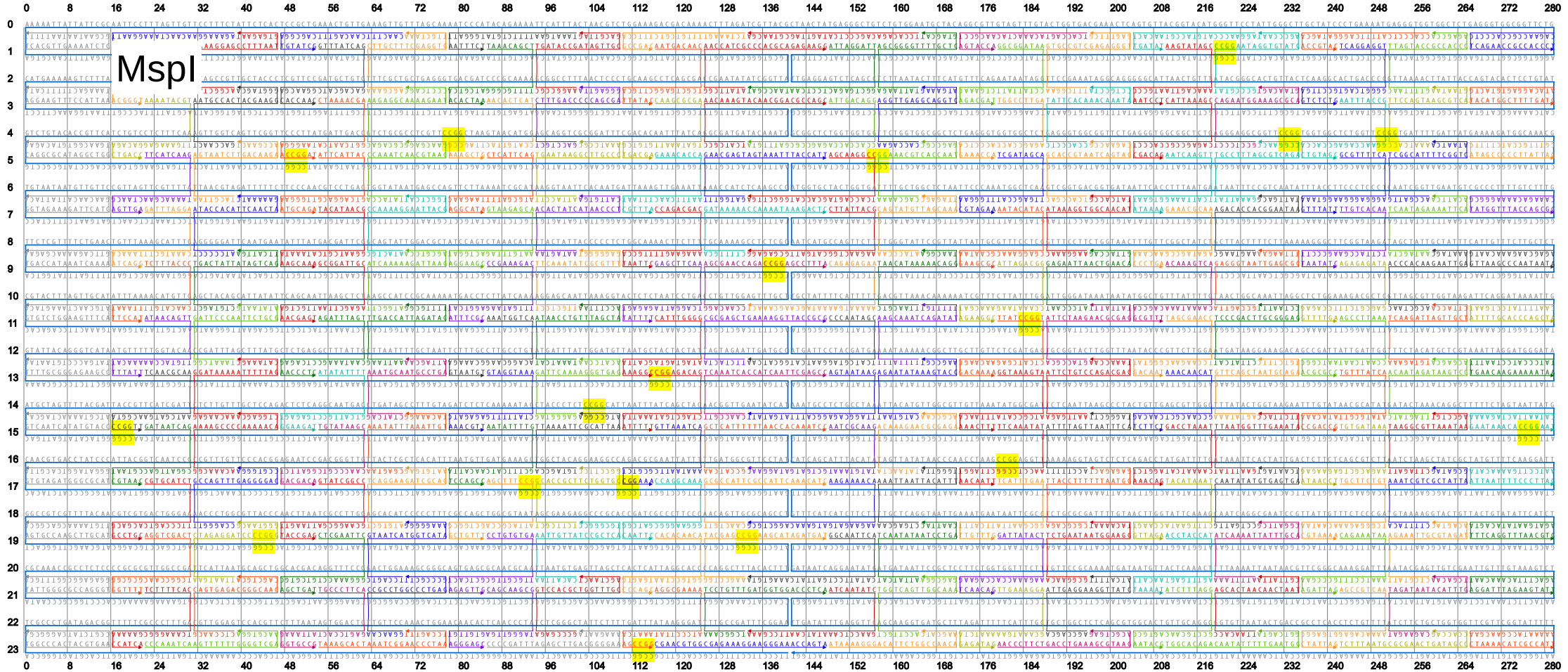
MspI

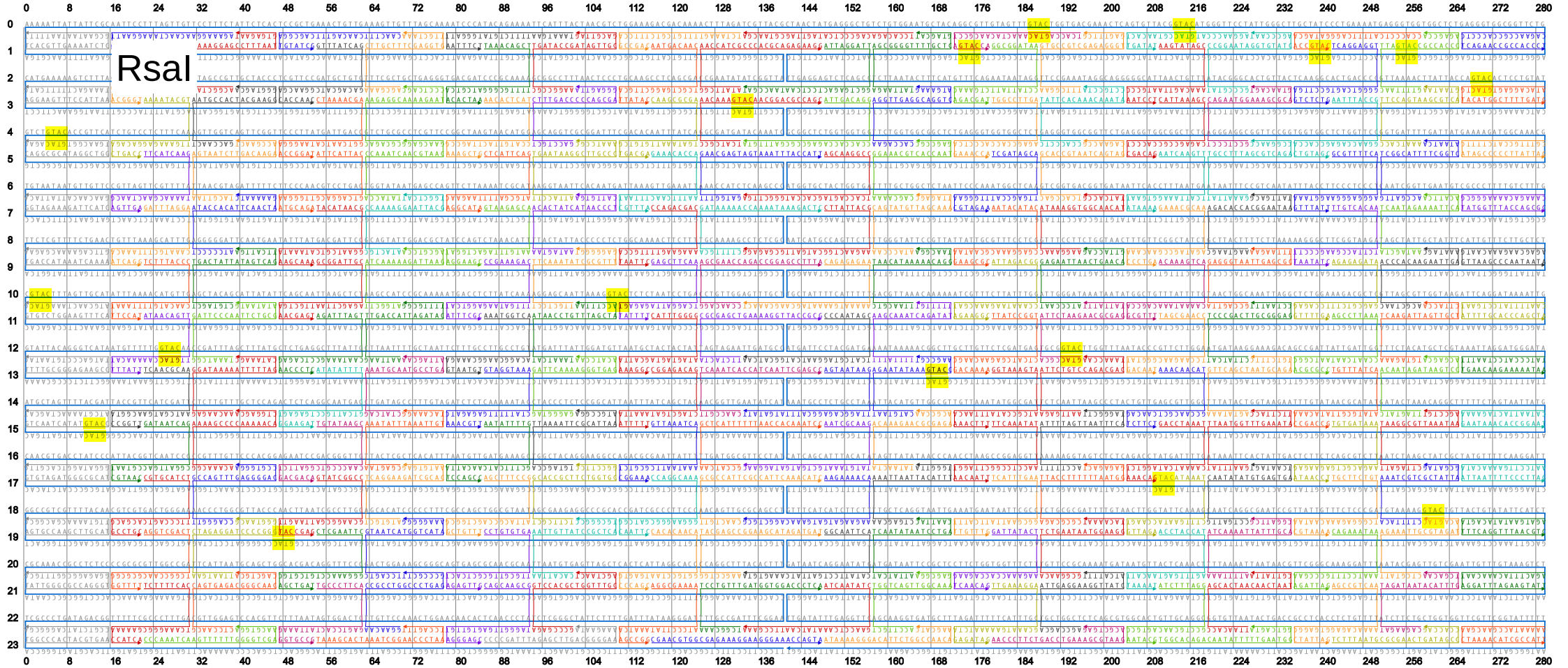
RsaI

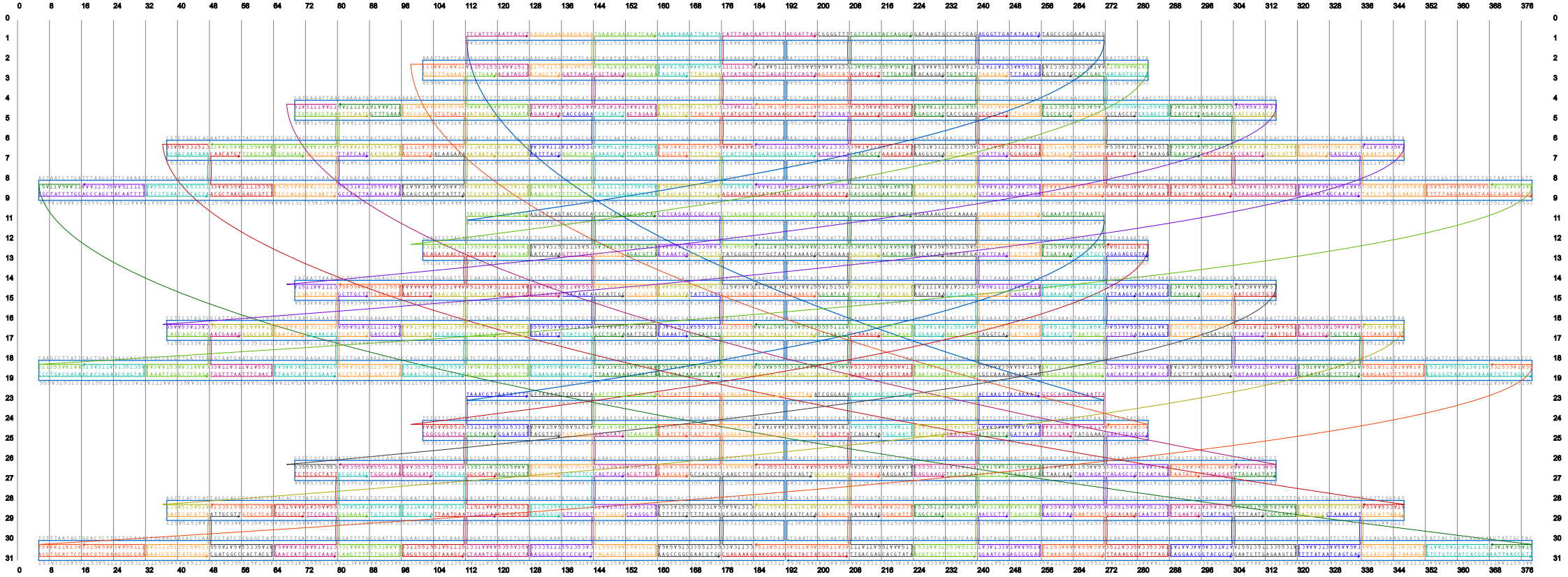

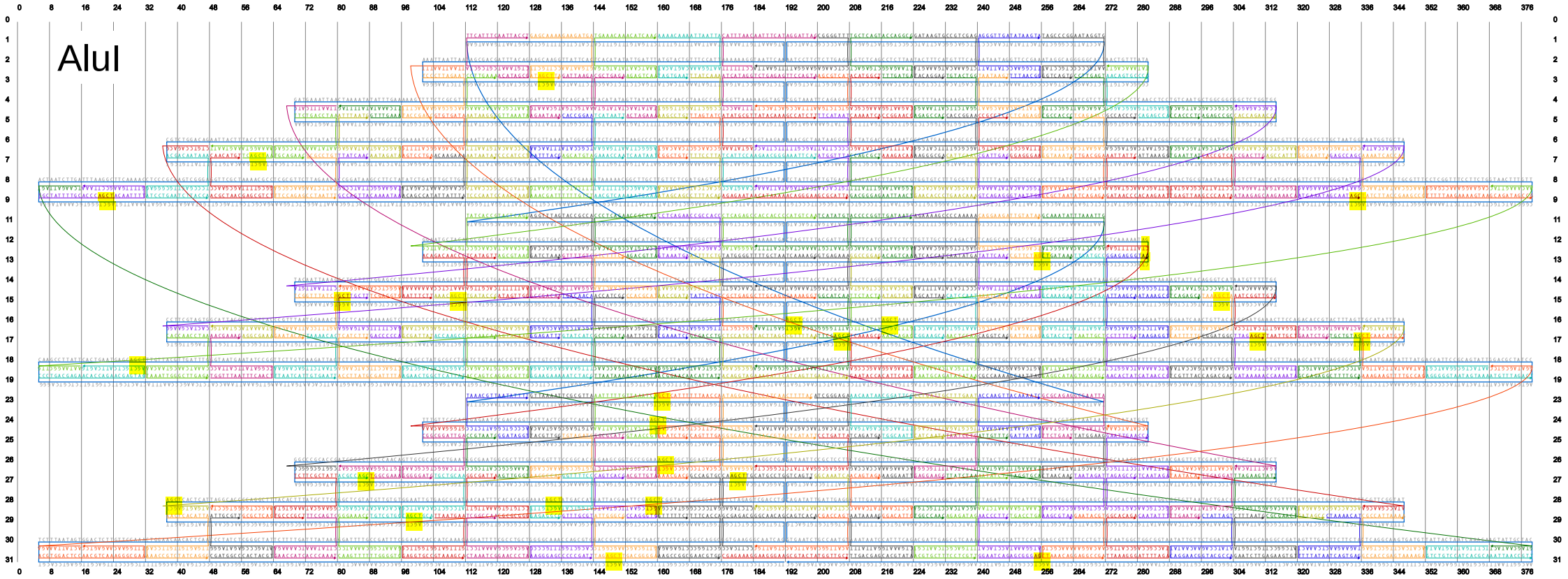
AluI

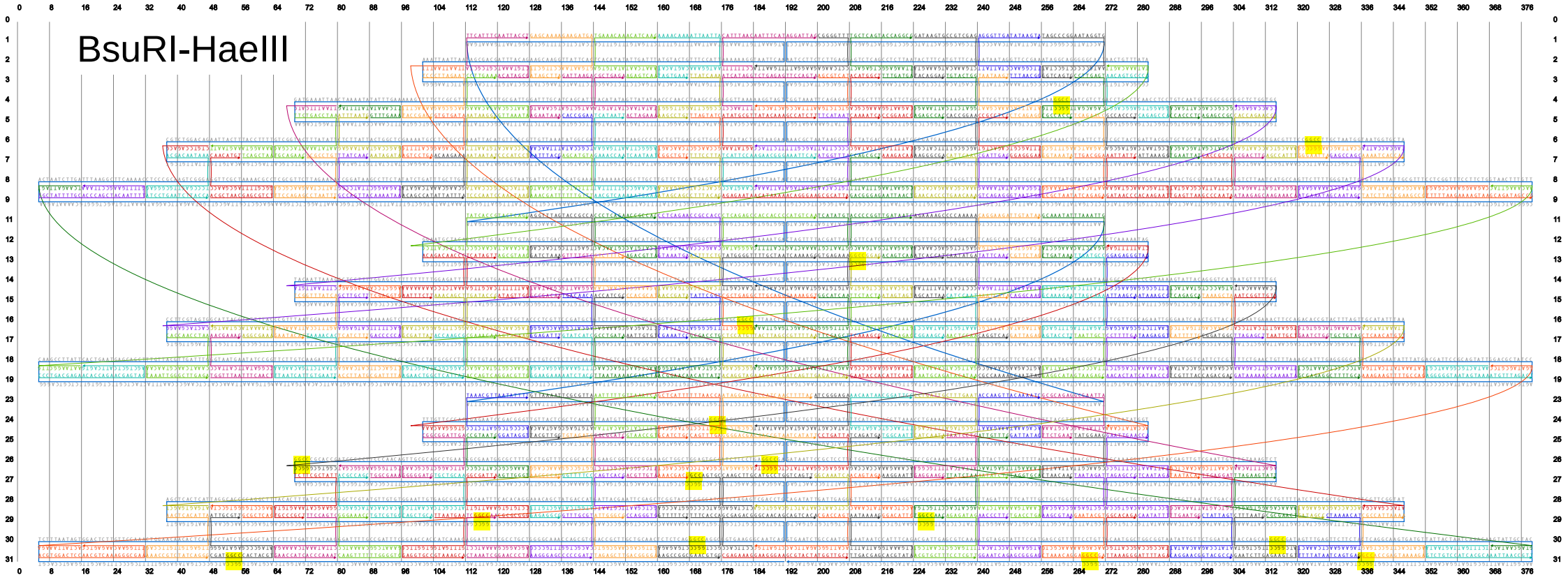
BsuRI-HaeIII

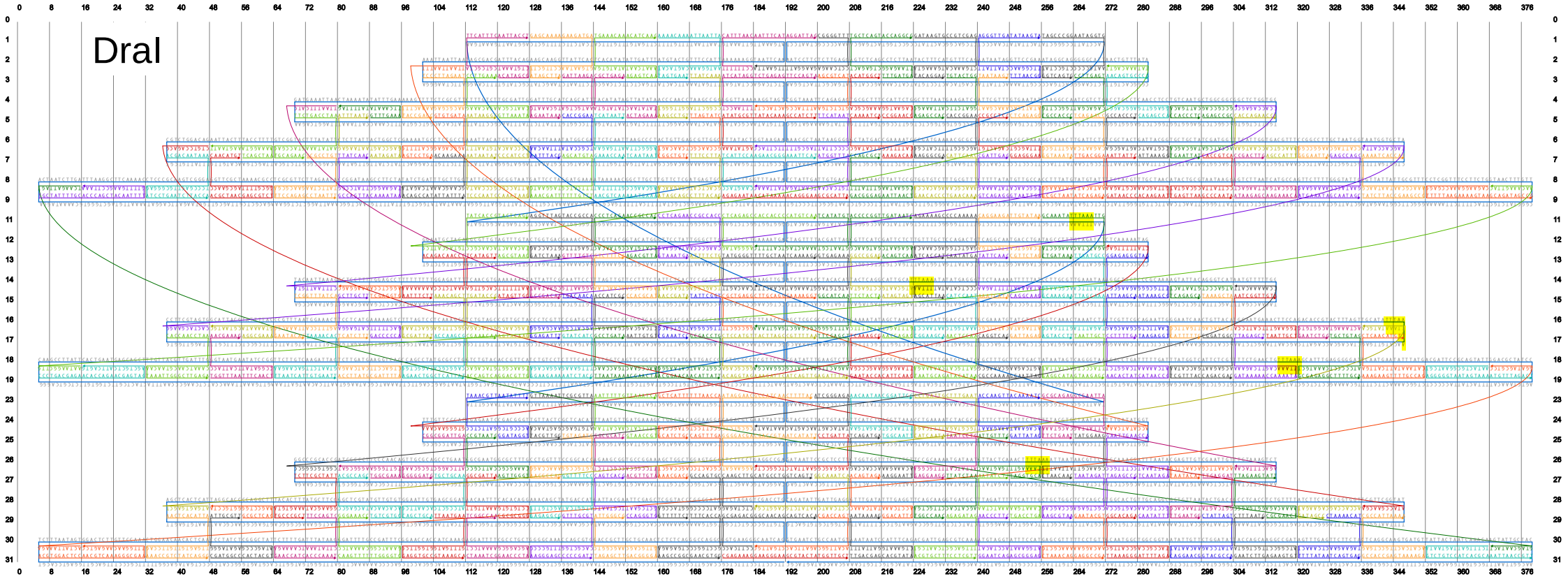
DraI

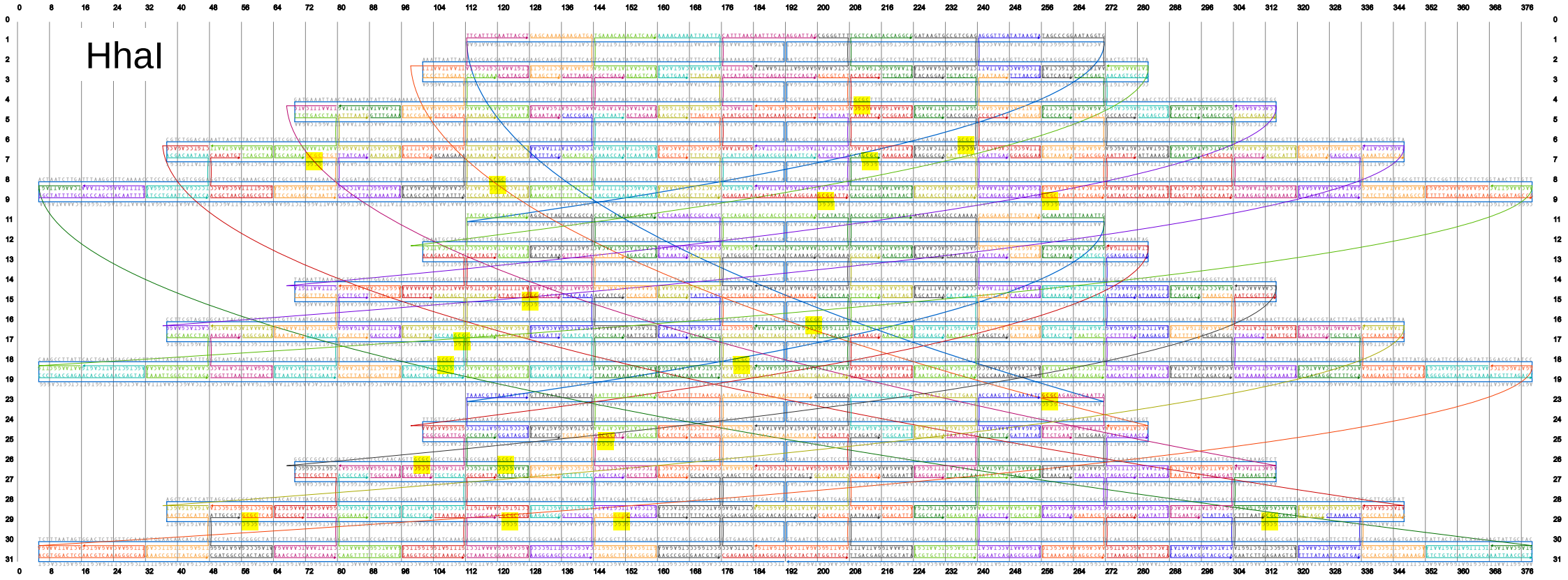
HhaI

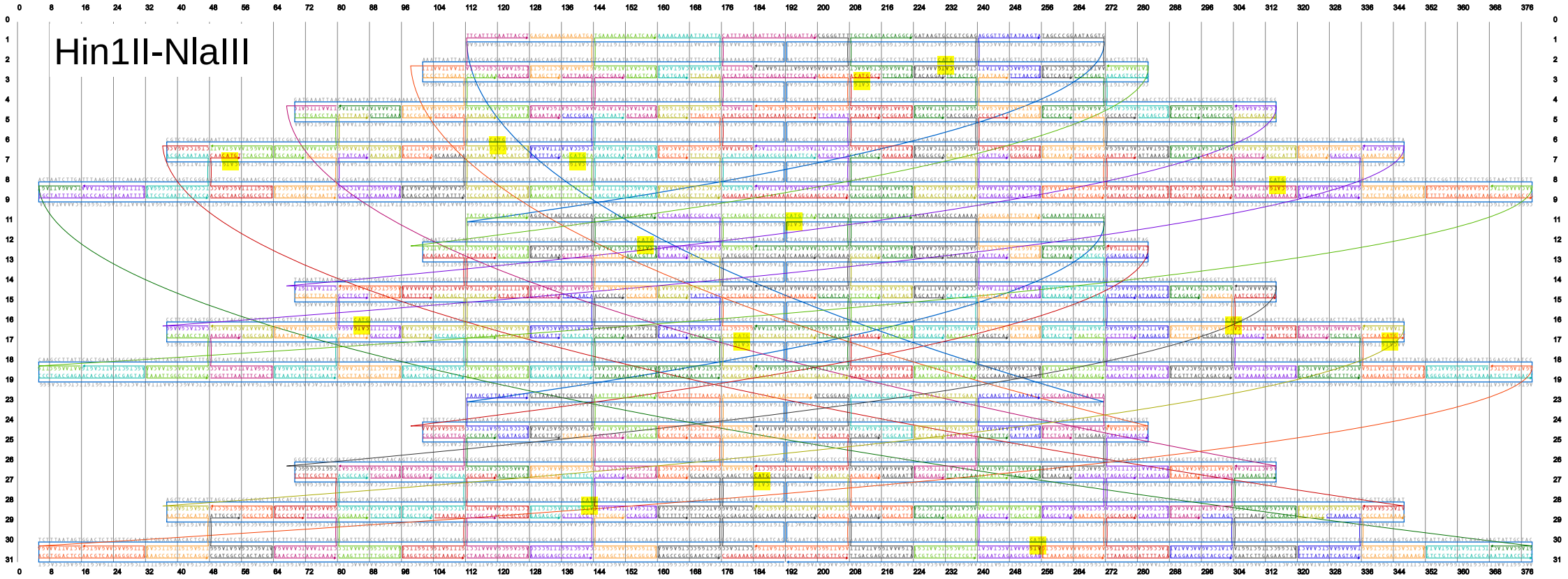
Hin1II-NlaIII

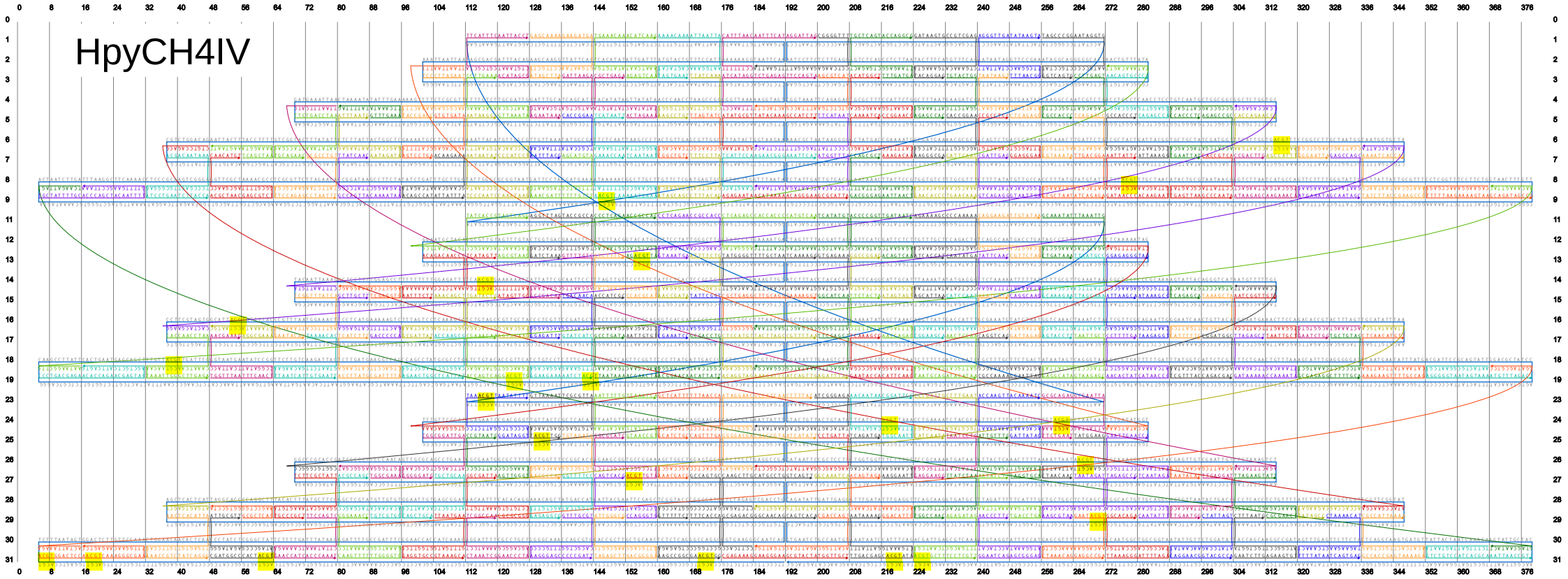
HpyCH4IV

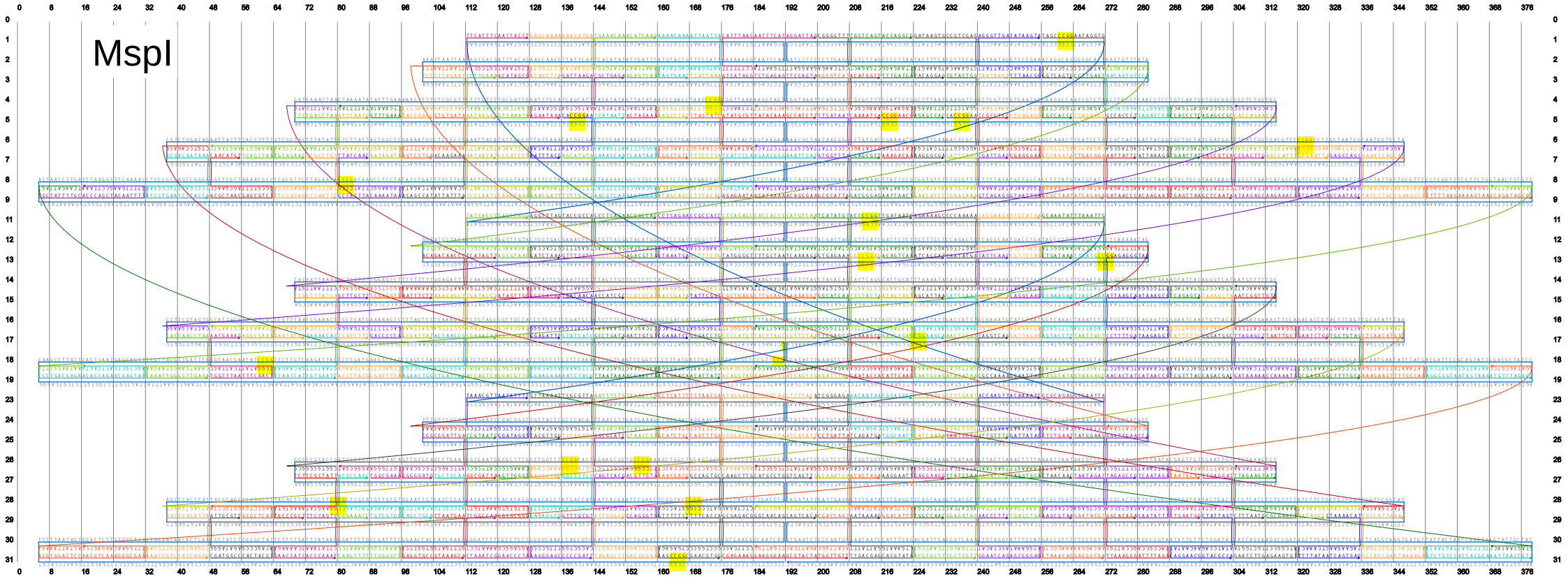
MspI

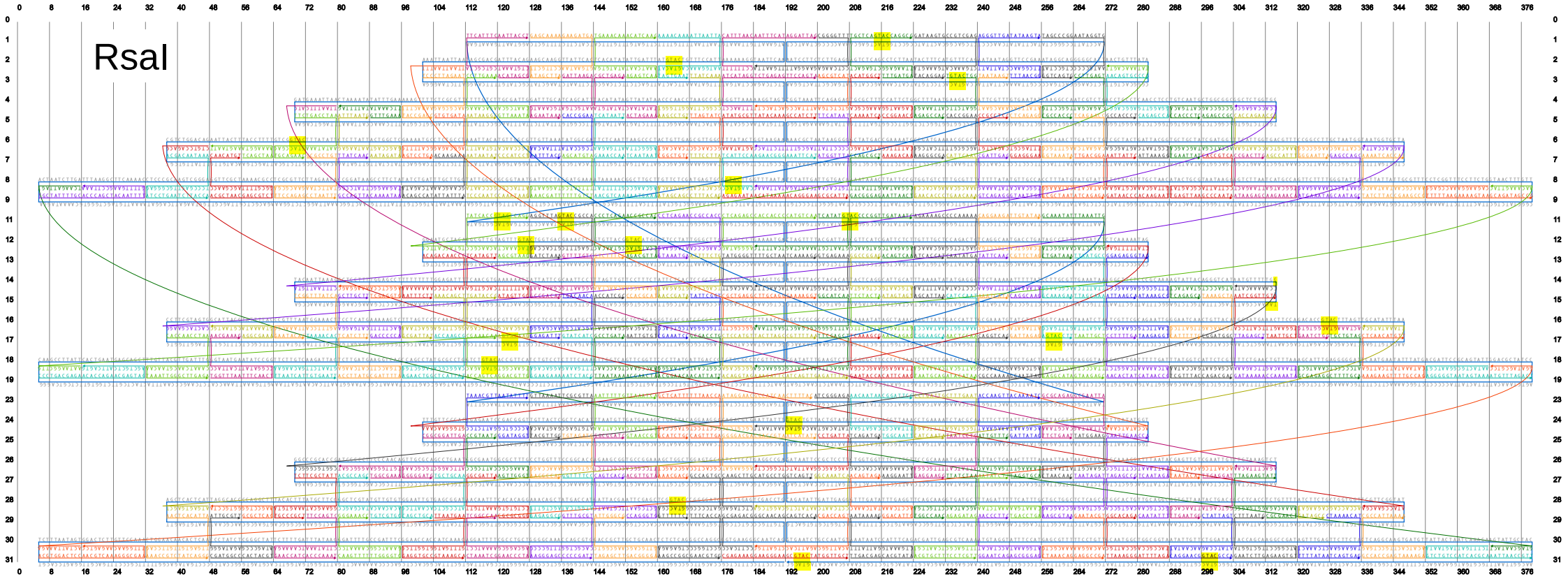
RsaI